Synergistic approach for the optimization of biodiesel production and property enhancement via nano-additive

Thesis submitted in partial fulfilment

for the award of the degree

Doctor of Philosophy

by

AJEET KUMAR PRAJAPATI

RAJIV GANDHI INSTITUTE OF PETROLEUM TECHNOLOGY

JAIS, 229304

Roll No.: 20CE0002

2025

CERTIFICATE

It is certified that the work contained in the thesis titled ***"SYNERGISTIC APPROACH FOR THE OPTIMIZATION OF BIODIESEL PRODUCTION AND PROPERTY ENHANCEMENT VIA NANO-ADDITIVE"*** has been carried out under my supervision and that this work has not been submitted elsewhere for a degree.

It is further certified that the student has fulfilled all the requirements of Comprehensive, Candidacy, and SOTA.

Dr. Rakesh Kumar

(Supervisor)

DECLARATION BY THE CANDIDATE

I, ***Ajeet Kumar Prajapati***, certify that the work embodied in this thesis is my own bonafide work and was carried out by me under the supervision of ***Dr. Rakesh Kumar*** from ***August 2020*** to ***June 2025***, at the *Department of Chemical and Biochemical Engineering,* Rajiv Gandhi Institute of Petroleum Technology, Jais. The matter embodied in this thesis has not been submitted for the award of any other degree. I declare that I have faithfully acknowledged and given credits to the research workers wherever their works have been cited in my work in this thesis. I further declare that I have not wilfully copied any other's work, paragraphs, text, data, results, etc., reported in journals, books, magazines, reports, dissertations, theses, etc., or available on websites and have not included them in this thesis and have not cited as my work.

Date:

Place: RGIPT, Jais, Amethi **Ajeet Kumar Prajapati**

CERTIFICATE BY THE SUPERVISOR

It is certified that the above statement made by the student is correct to the best of my knowledge.

Dr.Rakesh Kumar

(Supervisor) Signature & Seal of Head of Department

CERTIFICATE

CERTIFIED that the work contained in the thesis titled ***"Synergistic approach for the optimization of biodiesel production and property enhancement via nano-additive"*** by **Mr. Ajeet Kumar Prajapati** has been carried out under my supervision. It is also certified that he fulfilled the mandatory requirement of TWO quality publications that arose out of his thesis work.

It is further certified that the two publications (copies enclosed) of the aforesaid **Mr. Ajeet Kumar Prajapati** have been published in the Journals indexed by –

(a) SCI

(b) SCI Extended

(c) SCOPUS

Dr. Rakesh Kumar **Dr. Vivek Kumar**

(Supervisor) (Convener, DPGC)

COPYRIGHT TRANSFER CERTIFICATE

Title of the Thesis: Synergistic approach for the optimization of biodiesel production and property enhancement via nano-additive

Name of the Student: Ajeet Kumar Prajapati

Copyright Transfer

The undersigned hereby assigns to the Rajiv Gandhi Institute of Petroleum Technology Jais all rights under copyright that may exist in and for the above thesis submitted for the award of the **"DOCTOR OF PHILOSOPHY".**

Date:

Place: RGIPT, Jais, Amethi **Ajeet Kumar Prajapati**

Note: However, the author may reproduce or authorize others to reproduce material extracted verbatim from the thesis or derivative of the thesis for the author's personal use provided that the source and the Institute's copyright notice are indicated

Dedicated to my beloved parents

Acknowledgement

" The mind is everything. What you think, you become".

— Buddha

I would like to express my heartfelt gratitude to my supervisor, Dr. Rakesh Kumar, for his continuous motivation, unwavering support, and invaluable guidance throughout my research journey. His insightful discussions, patience, and encouragement have shaped both the direction and quality of my work. I am truly thankful for his time, expertise, and mentorship, without which this dissertation would not have been possible.

My sincere thanks also go to Dr. Deepak Dwivedi, whose steady guidance and support kept me focused and motivated throughout this endeavour. His thoughtful advice and constant encouragement have played a key role in helping me complete this work. I am deeply appreciative of Dr. Milan Kumar, Head of the Department of Chemical and Biochemical Engineering, as well as my committee members, Dr. Kaushik Guha Biswas and Dr. Debashish Panda, for their constructive feedback, valuable suggestions, and encouragement. I also extend my gratitude to the staff at Rajiv Gandhi Institute of Petroleum Technology, Jais, for their timely assistance and cooperation throughout my academic journey. On a more personal note, I would like to dedicate this work to my late grandparents, Mr. Gaya Prasad and Mrs. Manwati Devi, and my beloved late father, Mr. Ram Pratap Prajapati. Their blessings, love, and values have been a guiding light in my life. I am also deeply grateful to my mother, Mrs. Ful Bai Prajapati, for her constant support, sacrifices, and unshakable faith in me. To my wife, Mrs. Meena Prajapati, and my son, Aeric Kumar, thank you for your patience, love, and understanding during this journey. Your encouragement gave me the strength to keep going, even during the most challenging times. I would also like to thank my friends and colleagues who stood by me and offered help when I needed it. A special note of appreciation goes to Mr. Amit Kumar

Gomey, my research companion, for his constant support and collaboration. I am grateful to Mr Syed Saim Ali, Mr. Sunil Kumar, Mr. Rohit Kumar, Mr. Niyamt Ullaha Khan, Mr. Aash Mohammad, Mr. Sujeet Kumar Pandey, Mr. Harikeshwar Pandey, Dr. Yogendra Yadav, Dr. Belal Mohammah Haider, Mr. Siddharth Atal, Mr. Saurabh Mishra, Mr.Bhupendra Kumar, Mr. Amerandra, Mr. Waseem Ms. Swati, Ms. Shikha, Ms. Shalu Yadav, Ms Pooja Pandey, Ms. Swapna Patel and Ms. Akanksha Patel for their friendship and support. Lastly, I would like to thank Mr. Anuj Kumar, Mr. Umesh Kumar Sharma, Mr. Mahesh Kumar, Mr. Arun Kumar, and Mr. Surjit Kumar for their technical and practical assistance, which was invaluable to my work.

Date: **Ajeet Kumar Prajapati**

Table of contents

List of Figures

List of Tables

Nomenclature

η_m	Mechanical Efficiency
η_{bte}	Brake Thermal Efficiency
ηv	Volumetric Efficiency
K	Pseudo-voigt fit
λ	Wavelength of X-ray
β	Full width at half maximum

Abbreviations

AISI = American Iron and Steel Institute

AFR = Air-Fuel Ratio

Al_2O_3 = Aluminium Oxide

AV = Acid Value

B20 = Blended fuel (80% Diesel and 20% Biodiesel)

B30 = Blended fuel (70% Diesel and 30% Biodiesel)

BMEP = Brake Mean Effective Pressure

BP = Brake Power

BSFC = Brake-Specific Fuel Consumption

BTE = Brake Thermal Efficiency

C/H = Carbon to Hydrogen

C_3H_8OH = Isopropanol

CeO_2 = Cerium Oxide

CFD = computational fluid dynamics

CFI = Coil Flow Inverter

CH_3OH = Methanol

CN = Cetane Number

CNTs = Carbon Nanotubes

CO = Carbon Monoxide

Cr_2O_3 = Chromic Oxide

CSTRs = continuously stirred tank reactors

CV = Calorific Value

DBD = Discharge of Dielectric Barrier

DD-SDR = Dual-disk Rotating Disk Reactor

EDX = Energy Dispersive X-Ray

EGR = Exhaust Gas Recirculation

EU = European Union

FAAE = Fatty Acid Alkyl- Esters

FAME = Fatty Acid Methyl Ester

FBRs = Fluidized-Bed Reactors

Fe_2O_3 = Ferric Oxide

FESEM = Field Emission Scanning Electron Microscopy

FFA = Free Fatty Acid

FP = Frictional Power

GBA = Global Biofuel Alliance

GC-MS = Gas Chromatography -Mass Spectroscopy

H_2SO_4 = Sulfuric Acid

HCl = Hydrochloric Acid

HRR = Heat Release Rate

ICEs = Internal Combustion Engines

IEA = International Energy Agency

IMEP = Indicated Mean Effective Pressure

IP = Indicated Power

K_2NiF_6 = Potassium Hexafluoronickelate

KOH = Potassium Hydroxide

RSM = Response Surface Method

KOME = Karanja Oil Methyl Ester

M.W. = Molecular Weight

MeOH = Methanol

MnO = Manganese Oxide

MnO_2 = Manganese Dioxide

MOC = Material of Construction

MoO_3 = molybdenum trioxide

MR = Membrane Reactor

MTRs = mixed tank reactors

NaOH = Sodium hydroxide

Nb_2O_5 = niobium pentoxide

NER = net energy ratio

NHR = Net Heat Release

NMR = Nuclear Magnetic Resonance

NOx = Nitrogen Oxide

NPs = Nanoparticles

NZF = Net Zero Outflows

OFR = Oscillatory Flow Reactor

PM = Particulate Matter

RD = Reactive Distillation

Re = Reynolds Number

RIMM = Rectangle Inter-Digital Micro-Mixer

RPO = Refined Palm Oil

RSHCR = Rotary-Stator Hydrodynamic Cavitation Reactor

RS-SDR = Rotor-Stator Spinning Disc Reactor

RTR = Rotating Tube Reactor

SANS = South African National Standard

SDR = Spinning Disk Reactor

SFC = Specific Fuel Consumption

SIMM = slit inter-digital micro-mixer

SiO_2 = silicon dioxide

SMR = Static Mixer Reactor

SO = Soyabean Oil

SO_x = Sulphur Oxides

SPR = Shock-Wave Power Reactor

STR = spinning tube reactor

TBME = t-butyl methyl ether

TCR = Tubular Coil Reactor

TG = triglycerides

TiO_2 = titanium dioxide

TMR = Tubular microreactors

UCO = used cooking oil

USR = Ultrasonic reactor

VCR = Variable Compression Ratio

VF = Volume Fraction

WCFI = wavering coiled flow inverter

WHSV = Weight Hourly Space Velocity

ZnO = Zinc Oxide

Preface

The increasing global demand for energy, coupled with the depletion of fossil fuel reserves, has driven the search for renewable, sustainable, and environmentally friendly alternatives. Among these, biodiesel has gained significant attention as a viable substitute for conventional diesel due to its biodegradability, non-toxicity, and potential to reduce harmful emissions. Despite these benefits, widespread commercialization is hindered by several challenges, including high production costs, limited feedstock availability, sub-optimal fuel properties, and infrastructure compatibility issues. This thesis presents a comprehensive investigation into biodiesel production and performance enhancement, focusing on three key areas: reactor design innovations, nano-additive fuel enhancement, and corrosion behaviour of biodiesel blends. The research is systematically organized into seven chapters, each addressing a crucial aspect of the study:

Chapter 1 provides an overview of global and Indian biodiesel production trends. It discusses the advantages of biodiesel, available feedstocks, production methods, and the major limitations of conventional processes.

Chapter 2 reviews conventional and unconventional reactor technologies for biodiesel synthesis. It emphasizes innovative designs such as oscillatory flow reactors, spinning tube reactors, membrane reactors, and microreactors, outlining their operational principles, process advantages, and suitability for continuous biodiesel production.

Chapter 3 presents the experimental framework and compares the performance of batch reactors with flow-based systems, particularly tubular coil reactors (TCR) and coiled flow inverters (CFI). The study analyzes the effect of operational parameters such as molar ratios, flow rates, and reactor geometry on biodiesel yield and quality.

Chapter 4 explores the role of metal oxide nanoparticles (ZnO, Mg-ZnO, TiO_2, and SiO_2) in enhancing the physicochemical properties of biodiesel. These nanoparticles were

synthesized, characterized, and blended into pure biodiesel. Their impact on calorific value, viscosity, oxidation stability, and zeta potential was critically evaluated.

Chapter 5 focuses on the performance and emission behaviour of biodiesel blends incorporating SrO nanoparticles and tyre pyrolysis oil (TPO). Key engine performance parameters such as brake thermal efficiency (BTE), air-fuel ratio (AFR), brake-specific fuel consumption (BSFC), and emission outputs (CO, HC, NO_x, CO_2) were analyzed to assess the effectiveness of nanoparticle additives.

Chapter 6 investigates the corrosion effects of biodiesel blends on nickel-based alloys through prolonged immersion studies. Advanced surface characterization techniques, FESEM, XRF, XRD, and XPS, were employed to understand corrosion morphology, elemental changes, and surface chemistry. FTIR analysis was used to examine biodiesel degradation, and potential corrosion mitigation strategies were proposed.

This study emphasizes the potential of biodiesel as a renewable energy source, highlighting the need to enhance its fuel properties and operational reliability through nano-additive incorporation. It also underscores the importance of reactor design in optimizing biodiesel yield and process scalability. Through a comprehensive literature review, experimental investigations, and performance evaluation, the research demonstrates that nanoparticles can significantly improve biodiesel combustion efficiency, reduce emissions, and mitigate corrosion impacts, thus paving the way for industrial and commercial viability.

Chapter 7 concludes the work by summarizing the key findings and providing recommendations for future research, which include optimizing nano-additive formulations, exploring alternative and sustainable feedstocks, and scaling up reactor designs for industrial applications.

Chapter 1

General Introduction

1.1 Global scenario of biodiesel

Amid growing global pressure regarding climate change, numerous nations are focusing on renewable and clean alternative fuels for current and future applications. Alternative fuels such as ethanol, methanol, biodiesel, and hydrogen have gained significant attention due to their lower emissions and environmental advantages. Among them, biodiesel stands out as one of the most widely used renewable alternatives to petroleum diesel. The global production of biodiesel has shown a consistent upward trend, as illustrated in Figure 1.1, which highlights the steady growth in output from 2014 to 2023. The global production of biodiesel had approached 50 billion litres by 2023 (Statista Research Department, 2025; World Bioenergy Association, 2024). Indonesia led global production with about 14 billion litres, driven by its aggressive blending mandate and abundant palm oil resources. The country implemented a B35 mandate in 2023, requiring 35% biodiesel in all diesel fuel, with plans to raise it to B40 in 2025 and B50 by 2026 (BioEnergy Times, 2025; World Bioenergy Association, 2024). The European Union (EU) followed closely, producing around 13 billion litres, primarily using rapeseed oil and recycled cooking oil. The EU maintains a B7 blend mandate across most member states, though some countries adopt higher blends(Global Bioenergy Statistics Report 2024, 2024; World Bioenergy Association, 2024). Brazil, one of the pioneers in biodiesel production, generated nearly 7.5 billion litres using mostly soybean oil. The country currently follows a B14 mandate, having postponed a planned increase to B15 (fuelsandlubes, 2024; Ron Kotrba, 2025).

The United States, with its diverse blend policies across states, produced approximately 10.2 million tonnes, with widespread use of blends between B5 and B20 (U.S. Energy Information Administration, 2023). Soybean oil remains the dominant feedstock. Malaysia produced about 1.58 billion litres, supporting its current B20 policy in select regions, with plans to expand nationwide and evaluate a B30 mandate (Malaysia: Biofuels

Annual(USDA), 2023). Canada enforces varying provincial mandates, typically requiring 2– 4% biodiesel blends(Saini et al., 2021). As countries continue transitioning to renewable energy, biodiesel remains a crucial component in reducing carbon emissions and supporting sustainable transport systems.

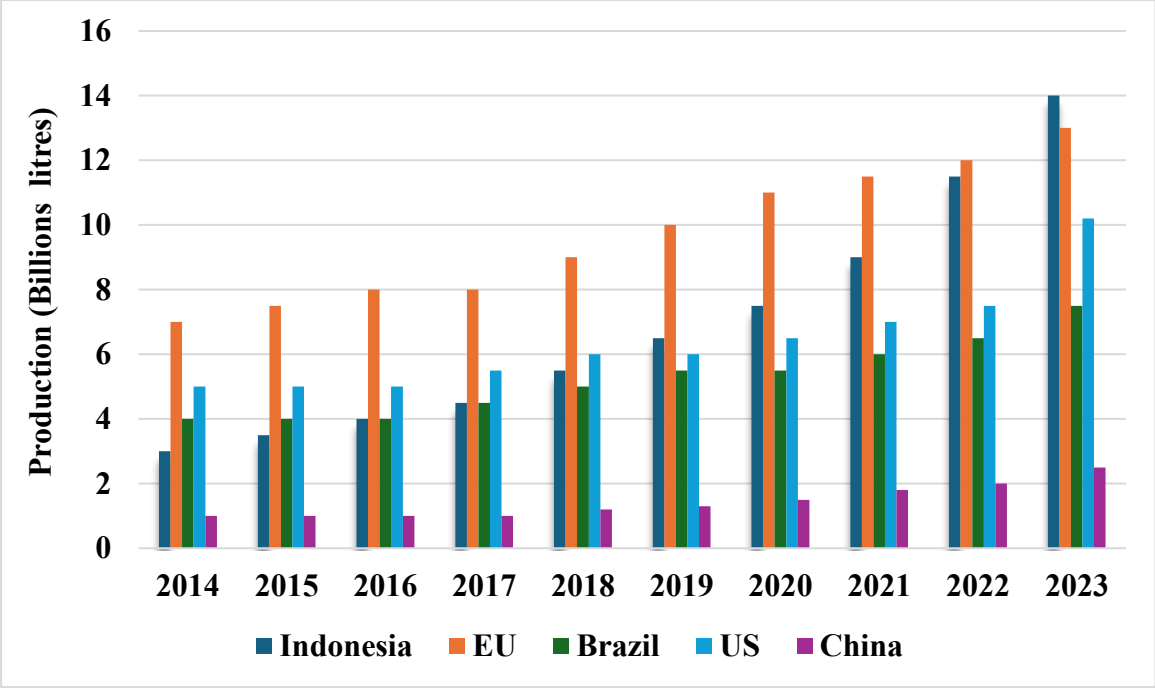

Figure 1. 1. Major biodiesel-producing countries (World Bioenergy Association, 2024)

1.2 Indian perspective of biodiesel production

In response to the growing demand for sustainable fuels, the Indian government launched a biodiesel purchase program in 2006, which was subsequently revised to meet evolving needs. Figure 1.2 illustrates the evolution of this initiative, while Table 1.1 outlines the current biodiesel market. India has made a substantial advancement in sustainable development by initiating the Global Biofuel Alliance (GBA) in 2023, collaborating with leaders from eight other countries to promote worldwide biofuel adoption. To support the development of the Global Biofuel Alliance (GBA), the International Energy Agency (IEA) released a report titled “Biofuel Policy in Brazil, India, and the United States:

Insights for the Global Biofuel Alliance"(Ministry of Petroleum & Natural Gas (PIB Delhi), 2024). The report emphasises the need to strengthen both emerging and established biofuel markets, noting that over 80% of global biofuel production is currently concentrated in just four regions: the United States, Brazil, Europe, and Indonesia, even though these regions account for only about half of the world's transport fuel demand. The IEA underscores the necessity of expediting technology deployment and commercialisation while achieving consensus on performance-based sustainability evaluations. The government aims to attain a 5% biodiesel blending target by 2030, necessitating almost 4.5 billion gallons of biodiesel each year, as per IEA projections (Jeremy Moorhouse, 2024). To stimulate production, India must establish a legislative framework like that employed for ethanol, encompassing production support, assured pricing, and feedstock incentives, especially for procuring used cooking oil and planting vegetable oils on marginal land.

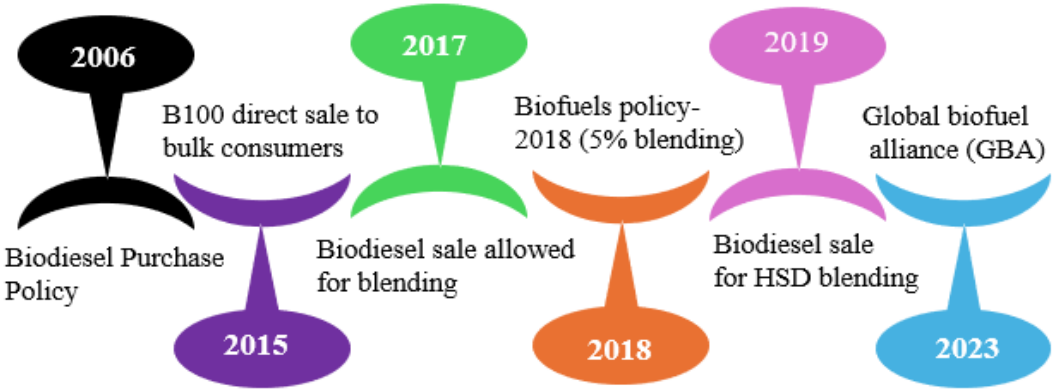

Figure 1.2. List of biodiesel policies in India

Table 1.1. Biodiesel production in India from multiple feedstocks (Shilpita Das, 2024)

Biodiesel (Millions of Litres)										
Calendar Year	2015	2016	2017	2018	2019	2020	2021	2022	2023	2024
Production	152	158	170	185	230	200	180	185	200	226
Consumption	118	119	165	180	185	140	165	186	190	220
Number of Biorefineries	6	6	6	6	6	6	6	7	10	12
Feedstock Use (1,000 MT)										
Animal fats	5	6	6	7	10	6	12	7	6	8
Recycled oils (UCO)	55	55	56	60	70	45	65	65	70	125
Other (mostly palm stearin)	85	90	100	110	140	140	95	105	115	83
Total	145	151	162	177	220	191	172	177	191	216
Market Penetration (Million Litres)										
Biodiesel, On-road use	41	48	72	83	100	50	10	40	40	105
Diesel, on-road use	52,239	55,179	56,715	59,220	60,145	44,400	52,927	57,002	62,000	65,850
Blend Rate (%)	0.08	0.09	0.13	0.14	0.17	0.11	0.02	0.07	0.06	0.16

1.3 Advantages of biodiesel

Biodiesel, especially in its pure form (B100), stands out as a cleaner and greener alternative to traditional petroleum diesel. One of its most notable environmental benefits is the complete elimination of sulphur emissions, which are a major contributor to acid rain. It also significantly reduces emissions of carbon monoxide and fine particulate matter that contribute to smog by nearly 50%. Hydrocarbon emissions, another key

pollutant, are cut by as much as 75% to 90%. Perhaps most importantly, biodiesel offers a powerful tool in the fight against climate change. When B100 is used, carbon dioxide (CO_2) emissions are reduced by over 75% compared to conventional diesel. Even using a lower blend like B20 (20% biodiesel and 80% petroleum diesel) can cut CO_2 emissions by around 15%, according to the U.S. Department of Energy. (United States Environmental Protection Agency, 2024). It also boosts engine performance by providing better lubrication, which helps reduce wear and minimizes the buildup of harmful deposits. With a high ignition point of around 176.7°C, biodiesel is also safer to handle and store than petroleum diesel. Moreover, biodiesel is biodegradable and non-toxic, making it a more environmentally friendly and safer alternative fuel. It also offers a range of additional benefits, as highlighted in Figure 1.3.

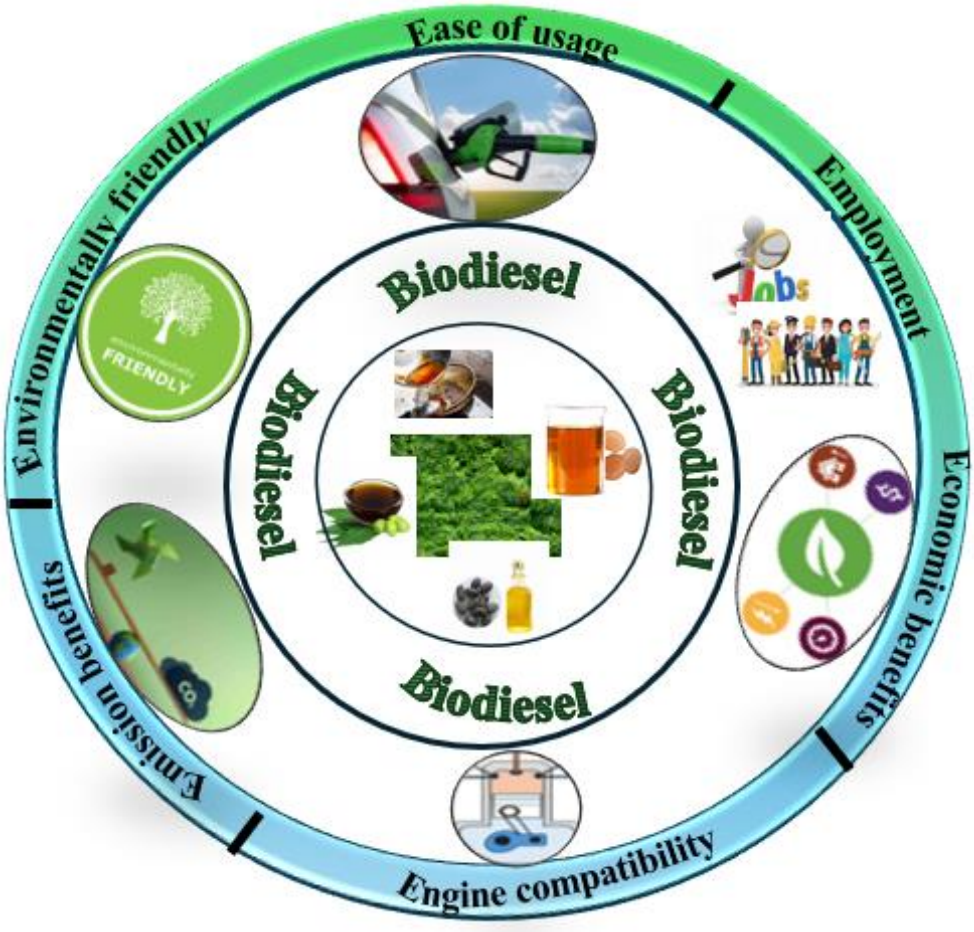

Figure 1.3. Holistic advantages of biodiesel

1.4 Biodiesel feedstocks

The availability of feedstocks for biodiesel production varies based on various factors, including geographic location, climate, pricing, and societal considerations. Certain regions, including Brazil and the United States, possess an abundance of biomass resources, such as soybeans, which are utilized as feedstock for biodiesel production. These nations have implemented regulations and incentives to encourage biodiesel utilization, resulting in a substantial increase in biodiesel output. Various sources for biodiesel production, including Jatropha, Karanja, Rapeseed, Soybean, Moringa, Neem seed, and Cottonseed, have been utilized as potential feedstocks for biodiesel synthesis. Technological advancements have significantly expanded the range of feedstocks available for biodiesel production, including vegetable oils, used cooking oils, animal fats, algae, and even genetically engineered algae. Feedstocks used in the production of biodiesel have been categorized based on their generation, as given in Table 1.2. The development of biodiesel is categorized into four distinct generations based on the type of raw materials used, the processing technologies applied, production costs, energy yields, and environmental impacts:

Table 1.2. Comparison of 1G to 4G biodiesel technologies

Generation	Raw materials	Processing Methodology	Feedstock Cost (USD/Gal)	Energy Yield (MJ/kg)	Cost Effectiveness (USD/Gal)	GHG Emissions (g CO_2-equivalent/MJ)	References
First-generation (1G)	Edible oils (e.g., soybean, rapeseed, palm oil)	Transesterification, fermentation	2.50-3.00	37-40	3.00-4.50	45-65	(Biodiesel Education, 2024.; Demirbas, 2009; Hirani et al., 2018; Rajpoot et al., 2025)
Second-generation (2G)	Non-edible oils, waste cooking oil, animal fats	Transesterification, biochemical, thermochemical	1.00-1.80	38-42	2.00-3.50	25-50	(Atabani et al., 2012; Monika et al., 2023)
Third generation (3G)	Microalgae	Transesterification, biochemical, thermochemical	4.00-7.50	45-55	4.50-8.00	10-30	(Ranjbari et al., 2022; Sharma et al., 2025)
Fourth generation (4G)	Genetically modified algae, photosynthetic organisms	Genetic modification, Transesterification, biochemical, thermochemical, electrochemical	5.00-10.00	50-60	5.50-10.00	0-15	(Shokravi et al., 2022; A. Singh et al., 2011; Y. Singh et al., 2025).

(i) First-generation (1G): 1G biodiesel is produced from edible oils such as soybean, rapeseed, and palm oil through processes like transesterification or fermentation. These feedstocks typically cost between 2.50 and 3.00 USD per gallon and provide an energy yield of 37 to 40 MJ/kg. An important consideration in biodiesel production is cost-effectiveness, which involves optimizing feedstock prices, processing techniques, and operational expenses to maximize fuel output per unit cost. However, despite its potential, this type of biodiesel tends to have relatively high greenhouse gas (GHG) emissions, estimated between 45 and 65 g CO_2-equivalent per MJ, which raises environmental concerns (Demirbas, 2009; Osman, Fang, et al., 2024).

(ii) Second-generation (2G): 2G biodiesel production employs non-edible oils, used cooking oils, and animal fats as primary feedstocks. These low-cost and more sustainable resources are converted into biodiesel through transesterification, as well as biochemical and thermochemical processing methods. Compared to first-generation counterparts, second-generation feedstocks are significantly more affordable, with costs ranging from approximately 1.00 to 1.80 USD per gallon. Additionally, they offer a slightly higher energy yield, between 38 and 42 MJ/kg. As a result, the process becomes more economically viable, with production costs generally falling between 2.00 and 3.50 USD per gallon. Furthermore, 2G biodiesel demonstrates environmental advantages, with lower greenhouse gas (GHG) emissions estimated at 25 to 50g CO_2-equivalent per MJ, making it a more sustainable alternative in both economic and ecological terms (Atabani et al., 2012; Monika et al., 2023).

(iii) Third generation (3G): 3G biodiesel places a strong focus on microalgae as the main feedstock due to its exceptional productivity, fast growth, and ability to thrive in various environments. Microalgae can be processed into biodiesel through

transesterification, as well as biochemical and thermochemical methods. One of its key advantages is a higher energy yield, ranging from 45 to 60 MJ/kg, which surpasses that of earlier-generation feedstocks. The production process remains costly, with expenses typically ranging from 4.00 to 7.50 USD per gallon, and total production costs falling between 4.50 and 8.00 USD per gallon. Despite the higher costs, microalgae-based biodiesel stands out for its environmental benefits, particularly its low greenhouse gas (GHG) emissions, which are estimated as 10 to 30 g CO_2-equivalent per MJ. This makes it a highly sustainable option for cleaner fuel alternatives (Ranjbari et al., 2022; Sharma et al., 2025).

(iv) Fourth generation (4G): 4G biodiesel represents a cutting-edge advancement in the field of renewable fuels, relying on genetically engineered algae and other modified photosynthetic organisms as feedstocks. These next-generation biodiesels are produced through a sophisticated combination of genetic modification, transesterification, biochemical, thermochemical, and electrochemical processes. Although the feedstock costs are the highest, ranging from 5.00 to 10.00 USD per gallon. 4G biodiesel delivers the most efficient energy output, with yields between 50 and 65 MJ/kg. Correspondingly, the total production cost is estimated in the range of 5.50 and 10.00 USD per gallon. A key distinguishing feature of 4G biodiesel is its remarkably low environmental impact, with greenhouse gas (GHG) emissions ranging from 0 to 15 g CO_2-equivalent per MJ (Shokravi et al., 2022; A. Singh et al., 2011; Y. Singh et al., 2025).

1.5 Biodiesel production techniques

Biodiesel production can occur via several techniques, such as the supercritical methanol process, enzymatic transesterification, thermochemical methods, pyrolysis, transesterification and hydrothermal liquefaction. Each technique offers unique advantages depending on the feedstock type, fuel quality requirements, economic factors,

and environmental implications (Ali Ijaz Malik, Zeeshan, et al., 2024). Supercritical methanol processing functions under elevated temperatures and pressures, eliminating the necessity for a catalyst and enabling the utilization of low-quality feedstocks. To enhance efficiency and minimize energy consumption, ultrasonic and microwave-assisted transesterification have been introduced, accelerating the reaction process. Enzymatic transesterification represents a more environmentally friendly approach, utilizing enzymes to generate high-purity biodiesel, albeit at a slower pace and higher cost. Thermochemical techniques such as pyrolysis and hydrothermal liquefaction effectively transform solid or mixed biomass into bio-oil, whereas biochemical conversion utilizes microorganisms to produce fuel precursors. Innovative advancements like electrochemical synthesis and synthetic biology present novel avenues for producing low-emission fuels through the utilization of CO_2 or genetically modified organisms (Zheng & Cho, 2025). Even with various techniques at hand, transesterification continues to be the predominant method for biodiesel production, owing to its straightforward application, reliable performance, and adaptability to various feedstock types.

1.5.1 Transesterification

The transesterification process is the most widely used method for producing biodiesel (B100). It significantly reduces the viscosity of oil feedstocks. This reduction improves the fuel's flow properties. As a result, biodiesel becomes more suitable for use in internal combustion engines (ICEs). In this process, oils or fats are reacted with alcohol in the presence of a catalyst to produce biodiesel, technically known as fatty acid alkyl esters, along with glycerol as a by-product (Mumtaz et al., 2017). Once the reaction is complete, the biodiesel and glycerol are separated, and any excess alcohol is recovered and recycled back into the process to improve efficiency. Since this method relies on alcohol, it's also commonly referred to as alcoholysis. A variety of alcohols can be used in the process,

including methanol, ethanol, propanol, butanol, and even amyl alcohol, with methanol being the most common due to its low cost, availability and reactivity. The chemical transformation occurs in steps: first, triglycerides (TG) are broken down into diglycerides (DG), then into monoglycerides (MG), and finally into glycerol. With each of these steps, molecules of biodiesel are formed specifically, and three molecules of alkyl esters are created for every molecule of glycerol (Brahma et al., 2022). The overall reaction is shown in Figure 1.4. One of the key advantages of transesterification is its flexibility, as it can be applied to a wide range of oil sources and operates under relatively mild reaction conditions (L. Yang et al., 2025). However, certain factors play a key role in how well the reaction proceeds, such as temperature, reaction time, pressure, alcohol-to-oil ratio, catalyst type and concentration, mixing speed, and the nature of the feedstock oil. Interestingly, the reaction can be carried out with or without a catalyst, and it works with both primary and secondary monohydric aliphatic alcohols. Overall, transesterification emerges as a sustainable and scalable method for converting renewable oils into clean-burning biodiesel.

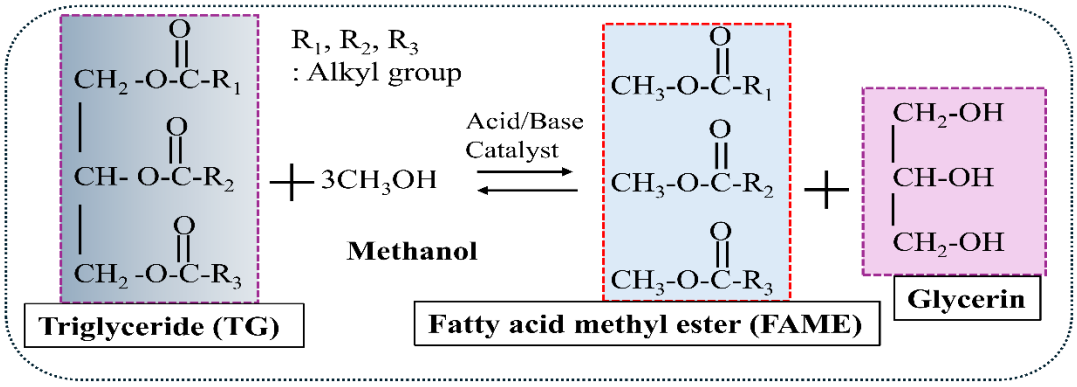

Figure 1.4.Transesterification of triglycerides with alcohol

1.6 Challenges in conventional biodiesel production

1.6.1 Production cost and feedstock availability

Biodiesel is widely regarded as a promising cleaner and more sustainable alternative to fossil fuels; however, its large-scale production is still hindered by several critical challenges (Gaurav et al., 2024). One of the most pressing issues is the high cost of production, which is largely driven by the price of raw materials. Feedstocks like vegetable oils, animal fats, and even used cooking oils form the bulk of the production expenses. The use of food-grade oils raises ethical concerns about food security (Osman, Nasr, et al., 2024). Another issue is feedstock availability and consistency. In many areas, the supply of suitable feedstock is irregular due to seasonal changes, limited collection systems, and varying agricultural outputs. This makes it difficult for producers to maintain stable production levels throughout the year. The processing technology also presents hurdles as impurities in low-cost feedstocks need to be removed through additional treatment steps, which increases energy use and operating costs (Maheshwari et al., 2022).

A primary issue in biodiesel production is achieving high yield while assuring consistent and dependable fuel quality. In the transesterification process, oils or fats are expected to react entirely with alcohol (Methanol or Ethanol) to produce biodiesel (Larimi et al. 2024). Nevertheless, in several instances, the reaction does not reach completion. Moisture, contaminants, and elevated free fatty acid levels in the feedstock can interfere with the process. This leads to insufficient yield, resulting in reduced biodiesel production and increased wastage of raw materials. A further difficulty is undesirable by-products, like soap and surplus glycerol. The by-products complicate the separation and purification of biodiesel to adhere to fuel quality regulations. Increased energy and time are required for cleaning and refining, resulting in higher production costs and diminishing overall

efficiency (Abdul Raman et al., 2019; Attarbachi et al., 2023). The catalyst type, reaction temperature, alcohol-to-oil ratio, and mixing speed are just some of the variables that must be carefully considered to achieve a complete reaction. Improving the yield of biodiesel and reducing waste are essential for rendering biodiesel production more dependable, cost-effective, and appropriate for widespread implementation.

1.6.2 Yield of the biodiesel

A primary issue in biodiesel production is achieving high yield while assuring consistent and dependable fuel quality. In the transesterification process, oils or fats are expected to react entirely with alcohol (Methanol or Ethanol) to produce biodiesel (Larimi et al. 2024). Nevertheless, in several instances, the reaction does not reach completion. Moisture, contaminants, and elevated free fatty acid levels in the feedstock can interfere with the process. This leads to insufficient yield, resulting in reduced biodiesel production and increased wastage of raw materials. A further difficulty is undesirable by-products, like soap and surplus glycerol. The by-products complicate the separation and purification of biodiesel to adhere to fuel quality regulations. Increased energy and time are required for cleaning and refining, resulting in higher production costs and diminishing overall efficiency (Attarbachi, Kingsley, and Spallina et al., 2023). The catalyst type, reaction temperature, alcohol-to-oil ratio, and mixing speed are just some of the variables that must be carefully considered to achieve a complete reaction. Improving the yield of biodiesel and reducing waste are essential for rendering biodiesel production more dependable, cost-effective, and appropriate for widespread implementation (Farouk et al., 2024).

1.6.3 Fuel properties

Despite its many environmental benefits, biodiesel still faces challenges when it comes to fuel properties, which can limit its widespread use. One of the main concerns is its higher viscosity compared to conventional diesel, especially at lower temperatures. This can lead to poor fuel atomization in engines, incomplete combustion, and the formation of deposits that may clog fuel injectors or filters (Ali Ijaz Malik, Kalam, et al., 2024). Another issue is cold flow performance. In colder climates, biodiesel tends to gel or solidify faster than petroleum diesel, making engine starting difficult and reducing fuel flow. To counter this, biodiesel often needs to be blended with conventional diesel or treated with additives, which adds to the cost and complexity (Bouaid et al., 2024; Hazrat et al., 2020). Biodiesel also has a slightly lower energy content, meaning vehicles may require more fuel to travel the same distance, especially when using pure biodiesel (B100). This can affect fuel economy and is a concern for users who rely on long-range efficiency. Moreover, oxidation stability is another area of concern. If biodiesel is stored for long periods, it may degrade, forming gums and sediments that can harm engine components (Verghese & Saeed, 2024). Addressing these fuel property limitations through better feedstock selection, advanced additives, or improved processing techniques is essential for making biodiesel more practical for everyday use.

1.6.4 Engine performance and emission

Although it is often acknowledged that biodiesel is a more ecologically responsible option than petroleum diesel, there are certain issues with engine performance and emissions. The fact that biodiesel, particularly in its pure form (B100), has a lower energy content than regular diesel is one of the main issues. This implies that, particularly in high-performance or heavy-duty applications, engines may see a decline in power output or fuel efficiency (Y. Zhang et al., 2021). Consequently, biodiesel-powered vehicles might

need more fuel as compared to petroleum diesel to cover the same distance, which could eventually impact operational expenses. Engine wear and deposits are another problem. Impurities like unreacted oils, moisture, or residual catalysts may have the potential to cause carbon deposits to accumulate in the combustion chamber, clogged fuel filters, and injector fouling (Csontos et al., 2019; Thangamani et al., 2021). This can shorten the lifespan of engine parts overall and lead to maintenance problems over time. Biodiesel does well in many areas when it comes to emissions. It dramatically lowers dangerous pollutants such as particulate matter, unburned hydrocarbons, and carbon monoxide. The tendency to emit a certain amount of nitrogen oxide (NOx) has been an ongoing issue, too. Smog is mostly caused by NOx, which can be harmful to the lungs.

The use of biodiesel is frequently associated with increased nitrogen oxide (NOx) emissions, which are mostly caused by higher combustion temperatures during engine operation. The generation of NOx is facilitated by these high temperatures. Even though numerous studies have supported this tendency, the issue is more complex than it may initially appear. According to several researchers, biodiesel continuously exhibits higher NOx emissions than regular diesel. Kolodnytska et al. observed that this increase becomes more obvious as engine load increases (Branco et al., 2025; Jayabal, 2025). The fact that biodiesel produced fewer NOx emissions than diesel when there was no load is interesting and suggests that engine load is a significant factor in emission results. Similarly, Hao Chen et al. found that while biodiesel's NOx emissions were generally greater than diesel's, they were equal to or even lower when the vehicle was moving at moderate speeds and low load. Further details were provided by Towhidul Islam et al., who tested blends of algae-based biodiesel, such as A5 (5% algal oil), A10 (10%), and A15 (15%), in comparison to pure diesel (M. T. Islam et al., 2021). Their findings indicated that the primary causes of elevated NOx emissions were improved injection timing and greater

intake and in-cylinder combustion temperatures. Nevertheless, blended algal biodiesel showed reduced NOx emissions compared to regular diesel while preserving satisfactory engine performance. This progress is being further supported by continuous advancements in engine calibration, exhaust after-treatment technologies, and fuel additives are assisting in lowering NOx emissions without compromising performance. With further research, biodiesel is becoming more engine-friendly and versatile, improving its potential as a cleaner, sustainable substitute for fossil fuels.

1.7 Scope of the present work

Although biodiesel has been extensively investigated as a renewable fuel, research has predominantly concentrated on isolated dimensions such as feedstock availability, catalyst development, process parameter optimization, and nanoadditive application. This fragmented approach limits progress in addressing persistent challenges related to yield, fuel properties, large-scale applicability and overall cost of the process. In the Indian context, where diverse non-edible and waste-derived feedstocks are abundant, there remains a lack of integrated strategies that combine multiple elements of biodiesel production to achieve superior outcomes.

In this thesis, the synergistic approach refers to the deliberate integration of four critical dimensions of biodiesel production: feedstock selection and blending, process parameter optimization, nano-additives development, and engine materials compatibility with biodiesel. The current study aims to achieve improvements in the biodiesel yield, physicochemical properties, and long-term usability by examining these factors collectively. This integrated strategy addresses the current knowledge gap and establishes a structured pathway for biodiesel production that balances technical performance and environmental sustainability. To address these aims, the following research objectives have been developed;

- To select non-edible oils and waste-derived sources as feedstock and their characterization.
- To optimize critical process parameters (molar ratio, temperature, reaction time, mixing speed) to maximize the biodiesel yield.
- To enhance the physicochemical properties of synthesized biodiesel through the application of nano-additives (NPs).
- To evaluate performance, combustion behaviour, and emission characteristics of nanoadditive blended biodiesel using a variable compression ratio (VCR) diesel engine.
- To assess the corrosion behaviour of biodiesel on engine materials, storage tank and delivery systems.

Chapter 2

A review on unconventional reactors for biodiesel production[1]

[1]The comprehensive review of the reactors discussed in this chapter has been published in Fuel. (2025);380:133263. https://doi.org/10.1016/j.fuel.2024.133263

2.1 Introduction

In the previous chapter, biodiesel was introduced as a renewable fuel, with transesterification identified as the principal synthesis route. While transesterification provides the fundamental basis for biodiesel production, further advancements are required to improve efficiency, reduce cost, and achieve scalability. These improvements depend largely on key factors such as feedstock quality, catalyst selection, and reactor configuration. Among these, reactor design is particularly critical, which ultimately governs the yield and scalability of the biodiesel process. Traditionally, this role has been fulfilled by conventional reactors such as batch and continuous stirred-tank reactors (CSTRs), which have long served as the backbone of biodiesel production.

However, the limited heat and mass transfer associated with these conventional reactors provides lower productivity of biodiesel. With the rising demand for sustainable fuel alternatives and the growing emphasis on higher process efficiencies, research efforts have increasingly shifted toward the development of novel reactor configurations. Accordingly, this chapter begins by briefly reviewing unconventional reactors for biodiesel production and highlighting their associated challenges. It then examines recently developed reactor designs that aim to enhance heat transfer, mass transfer, and reaction kinetics. In certain cases, these advanced systems also eliminate the need for catalysts, thereby reducing overall production costs. By enhancing reaction rates, novel reactor configurations offer strong potential for enabling continuous, intensified, and scalable biodiesel production.

2.2 Conventional reactors for biodiesel production: Challenges and Opportunities

Batch, semi-batch, and CSTRs (continuously stirred tank reactors) are among the conventional reactors capable of biodiesel production. Batch reactors necessitate a high catalyst concentration, a longer residence duration, and a higher alcohol-to-oil proportion, while the CSTRs with heterogeneous catalysts enable straightforward division from the biodiesel product and diminished soap formation. However, the complexity of multiphase reactions and the difficulty in combining incompatible reactant fluids (i.e., oil and alcohol) make the operation of conventional reactors challenging. The formation of byproducts is an additional concern that needs to be tackled with high energy consumption, contributing to the higher operational cost of the plant (i.e., complex biodiesel production and purification, removal of excess alcohol, and catalysts recovery during downstream processing) (Bashir et al., 2022). Also, since oils and alcohols are immiscible, mass transfer limitations exist for the biphasic reaction operated within a batch reactor and CSTRs (Díaz et al., 2023). Further, the slow reaction kinetics (especially at lower temperatures), catalyst deactivation, variation in quality and composition of feedstocks, high energy intake, and byproduct formation derive the need for a better-reacting system (or novel reactor) for biodiesel production.

2.3 Novel reactors for biodiesel production

A few recently developed reactors have been employed to perform the reaction (transesterification) and produce biodiesel from oily feedstocks. Novel reactors include mixers (static and chaotic), rotary-stator hydrodynamic cavitation reactors, OFR (oscillatory flow reactor), spinning-tube and rotating tube reactors, membrane reactors, reactive distillation, ultrasonic radiation reactors, microwave reactors, spiral reactors, and plasma reactors (see Figure 2.1). The next section discusses the usage and potential (novel reactors) mentioned above for biodiesel production.

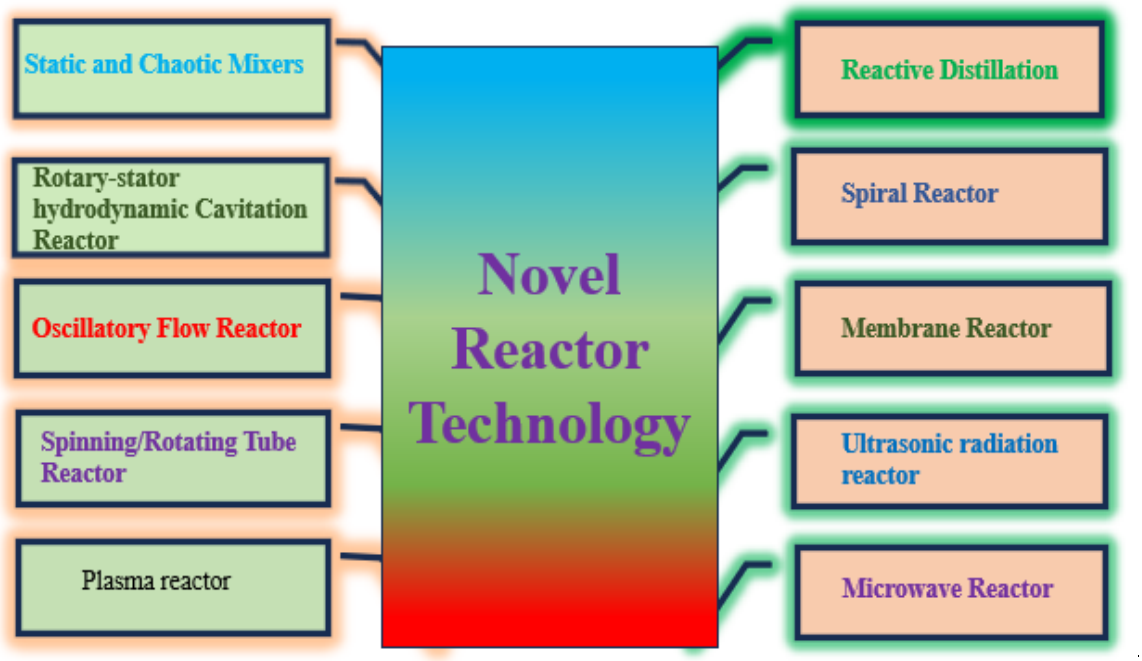

Figure 2.1. Novel reactors for the production and extraction of biodiesel

2.3.1 Static and chaotic mixers

Static mixers with compact designs remain efficient in conducting the reactions involving transesterification between waste cooking oil and methanol(Nguyen et al., 2018). The inline static mixers have been utilized extensively in the process industries due to their unique geometries, facilitating the transesterification reactions. The static mixer in the shape of helical coils allowed the fluids to flow by diffusion, especially at their tube cross-sections, enabling better mixing for incompatible reaction fluids(Alamsyah et al., 2010). The helical static mixer utilized for the generation of biodiesel is demonstrated in Figure 2.2. The helical mixer provided an excellent mixing rate and higher conversion in 30 minutes at 60 °C with a 1.5% sodium methoxide catalyst. The helical coils turn the flow direction by 90 degrees through the coils' bends, uniformly spaced apart, enabling good mixing amongst the immiscible canola oil and methanol. The number of bends within the

coils directly enhanced the fluid mixing efficiency. The CFIs mixers appeared promising for boosting biodiesel production in multiple ways, including (Aamir Bashir et al., 2021; Gupta et al., 2019):

- **Faster Reaction Times:** When compared to conventional batch reactors, CFIs can greatly shorten reaction times and increase production efficiency.
- **Improved Mixing**: CFIs facilitate effective mixing of the reactants (fats/oils, methanol, and catalyst) because of centrifugal forces and multiple shifts of the flow experienced within the coiled design. Higher rates of fat and oil conversion into biodiesel may result from this accelerated mixing.
- **Decreased Methanol Usage:** The CFIs can attain comparable conversion rates at lower methanol-to-oil ratios when it relates to the batch reactors. This, in turn, eliminates additional steps concerning excess methanol separation, thereby reducing the process complexity and overall cost.

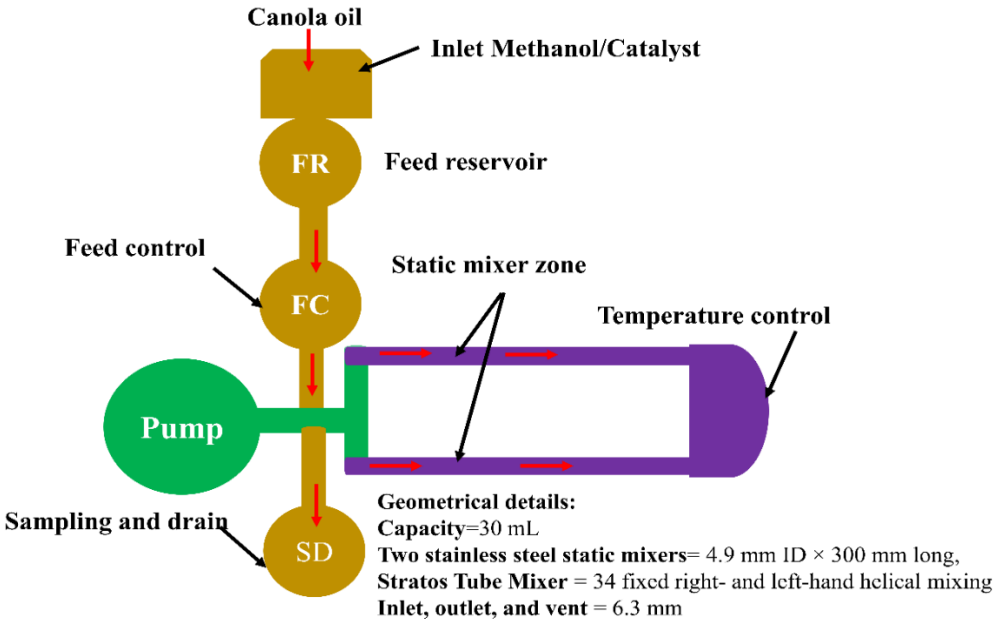

Figure 2.2. Schematic of static mixer closed loop system utilized for biodiesel production (Thompson & He, 2007a)

2.3.2 Rotary-stator hydrodynamic cavitation reactor

A rotary-stator hydrodynamic cavitation reactor (RSHCR) utilizes sonic or ultrasound energy to develop a cavitation phenomenon, which intensifies the process. Cavitation has the ability to improve the quality of waste or used cooking oil, naphtha, diesel, gasoline, and crude oil, resulting in more environmentally and economically advantageous products. Cavitation bubbles form and collapse aggressively when subjected to pressure fluctuations within the reactor. This causes shockwaves and microturbulence, which intensifies mixing and expands the oil-catalyst surface area in contact. Increasing mass transfer ultimately promotes the transesterification reaction and speeds up the generation of biodiesel. Additionally, cavitation can aid in better downstream separation, decreased soap production, and increased biodiesel yield. It is a promising technique for the manufacture of industrial biodiesel since it is robust and reasonably simple (Cako et al., 2022).

Cavitation induces liquid microcirculation and local turbulence, which boosts the degree of mass and heat transfer during this process of biodiesel generation (Farvardin et al., 2022; Fayyazi et al., 2018; Hosseinzadeh Samani et al., 2020; Safieddin Ardebili et al., 2015). Figure 2.3 illustrates the hydrodynamic cavitation reactor with a rotor-stator configuration.

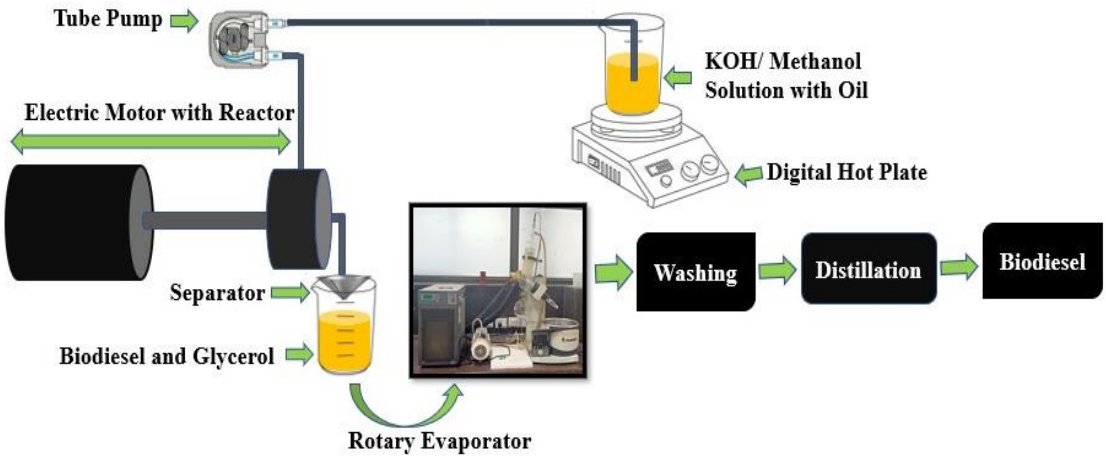

Figure 2.3. Rotor-stator hydrodynamic cavitation reactor (X. Sun et al., 2023)

In a report, hydrodynamic cavitation reactors show the free fatty acid (FFA) conversion to FAAE (fatty acid alkyl-esters) was 89.11% at 60 °C, 63.88 sec residence period, and 1:8.36 fatty acids: methanol (CH_3OH) ratio. The hydrodynamic cavitation reactors showed higher reaction rates than traditional reactors (batch) because they produce thinner and more uniform dispersions (Hamidi et al., 2023).

In controlled stream cavitation technology, ASTM 6751 B100 biodiesel is applied to produce a higher-quality fuel(Mishra et al., 2022). In another study, the cavitation-induced mixing of the reactants (oil and alcohol) is demonstrated using a Shock-Wave Power Reactor (SPR) during biodiesel production (Qiu, Engineering, et al., 2010). The SPR enhanced the transesterification reaction rates during biodiesel production because of its unique design/feature permitting controlled cavitation. In a typical SPR reactor, a carefully designed rotor continuously rotates and generates hydrodynamic cavitation within the rotor cavities. The hydrodynamic cavitation can be regulated by the rotor spin, which results in minuscule cavitation bubbles forming and collapsing, creating shockwaves. The shockwaves, once formed, are sent into the liquid mixture to facilitate the transfer of heat as well as mass. Therefore, in such a productive environment, animal

fats or vegetable oil transesterification takes place in only a few seconds, along with reduced saponification and emulsification (Meher et al., 2006). The SPR reactor empowers the utilization of a broader range of feedstock with higher concentrations of free fatty acids for biodiesel production (Atadashi et al., 2012).

Rotary-stator hydrodynamic cavitation reactors (RSHCR) have some restrictions (Blagojevič et al., 2023).

- **Effectiveness:** Although RSHCRs have the potential to generate cavitation effectively, attaining the ideal operating conditions can be challenging.
- **Complexity:** RSHCRs, in comparison to simpler systems such as orifice plate reactors, incorporate moving parts (rotor and stator), which adds intricacy to the design, manufacturing, and maintenance processes.
- **Shear Stress:** The intense shear forces occurring inside the reactor might cause harm to fragile materials or facilitate undesired side reactions.
- **Erosion:** Prolonged operation can result in the gradual wearing away of the rotor and stator components due to the repeated creation and collapse of cavitation bubbles. This can impact the performance of the reactor and require replacements.

2.3.3 Oscillatory flow reactor

OFR or oscillatory flow reactors include surfaces that are positioned transversely to the flow direction, resulting in well-organised mixing patterns and uniformity in the flow direction suitable for multiphase biodiesel production systems(Khelafi et al., 2022). The OFR is specifically designed with equally spaced orifice plates placed 1.5 tube diameters apart, providing a fractional open cross-sectional area of 0.25, as shown in Figure 2.4.

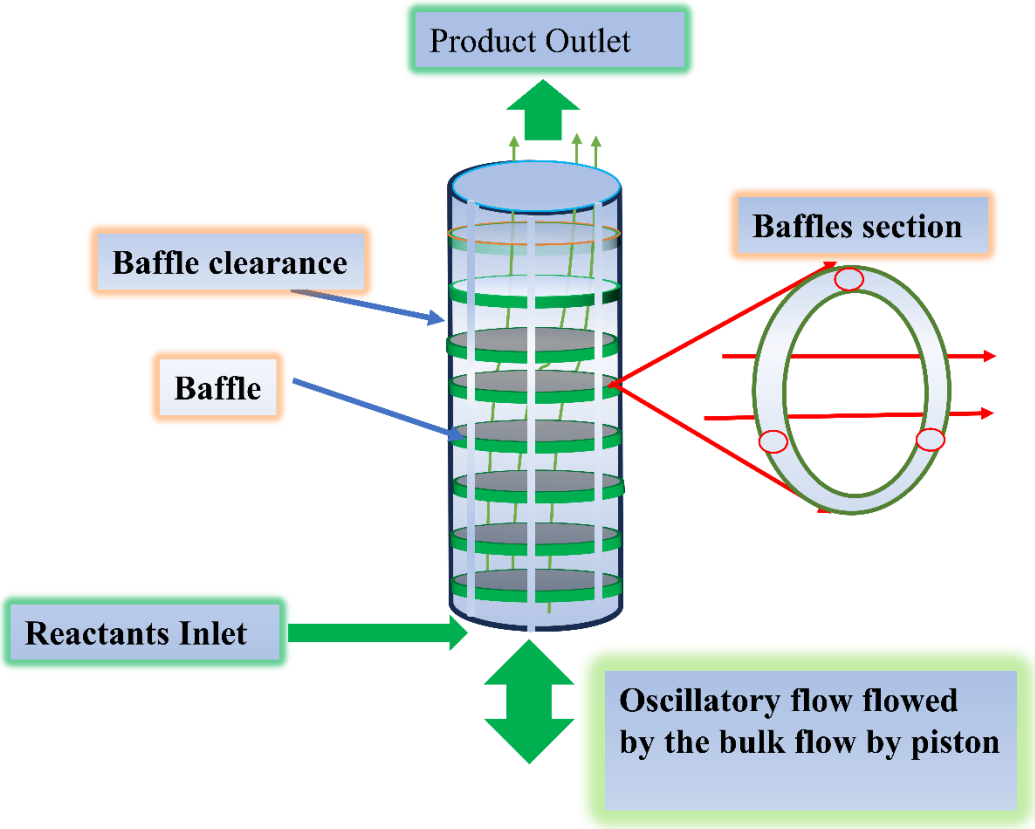

Figure 2.4. Demonstration of oscillatory flow reactor setup (Harvey et al., 2003a)

The incorporation of baffles allows OFR to initially function as stirred tanks and then eventually transition to resembling plug flow over time, making it a continuous reactor. However, unlike the PFRs (having a low Reynolds number), the pattern of interaction remains independent of the net flow in the OFR, permitting extended residence time("Reactors," 2008). This feature of OFR is promising for biodiesel production since the transesterification of oils, usually performed in a batch reactor, requires longer residence time. Conventional plug flow reactor designs are unsuitable due to their spacious length-to-diameter ratios that result in high capital costs, a big 'footprint', and challenging control. Further, the oscillatory motion created in the OFR is overlaid on the overall flow of the system's fluid (i.e., oil along with a methanol mixture), thereby facilitating a successful transfer of heat and mass while maintaining plug flow. The OFR

appeared as an efficient and cost-effective approach to resolving mixing and transport challenges of biodiesel production and enabling continuous process intensification. In a study, the OFR was utilized for the reaction (transesterification) of methanol-treated used cooking oil (1:6 molar ratio) (García-Martín et al., 2018). The reaction time of 30 minutes and an oscillatory frequency equal to 0.67 Hz resulted in a 78.8% biodiesel yield.

The OFRs represent an innovative category of continuous reactors; they are comprised of tubes that maintain equal spacing between the baffles of the orifice plate. Superimposing periodic motion over the total supply of the system's fluid generates flow patterns that facilitate the efficient transmission of mass as well as heat while controlling plug flow. In contrast to conventional plug flow reactors, which regulate the degree of mixing following the net flow, this design permits the attainment of extended residence durations in a reactor with a significantly reduced length-to-diameter (L/D) ratio. At present, numerous processes that require extended residence times are executed in batches. This is because conventional plug-flow reactor designs are unfeasible due to their substantial L/D ratio. It gives rise to issues including substantial capital expenditures, a significant "footprint," elevated pumping expenses, and challenging control. By enabling the conversion to continuous mode, the OFR effectively increases the process's intensity(Harvey et al., 2003a; Ghazi et al., 2008).

Furthermore, the development of OFR reactors with several operating conditions for biodiesel production was studied. For instance, the use of the response surface method (RSM) to ascertain temperature (30 – 50°C), oil to alcohol molar proportion (ranges from 1:6 to 1:12), catalyst concentrations (0.75% – 1.25%), and reactor length (1 – 3 m) on the biodiesel yield on OFR. The conversion increases by 8% when the temperature reaches 50°C, while it decreases by 4% when the temperature reaches 60°C. The biodiesel

conversion rate increases by 11% (from 58.70% to 69.51%) when the oil-to-alcohol molar proportion lies from 1:9 to 1:12. However, a 4% decline is observed at a 1:12 ratio. Similarly, at 1% catalyst concentration, conversion increased by 21% (from 48.82% to 69.51%); At 1.25%, it further decreased to 57.26%. An expansion of the reactor having a dimension (length) from 1 to 2 meters and the conversion rate increased by 20%, while an aggregate decrease of 4% was observed for reactors with a length of up to 3 meters. At a 1:9 oil-to-alcohol ratio, 40°C, 1% catalyst, and 3 to 9 meters of reactor length, the maximal conversion was 91.98 %(Kouhifaiegh et al., 2024). Additionally, modifying the OFR can reduce the residence and the process became 2-fold faster than the unmodified OFR and 12-fold faster than the batch process (Budi Utomo, 2013). Besides the benefits of the OFRs in biodiesel production, there exist some obstacles too that need to be addressed. Some of the constraints of OFR include:

- **Complex design and operation/control:** To ensure the best performance, the reactor must be designed with certain features, and the oscillation parameters (frequency and amplitude) must be precisely controlled to accommodate the oscillating flow. This can be complicated in comparison to conventional flow reactors.
- **Scalability:** Expanding the OFR operation from a lab-scale to a pilot/large-scale commercial operation for biodiesel production might present difficulties.
- **Maintenance:** The moving equipment, such as pumps or membranes, in the OFR to generate oscillation adds complexity and may necessitate more frequent maintenance compared to simpler flow reactors(Cruz et al., 2021).

2.3.4 Rotating or Spinning Tube Reactor

The principle of centrifugal force is the basis for the operation of the rotating tube reactor (RTR)or spinning tube reactor (STR), as illustrated in Figure 2.5. The rapid rotation of

the RTR/STR facilitates the development of centrifugal forces on the revolving tube surface, which induces shear stress in thin coatings (700–1400 μm). Thin films have a surface area/volume ratio (~ 1,000), which is quite large, due to their limited thickness, which facilitates surface interactions. Due to the components' dispersion within the film, the RTR approach enables a greater amount of mass and heat transfer. Additionally, it achieves efficient mixing by generating coiled films in the reaction mixture (i.e., oil or methanol) (Kuznetsov, 2011). This is demonstrated by the continuous synthesis of biodiesel in rotating tube reactors (RTR) using methanol and canola oil(Chanthon et al., 2021).

The synthesis was conducted with a 6:1 methanol-to-oil molar proportion, 1.5 wt.% NaOH (as a catalyst), 900 mL/min flow rate, 670 rpm tube rotational speed, and 45 seconds of retention period, resulting in a maximal conversion of 97.65%. The rotating disk reactor was employed in a separate study to generate biodiesel continuously by alkali-catalyzed reaction (transesterification) of soy oil and methanol(Lodha et al., 2012a). The operational conditions consisted of a 60 °C temperature, a 2400 rpm disc rotation, a 773 mL/min solution flow rate, and a 1.5 wt.% KOH catalyst, also the methanol-to-oil molar proportion of 6:1. The system achieved the highest yield of biodiesel (around 96.9%) at a residence time of 2–3 seconds. Further, the centrifugal force caused by the spinning disk effectively enhanced the biodiesel yield, particularly at higher flow rates. The STR provides a high shear rate, which eventually results in the high mixing of the reactants (i.e., soybean oil and methanol) and greatly accelerates reaction rates concerning biodiesel production. The reaction interface is constantly renewed because of the spinning motion, and it keeps eddy currents from dying. This constant refresh optimizes reaction efficiency by keeping reactants well-mixed for higher conversion rates and yields. Further, compared to conventional reactors, STRs can enable

the reaction time up to three-fold faster because of their improved mass transport and mixing (*COSTELLO | Spinning Tube in a Tube Reactor*, n.d.; L. Yang & Jensen, 2013).

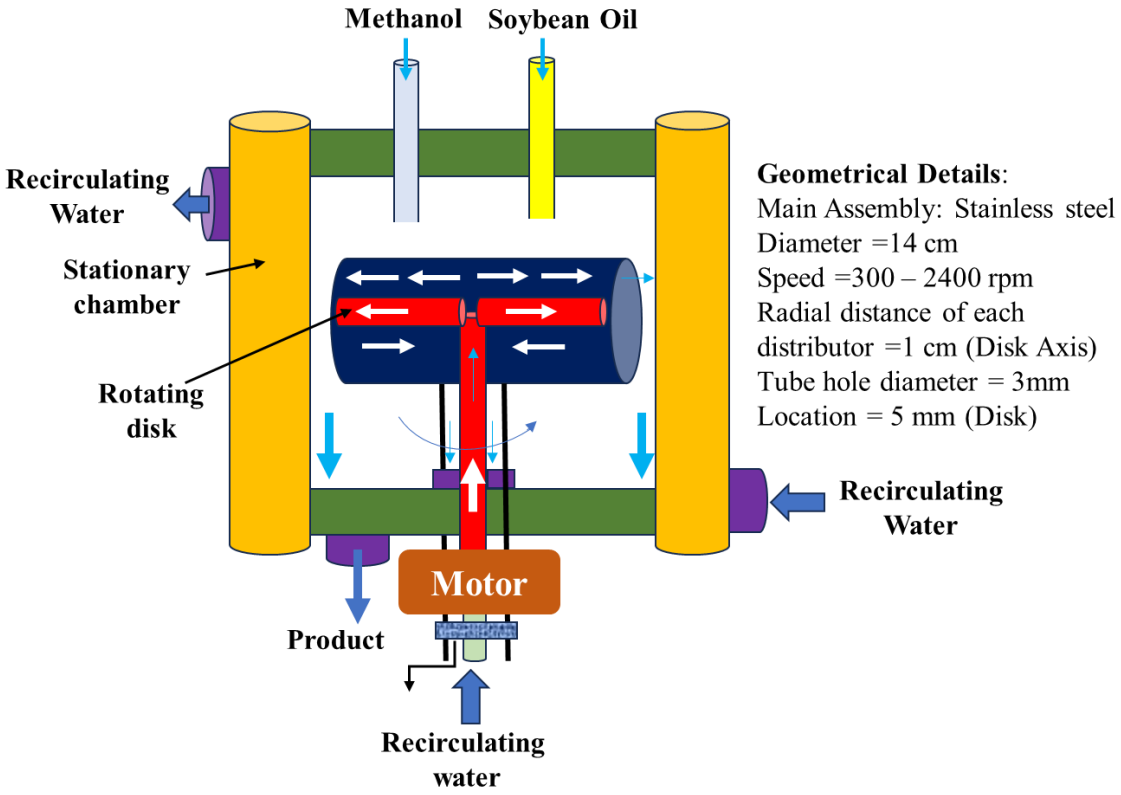

Figure 2.5**.** Experimental setup for spinning reactor (Qiu et al., 2012)

This is illustrated by the continuous conversion of soy oil and methanol into esters in a revolving or rotating reactor (disk). Another study examined the influence of the molar proportion of methanol to oil, temperature, catalyst type and concentration, flow rate, and rotating speed. The SDR showed 1.86 mol/min biodiesel production in a continuous transesterification reaction, which was significantly higher than that of other reactors. This suggested that the spinning disk reactor (SDR) holds great promise as a substitute for continuous biodiesel production (K. J. Chen & Chen, 2014). A similar FAME was also produced in a (rotor-stator spinning disc reactor) or RS-SDR. The RS-SDR enabled the production of intense shear forces within a narrow gap between a rapidly rotating disc

and a stationary wall, which eventually enhanced rates of heat and mass transfer during biodiesel production. The homogeneous base-catalyzed transesterification reaction can be conducted using both single-stage and multistage RS-SDR systems that have been scaled up to enhance mass transfer. The multistage RS-SDR enabled 82% conversion with a higher production rate of 7.78 × 103 mole/m^3.min (Chaudhuri et al., 2022). Further, a dual-disk rotating disk reactor (DD-SDR) consisting of two flat disks aligned in a coaxial and parallel configuration to each other was also utilized for biodiesel production. In a typical DD-SDR, the feeds are introduced in a coaxial manner, aligned with the central axis of each disk. Additionally, the mixing initiated from the middle of the inner disk space led to a substantial reduction in residence time of approximately 20 – 40 times less for establishing equilibrium, compared to the residence time recorded in a batch reactor (stirred) employed as a means of monitoring. The parameters that were considered in this study were the inter-disk spacing within the SDR; the reactor efficacy during the generation of biodiesel was drastically influenced by the surface morphology of the disks, reaction temperature, and its SDR(Qiu et al., 2012). Despite the advantages, the potential drawbacks associated with SDR are:

- **Complexity:** SDR exhibits greater complexity in both design and operation when compared to conventional stirred tank reactors.
- **Rapid rotation:** Significant energy consumption of SDR may result from the high rotational speeds required for mixing.
- **Limitations in scaling:** Increasing the size of SDR reactors for large-scale applications can be challenging since it requires the necessary space between components and assures structural strength at high rotational speeds.

- Control throughout the compound residence is restricted. The precise management of residence time can be challenging in SDR reactors due to their continuous flow of reactants.
- **Non-uniform flow distribution:** Attaining complete uniformity in flow distribution across the SDR reactor channel can be difficult, which may result in regions with suboptimal mixing efficiency (Visscher et al., 2013).

2.3.5 Plasma reactor

Biodiesel production using plasma technology is rapidly growing and holds great promise(Asghari et al., 2022). Utilizing a plasma reactor for the generation of biodiesel provided the following benefits.

- **Faster reaction rates:** When compared to conventional reactors, plasma activation dramatically accelerates the transesterification process, which results in higher manufacturing efficiency(Purwanto et al., 2020).
- **Decreased catalyst dependence:** The plasma may also function as a catalyst, obviating the necessity for chemical catalysts or lowering the needed amount of catalyst. This eliminates catalyst deactivation issues and thus reduces the overall process cost.
- **Possibility of different feedstocks:** The utilization of undesirable substances and used cooking oil among the expanded spectrum of renewable feedstocks for biodiesel production, which plasma technology offers promise for. This increases the possibility of producing biodiesel sustainably.

Utilization of plasma reactors for transesterification reactions has yielded encouraging outcomes. The plasma method can generate a diverse array of reactive and bond-breaking

species (as ions), resulting in a high level of selectivity in the reaction(Asghari et al., 2022). A study revealed that the discharge of the dielectric barrier (DBD) is a highly exceptional technique, and the plasma reactor, specifically DBD, can be utilized to generate biodiesel (by methanol and palm oil). The plasma reactor used in this study has a gas carrier 9 flow rate of 2.5 L/min, a TG/MeOH flow rate of 0.1318 L/min, and a 250 mm diameter for producing biodiesel (or FAME). The plasma DBD reactor was capable of converting TG/MeOH into biodiesel in homogeneous or heterogeneous systems without substantial amounts of glycerin byproducts (Fakhri et al., 2018). Another study showed FAME production in a continuous-streaming (dielectric-barrier discharge plasma) catalytic reactor. The catalytic reaction was conducted using a 5 wt.% K_2O/CaO-ZnO catalyst, at 1 atm, and 65 ºC. The catalyst flow in a continuous manner incorporates a voltage of 5 kV, a diameter of the catalyst of 5 mm, and WHSV (Weight Hourly Space Velocity) of 1.186/min, respectively, and produced 77.2% biodiesel(Buchori et al., 2016).

A plasma jet (produced through an internal high-voltage electrode and a ring outside electrode) in the ceramic tube was utilized to convert different molar proportions of methanol- oil (4:1 – 8:1) into biodiesel with 83% yield over 0.75 – 1.25 wt.% catalyst and in 30 – 90 secs (Ansari Samani et al., 2023). In another work, the methanol was allowed to react with the triglycerides (molar ratio 1:1) within the plasma DBD reactor at 40 °C, 1 atm, 120 mins, 1.3 mL/s liquid feed flow, 25.27 mL/s argon gas flow rate, and 10.2 kV AC plasma voltage to form biodiesel (Zara et al., 2019).

Despite benefits, there are a few issues that can affect plasma reactors' performance during biodiesel production. For instance, during the operation of the plasma reactor, the plasma-facing components, such as perfluorocarbons (PFCs), may cover the interior of the plasma reactor chamber and meet the intense heat and particles of the plasma. Perfluorocarbons (PFCs) undergo degradation over time because of erosion and

blistering, and thus may decrease the efficiency of the reactor, and potential contamination of the plasma affects the biodiesel production. Further, the dissipation of the thermal energy generated by the fusion reaction is required to be expelled from the reactor. Insufficient ventilation might result in excessive heat generation within the reactor, affecting biodiesel production(see Figure 2.6) (Linke et al., 2019). Nevertheless, the plasma approach of biodiesel production showed advantages over the traditional transesterification systems (typically conducted in batch reactors or CSTRs) by allowing biodiesel production without the need for catalysts that demand minimal generated energy and are unable to generate glycerol as a side product.

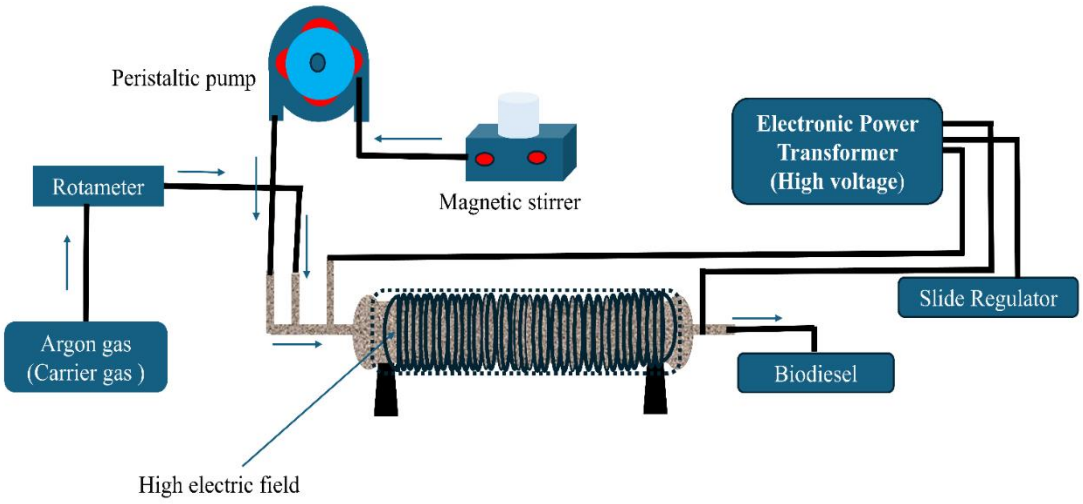

Figure 2.6. An experimental set of plasm reactors for biodiesel production (Zara et al., 2019)

2.3.6 Reactive distillation column reactor

RD (or reactive distillation) is also one of the fascinating techniques for producing biodiesel since it combines the separation of products (i.e., biodiesel and glycerol) with the reaction (transesterification) into a single unit (Petchsoongsakul et al., 2017). This can increase yields and improve product purity, thus declining the overall cost of the reaction. Further, it assists in changing the chemical balance in terms of increased biodiesel yields by constantly extracting the product (or biodiesel) by distillation inside the RD column.

By continually removing biodiesel from the reaction mixture, the RD can achieve high biodiesel purity and reduce the need for lengthy downstream purification processes. Research and development initiatives can substantially contribute to the advancement of biodiesel (mainly in generation) through the optimization of RD procedures(Noshadi et al., 2012). For instance, biodiesel synthesis through reactive distillation: a techno-economic analysis approach suggested the generation cost of biodiesel as $1288 per ton ($4.24 per gallon, for the heterogeneous system) and $1568 per ton ($5.18 per gallon, for the alkali-catalysed homogeneous system). The costs were determined by considering a 35 kilo-tonnes per year processing facility with an oil feedstock price of $1.1 per kilogram (while maintaining all other variables at their default settings). Nevertheless, the price previously stated was marginally higher than today's market pricing of biodiesel, putting it from $3.5 to $4.5 per gallon. The heterogeneous-catalysed process was economically preferable to the process of biodiesel generation catalyzed by alkali, as evidenced by the results(Poddar et al., 2015). In another report, the reactive separation method comprised two interconnected reactive distillation columns (RDCs) that accounted for the process of converting fatty acids (FFA) into esters and converting glycerides into esters using methanol, respectively, using Amberlyst 15 and MgO catalysts. The findings indicated that the amount of FFA included in the vegetable oil stream significantly influenced the performance esterification-transesterification reaction in the reactive distillation process (Pérez-Cisneros et al., 2016), (Sadiq Ali et al., 2019). The RD (reactive distillation) was also utilized for generating biodiesel out of algal oil with a yield of up to 99%. The typical processing condition includes a total of 15 trays (of which 11 are type of reactive- trays), heat duty of reboiler: 6.4 MJ/min, and a reflux ratio of 2, with an algal oil to methanol molar proportion of 1:4. Biodiesel was generated at the bottom of the column of RD with 65.5 % purity, which was relatively similar to the purity achieved through other

technological methods. Further, the recommended RD column achieved a 43.41% reduction in energy utilization compared to the conventional approach and thus a 52.96% decrease in total production cost. Moreover, it decreased CO_2 emissions by 40.11% indicating that the reactive distillation approach could be favourable in terms of energy efficiency, economic viability, and environmental impact of biodiesel generation (Mondal & Jana, 2019). In another study, biodiesel generation in the RD system was compared between the ethylic route and methylic approaches. The kinetic parameters of the ethylic route (rate constant = 8173 dm^3/(mol.min) and the activation energy = 27.48 kJ/mol) were determined to be more favourable than methylic approaches (Silva et al., 2019). At the sixth stage within the RD column, both ethylic and methylic approaches produce biodiesel with 60.1% and 67.8% yields, respectively (see Figure 2.7). Subsequently, a sensitivity analysis performed by taking 20 equilibrium stages revealed an ester conversion of 97%. An analysis of the energy use of biodiesel production in the RD column with a batch reactor suggested significant energy minimization in the former approach suitable for ethylic along with methylic routes (i.e., the batch reactor consumed 1210W/h for the route which is ethylic, 2430W/h for the route that is methylic, while the energy requirement was roughly 1000W/h for both ethylic and methylic ones) in distillation method (reactive) (Silva et al., 2019). M. Arif Khan et al. conducted techno-economic modelling to optimize catalytic reactive distillation (RD) for esterification reactions in bio-oil upgrading; their simulation approach and results provide a foundation for both large-scale industrial RD design and small-scale experimental RD design for bio-oil upgrading. While complex bio-oil RD will significantly impact the development of multi-component, multi-reaction bio-oil upgrading processes, RD simulation for simple bio-oil (such as acetic acid and water) can serve as a basis for Aspen modelling of dilute acid recovery from wastewater(M. A. Khan & Adewuyi, 2019).

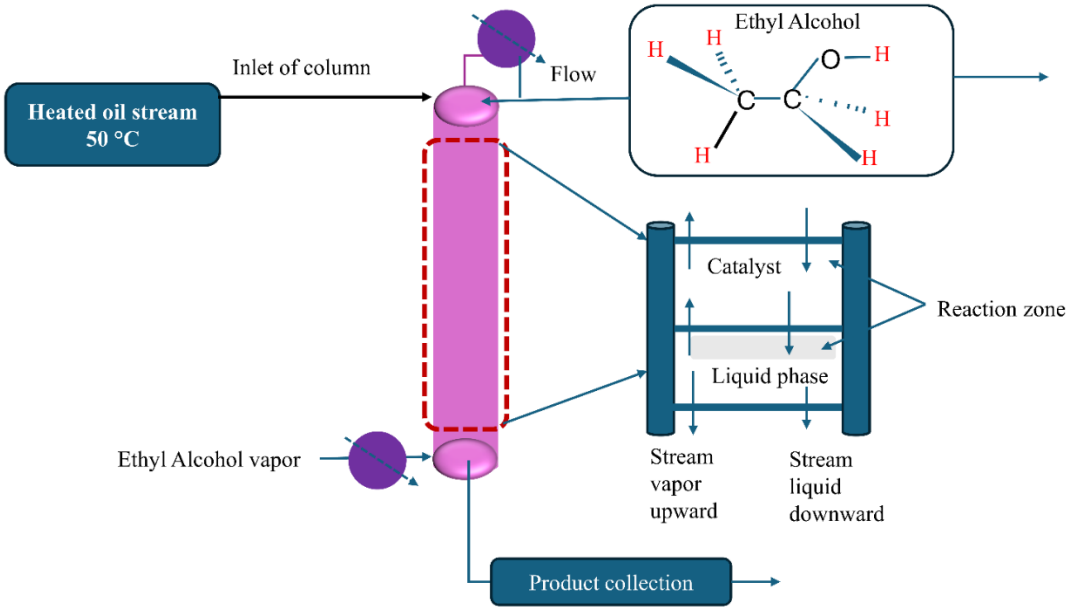

Figure 2.7. An experimental set of reactive distillation columns (Silva et al., 2019)

Although the reactive distillation (RD) approach provides benefits in biodiesel production, it also includes its unique difficulties, such as,

- **Design obstacles (**Optimizing the equilibrium from reaction to separation): The optimal design of a distillation column (reactive) must consider both the desired chemical reaction and the efficient separation of products.
- **Issues with the functioning and execution of tasks:** Restricted transformation. As a result of equilibrium, the effectiveness of reactive distillation in biodiesel production is often constrained by the state of reaction equilibrium. After reaching equilibrium, the subsequent conversion of reactants into products becomes challenging. This can have an impact on the ultimate purity of the final product(Silva et al., 2019; Simasatitkul et al., 2011)

2.3.7 Spiral reactor

The spiral reactor shows potential for biodiesel production when operating in severe environments that might involve extreme temperatures (i.e., hot or cold). Because of the coiled tube design, it provides enhanced heat transfer between the reacting mixture (i.e., oil and alcohol) during biodiesel production (Farobie et al., 2016). Compared to batch reactors, spiral reactors' continuous flow feature provides finer control over the reaction. The coiled tube functions as an enlarged heat exchanger. One can regulate the temperature of a jacket or bath that surrounds the reactor, as compared to the static conditions of a batch reactor (which operates in a cycle). Further, the compact coiled design makes it suitable for smaller-scale production facilities since it takes up less space than traditional stirred tank reactors (López-Guajardo, Enrique Ortiz-Nadal, Enrique Montesinos-Castellanos & Nigam, 2017). Supercritical or high-pressure biodiesel manufacturing, which utilizes high temperatures and pressures for improved conversion rates, usually uses spiral reactors. However, spiral reactors are rarely used for biodiesel production due to the complexity of operation than stirred tank reactors(Bernal et al., 2012). An analysis of a few studies suggested that the reactor, which is spiral, may function as a heat exchanger, allowing for an efficient recovery of heat. In a study, the reaction (transesterification of oil) with methanol in a spiral reactor was conducted from 270 to 400°C at 20 MPa. The molar proportion of oil-to-methanol is 1:40, and the reaction duration ranges from 3 – 30 minutes, which was utilized for biodiesel production. The reactor enabled 100% conversion of oil to FAME within 10 mins at 350°C. Thus, the spiral reactor enabled more production of biodiesel than batch reactors under similar reaction conditions (Farobie & Matsumura, 2015a). A separate investigation discovered that biodiesel can be produced without the catalyst, by employing supercritical conditions (having high pressure and temperature, surpassing its critical point) of t-butyl methyl ether or TBME. In the newly designed reactor (spiral). The reactor also functioned as a

heat exchanger, producing maximum biodiesel yield at 385°C in 20 minutes with 10 MPa pressures and an oil to TBME molar ratio of 1:4. The findings demonstrated that the spiral reactor outperforms a traditional reactor due to its enhanced generation of FAME and greater thermal efficiency (Farobie & Matsumura, 2015b). In another study, the spiral reactor at reaction temperatures 270 – 400 °Celsius, 20 MPa, 1:40 oil-to-ethanol molar proportion, and 3 – 30 minutes reaction times varying was utilized to generate biodiesel, as displayed in Figure 2.8. The spiral reactor demonstrated comparable efficacy to conventional reactors during the transesterification of the oil into biodiesel, while also exhibiting greater heat recovery capabilities (Farobie et al., 2015). Despite benefits, the spiral reactor also includes soap generation, pre-treatment prerequisites, reduced reaction rates, and stringent reaction conditions. Further, the heat recovery in the spiral reactor on a spacious scale could be more challenging. A continuous type of flow reactor can be utilized to resolve the heat recovery issue; however, it requires several prior investigations for the generation of biodiesel in supercritical ethanol. Moreover, it remained necessary to construct the heat exchanger condenser (or cooling system) as a separate entity, leading to an obstacle in the commercialization of the spiral reactor with the exorbitant cost of the equipment.

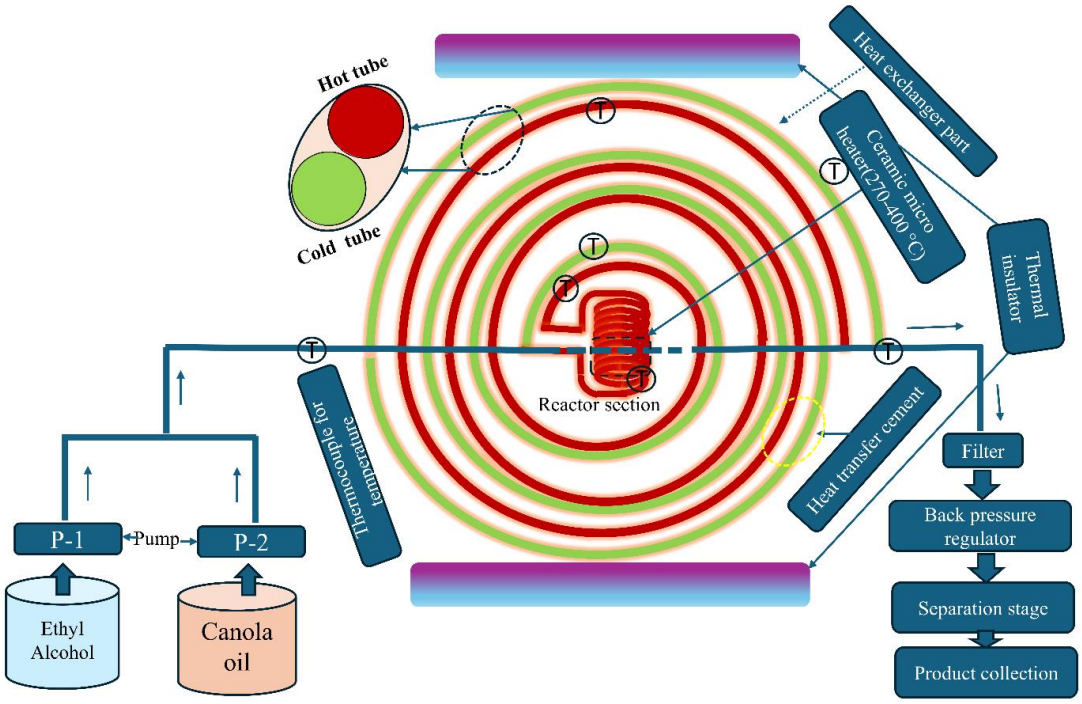

Figure 2.8. Experimental setup of the spiral reactor (Farobie et al., 2015)

2.3.8 Membrane reactor

A membrane reactor incorporates a barrier to enhance the transesterification reaction. It combines reaction along with separation in a singular moiety, enabling simultaneous performance of both processes, such as chemical transformations and selective separation of products. The membrane in the reactor can be selective, permitting specific moieties to proceed through yet engaging another. A membrane (or ceramic membrane) reactor was used for high-quality biodiesel (i.e., fatty acid methyl ester (FAME) yield of 94%). The production process engages using a methanol/oil molar ratio of 6:1 at a temperature of 65 °C for a duration of 150 minutes (Olagunju & Musonge, 2017). The methyl ester met both ASTM D6751 and SANS 1935 requirements for biodiesel. The ceramic membrane having a pore size of 0.02 µm exhibited high flux and permeate quality for the transesterification reaction and product separation. Moreover, the new biodiesel production method demonstrated a notable advantage by eliminating water

usage in the process, unlike conventional water washing methods used in biodiesel production that generate wastewater, contributing to environmental pollution and necessitating additional treatment, as shown in Figure 2.9. A study was conducted on a membrane reactor that showed 96.9% conversion at 65°Celsius, 90 minutes, a molar proportion of 4.2:1 between alcohol and oil, and a concentration of catalyst be 3 wt.%(Kong et al., 2022).

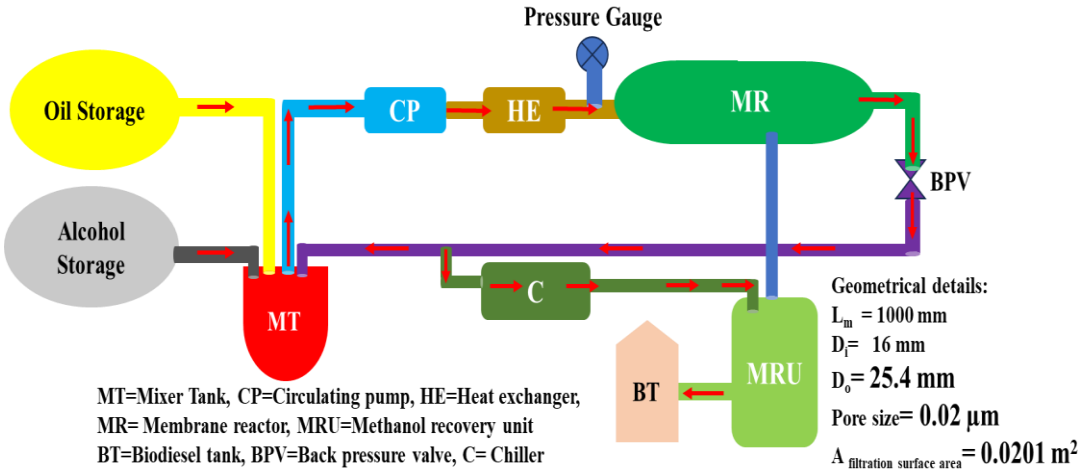

Figure 2.9. Schematic of the reactor (membrane) utilized for the generation of biodiesel (Kong et al., 2022)

A novel membrane reactor was implemented to produce biodiesel with methanol and canola oil. The reactor's membrane was responsible for the segregation of the unreacted emulsified oil from the product stream, which led to the production of an exceptionally purified fatty acid methyl ester (FAME). The initial influx of methanol/canola oil and the membrane's pore size were examined for their respective effects. Four distinct initial methanol volume moieties (φ1) (i.e., 0.29, 0.38, 0.47, and 0.64), as well as four-carbon membranes with varying pore diameters of 0.05, 0.2, 0.5, and 1.4 µm, were tested. It was determined that the reactor's canola oil was effectively contained by all four membranes. Permeation was observed at the initial methanol volume fractions of 0.38, 0.47, and 0.64,

but not at φ1 = 0.29. 11:1, 16:1, 23:1, and 46:1 are the methanol/oil mole proportions that correspond to the initial oil loadings. The phase that contained a high concentration of FAME did not contain any traces of glycerol. It was feasible to attain methanol/oil mole ratios of 6:1 through single recycling stages (Peigang et al., 2007).

The study investigated the utilization of a stationary or fixed membrane reactor that is filled with KF/Ca−Mg−Al hydrotalcite to generate biodiesel from soy oil. The production of biodiesel of superior quality was facilitated using ceramic membrane microfiltration in conjunction with solid base-catalyzed transesterification, without any residual oil. The catalyst quantity was 0.0531 g/cm^3, the reaction temperature was 70 °C, whereas the circulation velocity was 3.16 mL/minute, enabling maximum FAME production of 0.1820 g/min (Xu et al., 2013). Despite benefits, the membrane reactors may show fouling that significantly impacts the membrane reactor's performance. Further, it is challenging to model membrane reactor behaviour with precision. This is because of the interconnected nature of mass transfer, momentum transfer, and energy transfer within the membrane reactor (Jafari et al., 2021).

2.3.9 Ultrasonic reactor

The ultrasonic reactors appeared as a recent or effective reactor for the generation of biodiesel. In the typical operation, an ultrasonic sound is employed to increase the transesterification reaction's efficiency. This will result in the conversion of triglycerides, the primary ingredient in vegetable oil, into glycerin and biodiesel. Thus, the usage of ultrasound can considerably shorten the time of reaction (Badday et al., 2012). The cavitation bubbles are generated within the reaction mixture (i.e., oil and alcohol), which later collapse and result in strong shear pressures and higher localized temperatures. Under these conditions, the breakdown of the triglycerides takes place, facilitating the formation of biodiesel (Malani et al., 2019; Oza et al., 2024). The reaction can be sped up

by avoiding the mass transfer constraints because of ultrasound. Moreover, ultrasound helps to overcome mass transfer operations by micro-mixing, cavitation, and disruption of boundary layers. Further, the application of ultrasound also contributes to the prevention of soap production (byproduct) during the transesterification reaction and increases biodiesel yield (Cao et al., 2024).

An integrated dual-bandwidth ultrasonic (US reactor), equipped with a flat mechanical agitator, specifically built for the generation of biodiesel by methanol and palm oil using NaOH as catalyst, as shown in Figure 2.10. The findings indicated that the reactor achieved higher production of esters (methyl one) within 5 minutes of reaction with the methanol-to-oil molar proportion of 6, 1 wt.% NaOH, and a 55 mL/min feed flow rate. Even though the mechanically stirred (MS) reactor necessitated 60 minutes for a similar conversion of methanol/oil into esters (methyl). Furthermore, the biodiesel qualities derived from the ultrasonic reactor adhered to the standard of ASTM. The integration of the MS–US (reactor) resulted in improved biodiesel output compared to using the MS and US reactors alone (Choedkiatsakul et al., 2014).

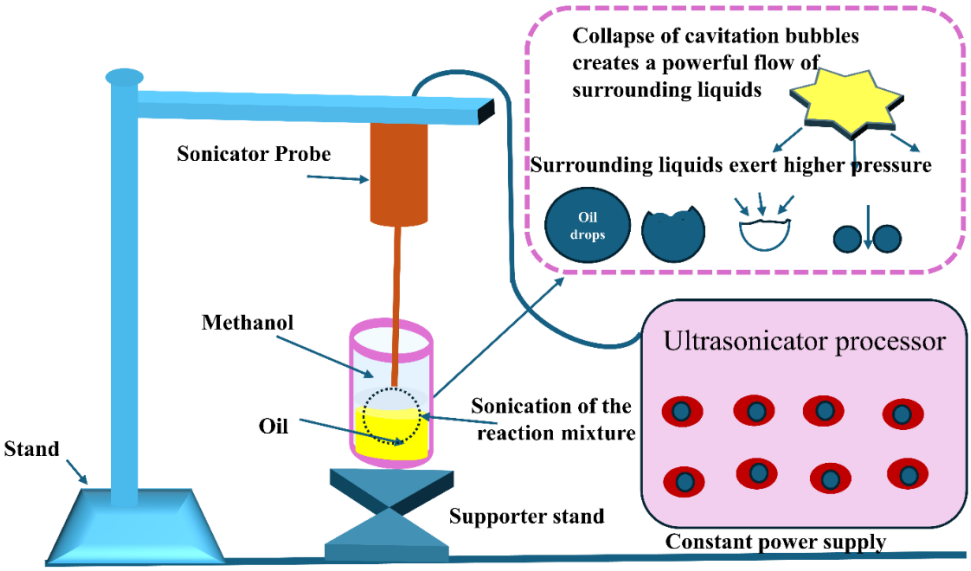

Figure 2.10. Schematic of ultrasound reactor for biodiesel production (Hoseini et al., 2018)

Another study focused on investigating the engagement of elevated frequency along with low-power ultrasound for biodiesel generation by soybean oil with methanol using a KOH catalyst, not considering outside heating or mechanical agitation. The ultrasonic power resulted in increased conversion rates. Furthermore, changing the frequency range of ultrasonic waves between 1 MHz and 3 MHz affects the conversion rates, increasing from 48.7% to 79.5% within the same duration of reaction time. Additionally, the findings suggested that the velocity of sound might be employed to assess the quality of the generated biodiesel subjectively. In addition, the ultrasound system demonstrated an electric consumption of 46.2 Wh, which was four times lower than conventional electric heating (212.3 Wh). Thus, the low-powered ultrasound frequency range for biodiesel production showed great potential to contribute to biodiesel production routes (Oliveira et al., 2021). Similar research using ultrasonic frequencies between 20 kHz to 611 kHz was conducted by Vishwanath Ganpat et al. Using 1% catalyst loading, a 9:1 methanol/oil molar ratio, and a reaction temperature of 65 °C, a 90% biodiesel yield was reached in 90

minutes (Deshmane & Adewuyi, 2013). Subsequently, Naresh N. et al. use the Taguchi approach to study how process parameters affect soybean oil transesterification by high-frequency ultrasound. According to its results, the ultrasonic frequency has very little effect on the amount of biodiesel produced in the range of 581 kHz, 143 W, and 0.75% (w/w) KOH loading at a 1:6 oil/methanol molar ratio. This produces more than 92.5% of the biodiesel in less than 30 minutes (Mahamuni & Adewuyi, 2010). In a different study, the synthesis of biodiesel is optimized using a multifrequency ultrasonic reactor for base-catalyzed transesterification of soybean oil with increased ultrasound properties. As per the results, in less than half an hour, over 90% of the FAME was obtained at a 6:1 molar ratio, 0.5 wt.% KOH, 611 kHz, and 139 W (Mahamuni & Adewuyi, 2009).

Shubham et al. performed an optimization study on the interesterification of karanja oil using response surface methodology (RSM) and investigated the intensification effects of ultrasound. Their studies demonstrated that ultrasound greatly increased yield, achieving 91% compared to only 60% with the usual approach. The greatest yield of fatty acid methyl esters (FAME) was produced under ideal conditions: a 35-minute reaction duration, a 1 wt.% catalyst loading, and a 1:9 reactant molar ratio(Kashyap et al., 2019). However, Edith Martinez-Guerra et al. investigated the combined effect of microwave and ultrasonic irradiation. As a result, in a synergistic effect that minimizes the heterogeneity of the transesterification reaction catalyzed by heterogeneous catalysts to greatly boost biodiesel yields (Martinez-Guerra & Gude, 2014).

Another study also claimed that biodiesel production under solid acid catalysts and ultrasound can enhance oil-to-biodiesel conversion by a factor of 300 and drop down the time of reaction, i.e., less than 1 hour (Boffito et al., 2015). S. Savvopoulos et al. produced biodiesel utilizing a sonicated system and a computational technique. Through the manipulation of both ultrasound intensity and methoxide flow rate, the system exhibits

flexibility in reaching high set points, ultimately reaching 60% in the biodiesel mole fraction (Savvopoulos et al., 2023).

Although in the developmental stage, ultrasonic reactors have shown the potential to benefit biodiesel production. However, building and implementing ultrasonic reactors at a large scale necessitates expertise in effectively managing operating variables such as frequency, power, and flow rates to attain the intended outcomes (or biodiesel yield)(Adamou et al., 2024; Kombe, 2024).

2.3.10 Microwave reactor

The microwave reactor is potentially being used in biodiesel production(Gude et al., 2013). Unlike conventional heating (conduction or convection), the microwave interacts directly with the oil/methanol molecules in the reaction mixture and enables their local heating (Gnaneswar Gude et al., 2013). The microwave quickly penetrates the reaction mixture and removes cold patches and temperature gradients (or provides uniform heating), thus it helps in facilitating the reaction. The reaction is further accelerated by this steady heating. Also, the uniform temperature aids in accelerating rates of reaction, increasing yields, and improving overall biodiesel quality (Gnaneswar Gude et al., 2013). The oleic acid (OA) was successfully converted into biodiesel in a microwave reactor under porous sulfonic acid functionalized (1.4437 mmol/g) utilizing the peel of banana waste (heterogeneous catalyst). Also, 8 wt.% acidic catalysts (with 4.62 wt% sulphur, i.e., equivalent to 1.4437 mmol/g of sulfonic acid) showed 97.9 ± 0.7% biodiesel with 20:1 methanol-to-OA molar proportion, 80 °C, and 55 minutes. A catalyst exhibited good stability and reached 5 cycles with negligible activity loss (Devasan et al., 2023). A similar OA was converted into biodiesel using a microwave reactor. The process of transforming oleic acid to biodiesel was carried out, and observed that 99.01 ± 0.3% at 9 wt.% catalysts involved, 1:16 OA-to-methanol molar proportion, 60 minutes duration of

reaction at 85 °C (Yadav et al., 2023). A microwave reactor at 2.45 GHz microwave radiation (which falls in the commercial microwave range) was also utilized for the generation of biodiesel (Motasemi & Ani, 2012). Further, the response surface approach suggested 68.4% to 96.71% conversion of oil/methanol into biodiesel under the microwave environment. The operating parameters include a 6:1 methanol/oil proportion, 1% catalyst, 138 seconds of microwave irradiation at 780 watts, and 7 bars of pressure. The biodiesel production increased when the radiation period was extended from 90 seconds to 138 seconds and the pressure from 5 to 7 bars (Safieddin Ardebili et al., 2019). Additionally, by employing a new biocatalyst and microwave irradiation, Olubukola et al. optimized the transesterification process of Kariya seed oil utilizing the Taguchi orthogonal array model. Using a methanol to KSO molar ratio of 10.5:1, 0.5 wt.% loading of calcined pawpaw trunk ash (CPTA), 300W of microwave heating power, and a 2-minute reaction duration, the transesterification procedure produced a maximum KSOME yield of 98.50±0.60 wt.% (Fadara et al., 2021).

The transesterification of Nyamplung (*Calophyllum inophyllum Linn*, a non-edible plant) was performed in a microwave reactor at 100 – 400 W power, 5 – 15 minutes, and 50 – 70 °C to produce biodiesel. A yield (84.62 %) of biodiesel was achieved at 200 W, 65 °C, and 5 minutes. The reaction rate was increased under microwave irradiation, compared to the conventional reactors (Nurhidayanti, 2021). A commercial-grade microwave reactor was also utilized for biodiesel production. The methanol (1:6 molar ratio) was permitted to react with the vegetable oil at a 7.2 L/min flow rate. Energy engagement simplifications indicated that the continuous-flow microwave reactor remained more energy-efficient than typical heated equipment (Barnard et al., 2007).

The generation of biodiesel by palm oil was also achieved using a commercial microwave reactor with a similar design. This reactor had a remarkable ester content of 99.4% and a

residence time of only 1.75 minutes. Compared to conventional reactors, the palm oil transesterification process consumed energy as low as 0.1167 kWh/L of biodiesel, indicating that microwave reactors may be a viable option for energy minimization and rapid biodiesel production. (Choedkiatsakul et al., 2015). The incorporation of microwave irradiation in biodiesel production greatly enhanced the reaction efficiency since microwave-based heating was considered superior to conventional heating because of the localized heating of the reaction mixture. Future biodiesel production techniques will likely incorporate microwaves at a certain point (Gude & Martinez-Guerra, 2015; Nomanbhay & Ong, 2017).

The Jatropha curcas oil transesterification under microwave irradiation utilizing activated carbon (derived from waste Oyster or Pyramidella shells) enabled the generation of biodiesel, as depicted in Figure 2.11. The waste shell-derived catalysts achieved an oil conversion of 93% within a 5-minute duration at 800 W microwave power, 15:1 methanol/oil molar proportion, along with 4 wt.% catalysts (Buasri et al., 2015).

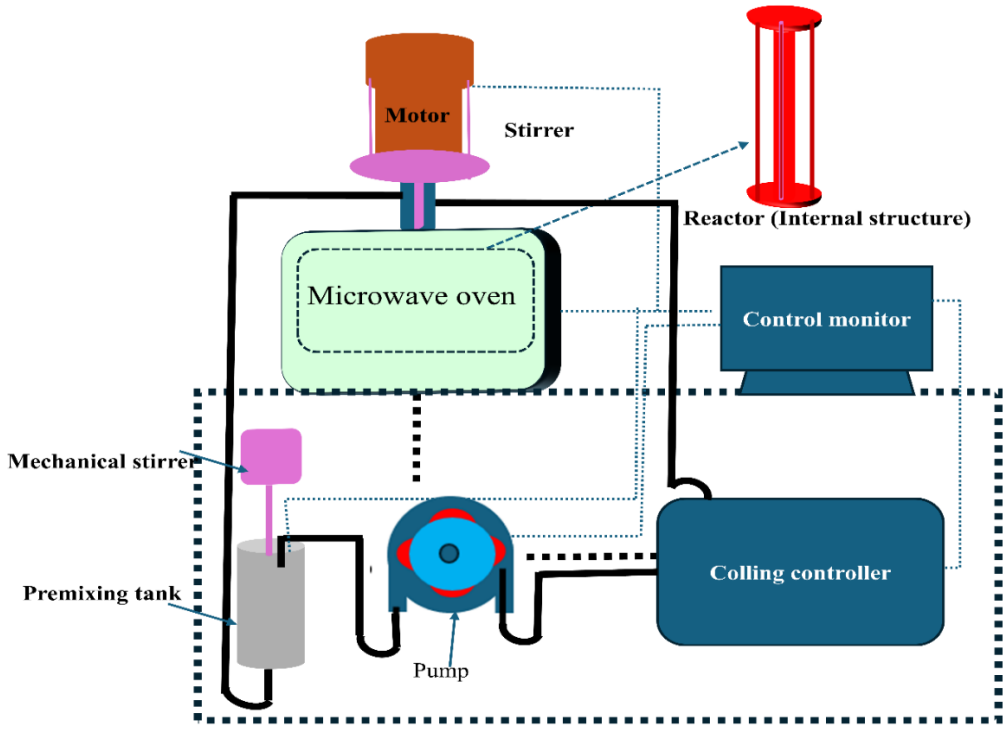

Figure 2.11. Microwave-assisted biodiesel generation experimental apparatus (Buasri et al., 2015)

Another study suggested the impact of the power of the microwave, methanol-to-oil molar proportion, catalyst KOH concentration or length of the tube, on the generation of FAME by palm oil in the microwave reactor. The findings indicated that at an ideal concentration of KOH, only a small amount of microwave power was sufficient for enhanced FAME production, thus, it allowed substantial energy saving during the biodiesel production (Ng et al., 2023). Further, the generation of biodiesel in a microwave reactor has resulted in the product (or biodiesel) yield between 80 – 94 % under varied conditions of oil–to–alcohol proportion, temperature, catalyst concentrations, and residence time, as reported elsewhere (Yuan et al., 2009), (Binnal et al., 2021), (Li et al., 2022).

Ana Karine et al. employed microwave radiation combined with enzymatic synthesis to convert the Mucor circinelloides lipid into biodiesel. This results in the attainment of 98.5% ethyl esters in 10 hours as opposed to 30 hours with traditional heating(Carvalho et al., 2018). Although microwave-assisted biodiesel production appeared as a quick and energy-efficient approach, microwaves were often limited by the penetration depth (a few centimetres) in the reaction mixture. Temperature regulation and quantification also remained difficult because of localized high heating through microwaves. Such localized overheating may not be suitable for a high viscosity reaction mixture, and it may also result in ruptures of the solid catalysts. Further, the microwave intensity remained another issue, especially for batch processing; thus, it became necessary to overcome the aforementioned constraints for the successful implementation of the microwave system (or microwave reactor) for large-scale biodiesel production (H. M. Khan et al., 2021), (Khedri et al., 2018; Motasemi & Ani, 2012).

2.3.11 Microreactors

Microreactor technology has recently demonstrated process intensification in biodiesel production because of its shortest diffusion path, enhanced surface area-to-volume proportion leading to elevated transfer rates of heat and mass, and enriched incorporation than the conventional reactors (Walter et al., 2005). Microreactors are categorized by several factors, including size, number, construction, and composition. It is categorized into tubular microreactor, microchannel reactor, and membrane microreactor (see Figure 2.12). The two most essential components of microreactors are a micro-structured shape for enhanced mixing and a microchannel for conducting biodiesel production reactions.

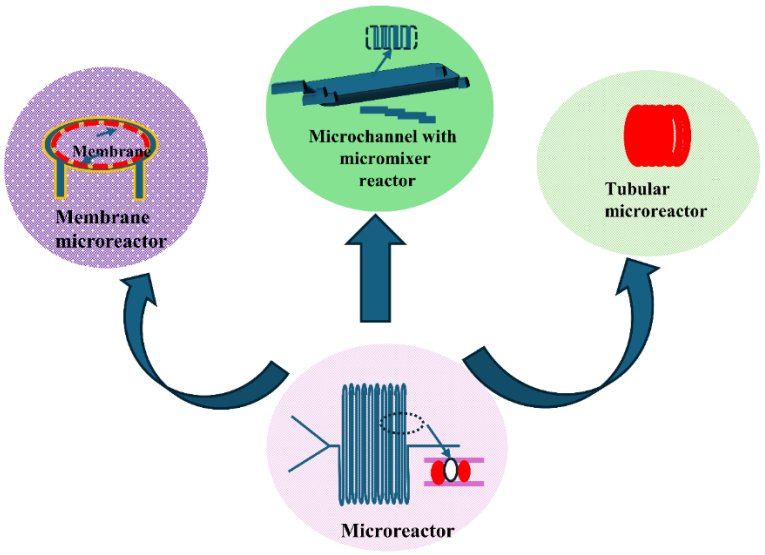

Figure 2.12. Microreactor for biodiesel production

2.3.11.1 Tubular microreactors

The tubular microreactors are recently being utilized for the generation of biodiesel. Biodiesel production by rapeseed or cottonseed oil, and methanol with the help of KOH as a catalyst was performed in a stainless-steel capillary microreactor (Sun et al., 2008). The tubular microreactor, having an inside diameter of 0.25 – 2 mm and a 30-meter length, provided 3.68 – 19.73 minutes residence time, good enough to yield 99.4% biodiesel in 1% KOH (catalyst) (Knothe & Razon, 2017). However, insights into the effect of the capillary microreactor's inner diameter on biodiesel production could not be elaborated. In addition to the reactor geometry, the influence of reactant flow direction (or pattern) within the tubular microreactor on biodiesel production was also studied. (Natarajan et al., 2019). The tubular micro-reactor was able to produce biodiesel in a time frame 15 times faster than a well-mixed CSTR with 99% conversion in 4 minutes residence time. The experimental findings were further supported through computational fluid dynamics (CFD) investigations, which revealed why the TMR provided a high conversion of more than 90% without employing high methanol-oil

molar ratios. This is because, as compared to previous systems, the TMR has a higher hydraulic diameter, employs a weight fraction of 0.7% of the catalyst that has a fixed molar ratio of 6:1 methanol: Oil(López-Guajardo, Enrique Ortiz-Nadal, Enrique Montesinos-Castellanos & Nigam, 2017). Tubular microreactor results surpass those of the lab-scale reactor because of (Tanawannapong et al., 2013)

- Increasing the contact surface area as compared to the lab scale reactor improves the transfer rates of heat and mass, facilitating better kinetics along with overall conversion.
- Smaller dimensions of microtubular reactors can result in better mixing of (oil and alcohol) as reactants, leading to a homogeneous reaction mixture. Better mixing can enhance the engagement of reactants as well as catalysts, thus improving the efficiency of the reaction.
- Small dimensions of microtubular reactors also lead to improved mass transport and allow the reactants to more readily reach the catalyst active sites, resulting in enhanced reaction rates with higher yields of biodiesel. Figure 2.13 and Table 2.1 demonstrate the microtubular reactor utilized for biodiesel production.

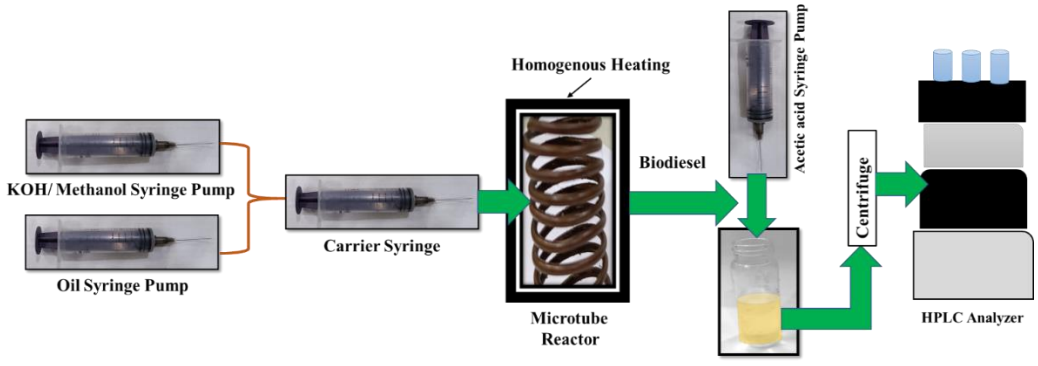

Figure 2.13. Microtubular reactor for biodiesel production

Table 2.1. List of Tubular microreactors for biodiesel synthesis

Microreactors	**Reactant**	**Alcohol/oil molar ratio**	**Temperature**	**Residence time**	**yield**	**Reference**
D = 250 µm L = 30 m	*Brassica napus* oil: Methanol	6:1	60	5.89 min	99.4	(Hazrat et al., 2023)
D = 0.8 mm L = 300 mm	*Helianthus annus* oil: Methanol	23.9:1	60	100 s	99	(Guan et al., 2009)
I.D. = 1.5 mm L = Nill	*Brassica napus* oil: Methanol	6:1	60	180 s	98	(Jachuck et al., 2009)
I.D. = 10 mm O.D. = 12.7 mm, L = 20 cm	Soy oil: Methanol	-	60	120 s	97	(Di Serio et al., 2006)
I.D. = 0.58 mm L = 1000 mm	*Arecaceae* oil: Methanol	21:1	60	180 s	95	(Azam et al., 2016)
I.D. = 0.38 mm	Soy oil: Methanol	7:1	40	53 min	95.2	(Bi et al., 2017)
D = 0.55 L = NS	Soy oil: Methanol	1:1	55	9 min	100	(Yeh et al., 2016)

Where, D=diameter; L= Length; I.D.=Internal diameter; O.D.= Outer diameter; N.S.=Not specified

Numerous works highlight the generation of biodiesel in tubular micro-reactors, covering enhanced heat-mass transfer, mixing, and hence increased reaction rates. A stainless steel microreactor (88 ml capacity, 1.59 mm OD, and 0.76 mm ID) was utilised for the continuous biodiesel production by oil (soybean) using ethanol (C_2H_5OH) and carbon dioxide (CO_2) as co-solvents (Bertoldi et al., 2009). The microtubular reactor's small-diameter channels enabled a great surface-to-volume proportion for enhanced diffusion, effective transfer of mass, and boosted the engagement of reactants with the catalyst, thus increasing the overall efficiency of the reaction. The soybean oil was transformed into (FAME) under supercritical conditions (i.e., high pressures ≈ 7.5 – 20 MPa and 300 – 350 °C). In another study, the reaction (transesterification) of soybean oil with methanol under the KOH catalyst occurred in a 316-cylindrical tube microreactor (make: American Iron and Steel Institute (AISI), OD = 12.7 mm, ID = 10 mm, and length = 200 mm) (Di Serio et al., 2006). The reactor was filled with AISI 316 Spheres to provide "microchannels" for oils and alcohol transport as well as enable resistance to corrosion in the synthesis of biodiesel. Differing fluid dynamic conditions were created with three different spherical diameters (0.39mm, 2.5mm, and 1.6mm) and lengths (1000m, 500m, and 300m), respectively. This leads to different flow patterns within the reactor. Further, the mass transfer and mixing of reactants (oil or methanol) were maximized because of fluid dynamics inside microchannels, leading to enhanced reaction efficiency. The reactor enabled up to 99% conversion in less than a minute, at 60°Celsius, with an oil-to-methanol proportion (1:6). The sunflower and castor oil blends with methanol were converted into biodiesel in a 1.6 mm-diameter milli-channel reactor(Jamil et al., 2016). The reaction (transesterification) with methanol-oil molar proportion (21:1), 5.4 wt.% KOH catalyst, 180 sec residence time, and 60 °C enabled 88.4% conversion. The effect of different ratios of sunflower and castor oil blends (40:60

to 60:40 to 80:20) was tested for biodiesel production. Amongst these, 80:20 sunflower to castor oil remained the most effective for FAME (or biodiesel) production with 88.4% yield. In another work, the continuous tubular microreactor transformed formic acid into fuel under the bimetallic catalyst AgPd@g-C_3N_4. The silver with palladium nanoparticles was supported on graphitic carbon nitride surfaces and was capable of converting acid into fuel (Tadele et al., 2017). The tubular microreactor was also utilized for biodiesel production through biological routes (Bi et al., 2017). The polytetrafluoroethylene (PTFE) coated microreactor (ID = 0.38 mm, OD = 0.78 mm, and length = 5 m) utilized an enzymatic catalyst (Lipase B from Candida Antarctica) to transform soybean oil into biodiesel. Soybean oil was further transesterified with methanol (1:7 ratio) into 95.2% biodiesel in 53 minutes, as opposed to a significant timeframe in the case of a conventional or traditional reactor (Mehboob et al., 2016).

The microfluidics technique for moving droplets (internal circulation) was also applied to produce biodiesel. A milli-metric coaxial flow system working on the droplets principle was developed, in which the reagents methanol and triglyceride flow together to create droplets that enhance the reaction and generation of fatty acid methyl esters (FAME), as shown in Figure 2.14 (Yeh et al., 2016). The droplet of methanol-containing catalyst is passed into the soybean oil for a transesterification reaction. The droplet-based system's high surface-to-volume proportion and internal circulation inside the moving droplets accelerated the transesterification reaction rate. This increased the volume of biodiesel production and decreased the use of excess methanol and hence its associated costs (cost of purifying and recovering excess methanol). The system resulted in 100% conversion of methanol and triglyceride at 55°C, methanol: oil = 1:1, 9-minute residence time, and 1% catalyst.

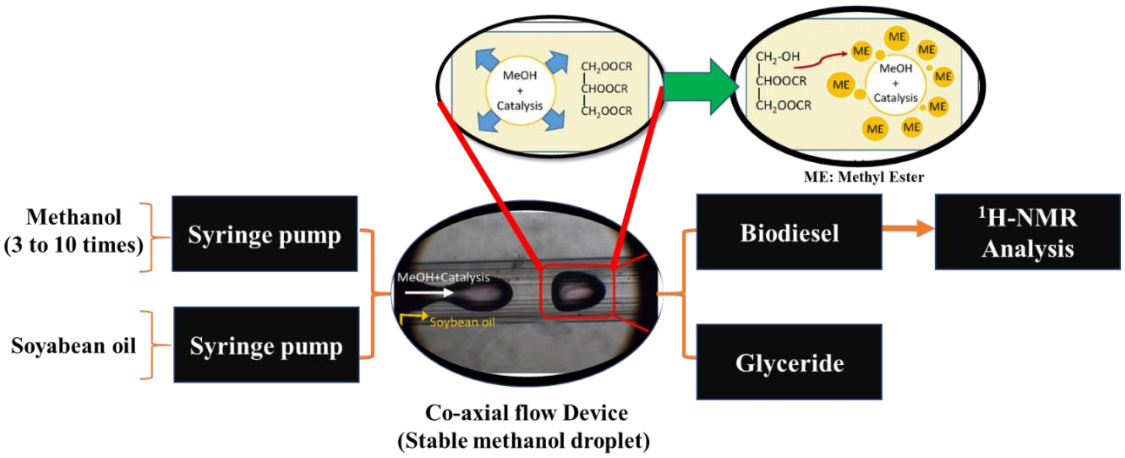

Figure 2.14. A droplet-based co-axial fluidic system for the generation of biodiesel (millimetric nature) (Yeh et al., 2016)

The tubular microreactors also include a few constraints (i.e., susceptible to obstruction, operation, and degradation of the reactor walls) (Awogbemi & Kallon, 2022), which as listed as:

- Challenging to monitor and regulate the temperature.
- Costly to construct and maintain.
- Significant abrupt decreases in pressure.
- Erosion and corrosion of reactor walls.
- Not suitable for use in industrial applications due to instability.
- Expensive construction expenses.
- Tubes of greater length.

2.3.11.2 Microchannel with micromixer reactors

The microreactors with simple designs, such as circular tubes, often resulted in higher fatty acid yields during biodiesel production. This alarmed the environmental conditions since the disposal of acids created the waste. To overcome this issue, micromixers were included in the microchannel reactors to accelerate the interaction of chemical species

and maximize biodiesel yield. The micromixers utilized for biodiesel production were (i) active micromixers and (ii) passive micromixers (Madhavan et al., 2018). Dynamic micromixers utilize an outside energy source, for instance, an electric or magnetic field, to mix the fluid, while passive ones exploit the energy (or mechanical energy) from the pumping system itself to mix the fluid.

2.3.11.2.1 Modelling and analyzing the microchannel system

To study the kinetics of generation (biodiesel) in the microchannel reactors, several mathematical tools, such as Minitab, GITT, ANSYS ICEM, CFD analysis, etc., were utilized. However, the validation of such models with the experimental results remained difficult because of the challenges with optimizing data at regular timeframes in the microchannel reactors.

Other reports also proposed the trans-esterification process of sunflower oil as well as soy oil with methanol and potassium hydroxide (KOH, as a catalyst) in a glass microchannel reactor (Bhoi et al., 2014). The zig-zag micromixer was provided for intermediate mixing between the oil and alcohol. The microchannel reactor produced a 99.5% biodiesel yield with 1.17 wt% KOH, 8.5 methanol/oil proportion ratio, 50° Celsius, and 14.9 seconds residence time. The work on utilizing methanol and KOH, having hexane as a co-solvent for soybean oil transesterification, produced 98% biodiesel in 9.05 seconds (Dai et al., 2014). For the transesterification reaction, three unique ways of micromixers with an inside diameter (d_i = 0.8 mm) and length = 1.58 mm (stainless steel tube) were utilized, as shown in Figure 2.15 (M. Rahimi et al., 2016). The micromixers, named E1(1), E2(2), and E3(3), were developed from a flat plate of polymethyl methacrylate (Plexiglass) with distinct angles (confluence) of 45°, 90°, and

135°. These micromixers enabled quick mixing and improved heat transfer from the reactants, thus providing aid in the generation of biodiesel.

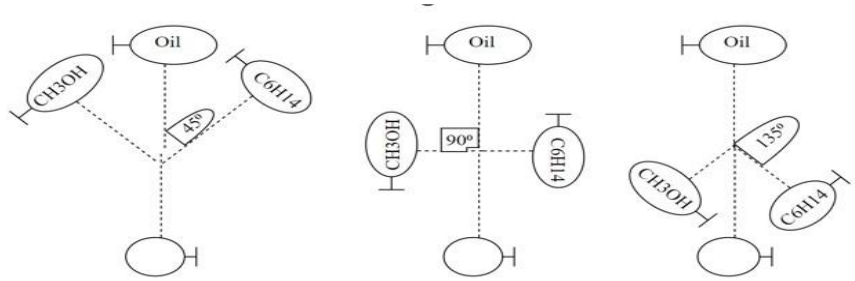

E1 (1) **E2 (2)** **E3 (3)**

Figure 2.15. Micromixer designs for biodiesel synthesis (M. Rahimi et al., 2016)

Thus, the application of micro-mixers in the micro-channel reactor enhanced the engagement of methanol in the oil. The heterogeneous catalyst was recommended since it reduced the overall process cost (Mohadesi et al., 2020). Further, the purpose of utilizing the cosolvent (i.e., n-hexane) was to enhance the solubility between the reactants and the reduction of the amount of methanol required to produce biodiesel (A. Rahimi et al., 2018). Moreover, scaling up of the micro-device-based biodiesel production remains an issue, although the different approaches of micromixers-embedded biodiesel production were studied.

Table 2.2 assembled the information on distinct novel reactors utilized for the generation of biodiesel, including biodiesel yields, scale of operation, merits, and demerits of the reactors. Each category of novel reactor has demonstrated the ability to produce biodiesel with yields ranging from 80% to 100% within reaction times of only a few milliseconds to several minutes. Furthermore, Table 2.3 presents a comparison between conventional reactors (such as batch and CSTR) and novel reactor configurations.

Table 2.2. Comparison of novel reactors for biodiesel production

S. No.	Reactors	Scale	Residence time (min)	Conversion (%)	Merits	Demerits	References
1.	Static mixers	Lab scale	30	80	Relative motion is zero, Low maintenance is required, and Operational cost is low.	Not suitable for non-continuous-flow systems	(Thompson & He, 2007)
2.	Chaotic mixer	Lab scale	6	99	No external mixer required, low alcohol to oil; Easy Separation	Scaling challenges (lab to pilot scale), High investment	(Boukhalkhal et al., 2020)
3.	Rotary-stator hydrodynamic cavitation reactor	Lab scale	1	89.11	Needs a low alcohol-to-oil ratio, low temperature, and low catalyst concentration	Long rotor and stator distances are not feasible.	(Samani et al., 2021)
4.	Oscillatory flow reactor	Pilot plant	30	99	Recovery is possible; Use of heterogeneous catalysts; No saponification	High operating cost; High temperature and pressure	(Harvey et al., 2003b)
5.	Spinning tube reactor	Commercial scale	-	98	High mass transfer rate, short mixing time	Not feasible for first and second-order reactions	(Qiu, Zhao, et al., 2010)

6.	Reactive distillation reactor	Pilot plant	240	82.69	Low operating cost; Easy separation	High reaction temperature, low conversion	(Harmsen, 2007) (Pradana et al., 2017)
7.	Membrane reactor	Commercial	25	>90	Higher conversion; Suitable for base catalyst	Not working in an acidic catalyst medium, slow reaction rate	(Dubé et al., 2007)
8.	Ultrasonic radiation reactor	Lab-scale	35	99.8	Non-corrosive. Eco-friendly	Ultracentrifugation is not needed.	(Fallah Kelarijani et al., 2020)
9.	Microwave reactor	Pilot-plant	30	100	Low cost; Faster operation	Corrosion of equipment	(Athar et al., 2020)
10.	Rotating tube reactor	Pilot plant	<1	98	High heat and mass transport; Low operating temperature and atmospheric pressure	Side products are produced,	(Lodha et al., 2012b)
11.	Spiral reactor	Pilot plant	3-30	93.7	Low catalyst requirement; Easy separation	High temperature, pressure	(Farobie et al., 2015)
11.	Chaotic mixer reactor	Pilot plant	6	99	Low production cost	High energy consumption	(Boukhalkhal et al., 2020)
12.	Plasma discharge	Lab scale	923 Mili-seconds	99.5	High mass transfer rate; Operate at room temperature	High power consumption, Stainless steel electrode only	(Wu et al., 2019)

Table 2.3. Comparisons of biodiesel (generation) using different types of reactors

S. No.	Reactors	Temperature (˚C)	Residence time (min)	Yield (Wt.%)	Reference
1	Batch reactor	40	80	96.2	(Wancura et al., 2021)
2	Continuous stirred-tank reactor (CSTR)	270-320	60	-	(Gonzalez-Quiroga et al., 2016)
3	Membrane reactors	70	40	90	(Hapo et al., 2019)
4	Packed bed reactors	200	11	97.5	(H. Liu et al., 2018)
5	Fluidized bed reactors	120	5	98.4	(Tabatabaei et al., 2019)
6	Trickle bed reactors	70	20	98	(Reactions, 2018)
7	Rotary/Spinning tube reactors	45	30	-	(Cintas et al., 2010)
8	Microwave reactors	60	5	95.95	(Universitesi & Soyhan, 2019)
9	Microreactors	25	0.67	98.6	(Mohd et al., 2020)
10	Cavitation reactors	35	35	99.8	(Fallah Kelarijani et al., 2020)
11	Ultrasound reactors		13	99	(Contreras-arias et al., 2020)
12	Hydrodynamic cavitation reactors	50	20	90	(Bokhari et al., 2017)

2.4 Future prospects and recommendations

The miscellany in biodiesel production enabled the researchers to seek diverse routes or systems to achieve the best results (or the best quality and higher biodiesel). Unfortunately, biodiesel production in conventional reactors faces limited mixing, transfer of heat and mass, enhanced time of reaction, high energy consumption, catalyst recovery, and reutilization problems. The heterogeneous catalytic system of biodiesel production appeared less complex than the homogenous one. Therefore, the optimization of production conditions and reactor configurations continues to be a critical area of

investigation in biodiesel research. The unconventional reactors discussed in this review can overcome the challenges of biodiesel production. However, most of the unconventional reactors of biodiesel production are still in the developmental stage and require comprehensive research in the future to achieve the best conditions for better yields and quality of biodiesel. There could be scope for data-driven techniques (such as machine learning and artificial intelligence) to predict the best combination of operating conditions for biodiesel production in unconventional reactors. Further, the cost minimization of unconventional reactor systems to make them suitable for commercial scale is another challenge that needs to be taken seriously. Moreover, the life cycle assessment and exergy analysis of unconventional reaction systems could be crucial for future research.

2.5 Conclusions

This review has examined biodiesel production using unconventional reactors. These systems intensify production through enhanced heat and mass transfer, reduced reaction time, and improved process efficiency, while also lowering operating temperatures and in some cases eliminating the need for catalysts. Examples include static and chaotic mixers, cavitation reactors, oscillatory flow reactors (OFRs), and microreactors for better mixing; spiral and microwave reactors for improved heat transport; micromixers, OFRs, microreactors, and rotary/spinning tube reactors for enhanced mass transfer; and reactive distillation or membrane reactors for easier separation. Plasma reactors, in particular, have shown promise by dramatically reducing reaction time and avoiding catalyst use.

Although unconventional reactors demonstrate significant potential, each category also presents challenges that limit their widespread adoption. Distinguishing between

conventional and unconventional systems and outlining their respective strengths and weaknesses is therefore essential.

Chapter 3 Performance evaluation of batch and flow reactors in biodiesel production[2]

[2]**The result discussed in this chapter have been published in Chemical Engineering and Processing - Process Intensification (2025);47:200-207.**

3.1 Introduction

Numerous studies emphasize single reactor systems for biodiesel production, but the absence of comprehensive comparisons among conventional and unconventional reactors hinders clarity on the most efficient design and operating conditions. Moreover, aspects such as scalability, energy efficiency, and the broader benefits of process intensification are not yet fully addressed.

Batch reactors, though widely adopted for laboratory and small-scale studies, are constrained by long reaction times (30 –120 minutes), dependence on multiple operating parameters, energy-intensive mixing, and limited production capacity. These drawbacks restrict their suitability for large-scale, continuous production (Dong et al., 2021; Foutch & Johannes, 2003).

In contrast, flow reactors, including tubular and continuous-flow intensified (CFI) systems, offer advantages such as enhanced heat and mass transfer, shorter residence times, and improved energy efficiency, though challenges remain in scalability and cost. Therefore, the current chapter focuses on the investigation of three reactor configurations: the conventional batch reactor (BR), the tubular coil reactor (TCR), and the coiled flow inverter (CFI).

3.2. Experimental procedure

3.2.1 Materials and chemicals

The oil produced using Karanja was acquired from Suyash Herbs Exports India Pvt. Ltd., located in Gujarat. The used cooking oil (UCO) was gathered from the mess of RGIPT,

Jais, Amethi, Uttar Pradesh. The physicochemical properties and fatty acid compositions are detailed in Tables 3.1 & 3.2 for Karanja oil and Tables 3.3 & 3.4 for used cooking oil, respectively (Hussain, 2018a). All analytical grade chemicals were used in this experimental analysis. Methanol (CH_3OH), 99.8% pure potassium hydroxide (KOH), 99.9% pure isopropanol (C_3H_8OH) alcohol, and 98% pure phenolphthalein were obtained from Sigma Aldrich (India) Pt. Ltd.

Table 3.1. Physicochemical properties of Karanja oil

S.No.	Properties	Value
1	Moisture (Dean and Stark) content	0.05%wt.%
2	Density @25°C	0.93 g/cc
3	Viscosity @40	40.07 cSt.
4	Colour in the inch cell on the Lovibond scale	34.90
5	Impurities (insoluble in hexane)	0.43 Vol.%
6	Acid value	23.56 mg KOH/g

Table 3.2. List of Fatty acid composition of Karanja oil

Fatty Acid	Molecular Formula	Carbon Chain	(%) Mass
Palmitic Acid (Hexadecanoic Acid, C16:0)	$C_{16}H_{32}O_2$	C16	13.28
Margaric Acid (Heptadecanoic Acid, C17:0)	$C_{17}H_{34}O_2$	C17	0.17
Linoleic Acid (9,12-Octadecadienoic Acid, C18:2)	$C_{18}H_{32}O_2$	C18	12.07
Oleic Acid (9-Octadecenoic Acid, C18:1)	$C_{18}H_{34}O_2$	C18	40.64
Stearic Acid (Octadecanoic Acid, C18:0)	$C_{18}H_{36}O_2$	C18	10.58
Eicosenoic Acid (cis-Methyl 11-Eicosenoate, C20:1)	$C_{20}H_{38}O_2$	C20	2.75
Arachidic Acid (Eicosanoic Acid, C20:0)	$C_{20}H_{40}O_2$	C20	3.01
Behenic Acid (Docosanoic Acid, C22:0)	$C_{22}H_{44}O_2$	C22	7.33
Erucic Acid (13-Docosenoic Acid, C22:1)	$C_{22}H_{42}O_2$	C22	0.21

Lignoceric Acid (Tetracosanoic Acid, C24:0)	$C_{24}H_{48}O_2$	C24	2.43
Hexacosanoic Acid (C26:0)	$C_{26}H_{52}O_2$	C26	0.14
Other minor fatty acids	-	-	7.39

Table 3.3. Physio-chemical properties of used cooking oil

S.No.	Properties	Value
1	Moisture (Dean and Stark) content	2.3 wt.%
2	Density @25°C	0.92 g/cc
3	Viscosity @40	38.7 cSt.
4	Impurities (insoluble in hexane)	0.43 Vol.%
5	Acid value	1.8 mg KOH/g

Table 3.4. Fatty acid composition of used cooking oil

S. No.	Fatty Acid	Molecular formula	Carbon chain	% Mass
1	Caprylic (C8:0)		C8	0.024
2	Capric (C10:0)		C10	0.016
3	Lauric (C12:0)		C12	0.216
4	Myristic (C14:0)		C14	0.794
5	Palmitic (C16:0)		C16	44.100
6	Palmitoleic(C16:1)		C16	0.208
7	Stearic (C18:0)		C18	4.121
8	Oleic (C18:1)		C18	39.000
9	Linolenic (C18:2)		C18	10.520
10	Linolenic (C 18:3)		C18	0.132
11	Arachidic (C24:0)		C24	0.146
12	Behenic (C22:0)		C22	0.060
13	Lignoceric(C24:0)		C24	0.054

14	Others	0.610

3.2.2 Sample analysis

To determine the FFA content in oil, the acid value (AV) is calculated according to ASTM D664 and EN 14104 standards. For biodiesel, both standards have set an optimum acceptable acid value of 0.50 mg KOH (Chai et al., 2014; Ramadhas et al., 2005). The acid value of Karanja oil (KO) and used cooking oil (UCO) was evaluated using the titrimetric method, and the FFA content was determined using equations (3.1) and (3.2) as shown below (Aricetti & Tubino, 2012).

$$\text{Acid value (AV)} = \frac{56.1 \times N \times V}{W} \tag{3.1}$$

$$\text{Free fatty acid (oleic acid)\%} = \frac{28.2 \times N \times V}{W} \tag{3.2}$$

where,

N = normality of standard potassium hydroxide (KOH) solution (N)

V = volume of standard potassium hydroxide (KOH) used, ml

W = the weight of the sample, g

The approximate conversion of biodiesel is assessed using the titration method. The acid values were compared at the initial and final stages for UCO and Karanja oils. The initial acid value was used to make a comparison of the feedstock and is calculated using Equation (3.3), as detailed below (Prasetyo et al., 2024).

$$\text{Conversion (\%)} = \left[\frac{(\text{Acid Value})_{t=0} - (\text{Acid Value})_{t=t}}{(\text{Acid Value})_{t=0}}\right] \times 100 \tag{3.3}$$

After esterification, transesterification was carried out at 60 °C for 2 hours, with a 1:9 molar ratio of oil to methanol and 1.5 wt.% KOH as the catalyst. The reaction mixture was then transported to a separatory funnel and left for 24 hours to separate into duel phases. The upper layer was biodiesel, whereas the bottom layer was glycerol. After

separation and washing, the biodiesel yield was determined using Equation (3.4) (Aslan, 2024; Takase, 2022).

$$\text{Biodiesel Yield (\%)} = \frac{\text{Biodiesel dry weight}}{\text{Oil dry weight}} \times 100 \quad (3.4)$$

3.2.3 Batch reactor experimental setup

The current study's experimental setup, depicted in Figure 3.1, primarily comprises a Hastelloy batch reactor (AmAr make, model no.: 4958) with a 1000 mL capacity. This reactor is outfitted with a thermocouple, a pressure gauge sensor, and a nitrogen inlet valve. It features a jacketed heating system to keep the reaction mass at the desired temperature. Additionally, a chiller connected to the reactor helps regulate the temperature, preventing it from exceeding the set point. The PID controller ensures that the reaction temperature remains at the set point by adjusting the coolant flow rate through the chiller as needed. To ensure the reaction mass remains homogeneous, constant stirring is provided by an impeller.

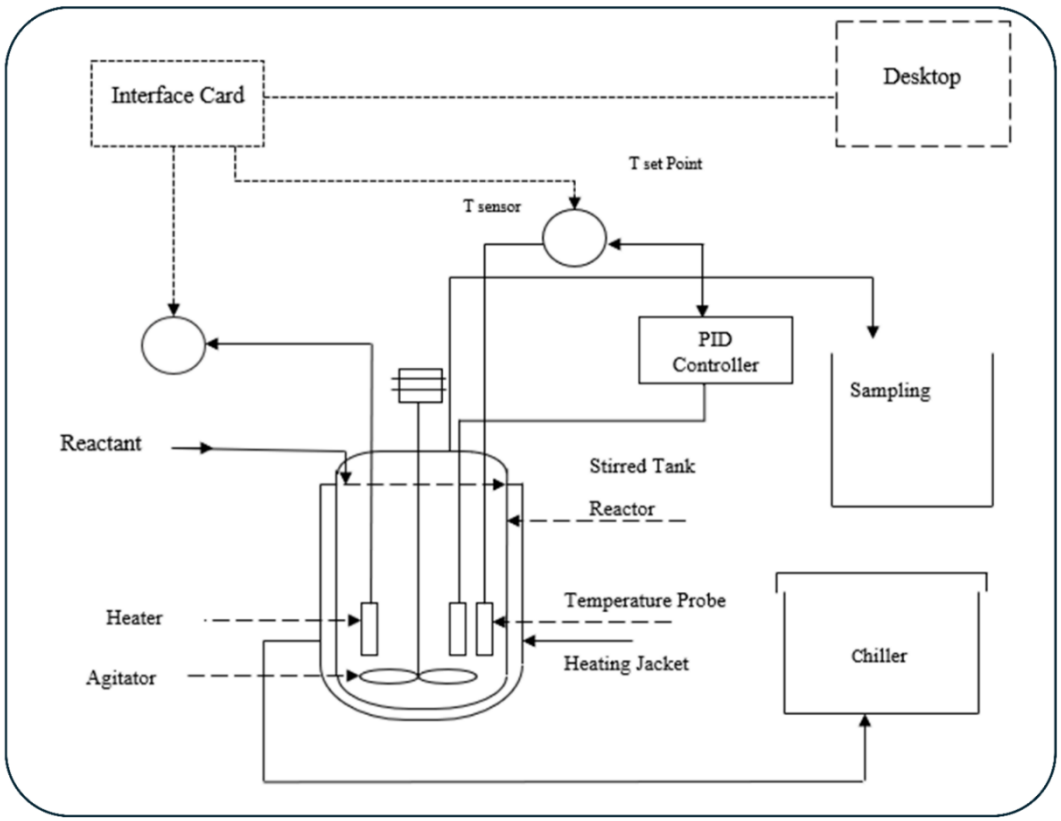

Figure 3.1. Schematic diagram of a batch reactor

3.2.4 Esterification and trans-esterification in a batch reactor

In this study, the methanol/oil molar ratio was varied from 3:1 to 12:1 to determine the optimal conditions for biodiesel production. A 9:1 methanol/oil molar ratio was determined to be optimal for maximizing yield and was subsequently chosen for further study. During the experiment, specific amounts (approx.500 gm) of pre-treated Karanja oil or UCO, methanol, and H_2SO_4 were placed in a stirred tank batch reactor, and the working temperature was 60°C. A mechanical stirrer was utilized to mix the components (RPM 900), maintaining a fixed methanol-to-oil molar ratio of 9:1 during the esterification process. The product obtained from the esterification was then transferred to a batch reactor for the trans-esterification. KOH catalyst at 1.5 wt.% of the oil was added and mixed at 900 RPM.

3.2.5 Flow reactor experimental setup

A stainless-steel tubular coil reactor (TCR) with a variable diameter and fixed length of 4m (SS316) was chosen for the transesterification reaction. The tubular coil was fully submerged in a water bath, with a hot plate used to regulate the reactor's temperature. To ensure uniform temperature distribution, a thermometer was positioned at the centre of the water bath, as shown in Figure 3.2. Two peristaltic pumps (SHENCHEN PUMP YZ1515 x) were utilized to separately feed the oil and methanol into the tubular coil reactor. The resulting products and any unreacted methanol were separated using a separating funnel. All experiments were conducted under identical operating conditions, namely a methanol/oil molar ratio of 9:1, a reaction temperature of 60 °C, and 1.5 wt.% KOH catalyst relative to the oil.

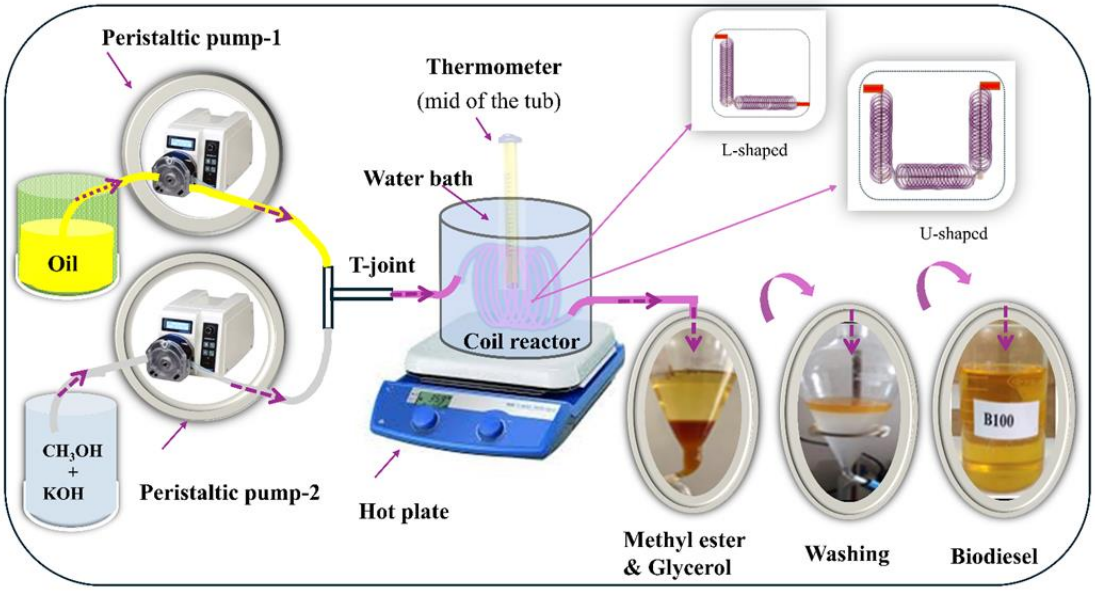

Figure 3.2. Schematic of the tubular coil reactor setup

3.2.6 Design of coiled flow inverter (CFI) & TCR

The coil flow inverter (CFI) was constructed exclusively from stainless steel (plate number 1). Two CFI variants were developed: L-shaped and U-shaped, each with consistent length (l) and tube diameter (d_t) as shown in Figure 3.3(a) & (b). The coiled configurations adhered to a constant curvature ratio ($\lambda_c = d_c/d_t$) and pitch (h) to facilitate comparison of design parameters.

For all configurations, including CFI (L), CFI (U), and TCR, the inner tube diameter (d_t) was 0.00165 m, corresponding to a surface-to-volume ratio of 2424.74 m^{-1}. The length (L) of the tube was 4 m, while the diameter of the coil (d_c) was 0.025 m, and the height (h) was 0.004 m. Additionally, the ratio of the inner tube diameter to the coil diameter (λ_c) was constant at 15.15 across all configurations. CFI (L) had 24 turns on each side and one 90° bend, while CFI (U) had 16 turns on each side and two 90° bends. TCR differs further, featuring a straight configuration and a total of 48 turns. Both coils were completely immersed in a water bath, which was positioned on a hot plate used to sustain the required temperature. To ensure uniformity, a thermometer was inserted into the middle of the water bath to monitor the temperature.

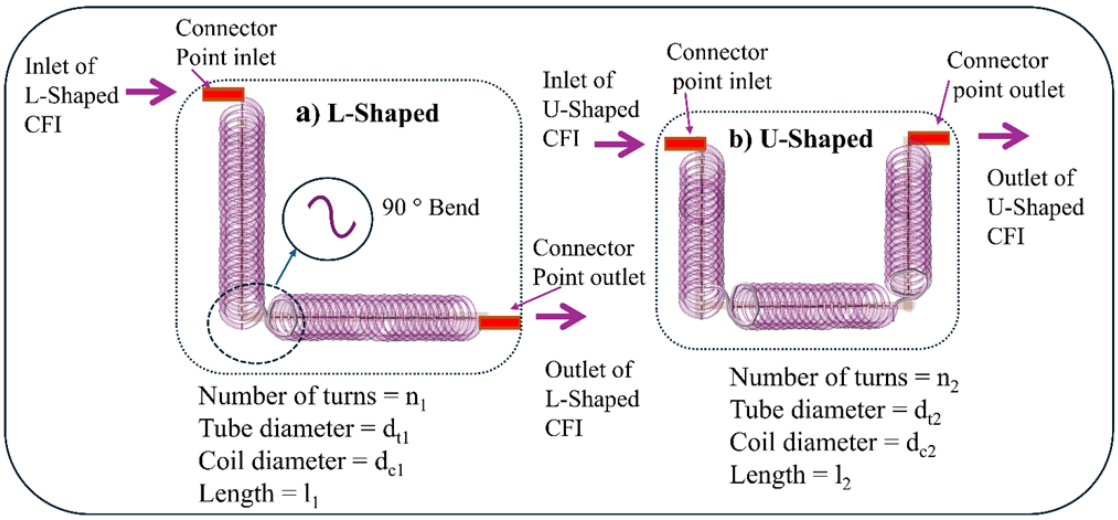

Figure 3.3. Pictorial depiction of the coiled flow inverter of the two aforesaid designs

a) L-shape CFI b) U-shape CFI

3.2.7 Characterization of biodiesel

Around the world, a variety of feedstocks are used to produce biodiesel, leading to different grades and qualities. To ensure its quality, biodiesel must follow international standards like the European EN 14214 and the American ASTM D6751-3. This study evaluated the thermophysical properties of the synthesized biodiesel according to the criteria outlined in Table 3.5, confirming its compliance with ASTM standards. The constituents of FAMEs were examined using Gas Chromatography-Mass Spectrometry (GC-MS) (*Agilent Model 8890 GC System with Single Quadrupole Mass Spectrometer, 5977B MSD, SAIF/IITM*) and Fourier Transform Infrared Spectroscopy (FTIR) (Thermo Electron Scientific Instruments LLC, Nicolet iS20, with a wavelength range of 11000-350 cm^{-1} and a spectral resolution of 0.4 cm^{-1}). The calorific value was measured with a bomb calorimeter (Hamco Model 6E, Automatic Bomb Calorimeter), density with a densitometer (Anton Paar, DMA 4100M), and viscosity with a rheometer (MCR 302e). Flash and fire points were determined using a Pensky-Martens closed-cup flash point tester, while oxidation stability was evaluated with a Metrohm Biodiesel Rancimat 893 at a flow rate of 10 L/h and a temperature of 110 °C.

3.2.8 Uncertainty analysis

Experimental uncertainties can originate from various sources, such as instrument selection, calibration errors, experimental conditions, environmental factors, observation techniques, measurement readings, and test preparation processes. A systematic uncertainty analysis was conducted to ensure the reliability and accuracy of the results. Also, error propagation was analysed using standard deviations, plotting error bars based on the average of three measurements. Uncertainty was determined by evaluating measured parameters, including motor speed, thermocouple readings, and pump flow rate, while accounting for the contributions of the instruments and methods used during the experiment. The overall uncertainty was calculated to be 2.3%, which falls well within the allowable limit (Hussain, 2018b).

3.3 Results & Discussion

This study presents a comparative performance evaluation of three types of reactors: the tubular coil reactor, the coil flow inverter, and the batch reactor. In the batch reactor, critical parameters, including the methanol-to-oil molar ratio, agitation speed, and reaction temperature, were analyzed. Conversely, for the tubular coil and coil flow inverter reactors, the research aimed at optimizing key parameters such as channel diameter, flow rate, and reaction temperature. The biodiesel properties were subsequently evaluated and examined according to the ASTM D6751 standard to determine their suitability and performance.

3.3.1 Gas Chromatography and Mass Spectroscopy (GC-MS) analysis

The ester content of Karanja-derived biodiesel was determined using a GC-MS for analysis and identification, as well as the separation of volatile components. The gas chromatogram of the FAMEs revealed that the mixture consists of five distinct fatty acid

esters with retention times of 5.579, 6.146, 6.703, 17.773, 18.22, and 20.788 minutes, as depicted in Figure 3.4. and Table 3.5. The esters were identified as methyl esters of palmitic, linoleic, oleic, linolenic, and stearic acids, as shown in Figure 3.5 and Table 3.2 by comparing the MS data of the oil sample with the computer's inbuilt database.

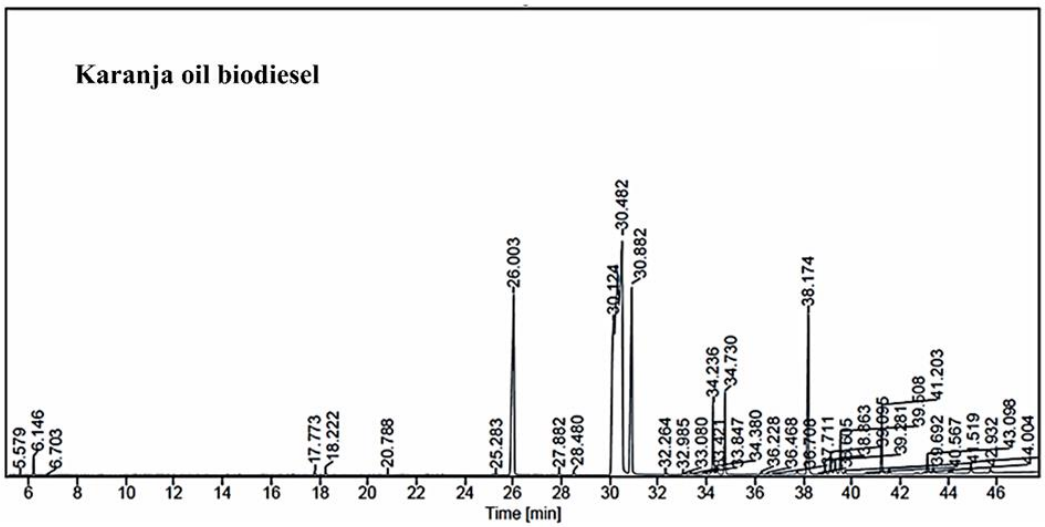

Figure 3.4. GC-MS of the Karanja oil-derived biodiesel

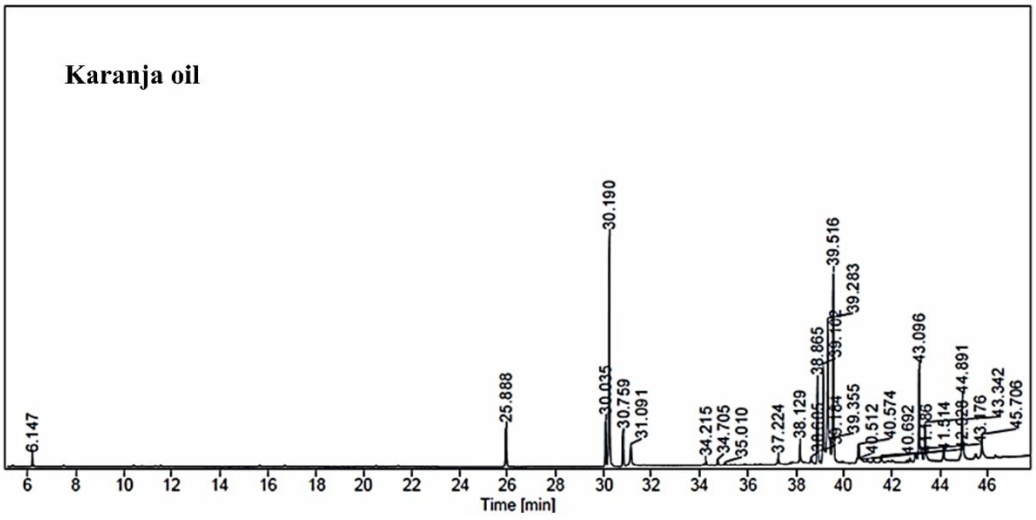

Figure 3.5. GC-MS spectrum of the Karanja oil

Table 3.5. Biodiesel (FAME) Composition from GC-MS Analysis

Fatty Acid Name	Molecular Formula	Molecular Weight (g/mol)	Carbon Chain	Saturation Type	Relative Area (%)

Methyl palmitate	$C_{17}H_{34}O_2$	270.45	C16:0	Saturated	13.28
Methyl oleate	$C_{19}H_{36}O_2$	296.49	C18:1	Monounsaturated	40.64
Methyl linoleate	$C_{19}H_{34}O_2$	294.47	C18:2	Polyunsaturated	12.07
Methyl stearate	$C_{19}H_{38}O_2$	298.5	C18:0	Saturated	10.58
Methyl arachidate	$C_{21}H_{42}O_2$	326.56	C20:0	Saturated	3.01
cis-Methyl 11-eicosenoate	$C_{21}H_{40}O_2$	324.54	C20:1	Monounsaturated	2.75
Methyl behenate	$C_{23}H_{46}O_2$	354.61	C22:0	Saturated	7.33
Tetracosanoic acid, methyl ester	$C_{25}H_{50}O_2$	382.66	C24:0	Saturated	2.43
Methyl myristate	$C_{15}H_{30}O_2$	242.4	C14:0	Saturated	0.06
Methyl palmitoleate	$C_{17}H_{32}O_2$	268.43	C16:1	Monounsaturated	0.05
Methyl heptadecanoate	$C_{18}H_{36}O_2$	284.48	C17:0	Saturated	0.17
Methyl linoleate	$C_{19}H_{32}O_2$	292.46	C18:3	Polyunsaturated	0.39

3.3.2 Fourier-Transform Infrared Spectroscopy (FT-IR)

The FTIR spectra of KO, UCO oil, and their derived biodiesel are illustrated in Figures 3.6 & 3.7. The presence of water molecules in both Karanja and used cooking oils is exhibited by the peaks at 3410 cm^{-1}. These peaks represent the stretching and bending vibrations of O-H bonds. Peaks at 2924.84 cm^{-1}, 2925.79 cm^{-1}, 2853.61 cm^{-1}, and 2854.31 cm^{-1} confirm the vibrations of C-H in CH_2 and CH_3 groups in(Peer et al., 2017; Rosset & Perez-Lopez, 2019; Subedi et al., 2020) Karanja and used cooking oils, respectively. The significant peaks at 1743.33 cm^{-1} and 1746.19 cm^{-1} are due to triglycerides' C=O vibration. The vibrations of CH_2 and CH_3 aliphatic groups are evident from the peaks between 1400-1200 cm^{-1}, with the HCH bending at 1377 cm^{-1} and the scissoring of CH_2 at 1463 cm^{-1}. The stretching vibrations of the C-O ester are shown by peaks between 1120

cm^{-1} and 1090 cm^{-1}, whereas the peak at 722 cm^{-1} confirms the rocking vibrations of (CH2)n. The presence of a peak at 1744 cm^{-1} confirms the stretching vibration of the C=O bond in esters. This is further corroborated by the presence of peaks in the range of 1300-1000 cm^{-1}, which match the stretching vibrations of the C-O bond. The stretching vibrations of CH_3, CH_2, and CH groups are detected at wavenumbers of 2980-2950 cm^{-1}, and 2950-2850 cm^{-1}, respectively. The bending vibrations occur at wavenumbers of 1475-1350 cm^{-1}, 1350-1150 cm^{-1}, and 722 cm^{-1}. The FT-IR spectra of Karanja oil used cooking oil, and their biodiesel are similar due to the presence of triglycerides and esters. However, slight variations are noted, with peaks in 1743, 1361, 1170, 1038, and 876 cm^{-1} in Karanja oil shifting to 1744, 1361, 1172, 1018, and 884 cm^{-1} in biodiesel. Similarly, peaks in used cooking oil in 1746, 1377, 1163, 1098, and 876 cm^{-1} shift to 1745, 1365, 1171, 1015, and 880 cm^{-1} in biodiesel (Devaraj et al., 2020; Kuppusamy et al., 2024). Consequently, the disappearance of peaks at 1443, 1096, and 965 cm^{-1} from the Karanja oil spectrum, along with the emergence of new peaks at 1435 cm^{-1} and 1196 cm^{-1}, conclusively indicates the transformation of Karanja oil and Used cooking oil into biodiesel. Furthermore, the lack of a broad peak between 3100-3500 cm^{-1} indicates low water content in Karanja and UC oil-biodiesels.

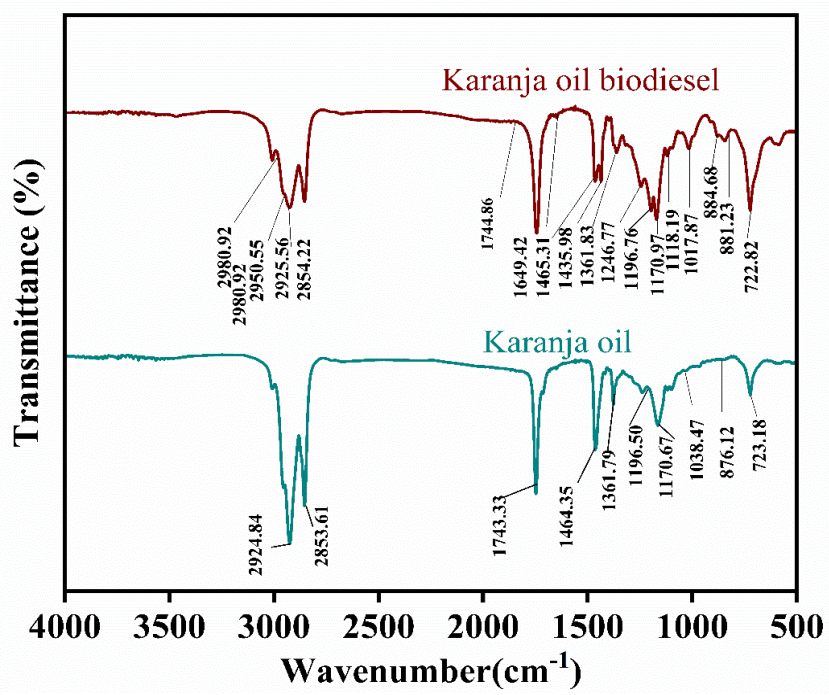

Figure 3.6. FTIR spectra of the Karanja oil and biodiesel

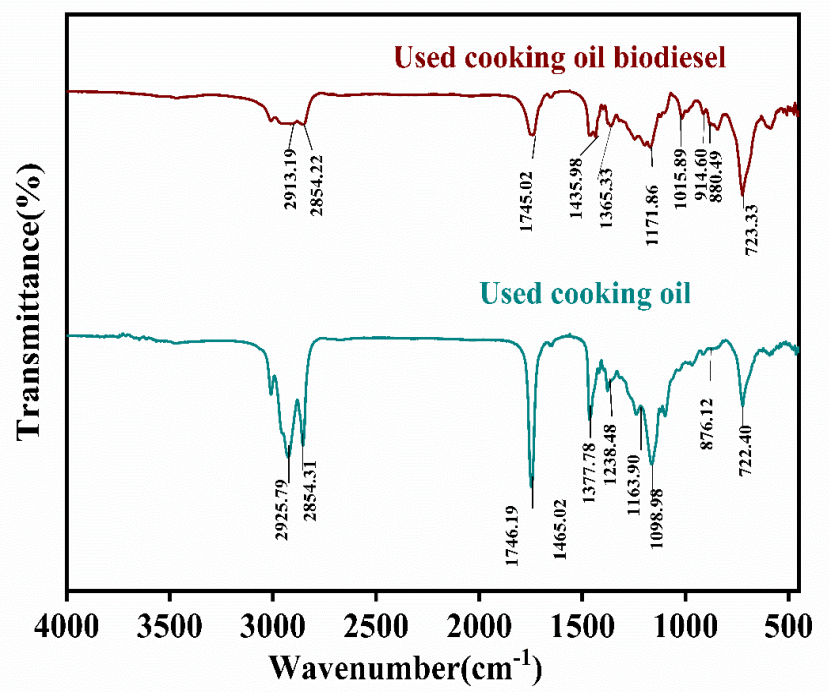

Figure 3.7**.** FTIR spectra of the used cooking oil and biodiesel

3.3.3 Effect of methanol/oil molar ratio in the batch reactor

The methanol-to-oil molar ratio plays a pivotal role in biodiesel production due to the reversible nature of the transesterification reaction (Musa, 2016). Increasing this ratio

shifts the reaction equilibrium toward ester formation, thereby enhancing biodiesel yield (Agarwal et al., 2013; Jazie et al., 2020). As demonstrated in the present study (Figure 3.8), increasing the methanol-to-oil molar ratio up to 9:1 significantly increases biodiesel yield. However, further increasing the ratio to 12:1 results in a yield decline, which can be attributed to the dilution effect on oil and possible catalyst deactivation (Hoque et al., 2013). Excess methanol also interferes with the separation of glycerol from the reaction mixture, leading to residual glycerol in the biodiesel phase and reducing the apparent yield (Encinar et al., 2007; Freedman et al., 1984). Furthermore, a higher alcohol concentration may help convert diglycerides to monoglycerides; an excessive amount can also favour the reverse reaction, where esters recombine with glycerol to form monoglycerides (Srinivasan et al., 2020). Kamari et al. (Kamari et al., 2020) also reported that retained glycerol in the mixture can shift the equilibrium backwards, thereby lowering ester yield. These results underscore the necessity of optimizing the methanol-to-oil ratio to maximize biodiesel production efficiency.

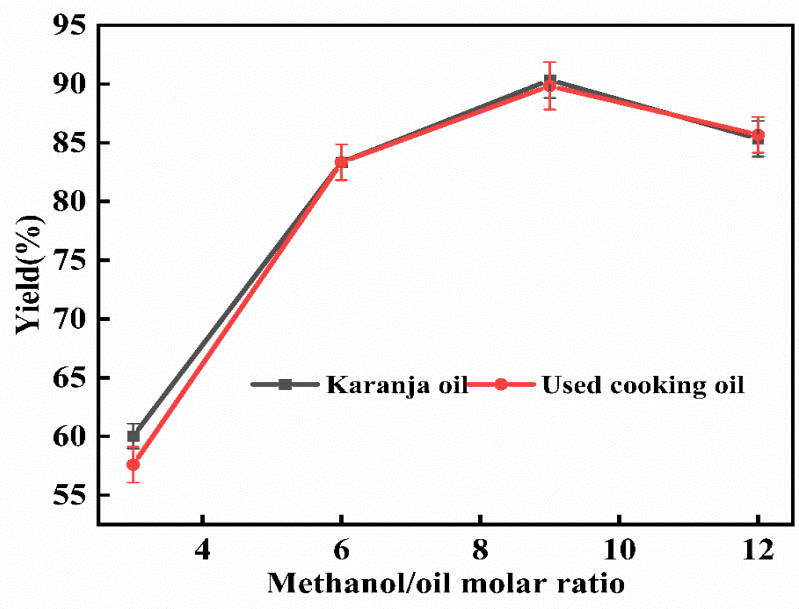

Figure 3.8. Effect of methanol/oil molar ratio on yield

3.3.4 Effect of agitation speed in the batch reactor

Agitation speed plays a critical role in mass transfer, significantly affecting biodiesel yield. Increasing agitation improves the mixing of oil and alcohol molecules, facilitating better contact and leading to a higher yield (Leevijit et al., 2006). As shown in Figure 3.9, the agitation speed varied from 600 to 1000 RPM at a constant reaction temperature of 60°C. The biodiesel yield was found to increase with agitation speed from 600 RPM to 900 RPM, reaching a maximum yield of 90.63% at 900 RPM. However, further increasing the agitation speed beyond 900 RPM led to a decline in yield. This reduction is attributed to mass transfer limitations and the reverse behaviours of the transesterification reaction at higher speeds. Higher agitation speeds above the optimal range may push the system to an excessively turbulent state, making it difficult for reactant molecules to effectively collide and react, which may reduce the biodiesel yield (Tesfay et al., 2019).

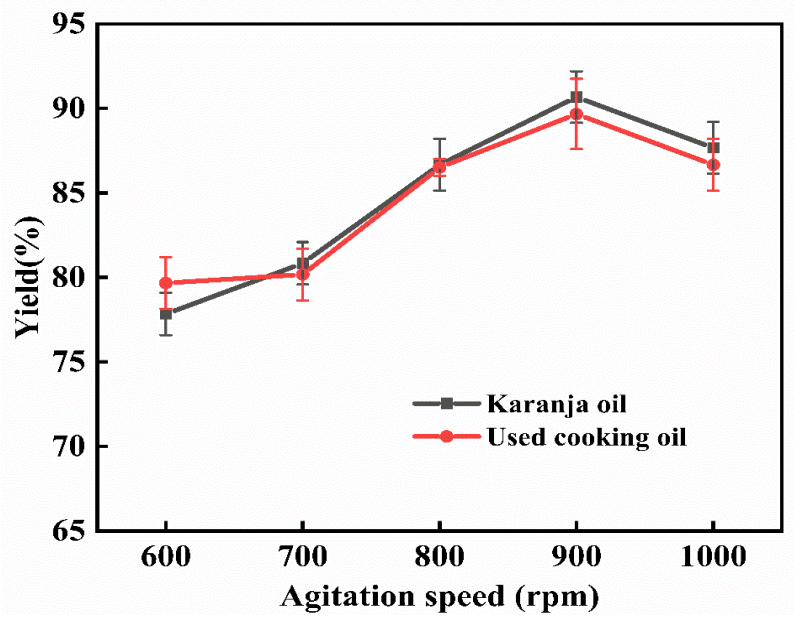

Figure 3.9. The effect of agitation speed on yield

3.3.5 Properties of biodiesel

The biodiesel derived from used cooking oil (UCO) and Karanja oil (KO) in this study demonstrates properties that largely conform to ASTM D6751 and EN 14214 standards. The viscosities of UCO biodiesel (UCOB) and Karanja biodiesel (KOB) were 4.5 mm^2/s and 4.0 mm^2/s, respectively, within acceptable limits. Density, essential for effective atomization in combustion systems, was recorded at 885.7 kg/m^3 for UCOB and 883.6 kg/m^3 for KOB, falling within the 860 – 900 kg/m^3 range specified by ASTM D6751. The flash points, critical for safe handling, were 160°C for UCOB and 155°C for KOB, both above the minimum 130°C requirement. Cold-flow properties were suitable, with cloud points of 11°C for UCOB and 10°C for KOB and pour points of 7°C and 8°C. However, the acid values (1.3 mg KOH/g for UCOB and 1.5 mg KOH/g for KOB) exceeded the standard's 0.5 mg KOH/g limit. A summary of these properties is provided in Table 3.6.

Table 3.6. Thermophysical properties of synthesized

S.no.	Properties	High FFA-based biodiesel (Jayaprabakar et al., 2024)	ASTM D6751 limit	EN 14214 limit	KOB	UCOB
1.	FAME content, %	97.13	NS	96.50	94%	93.78%
2.	Density @15°C kg/m^3	890	880	860-900	883.60	885.70
3.	Kinematic viscosity @40°C (mm^2/s) ISO 3104	5.13	1.90-6.00	3.50-5.00	4.00	4.50
4.	Acid value, mgKOH/g	0.38	Max. 0.50	Max. 0.50	1.50	1.30
5.	Calorific value (MJ/kg) D240	42	LS	LS	40.00	39.85
6.	Flash point (°C) ASTM D 93	163	130	101	155	160

7.	Cloud point (°C) ASTM D 2500	5	LS	LS	10	11
8.	Pour point (°C) ASTM D 97	1	LS	LS	8	7
9.	Cetane number D976	49	47	Min. 51	---	---
10.	Oxidation stability (h) @110°C	2.1	Min. 3	Min. 6	1.91	1.93

LS:Location & season dependent.
NS: Not specified.

3.3.6 Effect of reactant flow rate in TCR

The experiments were conducted in a tubular coil reactor (TCR) at a fixed temperature of 60 °C and a methanol-to-oil molar ratio of 9:1. The residence time (τ) in the tubular coil reactor (TCR) was calculated based on the internal volume of the reactor (8.55 mL) and the volumetric flow rate. The calculated residence times corresponding to the flow rates of 2, 4, 6, 8, and 10 mL/min were approximately 4.36, 2.18, 1.45, 1.09, and 0.87 minutes, respectively. Figure 3.10 illustrates the influence of volumetric flow rates on biodiesel yield in the TCR. As the flow rates of the reactants increased from 2 ml/min to 8 ml/min, biodiesel yield rose substantially, reaching 82.12% for Karanja oil and 82.52% for used cooking oil. This enhancement is primarily due to improved interaction between the immiscible phases, facilitated by the reactor's coiled geometry, which enhances mixing and mass transfer (López-Guajardo et al., 2017). However, beyond 8 ml/min, a noticeable decline in yield was observed. This drop can be attributed to reduced residence time at higher flow rates, which limits the extent of the transesterification reaction and may shift the equilibrium backwards, resulting in lower conversion. Interestingly, similar behaviour was reported by López-Guajardo et al.(López-Guajardo et al., 2017), who achieved higher yields at increased flow rates due to improved mixing but observed the opposite. Their results suggest that a shift in hydrodynamic behaviour, such as from slug flow to

parallel flow, may occur at elevated flow rates, leading to reduced interfacial contact, which leads to reduced mass transfer. A similar trend was also observed by Vural Gürsel et al.(Vural Gürsel et al., 2016), where a change in flow regime significantly lowered extraction efficiency due to the decrease in contact area between liquid phases. These observations further support that, while moderate flow rates can enhance performance, excessively high flow rates are counterproductive for biodiesel yield.

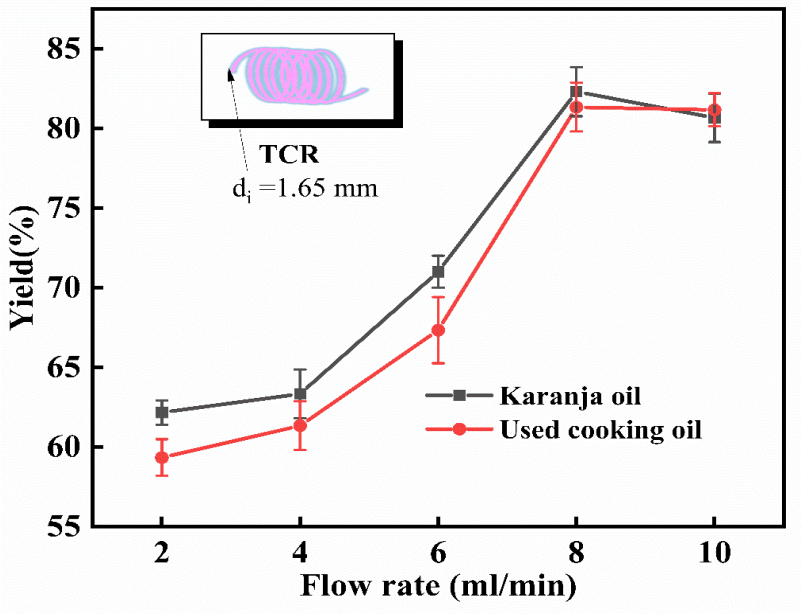

Figure 3.10. The effect of the reactant flow rate on the yield

3.3.7 Effect of the reaction temperature in TCR

Temperature has been observed to influence transesterification, impacting both the yield and rate of the methyl ester reaction. Figure 3.11 illustrates the effect of reaction temperature on the yield of KO and UCO in TCR of variable tube diameters (mm): 1.65, 2, and 3.2. The yield of fatty acid methyl ester (FAME) rises from 30% to 82.52 % as the tubular coil reactor's temperature increases from 40°C to 60°C. However, beyond 60 °C, the yield starts to decline due to the beginning of the vaporisation of methanol(boiling point 64.7 °C), forming small gas bubbles within the continuous liquid phase. These bubbles disrupt the flow regime in the TCR and reduce the effective interfacial area for

mass transfer, ultimately leading to lower biodiesel yield (Istiningrum et al., 2017). Additionally, the impact of tube diameter on mass transfer was discussed in the study by Ghaini et al. (Ghaini et al., 2010), who revealed that smaller tube diameters significantly increase the mass transfer coefficient due to a higher interfacial area between the two liquid phases. In contrast, larger diameters reduce the interfacial contact, leading to a reduced mass transfer rate. This supports our observation that reactors with smaller diameters (e.g., 1.65 mm) tend to produce higher yields than those with larger diameters.

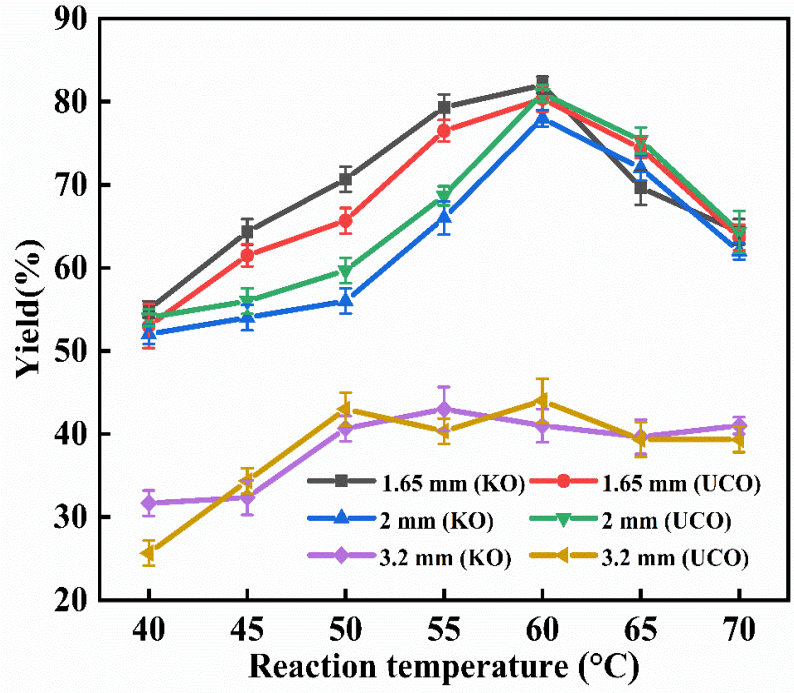

Figure 3.11. The effect of reaction temperature

3.3.8 Effect of tubular coil reactor diameter

Figure 3.12 illustrates the impact of coil diameter on biodiesel yield in a stainless-steel tubular coil reactor. Experiments were conducted with diameters ranging from 1.65 mm at a constant flow rate of 8 ml/min. It was observed that the smaller the diameter, the higher the biodiesel yield. The smaller the coil reactor diameter, the faster the velocity of the reactants, resulting in an increased Reynolds number, which enhances mass transfer. The highest yield, 82.52%, was achieved with the 1.65 mm diameter. Therefore, a 1.65 mm diameter was chosen for subsequent studies in this work.

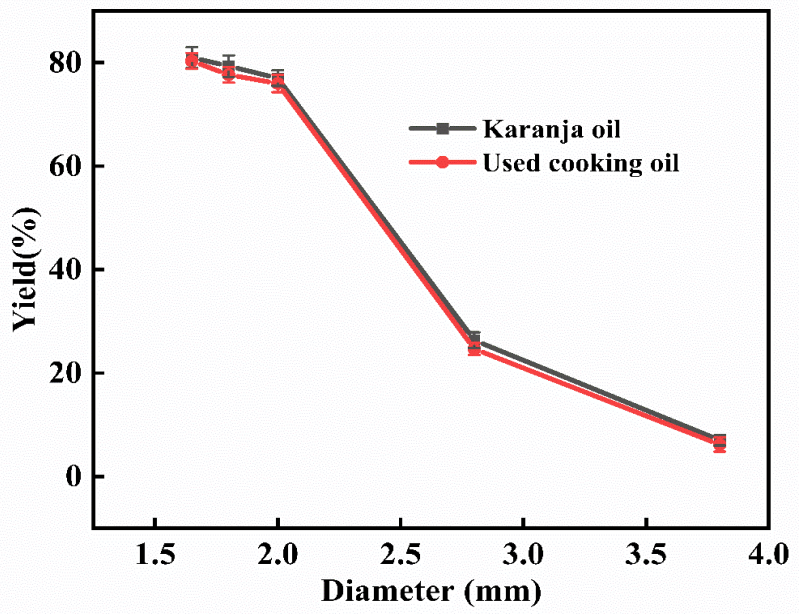

Figure 3.12. Impact of tubular coil reactor diameter on yield

3.3.9 Effect of flow rate in CFI and TCR

Figure 3.13 shows the effect of flow rate on biodiesel yield for different reactor configurations. As shown in Figure 3.13, biodiesel yield for all the reactors increases as the flow rate increases from 2-8 ml/min ($3.21 < Re < 25.71$). Further increasing the flow rate beyond 8 ml/min, the yield was reduced due to the shifting of the equilibrium reaction in the backwards direction. The U-shaped Coiled Flow Inverter (CFI) achieved the highest biodiesel yield, with 91% and 90% for KO and UCO, respectively, followed by the L-shaped CFI with 90% and 88.7%. In contrast, the Tubular Coil Reactor (TCR) showed the lowest yield, 81.23% and 80.23% for KO and UCO. The superior performance of the U-shaped CFI is attributed to its three-bend design, which strengthens secondary flows and Dean vortices, thereby inducing chaotic advection. This enhances micromixing intensity and promotes more efficient interfacial contact between immiscible phases compared to the two-bend configuration of the L-shape. The TCR, lacking these flow-inversion features, provides less efficient mixing, which limits mass

transfer. At higher flow rates, changes in hydrodynamics, such as the formation of parallel interfaces, likely reduce contact area, explaining the lower-than-expected conversions at 10 ml/min.

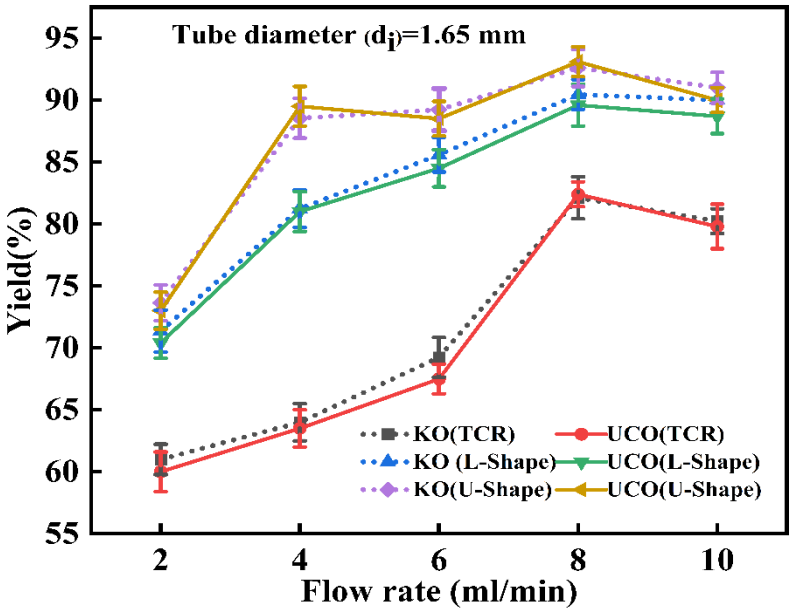

Figure 3.13. Comparative effect of flow rate on yield

3.4. Conclusion

A novel system for continuous biodiesel production was showcased, aiming to surpass traditional batch methods through process intensification using microtubular reactors. The experimentation utilized a batch reactor, a tubular coil reactor, and coiled flow inverters (both L and U shapes). Optimal results across all reactors were observed at 60°C with a 9:1 methanol/oil molar ratio, and KOH as the catalyst. The coiled flow inverter achieved the quickest yield to methyl esters, completing the process in just three minutes. In comparison, the batch reactor reached a 90.63% yield in two hours, and the tubular coil reactor (ID: 1.65 mm) accomplished an 82.52% yield at a flow rate of 8ml/min. Moreover, the U-shaped coiled flow inverter achieved a 92.6% yield, outperforming the L-shaped inverter, which attained a 90% yield.

Chapter 4

Enhancement of biodiesel property through the addition of nanoparticles[3]

[3]The result discussed in this chapter have been published in chemical Engineering Technology, Wiley, (2023);47:200-207. https://doi.org/10.1002/ceat.202300150

4.1 Introduction

In the current scenario, multiple process options have been developed for biodiesel production using the homogeneous transesterification route. These processes employ non-edible oils such as Karanja oil, used cooking oil, Jatropha oil, etc., along with methanol as reactants. Among these feedstocks, biodiesel derived from Karanja oil (KO) and used cooking oil (UCO) has been shown to meet ASTM specifications for density, viscosity, calorific value, flash and fire points, as well as pour and cloud points. Despite this, these biodiesels still show lower performance than conventional diesel. However, the purified biodiesel from KO and UCO follows property trends broadly similar to Jatropha biodiesel (BioEnergyTimes, 2025; Kumar Biswas et al., 2010; Riayatsyah et al., 2022). Considering its large availability in India, well-documented role as a reference non-edible feedstock, and properties aligning with KO and UCO, this chapter focuses on Jatropha biodiesel and its property enhancement using a nanoadditive.

The properties of Jatropha biodiesel, such as poor oxidation stability, reduced calorific value, and inadequate cold flow properties, were identified as major limitations, restricting its broader practical application. To address these shortcomings, the present chapter, as outlined in Chapter 1 objectives, has focused on improving the properties of Jatropha biodiesel through the incorporation of nanoparticles. For this purpose, ZnO, Mg-doped ZnO, TiO_2, and SiO_2 nanoparticles were dispersed into the biodiesel at concentrations of 50 ppm and 100 ppm, and their effects on the physicochemical properties of Jatropha biodiesel were systematically examined.

4.2 Materials and methods

4.2.1 Materials

To synthesize the nanoparticles, we have used the base materials a zinc acetate dihydrate [$Zn(CH_3COOH)_2 \cdot 2H_2O$: M.W = 219.50] was purchased from CDH Private Limited, India, tetra butyl Orth titanate ($Ti(OC_4H_9)4$: M.W = 340.32) was obtained from SRL Private Limited, India and used without further purification. Monoethanolamine (MEA) (100%, GR Merck) and ethanol were used as solvents. Magnesium (II) sulphate heptahydrate ($MgSO_4.7H_2O$) (99% extra pure, Sigma Aldrich), and Polydimethylsiloxane (PDMS) polymer with cross-linker were purchased from Sigma Aldrich. Deionized water (DI water) was used throughout the experiments, scale mechanical pump. To perform the experiments, analytical grade glass beakers (Durasil) were used. The pH of the solution was maintained through the digital pH meter (Toschcon CL 54+). The purity and source of the chemical used in this work are mentioned in Table 4.1. No further purification of precursor material was done for the synthesis of nanoparticle-based biodiesel. The jatropha oil (Jatropha carcus) was procured from the Might Scientific Sales 591 YA/605 B, New Baldev Vihar Telibagh, Lucknow-226029 U.P., India. Methanol (CH_3 OH) with 99.9% purity, potassium hydroxide (KOH) with 99.8% purity, Isopropanol (C_3H_8O) with 99.9% purity and phenolphthalein with a purity of 98% were procured from Sigma Aldrich (India) Pvt. Ltd. The composition of the jatropha is given in Table 4.2 (Bedassa Gudeta, 2016).

Table 4. 1. List of chemicals /precursor materials

Chemical Name	**Source**	**Molecular formula**	**Purity (%)**
Zinc oxide	SD Fine Chem Ltd	ZnO	99.999

Titanium dioxide	Merck	TiO_2	99.7
Silicon dioxide(	SD Fine Chem Ltd	SiO_2	99.995
Magnesium oxide	SD Fine Chem Ltd	MgO	99.99
Methanol	Molychem	CH_3OH	$\geq$ 99
Isopropanol	SD Fine Chem Ltd	C_3H_8OH	99.9
Zinc acetate dihydrate	CDH Private Limited India	$Zn(CH_3COOH)2{\cdot}2H_2O)$	99.99
tetra butyl Orth titanate	SRL Private Limited India	$Ti(OC_4H_9)4)$	98
Monoethanolamine (MEA)	GR Merck	$HOCH_2CH_2NH_2$	100
Ethanol	SD Fine Chem Ltd	C_2H_5OH	99.5
Magnesium (II) sulphate heptahydrate	Sigma Aldrich	$MgSO_4.7H_2O$	99
Potassium hydroxide	SD Fine Chem Ltd	KOH	99.8
Polydimethylsiloxane (PDMS)	Sigma Aldrich	$[Si(CH_3)2O]x[Si(CH_3)(R)O]y$, R = C16-C18	100

Table 4.2. Compositions of Jatropha oil

Fatty acids (FA)	**Systemic name**	**Chemical formula**	**Structure**	**Weight %**
Palmitic	Hexadecenoic	$C_{16}H_{32}O_2$	16:0	11.3
Stearic	Octadecanoic	$C_{18}H_{36}O_2$	18:0	17.0
Oleic	cis-9-Octadecenoic	$C_{18}H_{34}O_2$	18:1	12.8
Linoleic	cis-9, cis-12-Octadecandienoic	$C_{18}H_{32}O_2$	18:2	47.3
Arachidic	Eicosanoic	$C_{20}H_{40}O_2$	20:0	4.7

4.2.2 Synthesis methodology

The test fuels applied in this study were pure biodiesel (100%) with nanoparticle concentrations ranging from 50 ppm to 100 ppm. The jatropha-derived biodiesel meets the ASTM D6751 as well as European standards (EN 14214). Dispersion of nanoparticles with fuels is prepared by using an apparatus called Ultrasonicater (see Figure 4.1(a)) for

30 min to prepare the homogeneous JBD +50 ppm Mg-ZnO nanoparticles (JBD100Mg-ZnO50), JBD +50 ppm ZnO (JBD100ZnO50), JBD+50 ppm TiO_2 (JBD100Ti50), JBD +50 ppm SiO_2 (JBD100Si50), JBD +100 ppm Mg-ZnO (JBD100Mg-ZnO100), JBD +100 ppm Mg-ZnO (JBD100Mg-ZnO100), JBD+100 ppm TiO_2 (JBD100Ti100) and JBD +100 ppm SiO_2 test fuels. The synthesized test fuels are tested for stability in a 50 ml graduated scale glass test tube under static conditions and found to be stable for 12 hours. The sample collection photos before and after nanoparticle preparation are shown in Figure 4.1(b) and (c).

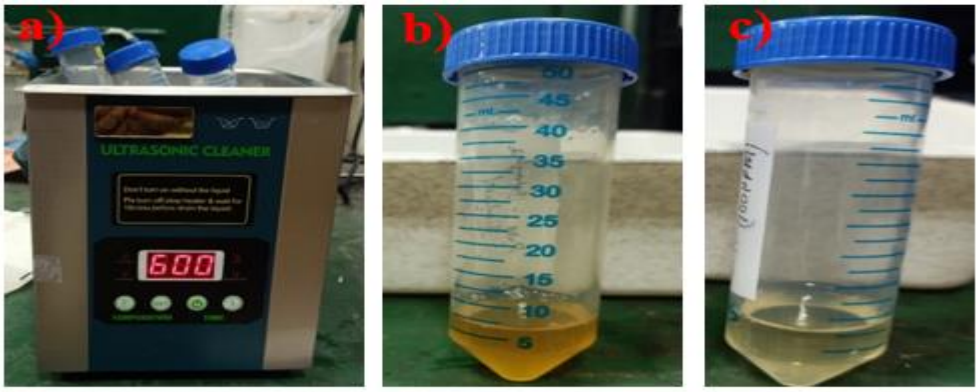

Figure 4.1. Preparation step for NPs

(a) Ultrasonicater bath, (b)Before nanoparticles, (c)After nanoparticles

4.3. Synthesis and characterization of ZnO, Mg-ZnO, TiO_2, and SiO_2 nanoparticles

4.3.1 Preparation of TiO_2, Mg-ZnO, and ZnO NPs from the Sol-Gel method

Using the sol-gel method, zinc oxide (ZnO) and TiO_2 sol have been prepared. The Mg-ZnO nanoparticles were then prepared by using magnesium element doping in the previously prepared ZnO sol. We have now discussed the ZnO and TiO_2 sol synthesis process in detail. As the precursor for ZnO sol, 1.09 g zinc acetate dihydrate was mixed with 3.05 ml Monoethanolamine at room temperature for 10 minutes. Following that, we

added 10 mL of ethanol as a solvent to the previous solution and continued stirring at 60ºC for 2 hours. The resultant ZnO sol is then discovered. For the preparation of TiO_2 sol, 1.70 ml of tetra-N-butyl orthotitanate (TNBT) [$Ti(OC_4H_9)_4$] and 3.05 ml of Monoethanolamine were taken initially and mixed at room temperature for 10 minutes. Later, 10 mL of ethanol was taken as a solvent to prepare the final TiO_2 sol. Then the mixture has been stirred at 60ºC for 2 hours. Monoethanolamine is used as a stabilization agent in this case. To obtain magnesium dopant nanoparticles, add magnesium (II) sulfate pentahydrate (2 wt.%) for Mg-ZnO nanoparticles to the previously prepared ZnO sol and continue stirring at 60ºC for 2 hours. The solution was completely transparent at the start of mixing and turned milky white at the end of the synthesis of Magnesium-doped Zinc oxide sol, confirming the synthesis of Mg-doped ZnO nanoparticles. Mg-ZnO nanoparticles have a yellowish-white powder colour, which aids in the formation of Mg-ZnO powder. After preparing the ZnO, TiO_2, and Mg-ZnO sols, we kept them at room temperature for 12 hours to allow the gelation to occur. This gelation-type was now preheated at 180ºC for 1 hour. As a result, these preheated gelation sols are calcined in a muffle furnace at 500 ˚C for 2 hours at a heating rate of 5 ˚C/minute, allowing the solid samples to be crushed in mortar pastel to obtain a fine powder of ZnO, TiO_2, and Mg-ZnO nanoparticles for further characterization.

4.3.2 Preparation of SiO_2 nanoparticles from Polydimethylsiloxane (PDMS) polymer

To synthesize SiO_2 NPs, the polydimethylsiloxane (PDMS) polymer was employed. Initially, oleophilic solid foam was synthesized using a mixture of PDMS with tetrahydrofuran (THF) solutions. In this process, the initially prepared PDMS mixed with THF solution was heated, which caused bubbles to form during the cross-linking reaction and led to the formation of an oleophilic solid foam. This foam was calcinated in a muffle

furnace with isothermal conditions at 500 °C for a fixed time interval of 2 h with 10 °C per minute. The final calcined product was SiO_2 NPs exhibiting a white colour, which was later characterised using different analytical techniques as mentioned in the Section. 4.6.

4.4 Transesterification reaction

The batch reactor was filled with known amounts of pre-treated oil, methanol, and KOH, and the reaction temperature was kept at 60°C; the overall reaction for transesterification is depicted in Figure 4.2. A mechanical stirrer was used to agitate the reaction mixture at 900 rpm, and the oil-methanol molar ratio was 9:1 during the 2 hours of residence time. Moreover, when the reaction was completed, the reaction mass was taken out and transferred to a separating funnel to separate all the phases. The formation of two layers (top: methyl ester, bottom: glycerine) was observed after 24 hrs. The catalyst (KOH) and excess methanol were removed from the methyl ester using a rotary evaporator.

Transesterification Process:

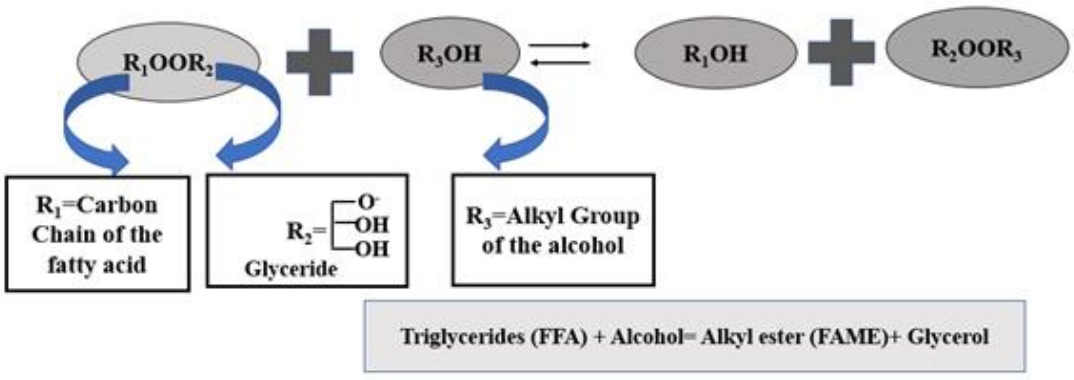

Figure 4.2. General reaction to the transesterification process

4.5 Experimental setup and procedure

The experimental setup to improve the properties of the biodiesel is depicted in Figure 4.3. First, a one-litre batch reactor (AmAr, Autoclave, model no. 4568) is used to convert

high free fatty acid (>10.51 FFA) to low free fatty acid (<5% FFA) through the esterification process. Reaction conditions include a reaction temperature of 60°C, a 9:1 oil-to-methanol molar ratio, and a 2-hour residence period. Since water is formed during esterification, and can be saponified. Nevertheless, before applying the basic transesterification, the acid is neutralised with the base in the pretreatment stages. Considering this, the transesterification process (as explained in Figure 4.2) is fed after hot water washing. Four distinct nanoparticles were blended with jatropha-derived biodiesel and evaluated for various fuel properties.

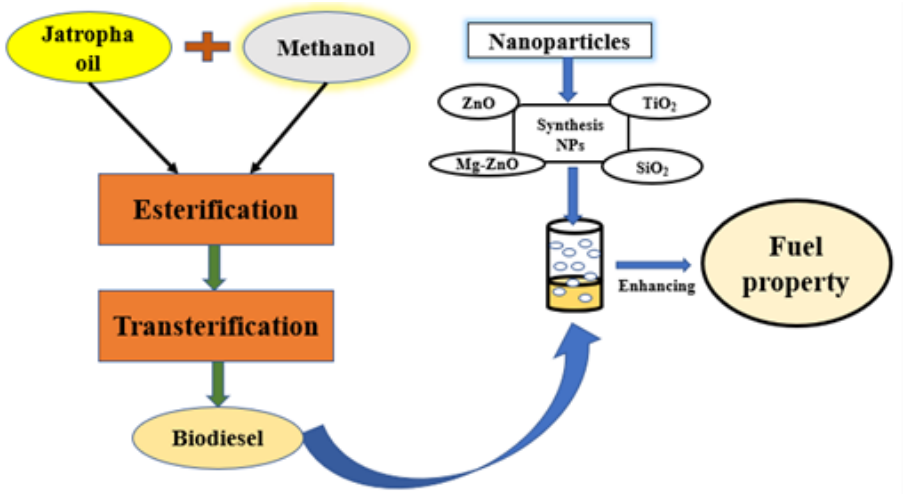

Figure 4.3. Preparation step for nanoparticles-based biodiesel

4.6 Characterization of nanoparticles

A thorough investigation of microstructural characterization of sol-gel synthesized ZnO, Mg-doped ZnO, TiO_2, and SiO_2 nanoparticles was carried out using a different combination of techniques, such as a powder X-ray diffractometer (EMPYREAN-QTY1, Malvern Pan Analytical, Netherlands). Powder XRD is used to determine phase, crystallite size, presence of strain etc., The qualitative elemental analysis was done by EDX, attached with FESEM (JSM-7900F, JEOL, JAPAN). Elemental mapping corresponding to BSE images was performed by EDXS. The XRD measurements of powder samples were carried out in the range of 2θ is 20° – 80° (step size is 0.003^0) with

Cu K_α ($\lambda = 0.15406$ nm) radiation. Before placing nanoparticles into the FESEM chamber for morphological analysis, gold (Au) was deposited on them for 90 seconds. These pictures were taken at an accelerating voltage of 5–10 kV.

4.7. Results And Discussion

4.7.1 (a) Structural properties (XRD) of nanoparticles

Structural and phase analysis of the synthesized pure ZnO, Mg-ZnO, and TiO_2 nanoparticles were carried out by X-ray Powder Diffractogram (XRD) as shown in Figure 4.4(a-c). The powder XRD of ZnO and magnesium-doped Mg-ZnO) shows a formation of the hexagonal wurtzite phase of ZnO, which can be indexed as a cubic system. Figure 4.4(a) represents, seven major peaks set at 31.88°, 34.57°, 36.36°, 47.71°, 56.80°, 63.09°, and 68.14° whose diffraction from the planes (100), (002), (101), (102), (110), (103), and (112) respectively, can be attributed to a lattice constant of a = b = 3.2539 Å and c = 5.2098 Å. (Abed et al., 2015; García-Martínez et al., 1993) Pure ZnO nanoparticles have a hexagonal wurtzite phase crystal structure (JCPDS: 01-080-0075), as demonstrated by the XRD patterns (Abed et al., 2015). Additionally, it can be seen from the diffraction that the Mg dopant in the ZnO crystal lattice has not caused any additional secondary phases to form, and the XRD pattern of the Mg-doped ZnO NPs has not undergone any notable modifications. However, it is also seen that Mg doping causes an increase in the XRD peak's intensity (as shown in Figure 4.4.b), which supports the slight crystallinity gain that resulted from the lattice distortion. A slight strain is added as a result of Mg^{2+} ions doping in the parent material ZnO crystal structure. This causes the lattice to be switched, which in turn causes the crystal's regularity to alter. When Mg is doped into the parent ZnO matrix, the peak position is seen to shift toward

lower angle values, according to extremely cautious conclusions. Particularly for the peak at (101) plane 36.36°, it is discovered that Mg doping causes it to shift towards a lower value, which can be explained by the substitution of Mg^{2+} ions for Zn^{2+} ions(Blinov et al., 2019). Furthermore, the dopant atom magnesium ions (Mg^{2+}) may replace the zinc ions (Zn^{2+}) in the parent lattice(Talam et al., 2012).

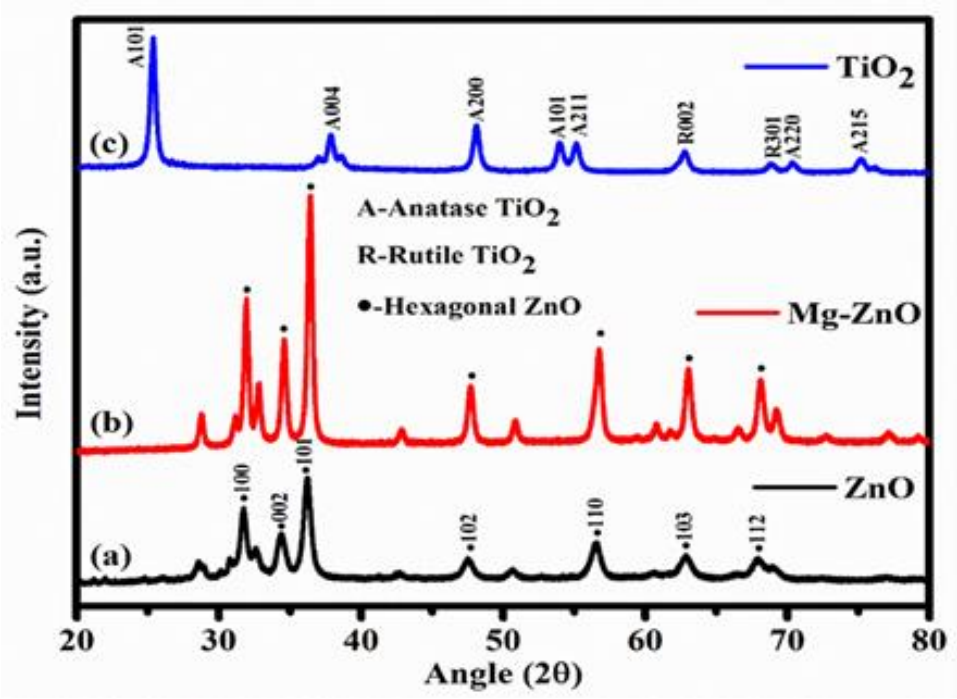

Figure 4.4 (a-c). X-ray diffraction patterns of powders ZnO, Mg-doped ZnO and TiO_2

In the literature, it has been extensively discussed how the insertion of dopant elements alters the host materials' lattice properties. This is due to their differences in atomic radii (Labhane et al., 2015). As a result, ZnO NPs maintain their original wurtzite structure, and their fundamental structure remains unaffected. This shows that the majority of the Mg^{2+} ions go into the lattice as substitution ions to replace the Zn^{2+} ions and do not enter the void spaces. Due to the ionic radius of the substituted dopant Mg^{2+} (R^{2+} = 0.57) being less than that of Zn^{2+} (R^{2+} = 0.60) (Labhane et al., 2015). On account of the substitution of Mg^{2+} into ZnO, a slight amount of lattice strain is detected to correlate with the XRD diffraction angle shift.

Figure 4.4 (c) also represents the XRD patterns of powder TiO_2 nanoparticles. All major diffraction peaks of powder TiO_2 were well indexed to purely anatase phase according to the standard JCPDS card No. 21-1272. Some lower-intensity action peaks were assigned to the rutile phase of TiO_2, which is confirmed by the JCPDS card No. 01-086-0147(Jalali et al., 2020).

4.7.1 (b) Morphological properties (FESEM) of nanoparticles

One of the important parameters influencing the density of the biodiesel blend is the surface morphology of the catalyst. The nanoparticles ZnO, Mg-ZnO, TiO_2, and SiO_2 were examined by using an SEM image, as shown in Figure 4.5(a-d). According to the SEM images, the ZnO particles were formed in a very uniform manner in a spherical shape(L. Wang & Muhammed, 1999).

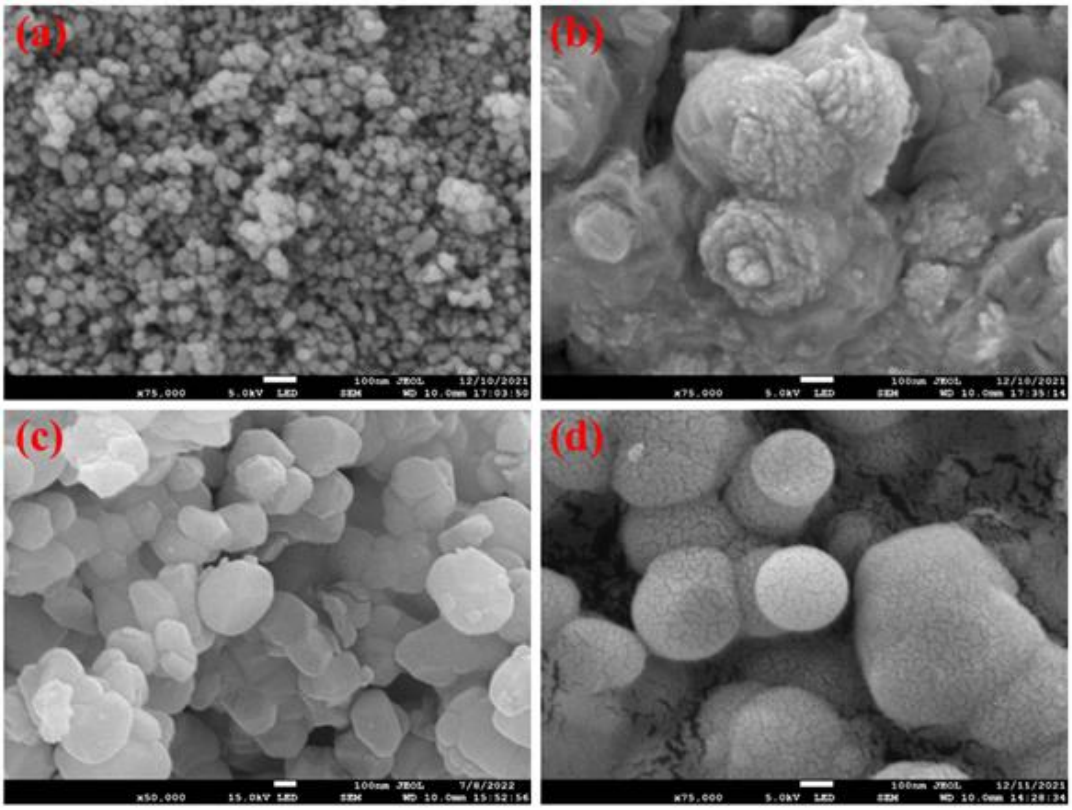

Figure 4.5 (a-d). Represents the FESEM of powder ZnO, Mg-doped ZnO, TiO_2, and SiO_2 nanoparticles with the same magnification at 75000X

SEM image of Mg-doped ZnO nanoparticles shows a huge agglomeration of ZnO particles and forms a bigger size of Mg-ZnO particle shown in Figure 4.5(b). It also forms a cluster-type morphology (Priscilla et al., 2019) with diameters in the range of 100 to 700 nm. As the analysis of SEM microphotographs of SiO_2 particles in Figure 4.5(d), silicon dioxide particles have a spherical shape at higher magnification, moderate polydispersity and an average diameter of about 200 nm (Blinov et al., 2019).

4.7.2 Characterization of synthesized biodiesel

The physicochemical specifications of biodiesel (synthesized by Jatropha oil) with the help of potassium hydroxide solution as a catalyst, were studied and done the comparison with ASTM standards. Table 4.3 contains the results of this characterization that fulfil ASTM criteria. FTIR was used to examine the relative content and recognition of several fatty groups (methyl esters).

Table 4.3. Properties of Jatropha oil, Jatropha biodiesel and diesel

Properties	**Jatropha oil**	**Jatropha biodiesel (Present work)**	**Diesel**	**Biodiesel standards**	
				ASTM D 6751	**EN14214**
Acid value (mg KOH/g)	28.0	0.50	----	< 0.80	< 0.50
Kinematic viscosity(mm^2/s)	24.5	4.7	2.60	1.9-6.0	3.5-5.0
Cloud point (°C)					
Pour point	4	--	-20	----	-----
Density at 15 °C (kg/cm^3)	940	879.20	850	----	860-900
Saponification number					
Oxidation stability (hr)100 °C		1.91	163		
Flashpoint (°C)	225	138	68	>130	>120
Calorific value (MJ/kg)	38.65	40.10	43.44	----	----

4.7.3 Fourier-transform infrared spectroscopy (FTIR) analysis

FTIR examination of the Jatropha oil as well as the derived biodiesel is depicted in Figures 4.6 & 4.7. The presence of water molecules results in a peak at 3410 cm^{-1} in Jatropha oil, indicating the stretch and bend vibration of the hydroxyl group. The occurrence of peaks at 2924.54 cm^{-1} and 2853 cm^{-1} confirms the presence of antisymmetric, symmetric stretching vibrations of methine in methylene groups and then methyl groups. The presence of the ketone group stretching vibration of carbonyl groups in triglycerides is responsible for the significant peak in 1748.76 cm^{-1}. The bending vibrations of methylene and methyl aliphatic groups were confirmed by the peaks at 1400-1200cm^{-1}. Similarly, the bending of hexachlorocyclohexane occurs at 1377 cm^{-1} and carbon and hydrogen are further cut at the 1463 cm^{-1} range. The stretching vibrations of the carbonyl group ester were represented by the peaks located between 1120 and 1090 cm^{-1}. The peak obtained at 722 cm^{-1} justifies the vibrations and shows $(CH_2)_n$ overlapping (de la Mata et al., 2012; Shalaby & Nour Sh. El-gendy, 2012). Furthermore, the peak at 1744 cm^{-1} validated the stretched vibration of the carbonyl group that is present in the esters, as did the peaks secured in the range of 1300-1000 cm^{-1}, which verified the ketone class with stretched vibrations(Guillén & Cabo, 1997; M. Tariq et al., 2011). The stretching vibrations of the methylene, methyl and methine groups were observed at 2980-2950, 2950-2850, and 3050-3000 cm^{-1}, respectively, while bending vibrations of the methyl, methylene, and methine groups were observed at 1475-1350, 1350-1150, and 722 cm^{-1} (Safar et al., 1994; M. Tariq et al., 2011). Because triglycerides and esters are present, the FTIR analysis of Jatropha oil and biodiesel made from it is suitable for comparison. However, very minor variations were detected, with the peaks appearing at 1743,1373,1155,1038, and 876 cm^{-1} in jatropha oil being displaced to 1744,1361, 1172, 1018, and 884 cm^{-1} in biodiesel. As a result, some peaks were absent in jatropha oil that

ranged from 1443,1096, and 965 cm^{-1}. The development of new peaks at 1435 cm^{-1} and 1196 cm^{-1} clearly shows that there is a generation of biodiesel. Moreover, the range of 3100-3500 cm^{-1} justified that the synthesized biodiesel from Jatropha oil has an insufficient amount of water content.

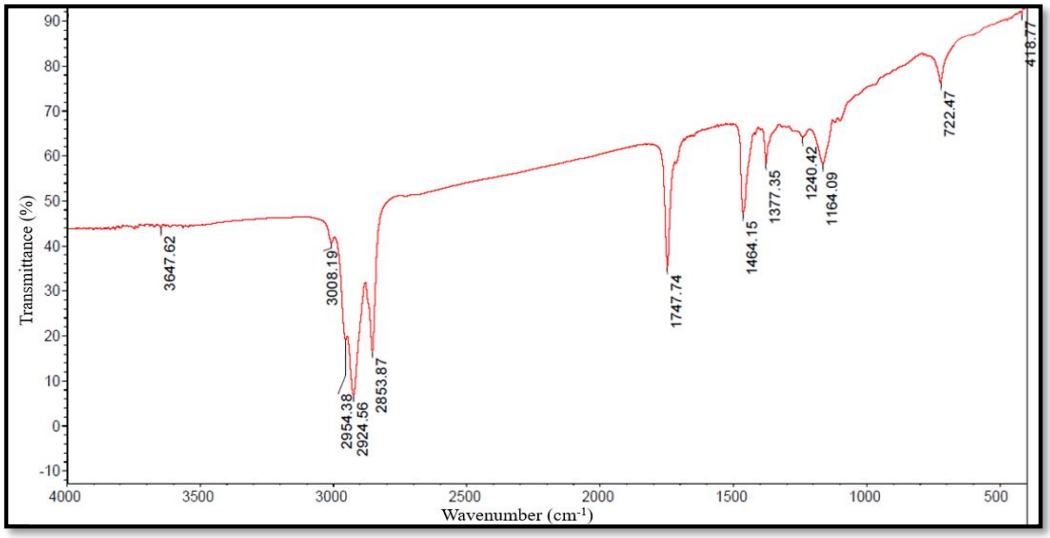

Figure 4.6. FTIR spectra of the Jatropha oil

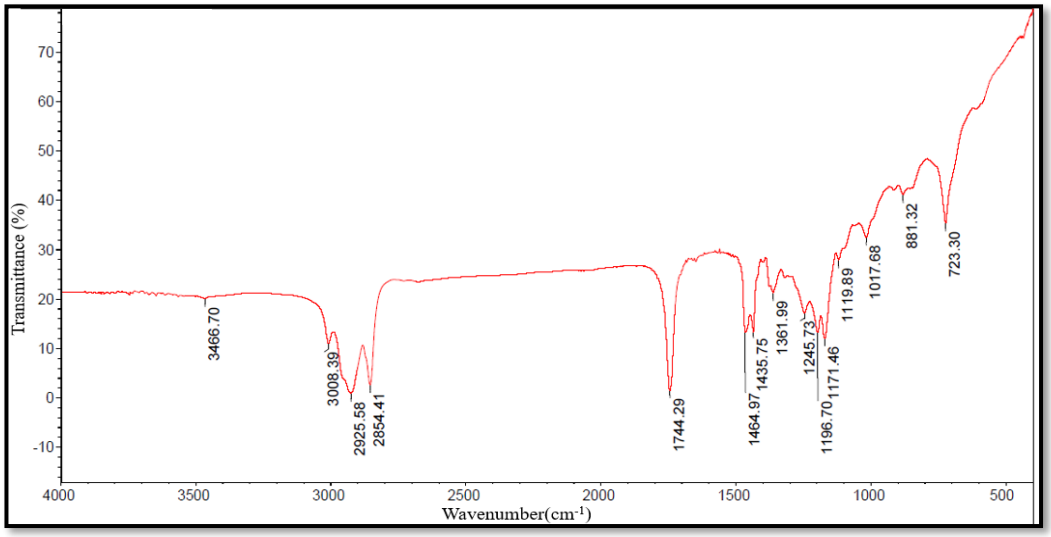

Figure 4.7. FTIR spectra of the jatropha-derived biodiesel

4.7.4 Effect on calorific value

Figure 4.8 depicts the calorific value of neat biodiesel and blends with different NPs such as ZnO, TiO_2, SiO_2, and Mg-ZnO. The biodiesel blended with nano-additives like TiO_2

and ZnO NPs (100 ppm) exhibited a higher CV than standalone biodiesel. This establishes the advantage of nano additives application as fuel/combustion property enhancers. It is noteworthy that biodiesel blended with ZnO NPs (at 100 ppm concentration) exhibited a higher CV than biodiesel blended with TiO_2, SiO_2, and Mg-ZnO. Interestingly, NPs blending at 50 ppm concentration in biodiesel depicted a higher CV for SiO_2 than Mg-ZnO, ZnO, and TiO_2. SiO_2 is a covalently bonded compound where silicon atoms are covalently connected with four oxygen atoms, whereas the oxygen atoms are bonded with two silicon atoms. Hence, more energy is expected to break the covalent bond. However, at higher concentrations, the application of SiO_2 NPs was not found to be favourable. It is believed that this is due to the cation-cation repulsion, which hinders the formation of dense anion oxygen layers and cations in the tetrahedral gaps in SiO_2. This brings cations closer to each other, and cation-cation repulsion gets promoted. Therefore, stability, which was evident at lower concentrations (50 ppm), was not obtained while using SiO_2 NPs at higher concentrations (100 ppm) in biodiesel. It is worth noting that Mg-ZnO performed better at lower concentrations (50 ppm) than at higher concentrations (100 ppm), and interestingly, was found to be better than ZnO at lower concentrations. This might be attributed to the difference in inherent bonding characteristics. ZnO NPs typically exhibit covalent bonding. However, Mg doping in ZnO led to the formation of additional metallic bonds along with covalent bonds. Hence, it is assumed that due to the mixed bonding characteristic, Mg-ZnO was found superior to ZnO for Enhancement at lower concentrations (50 ppm). The dominance of crystallographic planes, e.g. $(10\bar{1}1)$, $(10\,\bar{1}0)$, and $(11\bar{2}0)$etc, was evident in the XRD pattern (Figure 1). These surfaces depict higher surface energies than the other planes. Surface energies of $(10\bar{1}0)$and $(11\bar{2}0)$were calculated as 1.12 Jm^{-2} and 1.06 Jm^{-2}, respectively, for ZnO (Na & Park, 2009). Hence, it is believed that the application of ZnO NPs in biodiesel at higher concentrations

promotes the formation of crystallographic planes, e.g., $(10\bar{1}0)$ and $(11\bar{2}0)$, with high surface energies. This led to the stabilization of nano-additive-biodiesel blending due to more sigma bond formation. NPs with high surface energy and the presence of more sigma bonds demand more energy to break such blends (or bonds). Therefore, it is assumed that this phenomenon would have enhanced the CV of ZnO NP-blended biodiesel compared to another NP-blended biodiesel.

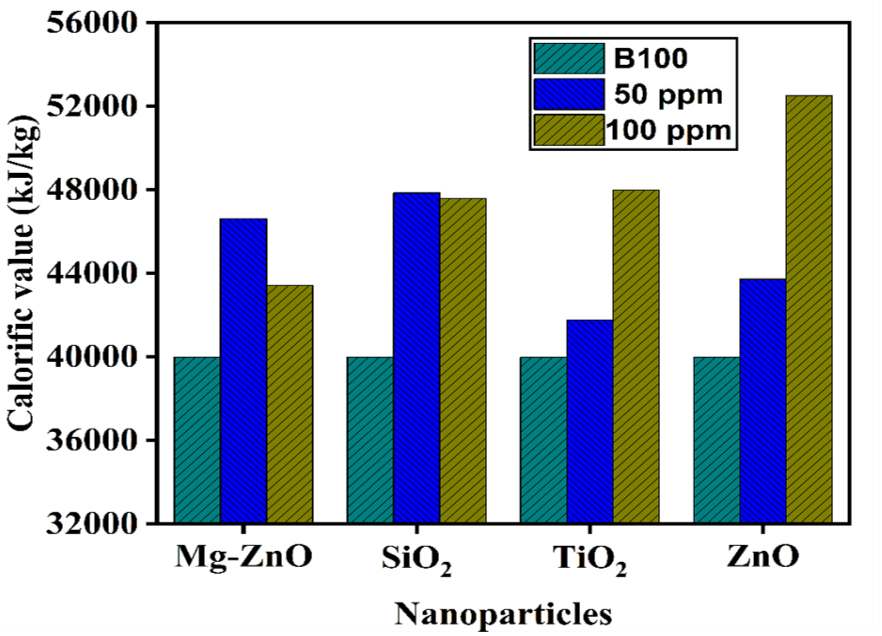

Figure 4.8. Comparison of biodiesel (and blends) calorific value with and without nanoparticles

4.7.4 Effect on density

Density is recognized as an influencing factor which affects the brake thermal efficiency of the engine and the ignition quality of fuel. Figure 4.9 shows the comparison of fuel densities at 15 °C of pure. Biodiesel with biodiesel blended with NPs at different concentrations. The densities of TiO_2, SiO_2, ZnO, and Mg-ZnO were found as 882.9, 883.3, 883.8, and 882.5 kg/m^{-3}, respectively, when used at 50 ppm. The Mg-ZnO NPs blended biodiesel exhibited the least density at 50 ppm, whereas ZnO-blended biodiesel had the highest density. On the other hand, at higher concentrations (100 ppm) of NP

dose, TiO_2-blended biodiesel showed the highest density, and Mg-ZnO NP-blended biodiesel exhibited the least density. Therefore, Mg-ZnO NPs were found suitable as efficient fuel property enhancers at low concentrations, which enhanced the CV and lowered the density (Sahoo & Jain, 2019).

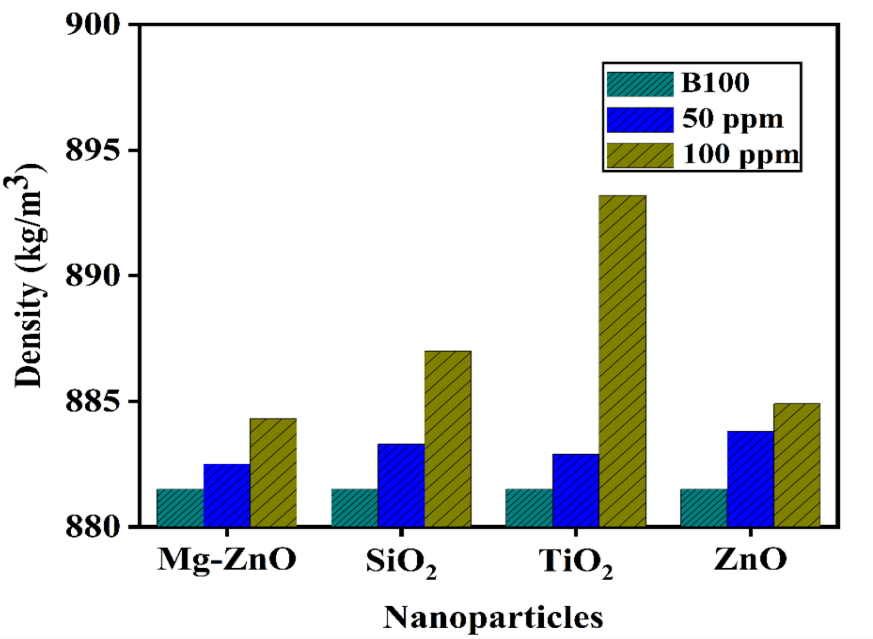

Figure 4.9. Density of biodiesel blend with various nanoparticles

4.7.5 Effect on oxidation stability

The presence of unsaturated acids makes the biodiesel highly reactive toward oxygen (O2). The double bond of fatty acid interacts with O_2 and gets transformed into alcohol, aldehyde, and carboxylic acid, which remain unstable by forming allylic hydroperoxides as well as various secondary oxidation state components. The oxidation stabilities of pure biodiesel and NP-blended biodiesels were studied using an 893 Professional Biodiesel Rancimat analyser (see Figure 4.10 and Table 4.4). The Mg-ZnO NP-blended biodiesel displayed the highest oxidation stability at a concentration of 50 ppm, whereas TiO_2-blended biodiesel exhibited the lowest oxidation stability for the same dosing concentration. On the other hand, at high- (see Table 4.4) induction time for nanoparticles blend biodiesel higher concentration (100 ppm) of NP dose, again Mg-ZnO-blended

biodiesel had the highest oxidation stability, whereas TiO_2-blended biodiesel exhibited the least oxidation stability. Therefore, Mg-ZnO NPs were found suitable as efficient oxidation stability enhancers of biodiesel at low and high concentration dosages. It is important to note that the same had enhanced the CV and lowered the fuel density. The XRD pattern of Mg-ZnO exhibited the crystallographic dominance of $(10\bar{1}1)$ than other planes; $(10\bar{1}1)$ elucidates lower surface energy than $(11\bar{2}0)$, and $(10\bar{1}1)$. Therefore, it is believed that the formation of Mg-ZnO NPs with the dominance of low surface energy crystallographic facets $(10\bar{1}1)$ would have led to higher oxidation stability than other NP-blended fuels.

Table 4.4. Induction time for biodiesel blended with different nanoparticles

Base feedstock: Jatropha biodiesel **Base induction time:**1.91 h		
Nanoparticle names	**Dosing level (ppm)**	
	50	**100**
ZnO	3.67	5.85
TiO_2	3.32	4.16
SiO_2	3.35	4.44
Mg-ZnO	5.14	6.93

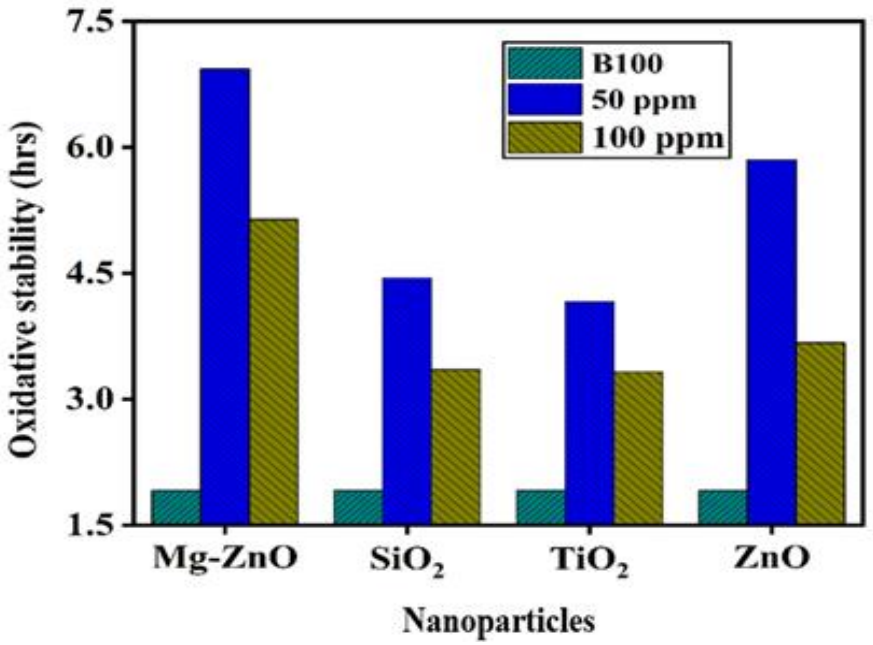

Figure 4.10. Effect on the induction time of biodiesel blend with various nanoparticles

4.7.6 Effect on viscosity

The dynamic viscosities of biodiesel and NP-blended biodiesels were measured at 30° ± 0.15 °C using a modular small rheometer. Figure 4.11 depicts the fluctuations in the viscosity of pure biodiesel (B100) and NPs such as TiO_2, SiO_2, ZnO, and Mg-ZnO-blended biodiesels as a function of the shear rate. As is evident from Figure 4.11, TiO_2 NP-blended biodiesel exhibited the lowest dynamic viscosity at the dosing concentration of 50 ppm, whereas ZnO-blended biodiesel showed the highest dynamic viscosity at the same dosing concentration. On the other hand, at a higher concentration (100 ppm) of NP dose, SiO_2-blended biodiesel revealed a higher dynamic viscosity, whereas Mg-ZnO-blended biodiesel exhibited the least dynamic viscosity. Therefore, Mg-ZnO NP-blended biodiesel was found suitable for automotive applications at 50 and 100 ppm dosing concentrations because it provides dynamic viscosity within the range mentioned in the ASTM standard (E. N. Frankel, 2012).

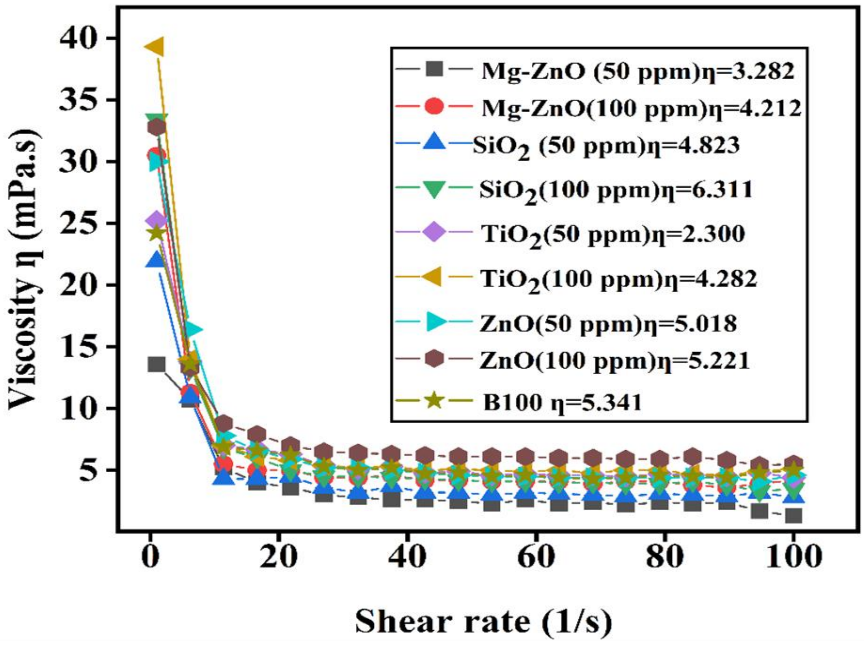

Figure 4.11. Effect on the viscosity of biodiesel blends with nanoparticles

4.7.7 Zeta potentials of various nanoparticle-blended biodiesels

Van der Waals forces between the NPs in NP-blended biodiesel affect the overall charge stability of the fuel system and may lead to the agglomeration or settling of NPs after some time. Therefore, it is important to examine the charge stability of the NP-blended biodiesels using zeta potential measurement. Figure 4.12 shows the dispersion stability of various NPs of sizes 30–80nm in Jatropha-derived biodiesel. At higher (100 ppm) and lower concentrations (50 ppm) of the NP dose, ZnO-blended biodiesel displayed higher stability for a constant volume fraction (VF) than other NP-blended biodiesels, whereas SiO_2-blended biodiesel exhibited the least stability under both conditions. Mg-ZnO-blended biodiesel was stated as the second most promising candidate in terms of blending stability, both at high and low concentration dosages of Mg-ZnO NPs. Hence, it must be highlighted that the Mg-ZnO-blended biodiesel is suitable for application in the automotive sector.

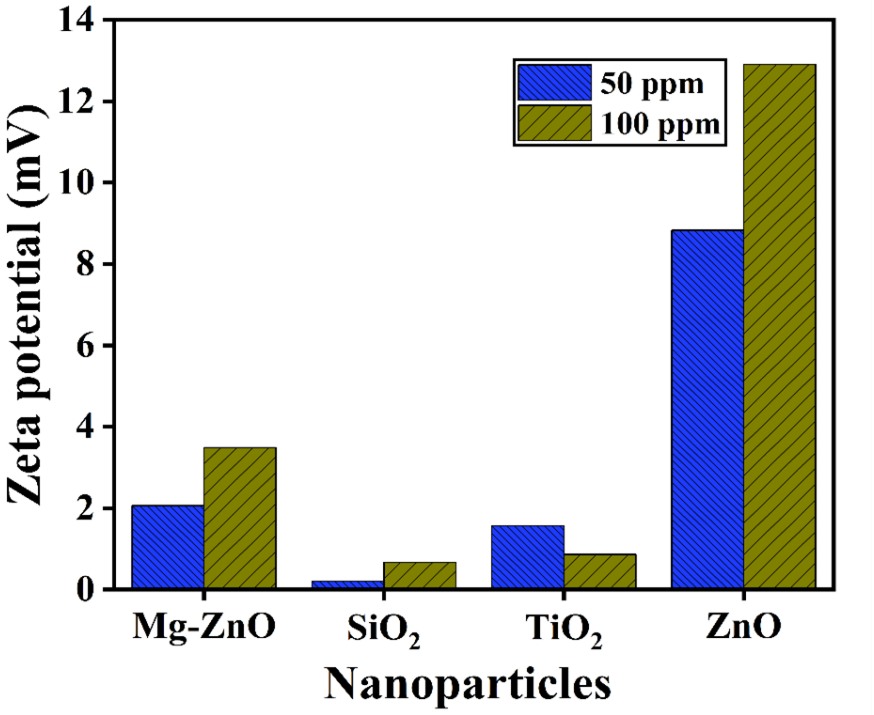

Figure 4.12. Variation of Zeta potential with nanoparticles

4.8 Conclusion

Four nanoparticles, ZnO, Mg-ZnO, TiO_2, and SiO_2 investigated for the physicochemical features and spray characteristics of the biofuel blends in this study. When the fuels were combined individually with clean jatropha oil, it was discovered that the addition of nanoparticles boosted the fuels' density, kinematic viscosity, oxidation stability, and heating value. Oil biodiesel with different dosages of nanoparticles (0-100 ppm). The density of the SiO_2 blends was lower than TiO_2 but higher than Mg-ZnO and ZnO mixtures. The calorific value was much higher for ZnO blends in comparison to Mg-ZnO, TiO_2, and SiO_2 mixtures. Its viscous nature was increased with both nanoparticles; however, ZnO gave smaller increases than Mg-ZnO nanoparticles. It was proven that the addition of zinc oxide gave better properties than TiO_2, SiO_2, and Mg-ZnO nanoparticles. Gains in density and viscosity would have a negative impact on the fuel supply systems and combustion of internal combustion engines, but increases in oxidation stability and heating value would have a favourable impact on fuel systems and engine combustion. So, in the secondary stage of the study, the effect of dosage level (0-100 ppm) addition in ZnO, Mg-ZnO, TiO_2, and SiO_2 nanoparticles biofuels was assessed to see how different concentrations of addition affect physicochemical properties and induction of period properties of the blends. The study found that the synthesis of four different nanoparticles by the sol-gel method and their use as to property improver of biodiesel. Determination of surface tension, engine performance, exhaust emission analysis, selection of suitable low-cost nanoparticles, and synthesis method are suggested as future work. The usage of various NPs and surfactants is coming in a distinct area of investigation (different fuels).

Chapter 5

Blending effect of nano additives[4]

[4]The result discussed in this chapter have been published in Journal of the Energy Institute. 2024;117:101825. https://doi.org/10.1016/j.joei.2024.101825

5.1. Introduction

Rising energy demand and growing dependence on fossil fuels have created an urgent need for sustainable alternatives. To address this, the Government of India, through the National Policy on Biofuels (2018), has set a target to increase biodiesel blending in diesel from 5% by 2030. Achieving this goal cannot be met through a single feedstock, as supply limitations restrict large-scale production. Consequently, researchers and policymakers are exploring multiple feedstocks, including Karanja oil, used cooking oil, Jatropha, and waste-derived sources to ensure sustainable biodiesel production, enhance energy security, and reduce reliance on fossil fuels.

In this direction, tyre pyrolysis oil (TPO) has gained significant attention. Derived from the thermal decomposition of scrap tyres, TPO offers a dual advantage: it supports effective waste management while simultaneously serving as a sustainable alternative energy resource. Its characteristics resemble those of light fuel oil, with a calorific value of 35–40 MJ/kg, and fuel experts have expressed optimism regarding its potential (Hood et al., 2018; Kumaravel et al., 2016; Tamizhdurai et al., 2025). Nevertheless, direct application of TPO remains limited due to high viscosity, elevated aromatic content, and the presence of impurities. Blending TPO with biodiesel offers a practical approach to overcoming these limitations, as biodiesel can improve combustion quality and reduce the environmental footprint of the mixture.

Similarly, used cooking oil (UCO) represents another promising feedstock. Large quantities of UCO are often discarded into drainage systems, dustbins, or directly onto soil, creating serious environmental issues. Instead of disposal, UCO can be utilised for biodiesel production, offering an economical route due to its low cost.

Building on these approaches, the present study introduces biosynthesised strontium oxide (SrO) nanoparticles, prepared via a green route using Moringa oleifera extract. Unlike chemically synthesised nanoparticles discussed in the previous chapter, these eco-friendly nanoparticles aim to enhance the physicochemical and combustion properties of biodiesel–TPO blends while minimising environmental and health concerns.

To validate this approach, the resulting fuel was tested in a single-cylinder, four-stroke diesel engine equipped with a variable compression ratio (VCR) system, where performance parameters such as brake thermal efficiency (BTE), heat release rate (HRR), and peak cylinder pressure (CP), along with emission characteristics including carbon monoxide (CO), hydrocarbons (HC), carbon dioxide (CO_2), and nitrogen oxides (NO_x), were systematically evaluated to determine its practical applicability.

5.2. Materials and methods

5.2.1 Raw material

Used cooking oil was collected from the mess of Rajiv Gandhi Institute of Petroleum Technology (RGIPT), Jais, India, and used in this work to synthesize biodiesel. Strontium precursor, $Sr(NO_3)_2 \cdot 6H_2O$, methanol (CH_3OH, 98% purity), sulfuric acid (H_2SO_4) and potassium hydroxide (KOH) were provided by Might Scientific Sales, Lucknow, India. The TPO was purchased from M/s Chemical and Instruments, Kanpur and was further processed in the green separation/biofuel lab, RGIPT, Jais, to be utilized in the current work. *Moringa oleifera* leaves were collected from RGIPT, Jais, India.

5.2.2 Synthesis and characterization of SrO nanoparticles

The SrO nanoparticles were synthesised using strontium nitrate hexahydrate ($Sr(NO_3)_2 \cdot 6H_2O$) salt as precursor and extract of *Moringa oleifera* leaves as reducing and capping agent. 20 g of dried leaves powder was boiled for 2 hours in 400 mL double-

distilled water to prepare the extract. The leaves were then vacuum-filtered using the Whatman filter paper. The final extract was then kept at 4 °C in a refrigerator. To synthesize SrO nanoparticles, 50 mL of the plant extract solution was mixed with 1mM $Sr(NO_3)_2 \cdot 6H_2O$ solution drop by drop using a burette. The process was completed on a magnetic stirrer at room temperature. This caused the solution to homogenize, giving a fine precipitate. The solution was then sonicated and centrifuged at 10,000 rpm. The obtained pellet was dried and ground into a fine powder for calcination, which was done at 1000 °C for 1 hour in the presence of inert gas, N_2. The obtained off-white powder was characterized by Jeol Field Emission Scanning Electron Microscope (FE-SEM) equipped with Energy Dispersive X-ray (EDAX) spectroscopy to analyse the morphological characteristics at an accelerating voltage of 15 kV. Pan analytical powder X-ray Diffraction spectrometer (XRD) with Cu Kα radiation was used to scan the sample from 2theta range of 20-80° at a scan rate of 0.0038 °/s.

5.2.3 Fuel preparation

5.2.3.1 Biodiesel preparation

The initial step in the synthesis of biodiesel is to identify the preparation technique based on the FFA content. The feedstock oils, such as Karanja, Jatropha, and used cooking oil, have a greater FFA content (>1% w/w), which is due to the increased triglyceride leading to a major reduction in product yield and an increase in saponification (Borugadda & Goud, 2012a). In such cases, a two-step technique is used, which includes esterification and transesterification. Firstly, esterification eliminates impurities by using an acid catalyst. The separated final product is then subjected to base-catalysed transesterification in the second step **(**as shown in Figure 5.1) (Ajeet et al., 2023a).

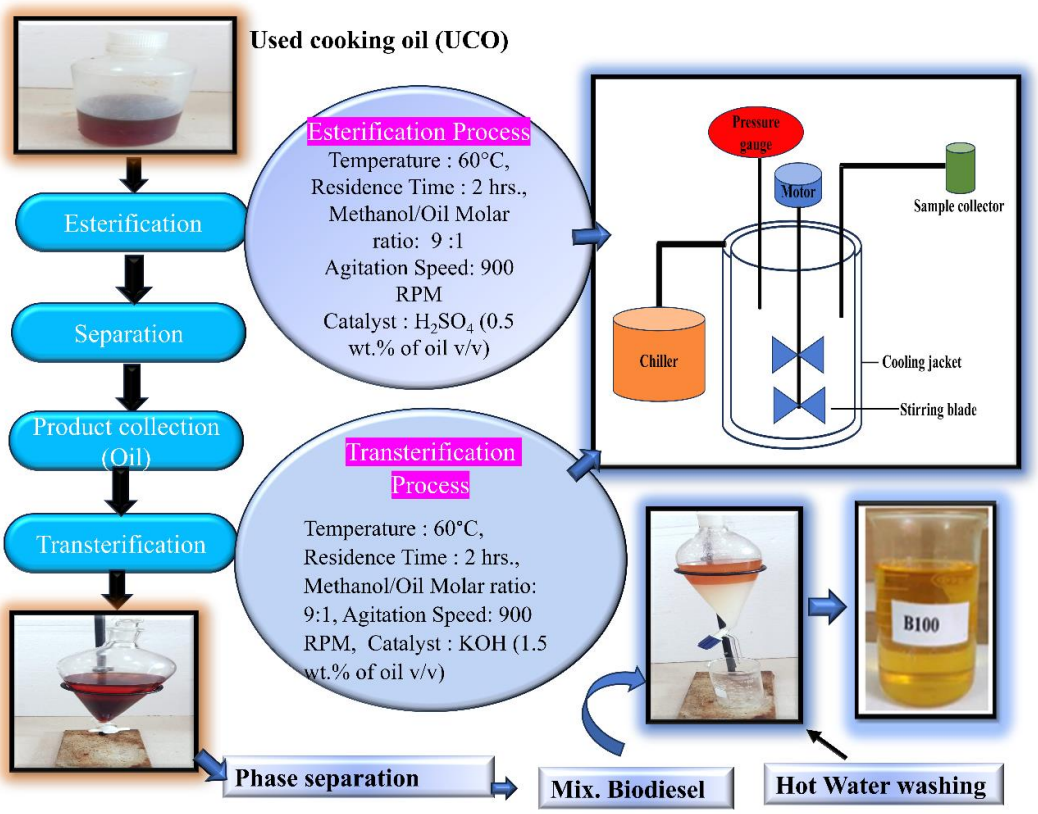

Figure 5.1. Steps involved in the production of biodiesel using high pressure-high temperature (HPHT) autoclave

5.2.3.2 TPO preparation

Raw tyre pyrolysis oil (TPO) is not directly used in engines due to its high content of organic compounds, which consist of 5-20% carbon and a significant proportion of aromatics (De Marco Rodriguez et al., 2001). The proportions of benzothiazole, aliphatic compounds, nitrogenous chemicals, and aromatics in TPO are measured at different pyrolysis process operating temperatures (M. R. Islam et al., 2013). When the operating temperature is adjusted from 300°C to 700°C, the percentage of aromatics increases from approximately 34.7% to 75.6%, while the percentage of aliphatic compounds ranges from about 19.8% to 59.2%. Additionally, it is found that over 30% of the TPO is easily distillable, with boiling points within the range of 70°C to 210°C(M. R. Islam et al., 2013;

Mia et al., 2017). In this study, a temperature range of 121-180°C was used for the fractional distillation of the raw TPO, as illustrated in Figure 5.2.

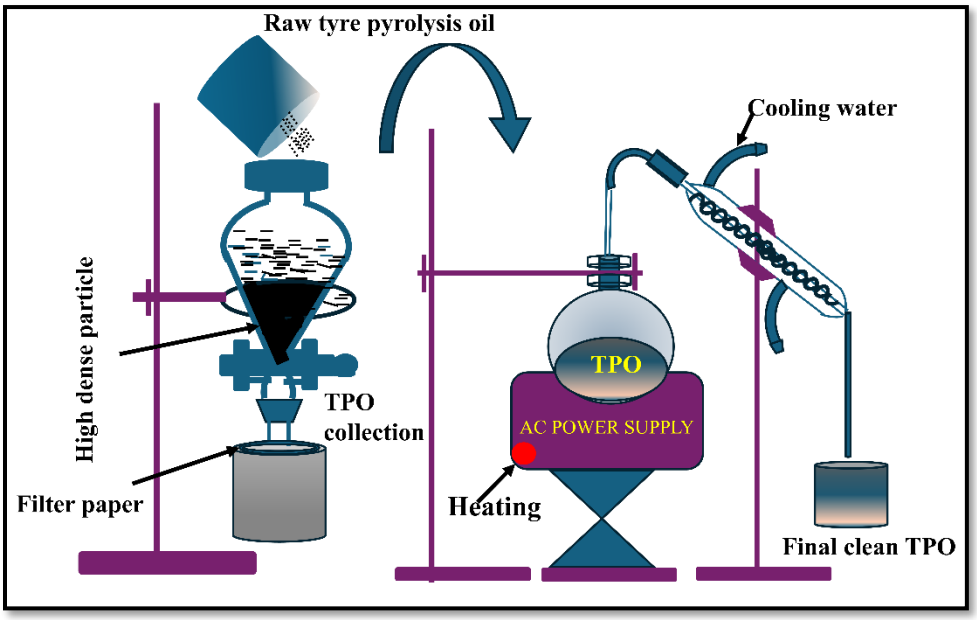

Figure 5.2. Purification of raw tyre pyrolysis oil

5.2.3.3 Blend preparation

In the present study, the blended fuel consisting of TPO, UCO biodiesel and strontium oxide (SrO) nanoparticles was prepared using an ultrasonic cleaner (Model: B089GMSMM2, ULEMA), as illustrated in the schematic, Figure 5.3. In this regard, NPs were accurately weighed by using a digital balance (MS304S) with a resolution of 0.1 mg. These nanoemulsions (NE) are dispersed by using the ultrasonication technique. The method prevents particle agglomeration and restores agglomerated nanoparticles to their nanometre range (Abishek et al., 2024; Sui et al., 2018; Tesfaye Lamore et al., 2023). The sample was kept in the water bath sonicator, which was set to a frequency of 40 kHz, 120 W for 48 hours. The prepared test fuels are labelled as B5TPO95SrO50 (5% biodiesel+95% tyre pyrolysis oil+50 ppm of strontium oxide nano additive); B10TPO90SrO100 (10% biodiesel+90% tyre pyrolysis oil+100 ppm of strontium oxide

nano additive); B50TPO50 (50% biodiesel+50% tyre pyrolysis oil). The above three blends were prepared by following a similar procedure using an ultrasonicator. Diesel and the biodiesel produced from UCO were used as references for testing. A portion of these blended fuels was extracted to ascertain their characteristics of sophisticated instruments, and the residual fuel was then filled into the fuel tank of the VCR diesel engine.

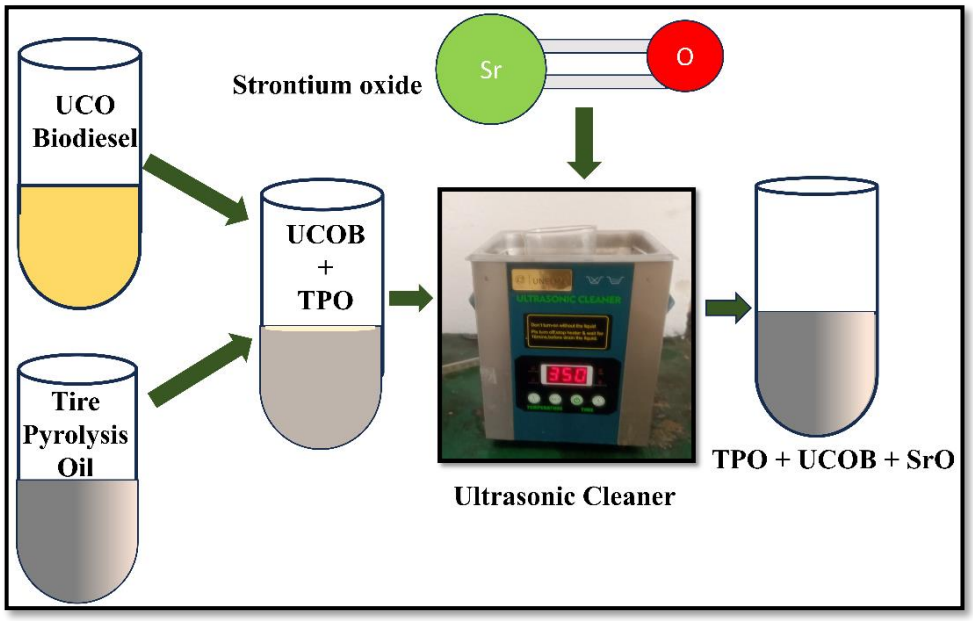

Figure 5.3. Schematic for the preparation of test fuel blends

5.2.4 Fuel characteristics assessment

The properties of all tested samples were evaluated according to ASTM standards, as listed in Table 5.1. The calorific value of the samples was determined using a bomb calorimeter (Model: Hamco 6E, Automatic Bomb Calorimeter). The density was measured using a density meter (Model: Anton Paar, DMA 4100M). Viscosity, a key property, was measured using a rheometer (Model: MCR 102e). The flash and fire points were measured using a Pensky-Martens closed-cup flash point tester. The obtained fuel qualities are listed in Table 5.1.

Table 5.1. Properties of UCO biodiesel blends with SrO nano additives

Properties ASTM D6751	ASTM Standards	Unit	TPO	Diesel	Biodiesel	B5TPO95 SrO50	B10TPO90 SrO100	B50TPO50
Density	D1448	gm/cc	0.812	0.827	0.885	0.828	0.848	0.829
Calorific value	D6751	MJ/kg	40.12	44.00	35.12	40.89	41.89	42.89
Kinematic viscosity	D445	cSt	2.10	2.72	5.20	2.50	2.85	2.40
Flash point	D93	°C	37	45	150	45	46	50
Fire point	D94	°C	39	55	180	48	49	55

5.3. Experimental setup

The basic components of the diesel engine arrangement consist of an electric start, four-stroke, single-cylinder variable compression ratio (VCR) engine with an asynchronous motor and loading unit. This specially designed adjustable bolt system on the cylinder block system makes it possible to vary the compression ratio (CR) without resting the engine (Anish et al., 2022). As illustrated in Figure 5.4, the engine setup is fully furnished with all the accessories needed to measure crank angle, combustion pressure, and injection pressure. The analysis parameters for this VCR engine, which runs at a constant speed (1500), are given in Tables 5.2 and 5.3. Fuel was injected using a multi-point fuel injection system (MPFI). The system is equipped with a panel board arrangement which consists of i) a data acquisition system, ii) a load controller, iii) a fuel sensor, and iv) a rotameter. The generated signals are transmitted to a computer via a data acquisition system, which enables further computations and deductions of the obtained results. The engine load varied from 2-27.9 Nm using the load controller, which was read with the help of attached torque measurement equipment. The amount of fuel consumed by the engine was indicated by a 50 mL burette attached to the panel board. The burette makes it easier to measure fuel usage over a predetermined amount of time by using a stopwatch.

The whole arrangement additionally permits the interaction of airflow, fuel flow, temperatures, and load measurements with a rotameter. The engine setup also includes an air intake measuring arrangement, which consists of an orifice plate with a diameter of 20 mm and a differential manometer (differential pressure transmitter to measure the flow of sucked-in air). The discharge coefficient of the orifice is about 0.64. Along with the requisite piping system that circulates the cooling water for the engine, there is an additional setup for monitoring the heat removed by the cooling water. The temperature sensor measures the inlet and outlet temperatures of the cooling water. The arrangement for measuring the heat carried away by the exhaust gases consists of a central tube and an outer jacket. To achieve an optimal temperature differential between the exhaust gases at the calorimeter's input and output, water is pumped within the outer jacket while the exhaust gases travel through the tube. The performance of VCR engines is determined by variables like air-fuel ratio (AFR), brake-specific fuel consumption (BSFC), volumetric efficiency, indicated power, frictional power, brake thermal efficiency (BTE), etc. Among them, AFR, BSFC, and BTE were used for performance analysis in our study. Combustion characteristics such as CP, HRR, and crank angle were measured at full loading conditions. Five gas analyzers (Model no.-AVG-500) were used to assess the exhaust emission of the VCR diesel engine that was attached to the sample probe. During the testing, the probe was inserted in the outlet of the exhaust of the gas calorimeter (mentioned in Table 4) for analysis of HC, CO, CO_2, NOx, O_2 and lambda. The software package "ICEngine_SoftV9.1," which is based on Lab-view, was used for online performance assessment. An IC engine's performance in combination with conventional diesel, biodiesel blends, and nano additives was tested. Before starting the experiment, the necessary parameters like engine oil level, water coolant, and other testing conditions were checked. The test engine was allowed to run once it was stabilized, and gradually

the load was applied. Simultaneously, the measurements were properly configured by using the instruction manual. The engine was first operated for more than 15 minutes using diesel fuel to reach its nominal and considerable operating temperature. After the warmup, diesel fuel was removed from the fuel tank and fuel pump lines and replaced with test fuels such as B5TPO95SrO50, B10TPO90SrO100, and B50TPO50. At each load, measurements were done for brake power and torque, fuel consumption, intake air temperature, exhaust gas temperature, engine coolant temperature, and combustion pressure, along with emissions records of hydrocarbon (HC), CO, NOx, and CO_2 gases. To remove any leftover biodiesel blends, especially in the fuel system, each test engine was run with diesel again. In addition, the experiment was conducted three times to ensure repeatability and accuracy.

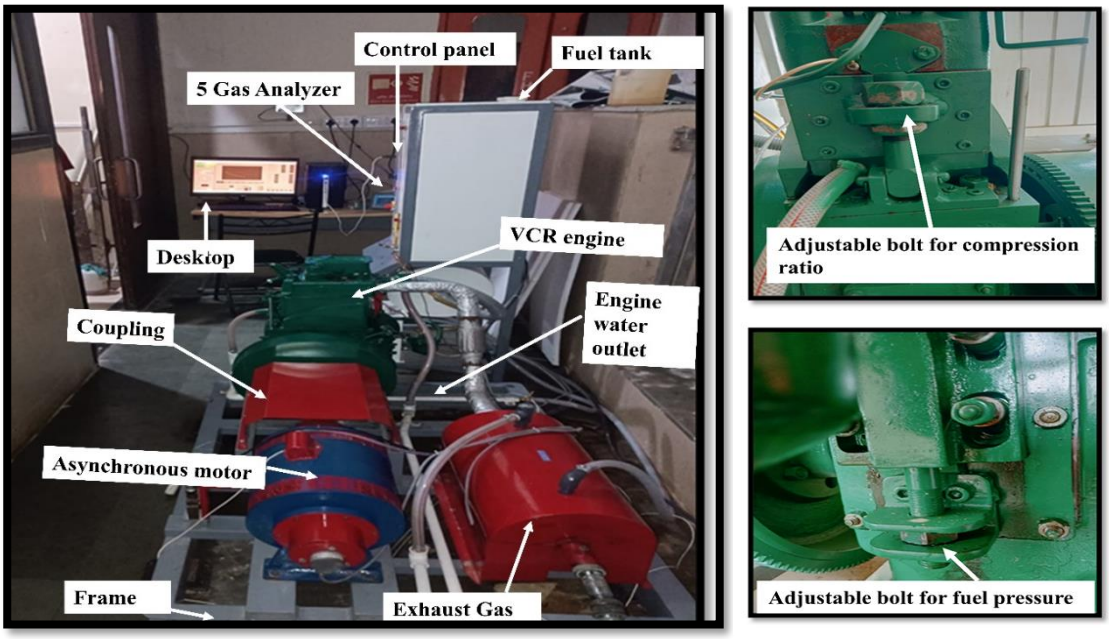

Figure 5.4. Experimental VCR diesel engine setup

Table 5.2. Engine specifications

Product GIC-TD203D	**Single cylinder, four-stroke, diesel/Biodiesel (VCR computerised) electric start with battery and battery charger**
Injection Pressure and Injection Timing	Mechanical type continuously variable injection pressure:180,190,200,210,220,230 &240 bar Mechanical type variable injection timing: advance and retard 15-20 deg
Dynamometer Type	Eddy current type (water-cooled with control panel) Asynchronous motor with regenerative
Propeller soft	Hindustan Hardy with universal joints Force transmission from the engine to the brake unit means using a coupling.
Airbox	M S box with orifice meter and manometer
Fuel tank	5 Litres 2 fuel tank with glass fuel metering column
Calorimeter	Pipe in pipe type, with heat-resistant hose
Piezo sensor	PCB Piezotronics (New York) Diaphragm stainless steel type & hermetically sealed, Piezo sensor for head pressure, range 350 bar, with low noise cable, and signal conditioner
Crank angle sensor	PPR: 360 resolution 1 deg, speed 6000 rpm, with TDC pulse 10-30 V DC,
Temperature sensor	J type, range 0-700 deg crank K type, range 0-1200 deg crank
Load sensor	Load cell, strain gauge type, 0-50 kg
Fuel flow transmitter	500 mmWC, output 4-20ma,
Airflow transmitter	Pressure transmitter, range (-) 250 mm WC
Water flow sensor	0-30 LPM turbine-type cooling water flow sensor with controlling valve
Analysis Software	Windows-based engine performances' IC Engine Soft" Model:1.4, Ver:1.3
Space (Overall dimensions)	W 4000 x L3800 x H2000 mm

Table 5.3. Engine test rig specifications

Make Type	VCR Four Stroke water-cooled
No of cylinder	Single
Power	5.2 kW@1500 rpm
Bore	85 mm
Stroke	110 mm
Combustion principle	Compression ignition
Cubic capacity	661.5 cc
Compression ratio	12:1, 22:1 (Variable Type) Changing during engine running
Fuel	Run on diesel, biodiesel, as well as biodiesel blends
Max speed	1800 rpm
Min. idle speed	750 rpm
Min operating speed	1200 rpm
Rated operating speed	1500 rpm
Max operating speed	1600 rpm
Fuel timing for standard engine valve timing	23-degree BTDC Inlet open BTDC 4.5 degrees Inlet close ABDC 35.5 degrees Exhaust open BBDC 35.5 degrees Exhaust close ATDC 4.5 degrees
Inlet valve clearance	0.18 mm
Exhaust valve clearance	0.20 mm
Lubrication oil	3.5 litre (20w40)

Table 5.4. AVG-500 specifications

	Gas channel	Range	Resolution

Measured components	Hydrocarbon (Hexane)	0 to 15000 ppm	1 ppm
	Carbon Monoxide	0 to 15 %	0.001%
	Carbon Dioxide	0 to 20%	0.01%
	Oxygen	0 to 25%	0.01%
	NOx	0 to 5000 ppm	1 ppm
	Lambda	0.500 to 9.999	0.001
	AFR	7.90 to 27.60	00.01
Accuracy	Hydrogen Carbon Monoxide Carbon Dioxide Oxygen	± 12 ppm Vol. ± 0.06% Vol. ± 0.40% Vol. ± 0.10% Vol.	
Response time Repeatability		≤ 15 sec. for Final value ± 1% of the First Sample value	
Auto Zeroing		≤20 Seconds (Performs automatically at every measurement cycle)	
Warm-up time		≤5 Minutes	
Samples flow rate		4 Litres/Minute	
Fabrication		Full Metal Body	
Dimensions		L 280 mm ×W 250 mm ×H 140	
Operating conditions		Temperature Range: 0 to 50 degrees Celsius Atmospheric pressure: 700 to 1150 mBar Humidity to 90% (non-condensing)	

5.3.1. Uncertainty analysis

The different types of instruments used, the measuring technique, the surrounding circumstances, and the experimental setting are some of the variables that could lead to uncertainty in an experiment. After applying the engine loads and engine speed for five minutes, engine performance and emission measurements were carried out for every situation to ensure the measured parameters remained unchanged. In addition, the propagation of error was studied using standard deviations by plotting error bars, where error bars were derived considering the average of three readings and uncertainty was

determined using measured parameters, including torque, AFR, HRR, CT, BTE, BSFC, CO_2, HC, and NOx. The root-mean-square approach, as described by Holman, is used to calculate the total uncertainty. Table 5.5 presents the uncertainty analysis for different parameters. Equation (5.1) is utilized to compute the overall uncertainty(Panithasan et al., 2020).

Overall, the uncertainty percentage in the experiment

$$= \pm\sqrt{\begin{matrix}(\Delta T)^2 + (\Delta AFR)^2 + (\Delta BTE)^2 + (\Delta BSFC)^2 + (\Delta CO)^2 + (\Delta HC)^2 + \\ (\Delta CO2)^2 + (\Delta NOx)^2 + (HRR)^2 + (\Delta CT)^2\end{matrix}} \quad = \pm 2.55 \quad (5.1)$$

The result for overall uncertainty was found to be 2.5 %, which is well within the allowable limit (O. Khan et al., 2024; Shrivastava et al., 2020; T. S. Singh & Verma, 2019).

5.4. Results and discussion

Table 5.5. Uncertainty analysis of different variables

Measurement	Accuracy	Uncertainty (%)
Torque (Nm)	-	±0.29
Brake thermal efficiency (%)	-	±1.25
Brake-specific fuel consumption (%)	-	±1.30
AFR	-	±1.00
Heat release rate (J°/CA)	-	±1.28
Cylinder Temperature		±0.56
CO (Vol.%)	±0.06 % Vol.	±0.06
HC (ppm)	±12 ppm	±0.14
NO_x (ppm)	±12 ppm	±0.20
CO_2 (Vol. %)	±0.40 % Vol.	±0.40

5.4.1 Characterization and role of SrO nanoparticles

The morphological characteristics and elemental analysis of SrO have been assessed using FE-SEM and EDAX, as shown in Figure 5.5. FE-SEM is a versatile technique

which is used to observe nanoparticles of varying morphologies using an electron gun as the source. The typical shape of the SrO nanoparticles calcined at 1000 °C was found to be nearly spherical. Partial agglomeration of the particles can also be seen, which could be attributed to high surface energy. It was observed that the spherical particles tend to form rods (highlighted red) if calcined for a longer time after the growth process. The histogram in Figure 5.5(below) depicts the mean diameter of the particles that were calculated using Image J software and found to be 66 nm. EDAX analysis has been used to examine the stoichiometry and composition of SrO. The obtained profile picture exhibits different peaks for Sr, O, C and N. The presence of C and N peaks is due to the green route synthesis of SrO. Moreover, it is evident from the obtained results that the synthesis of SrO nanoparticles using *Moringa* extract could be a better substitute for chemical synthesis that utilizes harmful chemicals.

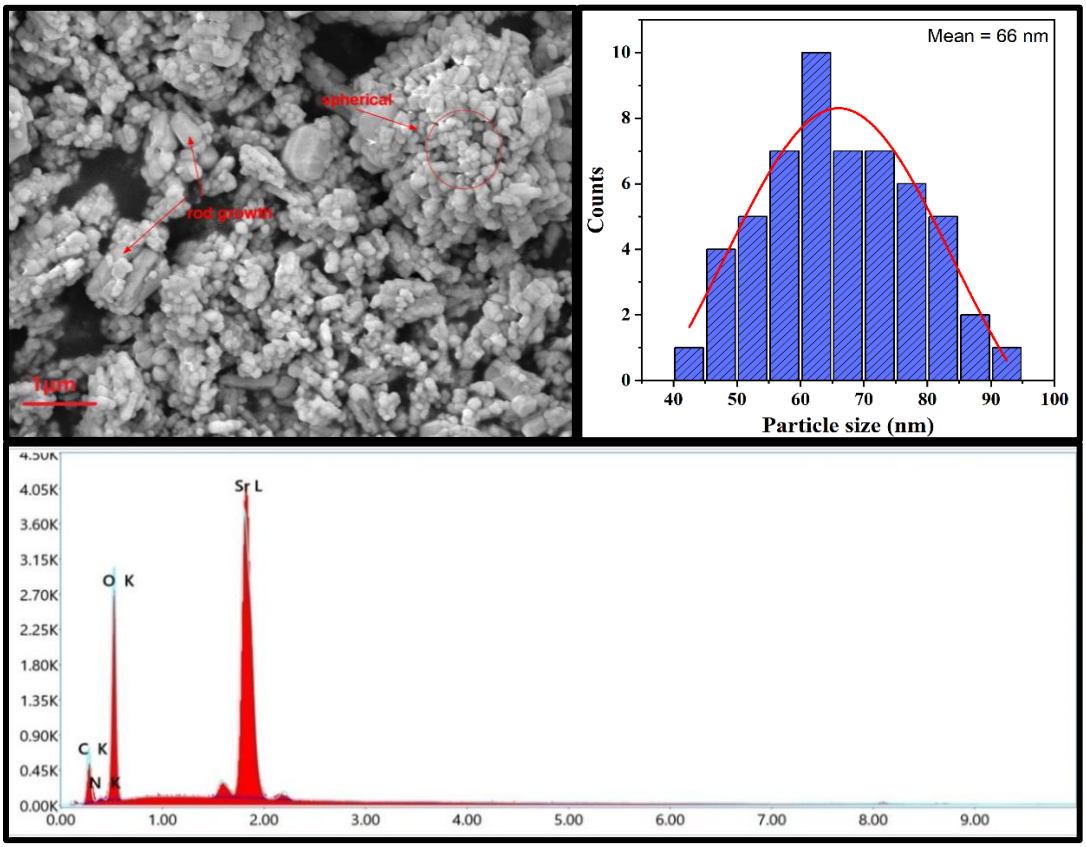

Figure 5.5.(a) FESEM Analysis with histogram (top) and (b) EDAX analysis (bottom) for SrO

The crystal patterns, phase composition and crystallite size of SrO NPs were investigated and identified using XRD (Figure 5.5). The nanoparticles without calcination exhibit predominant peaks for $SrCO_3$ (COD ref. 96-901-3803), while after calcination at 1000 °C, the carbonate was lost as CO_2, and the twin peaks at 25.10°, 25.79° and 49.88° (highlighted part) for $SrCO_3$ had disappeared, and new peaks were formed for SrO. The major peaks observed at 28.5°, 33.22°, 47.55° and 56.6° assigned to the planes (100), (110), (220) and (311) impeccably match the face-centred cubic structure of SrO (JCPDS 48-1477). The formation of intense and sharp peaks is indicative of the phase purity and crystallinity of the synthesized SrO nanoparticles. The average crystallite size (D) was calculated for SrO nanoparticles using Scherr's equation,

$$D = K\lambda/(\beta \cos \theta)$$

where β is the full width at half maximum that was obtained after fitting the plot using Pseudo-voigt fit, $K = 0.94$ (constant) and $\lambda = 1.5405$ nm, which is the wavelength of X-ray.

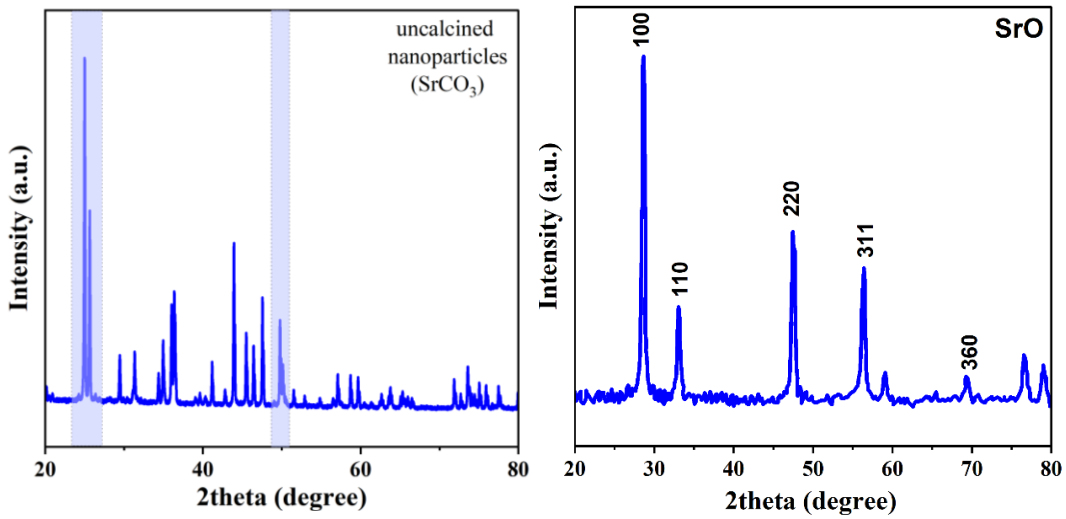

Figure 5.6. XRD patterns of uncalcined and calcined nanoparticles (highlighted part shows twin peaks specific to $SrCO_3$ that are absent in SrO)

The addition of biogenic SrO nanoparticles to biodiesel blends led to significant changes in thermophysical properties, like an increase in calorific value and a decrease in kinematic viscosity (Table 5.1). These nanoparticles were able to enhance engine characteristics by overcoming the limitations associated with biodiesel. Biodiesel is oxidatively less stable compared to diesel; hence, the formation of secondary products like hydroperoxides and acidic components is expected. Among alkaline earth metal oxides, SrO nanoparticles possess the highest base site density; hence, they can increase the stability of biodiesel by minimizing its auto-oxidation by balancing the acidic components formed during the combustion of fatty acids, thereby reducing engine wear and corrosion (Pullen & Saeed, 2012a). On the other hand, they can act as catalysts during the combustion stages of fuel, leading to complete combustion with lower fuel consumption (Saxena et al., 2017).

5.4.2 Performance characteristics

The engine performance characteristics, such as brake thermal efficiency, air-fuel ratio and brake-specific fuel consumption of all blended fuels were carried out on the VCR diesel engine at a constant speed of 1500 rpm, the compression ratio of 21.5 and at different torques (load): 4.7, 8.06, 14.5, 18.6, 24.2, and 27.9 Nm.

5.4.2.1 Effect of NPs on brake thermal efficiency

The brake thermal efficiency (BTE) of blended fuel with and without nano additives has been shown in Figure 5.7. An upward trajectory of BTE was noted when the engine load gradually increased from 4.7 Nm to 27.9 Nm for all fuel blends. The BTE of all the blends of tyre oil was plotted. Initially, the BTE was lower as a low load and further increased when the load increased up to 27.9 Nm. In the beginning, the air is mostly at atmospheric temperature and pressure, and with a fixed compression ratio (CR 21.5), the energy consumed during compression is more or less fixed regardless of the power output. However, since the energy produced during expansion is lower, the brake thermal efficiency (BTE) also decreases. Furthermore, a minuscule amount of 50 parts per million (ppm) of a nano additive was introduced to a B5TPO95 mix. This resulted in a decrease of 17.13% in the BTE as compared to the diesel fuel. However, the B10TPO90SrO100 blend exhibits a 1.77% increase in BTE compared to diesel fuel. Fuels containing nano additives typically have higher calorific values as well, and these blends facilitate full combustion by effectively using oxygen and employing high-quality splashing fuel. For example, a higher surface-to-volume proportion allows for a greater amount of fuel to react with air, improving BTE (Venkatesan & Kadiresh, 2016). However, under full load conditions, the BTE is 30.03% for diesel, 31.66% for B10TPO90SrO100, 25.50% for B5TPO95SrO50, 28.10% for B50TPO50, and 25.66% for neat biodiesel. The decrease in

efficiency is because of the resistance in the flow of fuel, slowing down combustion, poor atomization, and fuel vaporization.

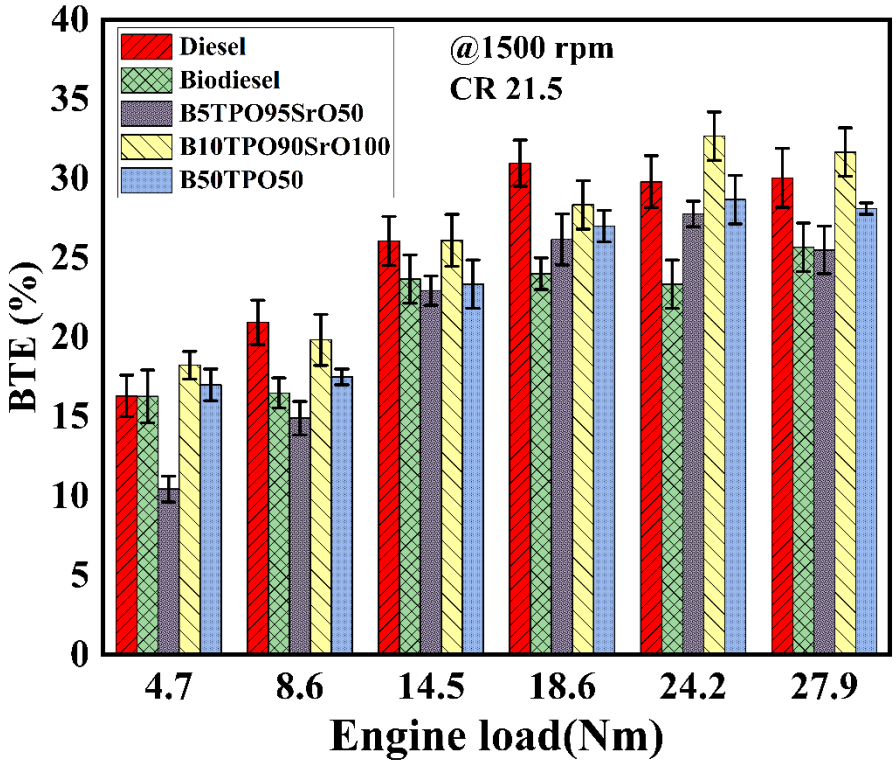

Figure 5.7.Variation of brake thermal efficiency with engine load

5.4.2.2 Effect of NPs on air–fuel ratio (AFR)

The term "air-fuel ratio," or AFR, refers to the mass ratio of air to fuel supplied into the engine (“Combustion of Hydrocarbons,” 2011). The maximum temperature, the flame front, the flame propagation velocity, the net heat release in the combustion chamber, and the degree of combustion completion are all influenced by the mixture's AFR, which also affects the combustion phenomena (N et al., 2014; Parikh et al., n.d.). Figure 5.8 depicts the impact of engine load fluctuations on air-fuel ratios for diesel, biodiesel, and TPO mixes with nano-additives at 50 and 100 parts per million. It was observed that B10TPO90SrO100 has a lower AFR compared to B5TPO95SrO50 at all loads. Furthermore, at full load, the AFRs of biodiesel, B5TPO95SrO50, B10TPO90SrO100,

and B50TPO50 decreased in comparison to diesel by 2.16%, 2.05%, 5.39%, and 3.53%, respectively. This is because of the higher amount of oxygen available in biodiesel, which improves the air-fuel ratio and promotes the combustion inside the cylinder(Parikh et al., n.d.). Moreover, the addition of NPs enhances the physical characteristics, including thermal conductivity, evaporation rate, secondary atomization, and reduced ignition delay time. These properties also create an environment that is favourable for the generation of micro-explosions during combustion, which results in air-fuel mixing and complete combustion (Keskin et al., 2007; Khond & Kriplani, 2016; Soudagar et al., 2018).

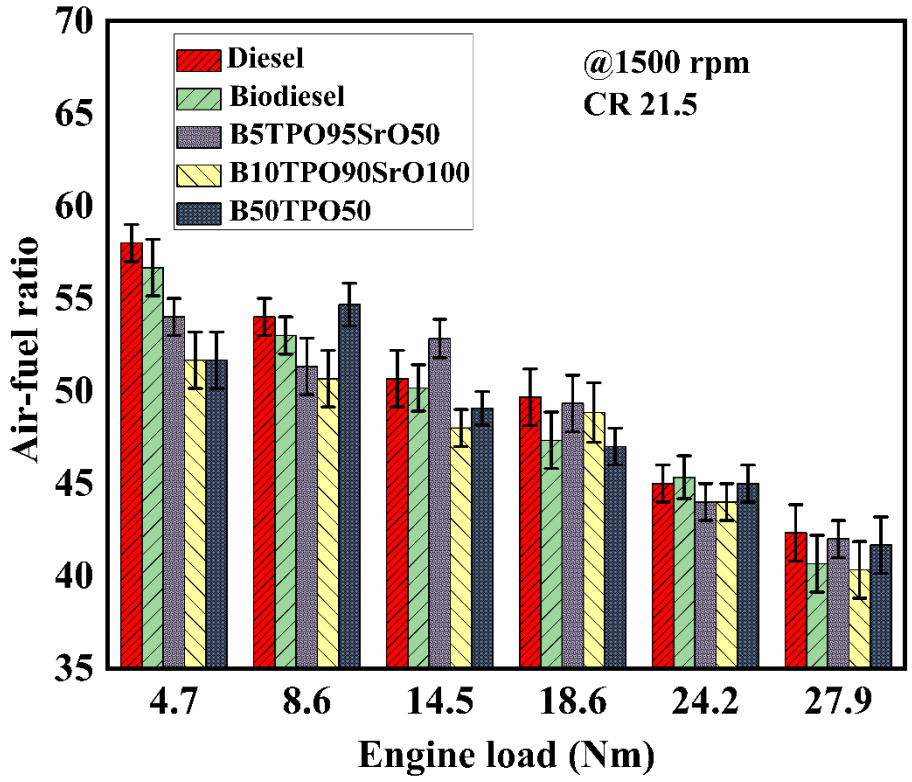

Figure 5.8.Variation of air-fuel ratio with engine load

5.4.2.3 Effect of NPs on brake specific fuel consumption (BSFC)

Break Specific Fuel Consumption (BSFC) quantifies the fuel efficiency of an engine that consumes fuel and generates rotational or shaft power**.** Figure 5.9 depicts the BSFC of the engine at varying engine loads. The fuel's calorific value, density, viscosity, cetane number, rate and duration of combustion are among the many parameters that determine

the BSFC (Ajeet Kumar Prajapati, Yogendra Yadawa, Dr. Deepak Dwivedi, 2023a; Emiroğlu & Şen, 2018; Karagoz et al., 2020). Out of them all, test fuels' lower heating values may be the most significant BSFC characteristic (Emiroğlu & Şen, 2018). The minimum values of BSFC 0.10, 0.40, 0.21, 0.11, and 0.19 kg/kWh were recorded at a 27.9 Nm engine load for diesel, biodiesel, B5TPO95SrO50, B10TPO90SrO100, and B50TPO50, respectively. All the fuels that were evaluated had average BSFC values of 0.23 (diesel), 0.44 (biodiesel), 0.38 (B5TPO95SrO50), 0.21 (B10TPO90SrO100), and 0.26 (B50TPO50) kg/kWh. Under all load conditions, it is noticeable that the diesel fuel exhibits the lowest BSFC, while the B5TPO95SrO50, B10TPO90SrO100, B50TPO50, and biodiesel fuels display higher BSFC values. This is mostly caused by the fuel's calorific value and the presence of additional aromatic components (Madiwale et al., 2017). The BSFC exhibited a consistent reduction when the load was increased across all tested fuels. This phenomenon is a result of the rise in temperature within the cylinder and the reduction in primary frictional losses. Nevertheless, the use of SrO nanoparticles enhances the BSFC outcomes. The BSFC of B10TPO90SrO100 decreased by 5.18 % in comparison to diesel (see Figure 5.9). The enhanced combustion reactivity can be ascribed to elevated quantities of nanoparticle incorporation in the mix (Murugesan et al., 2022). However, in the absence of nanoparticle additions, B50TPO50 exhibited inferior results due to weak fuel mixture formation and delayed vaporization during the premixed combustion stage. On the other hand, nanoparticle blends cause a micro-explosion of fuel droplets within the engine cylinder, improving combustion and resulting in an increase in engine performance, BSFC (Mofijur et al., 2024).

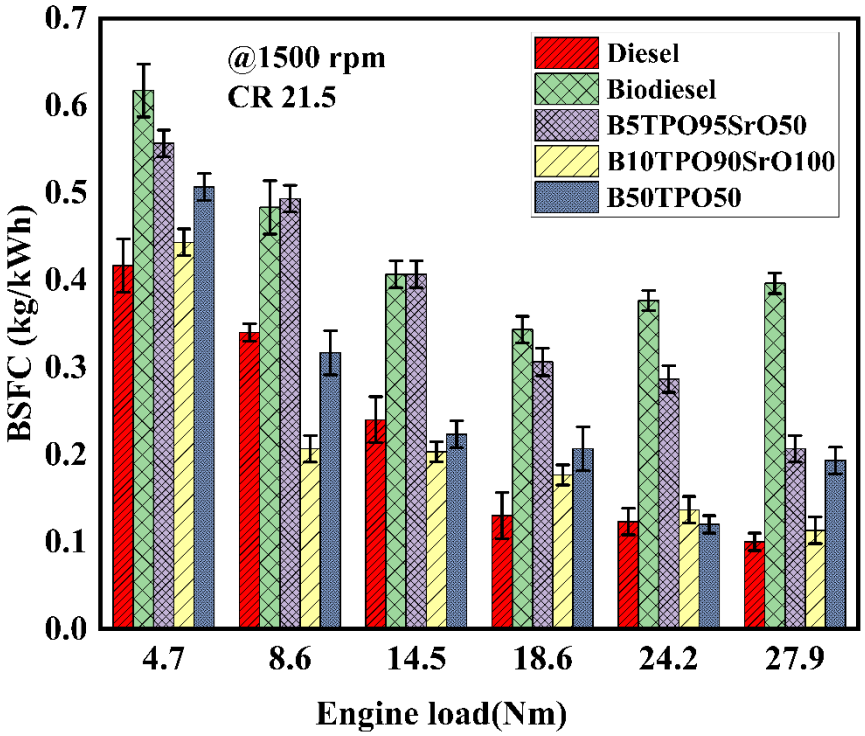

Figure 5.9. Variation of brake-specific fuel consumption with engine load

5.4.3 Combustion characteristics

This part focuses on analysing the combustion of test fuels by examining the graphs of heat release rate (HRR) and in-cylinder pressure (CP) concerning crank angle (θ), while considering different engine-varying loads. One important feature that helps with a thorough understanding of the combustion behaviour in the cylinder is the variation in the CP of ICEs, which is reliant on the state of the crankshaft (Borugadda & Goud, 2012b). The CP and HRR metrics exhibit a significant correlation with the oxygen content, viscosity, heating value, and CN of the test fuels. Figure 5.10 depicts the fluctuation of HRR at 100% loading conditions. As the working load grows from 4.7 Nm to 27.9 Nm, the in-cylinder temperature likewise rises because more fuel is being fed into the combustion chamber at higher loads(Rimkus et al., 2021). The rise in internal combustion temperature is correlated with the increase in inside cylinder pressure (CP). Upon evaluating the CP of each load collectively, it becomes evident that the top point

value of the CP rises as the engine load increases. The maximum CP was observed for B50TPO50 as 52.13 bar at full load, which is the highest among all load circumstances for the experimental blend test fuel. The maximum CP of Biodiesel, Diesel, B5TPO95SrO50, B10TPO90SrO100, and B50TPO50 at full load (27.9 Nm) was measured to be 49.63, 46.14, 48.34, 48.6, and 52.13 bar, respectively, as seen in Figure 5.11. The maximum HRR values of Biodiesel, Diesel, B5TPO95SrO50, B10TPO90SrO100, and B50TPO50 are determined to be 39.4, 49.72, 39.78, 49.16, and 41.92 J/°CA in 27.9 Nm, respectively. These CP and HRR values of B50TPO50, B10TPO90SrO100, and biodiesel test fuels exhibit higher values when compared to the regular diesel test fuels. Overall, B50TPO50 & B10TPO90Sr100 test fuels exhibit the greatest CP and HRR values for applied engine load. The source of this phenomenon can be attributed to the fuel oil's high oxygen concentration, low CN and high viscosity. These factors lead to poor fuel atomization and, as a result, a prolonged ignition delay time (Q. Zhang et al., 2022).

Additionally, in a premixed combustion zone, the fuel accumulation is higher, causing more fuel to burn during the combustion stage, which increases the pressure and cylinder temperature (Shahridzuan Abdullah et al., 2021). As the amount of TPO (max. 50%) was increased in the blends, the cylinder temperature increased because of factors such as the calorific value, density, viscosity, atomization of fuel, and volatility of the fuel, which directly affect the CT (mean gas temperature) (Babu & Anand, 2019). Figure 5.12 shows the variation of the cylinder temperature vs crank angle of blends at full load.

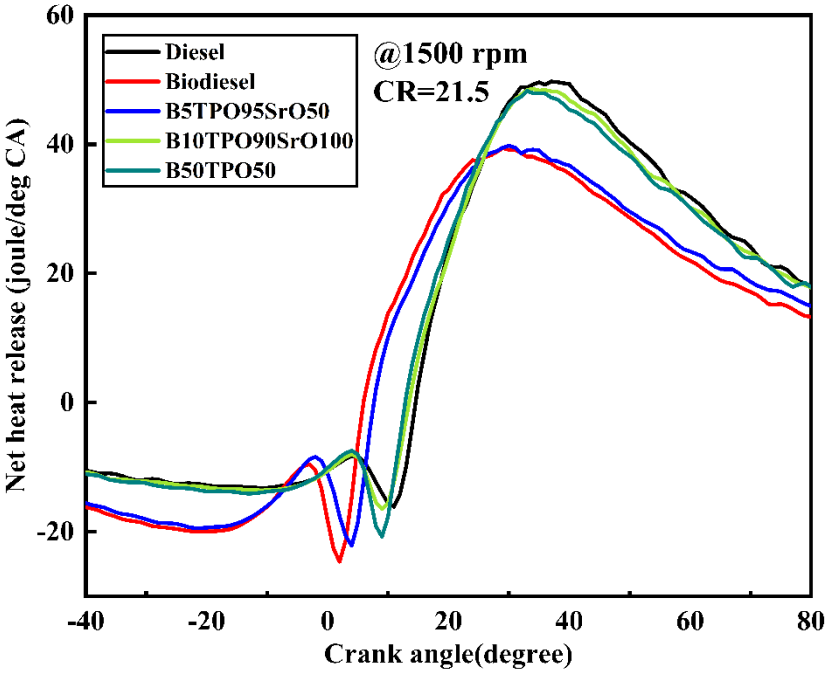

Figure 5.10. Variation of HRR at 100% loading conditions

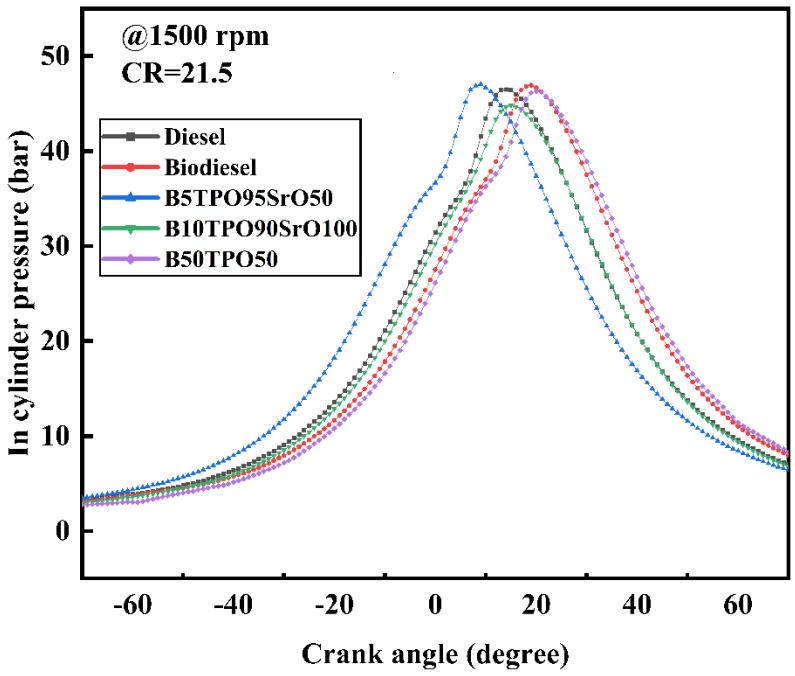

Figure 5.11.Variation of CP at 100% loading conditions

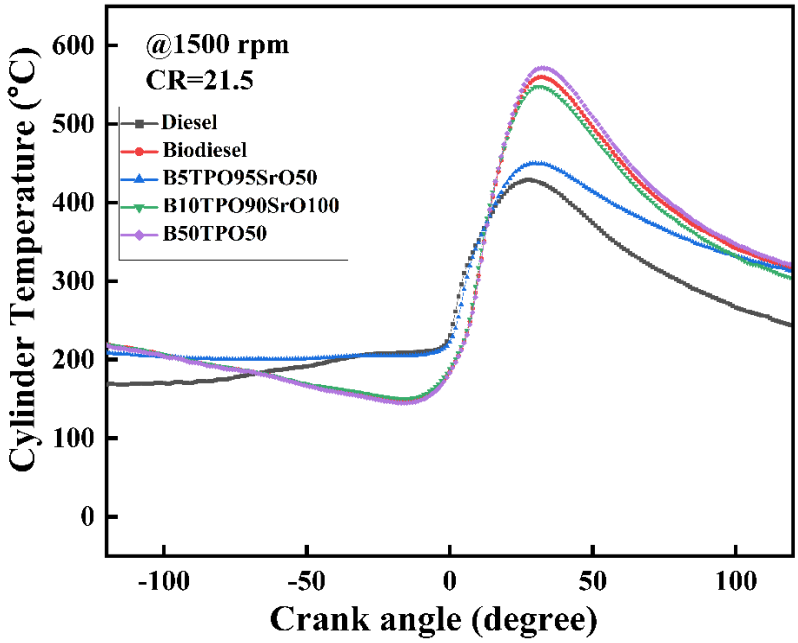

Figure 5.12.Variations of CT at 100% loading conditions

5.4.4 Emission characteristics

5.4.4.1 Effect of NPs on CO

Carbon monoxide (CO) emissions are produced due to the incomplete combustion of fuel within the engine cylinder(An et al., 2012). The key factors that determine the production of CO emissions from the exhaust are as follows: insufficient AFR, insufficient oxygen molecules, areas with excessive fuel, and insufficient time for CO to be converted to CO_2 by oxidation(Patel et al., 2019). Figure 5.13 illustrates the change in CO emissions based on engine load for blends of tyre pyrolysis oil, both with and without the use of nano-additives. In addition, the introduction of NPs into the mix of biodiesel-waste tyre pyrolytic oil resulted in decreased CO emissions. This is because the oxygen content increases when biofuels are added to the fuel blends(Erol et al., 2023; J. Liu et al., 2023). If the oxygen level in the mixes is higher, full combustion will occur(El-Shafay et al., 2023). Similarly, when there is a shortage of oxygen atoms, the fuels cannot undergo

complete oxidation or may only undergo partial oxidation. This will result in an increase in CO emissions, which is a byproduct of incomplete combustion(Lott & Deutschmann, 2023). The fuel/air equivalency ratio had a substantial impact on CO emissions because biodiesel oxygen content allows for leaner combustion than diesel(Kaya & Kökkülünk, 2023; Vellaiyan et al., 2018). The highest levels of CO emissions are seen when the engine is fuelled with regular diesel fuel and operated at a certain engine load. Another contributing factor to the increased CO emissions in conventional diesel is the greater carbon-to-hydrogen (C/H) ratio compared to other fuel additives(Zuo et al., 2022). The visibility of CO emissions altered when additives were introduced into normal diesel fuel, considering the cumulative engine loads.

In this regard, the addition of 50ppm NPs tyre pyrolysis oil (B5TPO95SrO50) resulted in a 2.72 % increase. Nevertheless, the B10TPO90SrO100 test fuel had a decrease of 15.27 %, while the B50TPO50 and biodiesel test fuels saw declines of 5.49 % and 27.59 % respectively. In brief, the introduction of biofuels increased the amount of oxygen in the biodiesel blends derived from waste tyre pyrolysis oil, resulting in an optimised reduction of CO emissions. The existing literature has provided evidence of similar results and their underlying causes, demonstrating that the use of biodiesels, alcoholic fuels, and pyrolytic oils in diesel engines leads to a reduction in CO emissions. Akcay and Ozer (Akcay & Ozer, 2019) found that adding fuel oil to mineral diesel fuel resulted in decreased CO emissions across all engine load situations. The reduction increased as the ratio of fuel oil in the blend increased. Ultimately, the improved combustion efficiency is a result of the increased oxygen content seen in alcohol-based fuels.

The researchers noted that the CO emissions seen under various loading situations were caused by the distinct features of the fuels used. Patel et al.(Patel et al., 2019) reported that biodiesel fuels exhibited greater levels of CO emissions compared to conventional

diesel fuels under most loading settings. This can be attributed to the somewhat higher viscosity properties of biodiesels, which result in inadequate spray atomization and therefore increased droplet size dispersion.

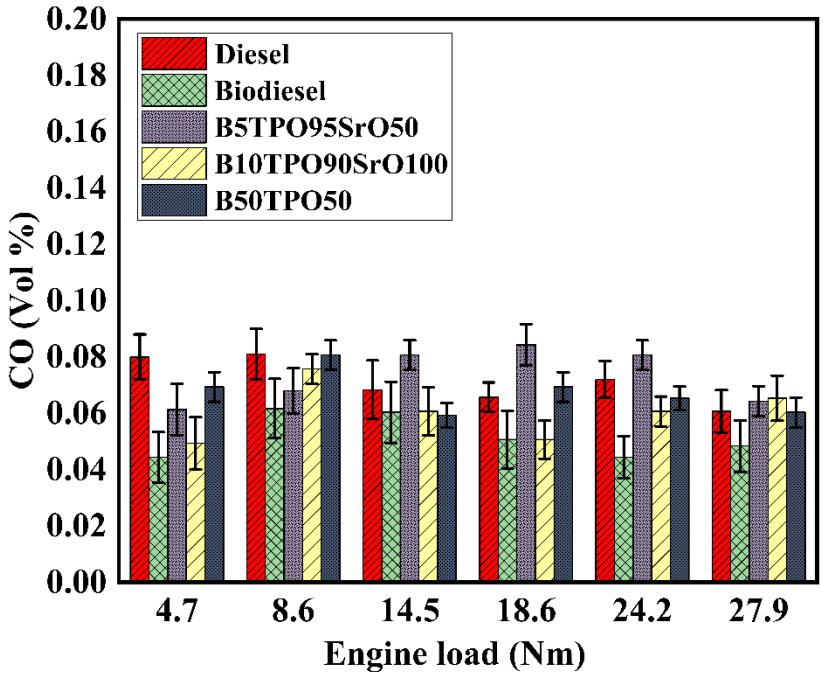

Figure 5.13.Variations of CO emissions as a function of engine load

5.4.4.2 Effect of NPs on HC

The hydrocarbon emissions of the nano-additive blends are lower than those of standard diesel due to the complete combustion process, as illustrated in Figure 5.14. This reduction in HC emissions is attributed to many factors and is known to be primarily dependent on engine operating conditions, fuel properties, and fuel atomisation, as highlighted in previous studies (X. Wang et al., 2022). All blends, such as B5TPO95SrO50, B10TPO90SrO100, B50TPO50, and biodiesel, showed a noticeable reduction in HC emissions as compared to the reference (commercial diesel). The nano-additive blends, on average, showed a significant decrease in HC emissions. Specifically, biodiesel, B5TPO95SrO50, B10TPO90SrO100, and B50TPO50 exhibited reductions of 13.38%, 15.56%, 15.84%, and 2.78 %, respectively, compared to regular diesel. The large

reactive surface area of nanoparticles and the high oxygen concentration in oxygenated alcohols may have contributed to the notable decrease in HC emissions by improving fuel combustion. Furthermore, the decrease in HC emissions to the elevated temperature within the cylinder and the quick pace at which heat is released may have promoted the oxidation process of unburned hydrocarbons(A. I. Tariq & Saleh, 2023). Consistent observations were reported by Ghanbari et al. (Ghanbari et al., 2021) and Najafi (Najafi, 2018), further supporting the positive impact of fuel additives on reducing HC emissions.

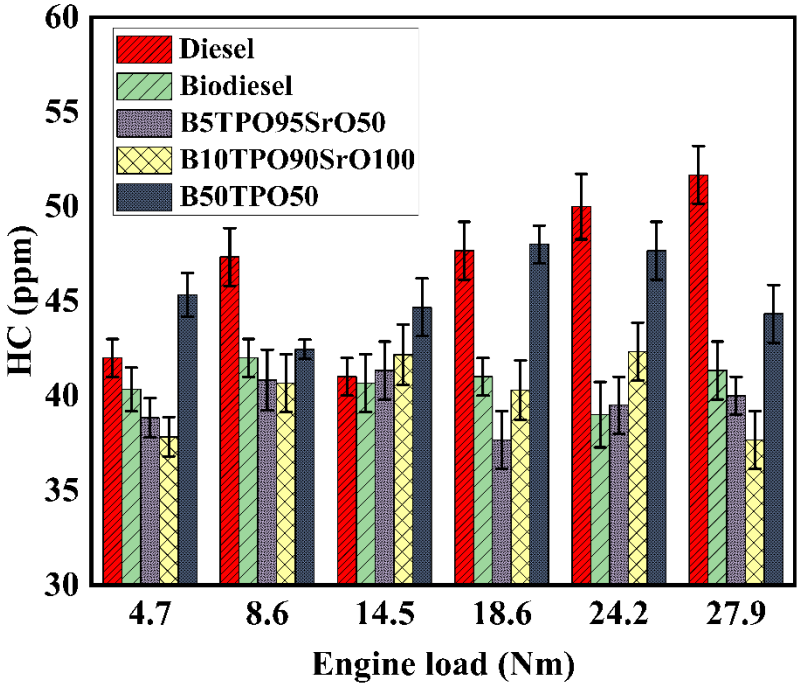

Figure 5.14.Variations of HC emissions as a function of engine load

5.4.4.3 Effect of NPs on NOx

NOx emissions arise as a result of elevated temperatures within the combustion chamber(Sharon et al., 2013). As the engine load rises, the temperature within the cylinder also rises, leading to an increase in NOx emissions with increasing engine loads, as shown in Figure 5.15. The NOx emissions of biodiesel, B5TPO95SrO50, B10TPO90SrO100, and B50TPO50 are greater than those of ordinary diesel due to the higher CN of the test

fuel. This higher CN improves the fuel's combustion performance, leading to an increase in CP and subsequently higher NOx emissions. Conversely, a lower CN and shorter ignition delay result in less retention of hot gases in the combustion chamber during high temperatures, hence resulting in decreased NOx emissions. Numerous studies in the literature have extensively discussed these underlying causes(Atmanli et al., 2014; Valentino et al., 2012). Also, without the addition of nanoparticles in the tested sample, the B50TPO50 has the highest NOx emission due to the biodiesel work, as high oxygen content rises, the CP and the gas temperature rise. Nevertheless, the presence of oxygen and the release of latent heat during evaporation have a beneficial impact on combustion, particularly in terms of reducing NOx emissions. The findings of this study indicated that the influence of those two parameters outweighed the impact of CN on NOx emissions. The increase in temperature and pressure within the cylinder was a result of the enhanced combustion of diesel fuel, achieved by including SrO as a fuel additive. Pan et al.(Pandey et al., 2023) asserted that emissions rise for both diesel and TPO blends, with a progressive increase in the loads. Their research findings indicate a significant rise in NOx emissions due to elevated temperature and pressure within the combustion chamber, which is opposite to the present study. The increased NOx emissions can be attributed to the substantial oxygen concentration in ternary fuel blends, resulting in thorough fuel combustion and elevated in-cylinder temperatures(Pote & Patil, 2019).

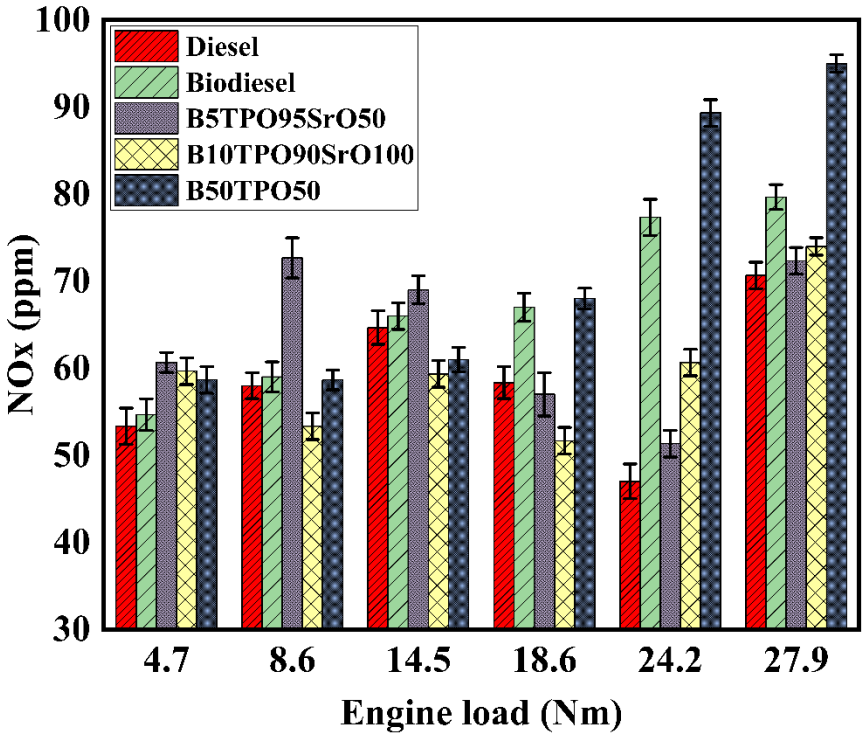

Figure 5.15.Variations of NOx emissions as a function of engine load

5.4.4.4 Effect of NPs on CO_2

When fuels with carbon atoms in their chemical compositions are burned at high temperatures during the post-combustion phase of ICEs, CO_2 is the byproduct of full combustion (Nanthagopal et al., 2018). Enough oxygen present in the combustion chamber is responsible for the CO_2 in the exhaust emissions. Additionally, CO is converted to CO_2 by the hydroxyl radical with the adequate participation of oxygen (Nema et al., 2023). In actuality, a large portion of the greenhouse gases produced worldwide is accounted for by CO_2 emissions alone (Chataut et al., 2023). The carbon-to-hydrogen (C/H) ratio and oxygen content of the test fuels have a direct impact on the variation in CO_2 emissions (Çakmak & Özcan, 2022). In this investigation, Figure 5.16 illustrates the CO_2 emission profile at various engine loads for the conventional diesel test fuel compared to biodiesel blends B5TPO95SrO50, B10TPO90SrO100, and B50TPO50. The biodiesel showed a 5.76 % decrease in CO_2 emissions, while B5TPO95SrO50

exhibited a 2.69 % increase. In contrast, B10TPO90SrO100 resulted in a 7.69 % reduction, and B50TPO50 demonstrated a 4.35 % decrease in CO_2 emissions compared to the conventional diesel test fuel. Therefore, it was determined that the higher fuel injection volume in the combustion chamber was the cause of increased CO_2 emissions with increasing engine load(Mohamed Shameer et al., 2017; Park et al., 2012). Furthermore, several studies noted that for a particular test fuel, higher CO_2 emissions have been associated with a thorough combustion process(Babu & Anand, 2017). Although diesel fuel has a higher carbon-to-hydrogen (C/H) ratio than biodiesel, it generally shows lower CO_2 emissions when compared to other test fuels (Prabhu et al., 2023). According to Zareh et al. 2017 (Zareh et al., 2017) and Amid et al. 2020 (Amid et al., 2020), mixing biodiesel with diesel or other fuels significantly reduces fuel consumption, which can outweigh their lower energetic content when compared to diesel fuel for the same amount of work. Another explanation is that biofuels' higher oxygen atoms are reacting with higher carbon atoms of the tyre pyrolysis oil, thereby increasing CO_2 emission for B5TPO95SrO50 but decreasing in the case of B50TPO50 and B10TPO90SrO100.

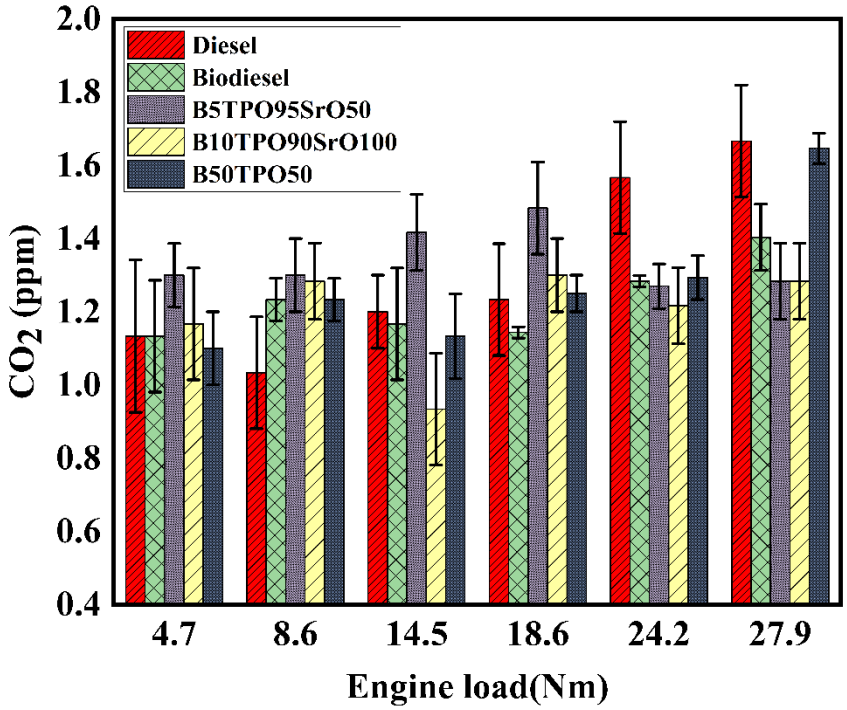

Figure 5.16.Variations of CO_2 emissions as a function of engine load

In general, the addition of nanoparticles (NPs) can enhance fuel combustion efficiency, reduce pollutant formation, and thereby improve overall engine performance. Their high surface area facilitates better fuel atomization and more complete combustion, leading to cleaner and more efficient operation (M. Mofijur, 2024). However, during combustion, NPs may undergo oxidation or chemical transformation due to elevated in-cylinder temperatures, while some may agglomerate into larger particles or remain unreacted. Depending on their size, composition, and stability, they may subsequently deposit on engine components or be released through the exhaust stream (Tran, 2024). Such post-combustion processes, though important, are not examined in the present study as they lie beyond the scope of this thesis.

5.6 Conclusion

This study offers the prospect of employing the blend of waste tyre pyrolysis oil, UCO biodiesel, and nano-additives in diesel engines. The following results were obtained:

- Performance parameters such as BTE, AFR, and BSFC improved significantly compared to the diesel. The addition of 100 ppm SrO nano additive to the B10TPO90 fuel blend resulted in a 1.77 % increase in BTE compared to diesel. The BSFC of the B10TPO90SrO100 blend decreased by 5.18 % while the AFR for B10TPO90SrO100 decreased by 5.39 % in comparison to diesel.
- The B50TPO50 mix exhibited a cylinder peak pressure of 52.13 bar, whereas the inclusion of nanoparticles in the B10TPO90 blend resulted in a drop to 48.6 bar. The decrease in pressure was ascribed to the nanoparticles' enhancement of combustion processes, therefore approaching the 46.14 bar pressure of diesel fuel. The heat-release rate of the nano-additive-doped tyre oil blend is 48.6 J/°CA, which is greater than the blend without nano-additives, similar to the energy content of diesel fuel, 49.72 J/°CA.
- B10TPO90SrO100 decreased HC, CO, and NOx emissions by 15.27 %, 15.84% and 1.89%, respectively, in comparison to diesel fuel. The reason for this might be attributed to the increased surface-to-volume ratio, which leads to a more efficient mixing of fuel and air in the combustion chamber.
- Overall, biosynthesised SrO nanoparticles of 50 and 100 ppm were successful in improving the thermo-chemical properties of the fuel to a certain extent when compared to diesel. These additives are eco-friendly and can be mass-produced.

Chapter 6

Effect of different biodiesels on corrosion of nickel alloy[5]

[5]The result discussed in this chapter have been published in Journal of the Materials Today Sustainability. 2024;28:100968. https://doi.org/10.1016/j.mtsust.2024.100968

6.1. Introduction

Biodiesel is mostly compatible with existing diesel engines, as its thermophysical properties, such as density, viscosity, oxidation stability, flash and fire points, pour and cloud points, and calorific value, closely resemble those of conventional diesel (Tsoutsos et al., 2019). However, a significant concern arises regarding its susceptibility to corrosion. The corrosive tendency of biodiesel is primarily linked to its higher free fatty acid and water content, which makes it more aggressive than conventional diesel (Oni et al., 2022; Sorate & Bhale, 2015). The extent of this degradation depends strongly on the type of feedstock used and often affects critical components such as fuel tanks, pipelines, and injection systems. Prolonged exposure intensifies this damage in metals such as copper, carbon steel, aluminium, and stainless steel, ultimately undermining durability, efficiency, and safety (Abdulqadir, 2017; Kumar & Ashok, 2023; S. Zhang et al., 2020).

To address these challenges, the present chapter moves beyond UCO biodiesel alone and incorporates Jatropha Oil Biodiesel (JOB) and Karanja Oil Biodiesel (KOB) in order to comparatively evaluate their corrosive behaviour. This broader investigation enables the identification of which biodiesel feedstock is more aggressive toward metallic materials under realistic conditions. At the same time, attention is directed toward identifying materials capable of resisting such degradation. Nickel-based alloys, particularly UNS718 (Inconel 718), have demonstrated superior resistance to corrosion, high mechanical strength, durability, and stability against oxidation at elevated temperatures (Abdulqadir, 2017). Nevertheless, they are not completely immune to all forms of degradation, especially in environments prone to pitting or crevice corrosion, such as fuel blends with high oxidative potential. Against this background, the present chapter

investigates the corrosion behaviour of UNS718 when exposed to biodiesel derived from used cooking oil (UCO), Jatropha, and Karanja. The objective is to evaluate the extent to which this alloy resists or reacts to the chemical environment of these biodiesels under realistic conditions. By systematically assessing its corrosion performance, this study aims to determine whether UNS718 can serve as a more reliable material for biodiesel storage tanks and fuel delivery systems, thereby contributing to the safe and efficient adoption of alternative fuels in the transportation sector.

6.2. Materials and methods

6.2.1. Biodiesel production

Steps involved in the production of biodiesels derived from Karanja (KOB), Jatropha curcas (JOB), and used cooking oil (UCOB) using high-pressure-high temperature (HPHT) autoclave technology are delineated in detail elsewhere (**as shown in Figure A1**) (Ajeet et al.:2023b).

6.2.2 Coupons preparation

A test was conducted to measure the corrosion resistance of Ni alloy (UNS718) in three different types of biodiesel fuels: Karanja (100%), Jatropha curcas (100%), and used cooking oil (UCOB) (100%). To prepare for the test, specimens were cut from the Ni alloy rod purchased from *M P Steel Solutions, Mumbai* (material composition as shown in Table 1). Round bars were used to machine and grind test coupons (Coupons with dimensions of 11.9038 mm (length), 11.9038 mm (width) and 1mm (thickness)), which were then polished with silicon carbide papers (grade: 400 to 1,200), washed with distilled water, degreased with acetone and dried with argon gas. Each coupon was then immersed in a biodiesel fuel containing 30ml of biodiesel samples (Karanja (100%), Jatropha curcas (100%), and UCO (100%)) for different time durations (e.g. 720, 1440 and 2160 hrs) at

27±2 °C. After each immersion test, the coupons were cleaned with an ultrasonic cleaner (*Spire Automation*, model no. US-2) for 5 minutes in acetone to remove any corrosion products. The weight loss of each coupon was measured using a digital balance with up to four-digit accuracy. The corrosion testing has been performed three times by weighing each sample thrice to ensure reproducibility and minimize the experimental error (experimental errors were in the range of ~1.15% -1.65% in CR measurement).

Table 6.1. Composition of Ni alloy (UNS718)

Elements	**C**	**Si**	**Mn**	**P**	**S**	**Cr**	**Mo**	**Ni**	**Al**	**Co**	**Cu**	**Nb**	**Ti**
Composition (in wt.%)	0.0430	0.200	0.400	0.090	0.100	18.200	2.900	52.200	0.400	0.500	0.200	4.900	0.700

6.2.3 Surface characterization and spectroscopic analysis

The morphology of corrosion products on both pure and corroded Ni alloy samples was examined using a field emission scanning electron microscope (FESEM) (*JSM-7900F,* JEOL, Japan), with an attached EDS for qualitative elemental analysis, and elemental mapping corresponding to BSE (backscattered electron) images was recorded by energy dispersive spectroscopy (EDS). The surface properties of the biodiesel-immersed coupons were comprehensively analysed using various techniques, including X-ray fluorescence analysis (XRF), X-ray diffraction analysis (XRD) [*Empyrean-QTY1* diffractometer (Malvern PANalytical) with a *Cu Kα* (1.54 Å) radiation source, 2θ range (5–90 degrees) with step size of 0.0070] and Fourier transform infrared spectroscopy (FTIR) [*Nicolet iS20* model from Thermo Electron Scientific Instruments, LLC (spectra range from 400 cm^{-1} to 4000 cm^{-1} with the resolution of 0.09 cm^{-1}) spectral resolution of 0.25 cm^{-1} and single-to-noise ratio (50,000:1)]. X-ray photoelectron spectroscopy (XPS) [Thermo Fisher Scientific, *K-Alpha* (monochromatic *Al Kα* source (15 mA, 14 kV)] was

used to investigate the compositional features of the corroded surface of the Ni alloy, whereas XRF [*LE neo^{R} Fusion (Claisse LE neo FLUXER)* PANalytical] provided additional insights on compositional features of the corroded surface of the Ni alloy with its versatile excitation parameters and concentration range. A *JEOL 400 YH NMR* machine was used to record proton and ^{13}C NMR spectroscopic data in CdCl3 at 25 °C.

6.3. Results and discussion

6.3.1 Corrosion rates calculation

At the end of the test, we determined the average weight loss for the coupons and measured the corrosion rate using Equation (6.1)(Sterpu et al., 2024)

$$\text{Corrosion Rate (CR)} = \frac{8.76\times10000\times\Delta m}{\rho\times A\times T} \quad \ldots\ldots\ldots\ldots\ldots\ldots \quad (6.1)$$

The corrosion rate is measured in millimetres per year (mm y^{-1}). Here in eq. (1), W_1 is the weight before corrosion (in grams), W_2 is the weight after corrosion (in grams), Δm is the weight loss (in grams), ρ is the metal density (in grams per cubic centimetre), T is the exposure time (in hours), and A is the exposed surface area (in square meters). The density of the Ni alloy (UNS718) was determined to be 8.19 g/cm³, and the exposed surface area was 1.417 cm².

Coupons of Ni alloy (UNS718) were exposed to different biodiesel fuels (e.g. JOB, KOB and UCOB) and remained immersed for 30 days (720 hours), 60 days (1440 hours) and 90 days (2160 hours). It was evident that the corrosion rate of the Ni alloy exposed to all three biodiesel solutions was found to decrease with increasing immersion time. This elucidates the formation of passivating films on the surface of the Ni alloy (UNS 718) coupons. It was noteworthy that the corrosion rate of JOB (0.000699 mm/year) was found to be lower than the other two biodiesels, such as KOB (0.001048 mm/year and UCOB (

0.001398 mm/year) after 2160 hours immersion (see Figure 6.1). On the other hand, it was highlighted that the corrosion rate of Ni alloy (UNS718) was higher for all three biodiesels for the short period of exposure (720 hours) than for the longer exposure time (2160 hours). KOB was found highly corrosive for Ni alloys as compared to the other two biodiesels (see Figure 6.1); however, from the industrial engineering point of view, Ni alloy was found suitable as the material of construction (MOC) of biodiesel storage tanks, particularly at low temperature (at 27±2 °C).

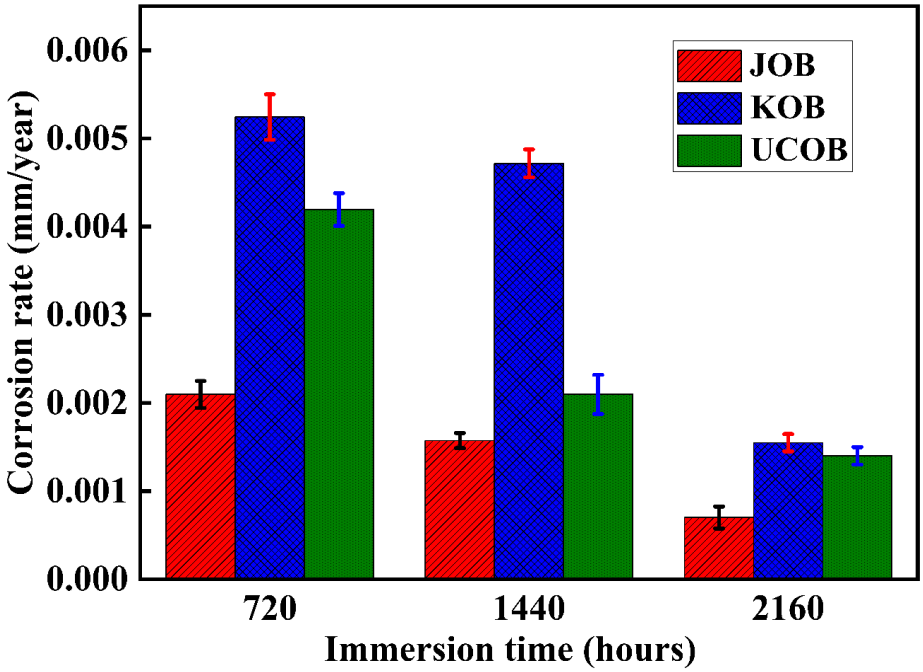

Figure 6.1. Corrosion rate (in mm/year) of Ni alloy (UNS 718) exposed to KOB, JOB and UCOB for 720, 1440 and 2160 hours

6.3.2 Surface characterization

Field-emission Scanning Electron Microscopy (FESEM) images of a Ni alloy exposed to different biodiesels (JOB, KOB, and UCOB) confirmed the formation of corrosion products on the surface due to the degradation of the biodiesels over time (Chandran et al., 2023a). Elemental mapping and Energy Dispersive X-ray Spectroscopy (EDS) were

conducted for all corroded samples, as shown in Figure A2. Additionally, the optical microstructures of the corroded samples are provided in Figure A3.

6.3.2.1 Morphological analysis of corroded alloy after 720 hours using FESEM

The Ni alloy exposed to KOB, JOB, and UCOB showed the formation of corrosion products on the surface, as confirmed by FESEM and EDS analysis. The EDS spectra indicated the presence of Cr, O, Ni, and Fe, along with Al, Mn, and Zn (not shown in the figure), as well as carbon. This is attributed to the development of passive oxides on the surface. As previously mentioned, the corrosion rate of the Ni alloy after 720 hours was higher for all three biodiesel solvents compared to the alloy exposed for 1440 and 2160 hours. We anticipate that the formation of a denser and more coherent corrosion product/oxide layer would have formed as the immersion time increases. While the film growth began after 720 hours of exposure, we believe there was a sufficient supply of diffusing species (e.g., O) and alloying elements (e.g., Cr, Fe, etc.) from the parent alloy (through outward diffusion) after 720 hours, which could have led to the formation of a dense passive layer, resulting in a lower corrosion rate as the exposure time increased. Figure 6.2(a), (b), and (c) show FESEM and EDS images of coupons submerged in KOB, JOB, and UCOB environments for 720 hours. The corrosion products formed on the surface exhibited cracks and pits, as shown in Figure 6.2(b) and 6.2 (c)(Chandran et al., 2023b; G. S. Frankel & Sridhar, 2008; Haseeb et al., 2010; Ramos et al., 2009)

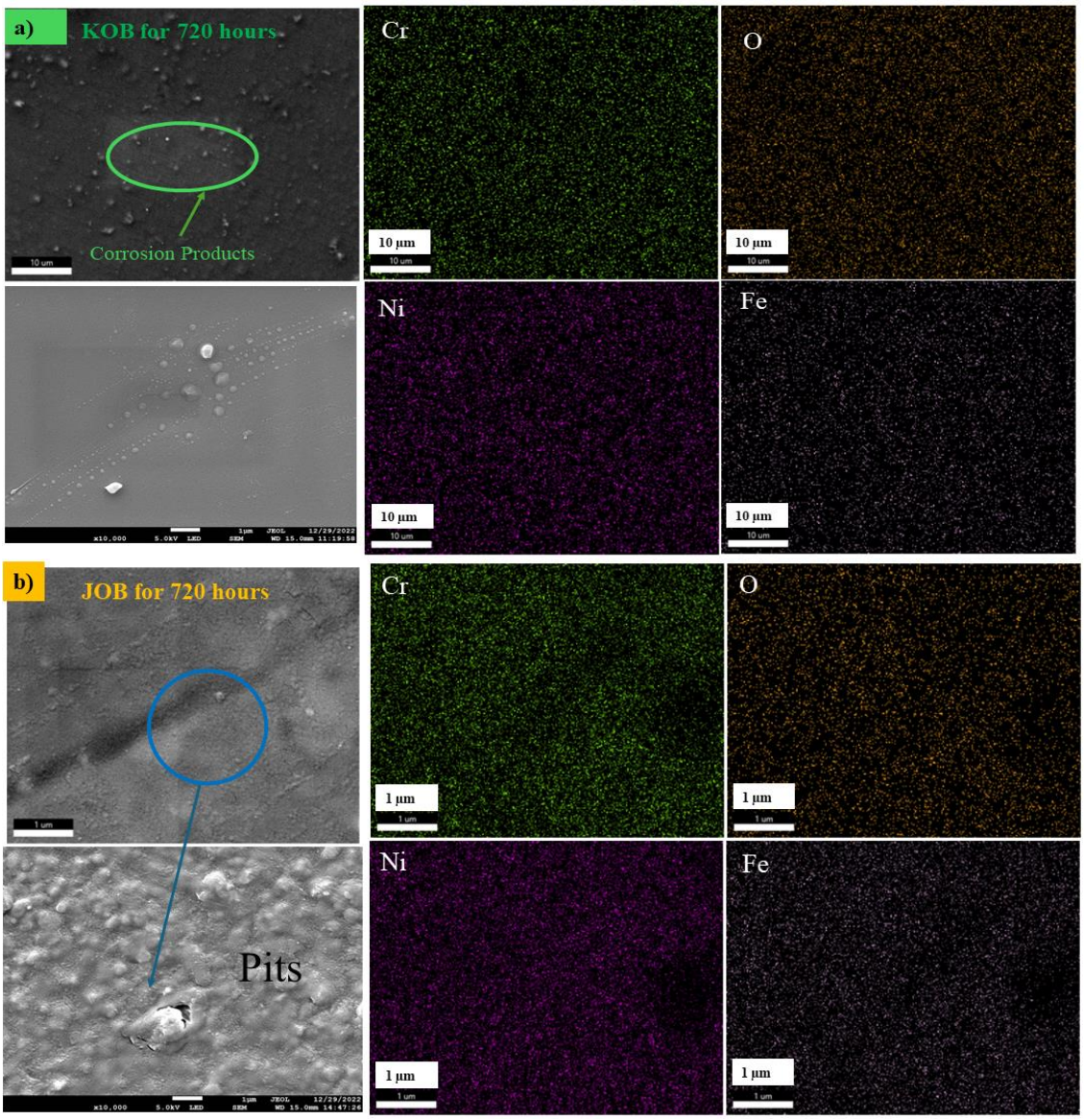
a)
KOB for 720 hours
Corrosion Products
Cr
O
Ni
Fe
b)
JOB for 720 hours
Pits
Cr
O
Ni
Fe

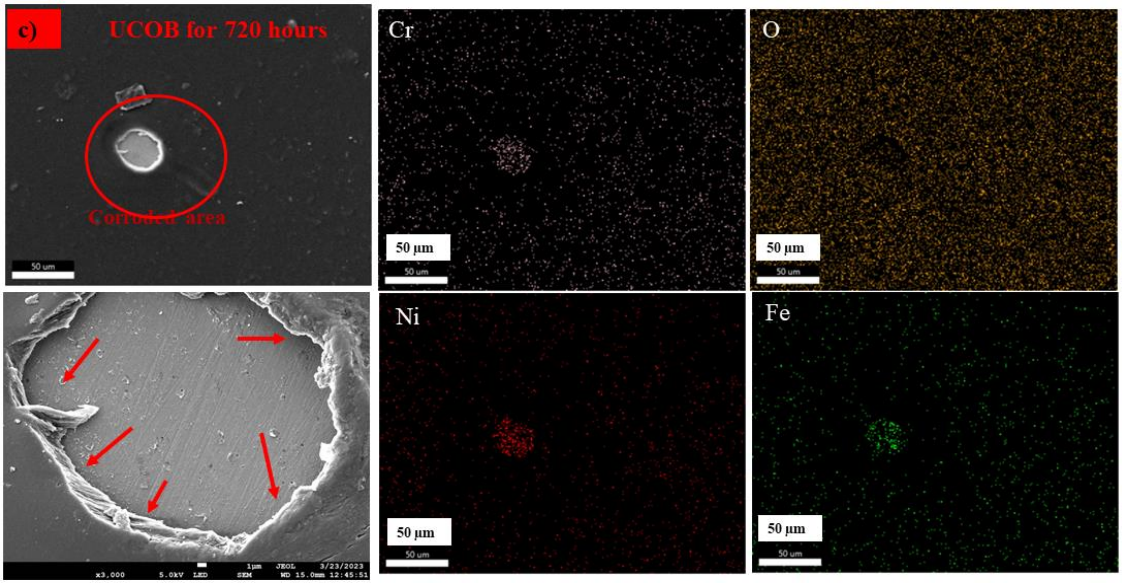

Figure 6.2. FESEM and EDS images of Ni alloy (UNS718) for exposure time 720 hours in (a) KOB, b) JOB, c) UCOB

6.3.2.2 Morphological analysis of corroded alloy after 1440 hours using FESEM

Images 6.2(d), 6.2(e), and 6.2(f) show the formation and chemical mapping of corrosion products on the Ni alloy after exposure for 1440 hours in JOB, KOB, and UCOB. Micro holes were observed in addition to the oxide film (see Figure 6.3(d)(Meenakshi & Shyamala, 2015a). Figure 6.3 (e) indicates localized corrosion (UCOB) and surface degradation of the Ni alloy, along with inconsistency in oxide formation. On the other hand, Ni alloy exposed to JOB shows an intact dense passive layer (with some cracks), which makes JOB less corrosive for Ni alloy compared to other biodiesels (see Figure 6.3 (f)). In conclusion, KOB, JOB, and UCOB are found to be corrosive to Ni alloy, similar to other biodiesels derived from different feedstocks such as palm (Meenakshi & Shyamala, 2015b), ghee butter (Milano et al., 2021), Moringa oleifera Lam (Fernandes et al., 2019), sunflower (Cursaru et al., 2014), Aegle marmelos Correa (R et al., 2022; Thangarasu & Anand, 2019), rapeseed (Su et al., 2013), and poultry fat (Geller et al.,

2008) biodiesel, however, JOB was found better than KOB and UCOB in terms of offering corrosion in Ni alloy.

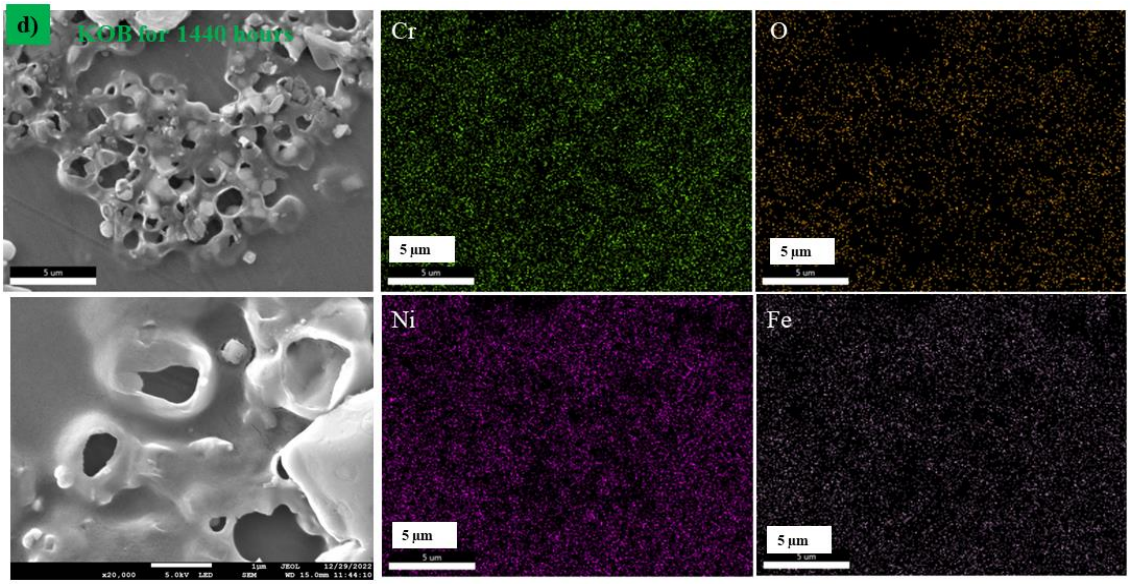

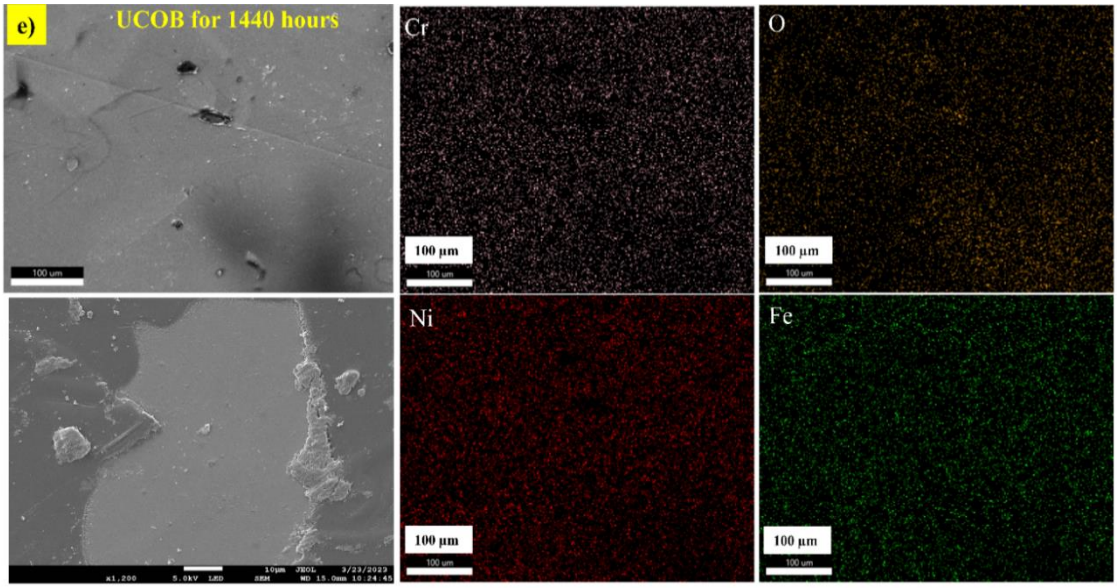

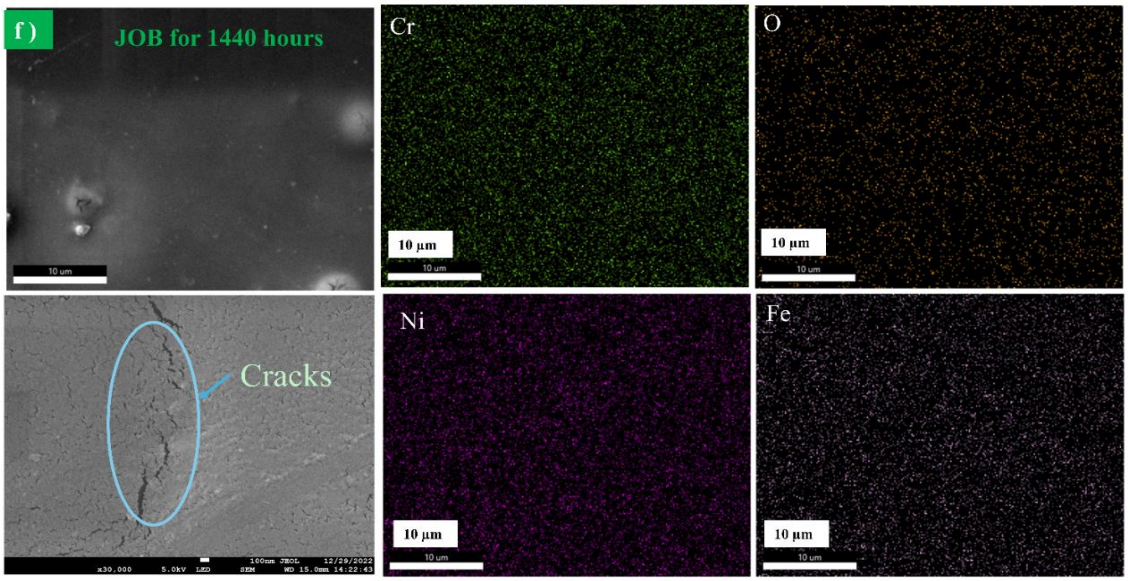

Figure 6.3. FESEM and EDS images of Ni alloy (UNS718) for exposure time 1440 hours in d) KOB, e) UCOB, f) JOB

6.3.2.3 Morphological analysis of corroded alloy after 2160 hours using FESEM

The corrosion products formed on Ni alloy (UNS718) samples immersed in KOB, JOB, and UCOB for 2160 hours are shown in Figure 6.4(g), (h), and (i) along with corresponding EDS spectra. It is important to note that the corrosion rate for JOB was the lowest compared to KOB and UCOB. The Ni alloy immersed in JOB for 2160 hours exhibited the lowest corrosion rate due to the formation of a dense protective layer on its surface, with nano-sized cracks (refer to Figure 6.4(h)). On the other hand, examination of the morphologies developed on the Ni alloy surface after exposure to KOB and UCOB for 2160 hours confirmed the presence of a discontinuous corrosion film with pits (see Figure 6.4(g) and Figure 6.4(i)). Additionally, large micron-sized pits were observed on the Ni alloy exposed to UCOB, indicating localized accelerated attack, which resulted in a higher corrosion rate compared to KOB, where only small pits in the nanometre range were observed.

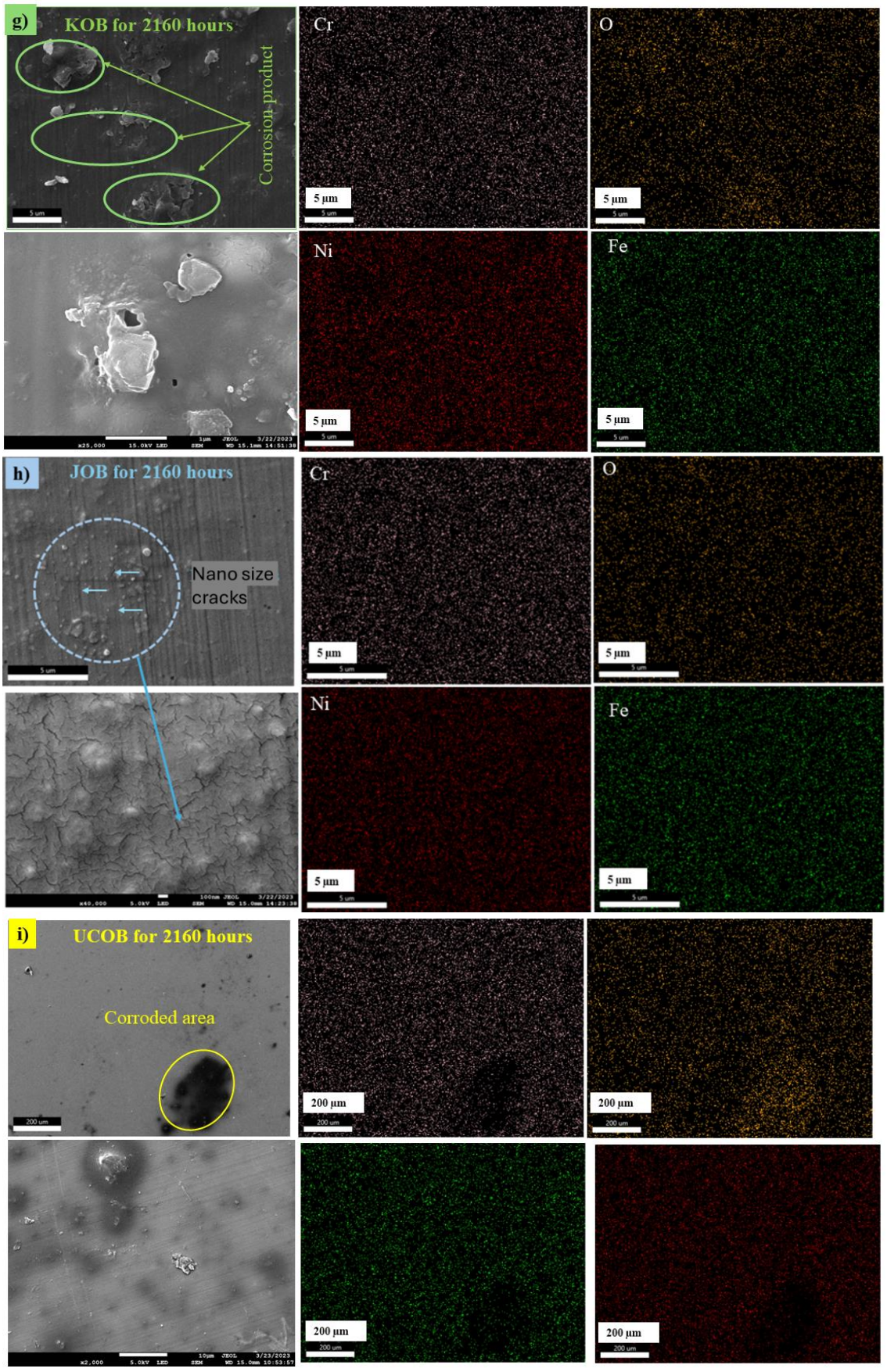
g)
KOB for 2160 hours
Corrosion product
Cr
O
Ni
Fe
h)
JOB for 2160 hours
Nano size cracks
Cr
O
Ni
Fe
i)
UCOB for 2160 hours
Corroded area

Figure 6.4. FESEM and EDS images of Ni alloy (UNS718) for exposure time 2160 hours in g) KOB, h) JOB, i) UCOB

6.3.3. XRF analysis

To better understand the corrosion mechanisms of Ni alloy (UNS 718) when exposed to different biodiesels derived from various feedstocks, XRF analyses were performed on samples subjected to KOB, UCOB, and JOB for 720 and 1440 hours, respectively (refer to Tables 6.2 & 6.3). Additionally, a fresh Ni alloy (UNS 718) substrate was characterized using XRF. Notably, the formation of passive corrosion products such as Cr_2O_3, Al_2O_3, Fe_2O_3, MnO, NiO, etc., was observed on the fresh Ni alloy (UNS 718) substrate, contributing to its passivation. However, upon exposing the same substrate to UCO for 720 and 1440 hours, it was observed that the NiO passive layer remained largely intact until 720 hours but began to detach after 1440 hours. This detachment could be attributed to ion migration at the liquid (UCO)-solid (substrate) interface. NiO was found to be unstable in KOB solutions when Ni alloy coupons were immersed for 720 and 1440 hours. It was observed that the wt. % of NiO increased gradually over time, indicating unstable NiO layer formation on the Ni alloy when exposed to KOB. Conversely, stable NiO was found in the case of JOB. XRF analysis of the JOB solution after 720 and 1440 hours confirmed a lower amount of NiO present in terms of percentage in the solutions, affirming the passivation of Ni alloy through intact NiO formation. These results were further confirmed by measuring the corrosion rate of the Ni alloy after exposure to JOB for 720 and 1440 hours, which was lower than that of KOB and UCOB (refer to Figure 6.1). Moreover, a higher corrosion rate of the Ni alloy was observed for KOB (720 and 1440 hours) compared to the others, which was supported by XRF analysis. XRF analysis revealed the aggressive nature of KOB, hindering the formation of coherent passive layers such as NiO, Fe_2O_3, and Cr_2O_3, as seen in Table 6.2. These results were also supported

by FESEM images captured of Ni alloys exposed to KOB for 720 and 1440 hours, where a significant number of cracks were noticed, indicating passivation disturbance and leading to a higher corrosion rate. The Ni alloy exposed to UCO biodiesel exhibited a lower corrosion rate than KOB until 1440 hours; however, it was found to be more aggressive towards Nb_2O_5, as confirmed by XRF and FTIR (refer to Figure 6.15). These passive corrosion products were also found in KOB, JOB, and UCOB.

Table 6.2. XRF analysis after 720 hours of immersion

Oxide (wt. %)	**KOB**	**JOB**	**UCOB**	**Nickel alloy UNS718**
Al_2O_3	0.682	0.652	0.485	0.746
SiO_2	0.125	0.306	0.0768	0.123
TiO_2	1.223	1.153	1.125	1.208
Cr_2O_3	18.898	16.780	15.753	18.499
MnO	0.123	0.114	0.105	0.128
Fe_2O_3	17.727	15.564	14.744	17.448
NiO	42.725	39.109	35.331	41.335
Nb_2O_5	4.172	2.291	3.446	4.005
MoO_3	2.566	2.291	2.148	2.492

Table 6.3. XRF analysis after 1440 hours of immersion

Oxide (wt. %)	**KOB**	**JOB**	**UCOB**	**Nickel alloy UNS718**
Al_2O_3	0.783	0.522	0.688	0.746
SiO_2	0.187	0.088	0.110	0.123
TiO_2	1.227	1.097	1.225	1.208
Cr_2O_3	19.188	14.906	19.104	18.499
MnO	0.133	0.101	0.138	0.128
Fe_2O_3	17.979	14.002	17.947	17.448
NiO	43.144	33.513	43.423	41.335
Nb_2O_5	4.202	3.257	4.266	4.005
MoO_3	2.593	2.027	2.619	2.492

6.3.4 XRD analysis

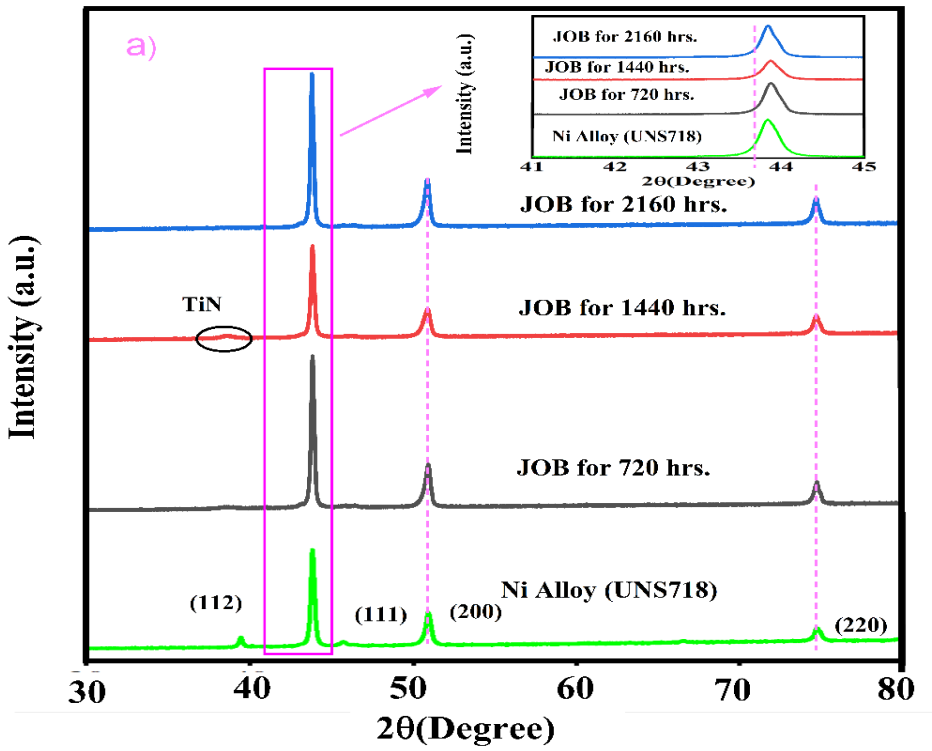

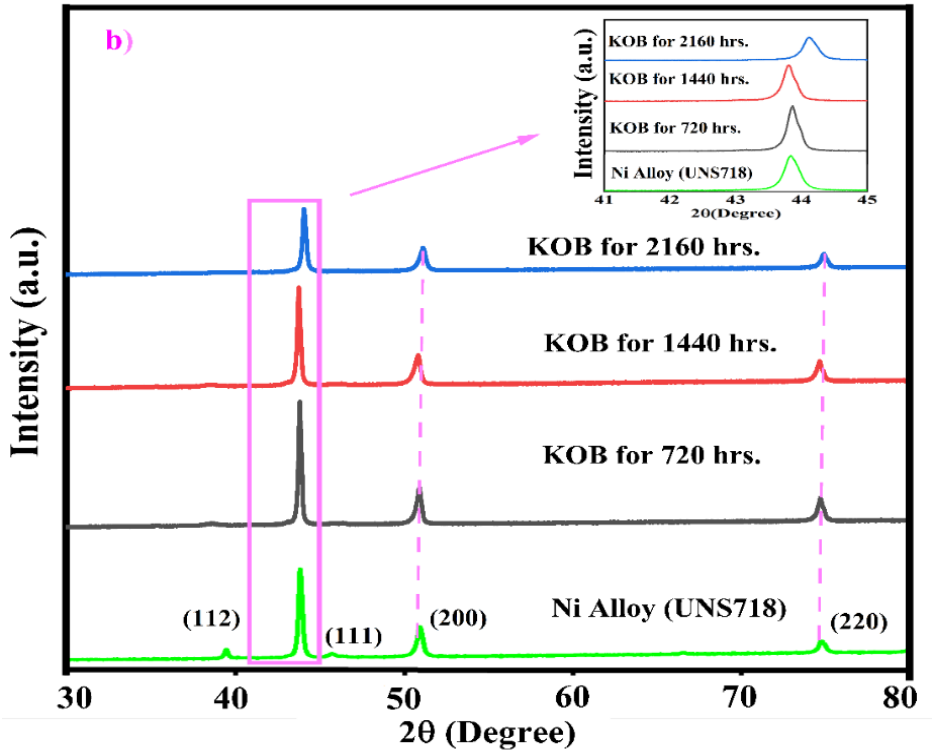

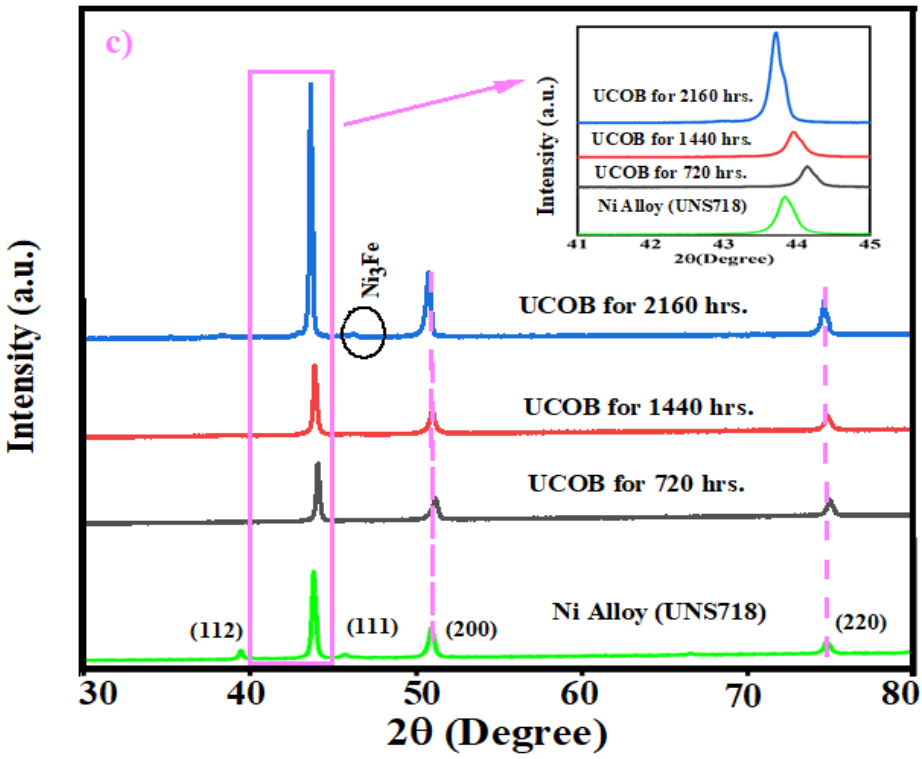

Figure 6.5. XRD spectra of a) Jatropha oil biodiesel, b) Karanja oil biodiesel, c) Used cooking oil biodiesel

To explore the phase transformation occurring when samples were exposed to various biodiesels over different durations, XRD analyses were conducted on Ni alloys immersed in JOB, KOB, and UCOB, as depicted in Figure 6.5 (a), (b), and (c). Notably, the Ni alloy immersed in JOB for 1440 hours showed TiN formation. Significantly, the microstrain values decreased as the exposure time increased till 1440 hours; however, it got further decreased for the Ni alloy exposed for 2160 hours (refer to Figure 6.5 (a-c)). The highest strain was observed for the Ni alloy exposed for 1440 hours. Corrosion products like NiO, MnO_2, and others were observed in the XPS analysis of Ni alloy samples exposed to JOB between 720 and 2160 hours, which remained undetected in XRD, which might be due to these products' amorphous nature. The Ni alloy exposed to JOB exhibited the lowest corrosion rate, as evidenced by the formation of passive or protective layers at 720 hours, which remained intact up to 2160 hours. In contrast, Ni alloys exposed to KOB showed

a rightward shift in all characteristic peaks for the Ni alloy exposed for 2160 hours, without any indication of corrosion product formation. This suggests a lower strain presence after 2160 hours compared to the alloy exposed for 720 hours. Notably, the strain values decreased with increased exposure time for the Ni alloy immersed in KOB. The minimum strain was observed for the Ni alloy exposed to KOB for 2160 hours, as shown in Figure A4 (d-f). Conversely, there was no indication of Ni_3Fe in the XRD patterns for the Ni alloy exposed to UCOB up to 720 and 1440 hours, but it became apparent after 2160 hours. Notably, the XRD pattern for the Ni alloy exposed for 1440 hours showed the highest strain compared to both the 720-hour and 2160-hour exposures (refer to Figure A4 (g-i)). This is consistent with the corrosion rate findings presented in Figure 6.1, where the Ni alloys exposed to UCO up to 1440 hours had a higher corrosion rate than those exposed to 2160 hours. Strain values were determined using the Rietveld refinement method, as illustrated in Figure A6 (a-i), with the methodology for strain calculation via Rietveld Refinement detailed in another source (Rocha et al., 2020).

6.3.5 XPS analysis

X-ray Photoelectron Spectroscopy (XPS) is the most prevalent technique for surface characterization. It is crucial for analysing surfaces, particularly in corrosion evaluation, as it provides a quantitative chemical composition of the material's surface up to 10 nm depth (Krishna & Philip, 2022). Depending on the conditions, the corrosion product may form either a thin or a thick layer. The survey scans also display minor peaks attributable to auger electrons, impurities, and elements in low concentrations, which remained without labelling (Ilyin, 2017; Turner & Schreifels, 2000). The absence of 2P1/2 components in the XPS survey scan was observed, which could be attributed to the overlap of the peak with the Auger electron peak or plasmon resonance(Nesbitt & Banerjee, 1998a; Stevie & Donley, 2020; L. Wang et al., 2020).

6.3.5.1 XPS analysis conducted for Ni Alloy immersed for 720 hours in KOB

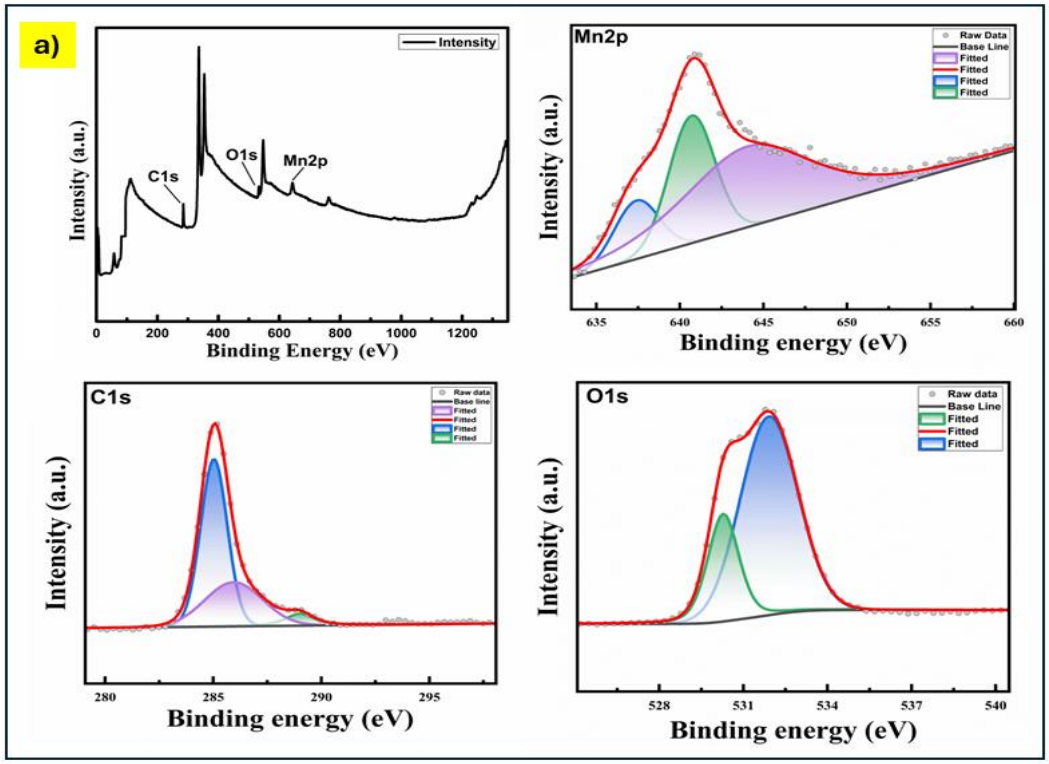

Figure 6.6. (a**)** XPS curve of the sample after 720 hours of immersion in KOB

The XPS survey scan of samples immersed in KOB for 720 hours reveals elements with oxidation states such as C1s, O1s, and Mn2p. Upon peak fitting, peaks at binding energies of 638.7 eV, 641.4 eV, and 641.8 eV are observed, corresponding to Mn metal, Mn_2O_3, and MnO_2, respectively, as indicated in Figure 6.6(a) (Hendi1 et al., 2016). For the C1s peak fitting, peaks at binding energies of 284.9 eV, 286 eV, and 288.7 eV are identified for the alkyl (C-C) group, ester group (C-O-C), and carbonyl group (O=C-O) (from biodiesel), respectively. Likewise, the O1s peak fitting yields peaks at binding energies of 530.5 eV and 531.9 eV(Frankcombe & Liu, 2023) associated with metal oxides.

6.3.5.2 XPS analysis conducted for Ni Alloy immersed till 1440 hours in KOB

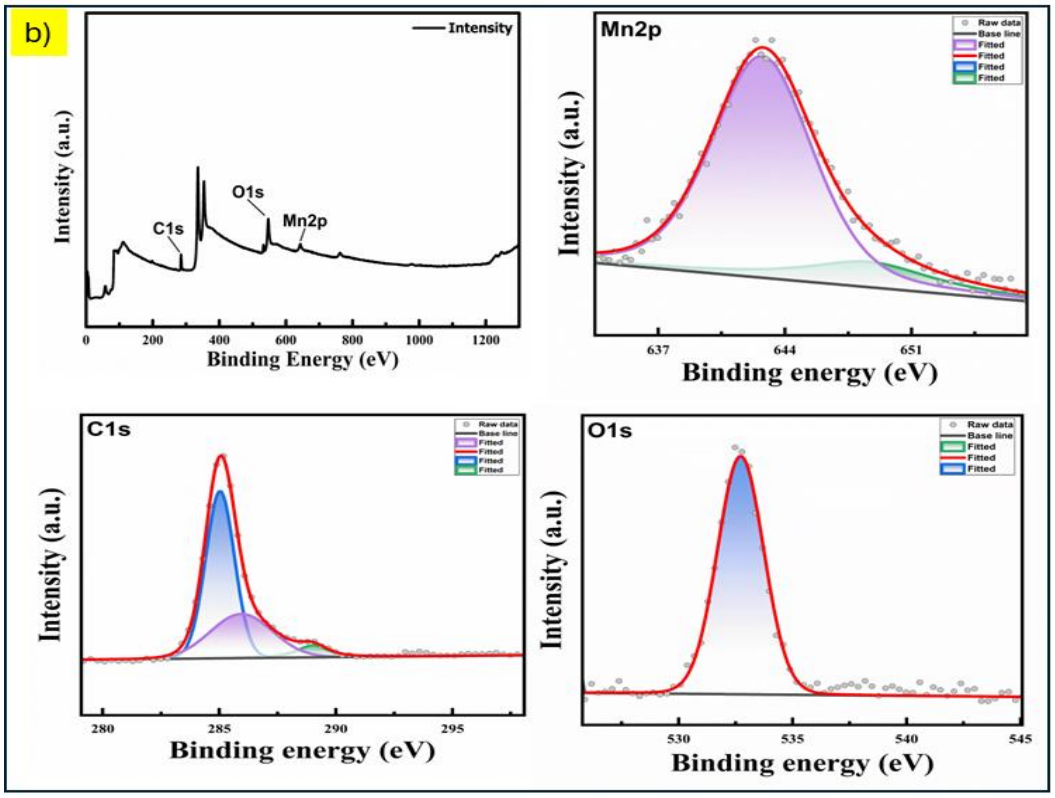

Figure 6.7.(b) XPS curve of the sample after 1440 hours of immersion in KOB

The XPS survey scan for the sample immersed in KOB for 1440 hours indicates the presence of elements in oxidation states, including C1s, O1s, and Mn2p. Subsequent peak fitting reveals peaks that correspond to a binding energy of 642.1 eV, indicative of MnO_2 (Nesbitt & Banerjee, 1998b), as depicted in Figure 6.7(b).

6.3.5.3 XPS analysis conducted for Ni Alloy immersed till 2160 hours in KOB

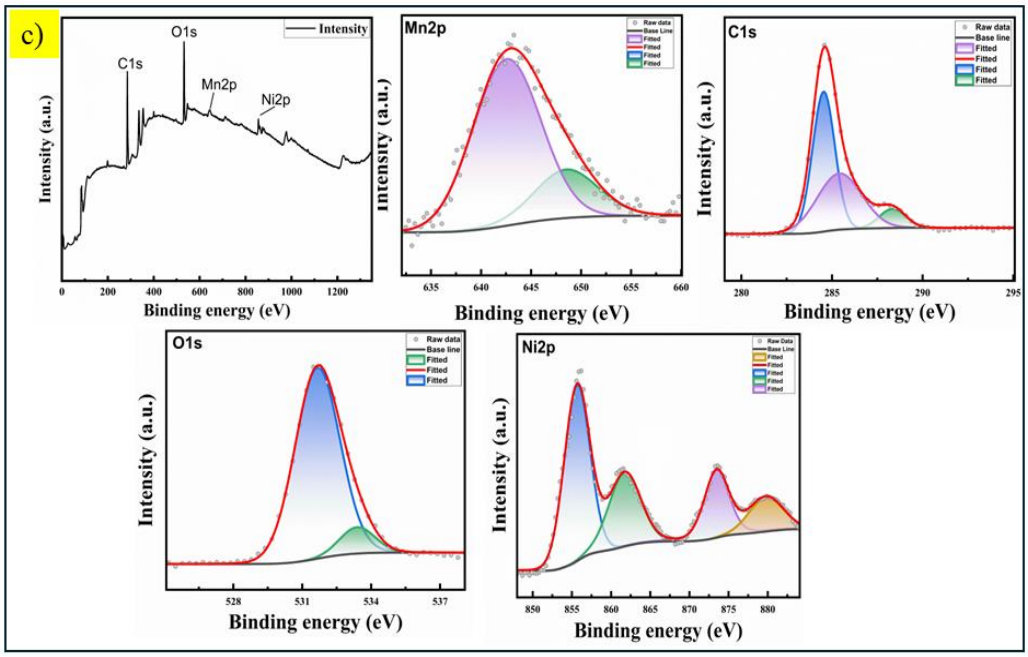

Figure 6.8. (c) XPS curve of the sample after 2160 hours of immersion in KOB

The XPS survey curve for the sample immersed in KOB for 2160 hours indicates the presence of elements in oxidation states such as Mn2p, C1s, O1s, and Ni2p, as depicted in **Figure 6.8**(c). Peaks were observed corresponding to binding energies of 835.8 eV for NiO (Pu et al., 2013), 855.9 eV for $Ni(OH)_2$ (Feng et al., 2021), 640.7 eV for MnO, 284.55 eV for alkyl (C-C) group, 286.4 eV for the ester group (C-O-C), and 288.61 eV for the carbonyl group (O=C-O)(Gengenbach et al., 2021). Additionally, the O1s peak fitting revealed peaks at a binding energy of 531.2 eV associated with $Ni(OH)_2$(Payne et al., 2012).

6.3.5.4 XPS analysis conducted for Ni Alloy immersed till 720 hours in JOB

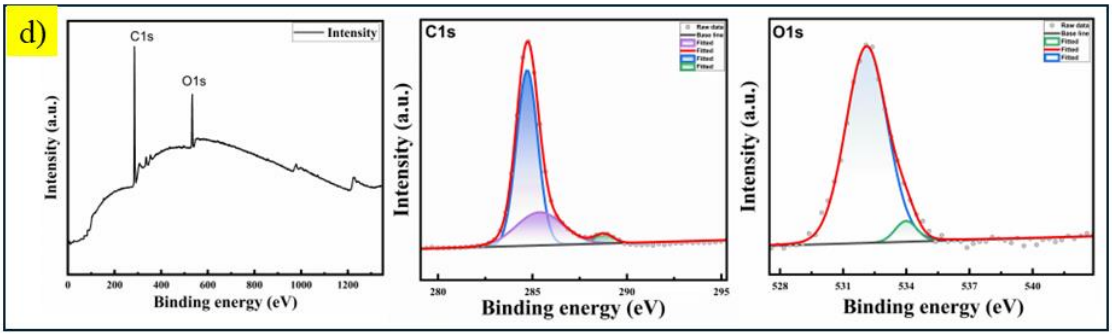

Figure 6.9.(d) XPS curve of the sample after 720 hours of immersion in JOB

The XPS survey scan of the sample, after immersion in JOB for 720 hours, reveals the presence of elements in oxidation states such as C1s and O1s, as depicted in Figure 6.9(d). Subsequent peak fitting yield peaks at binding energies of 284.9 eV, 286 eV, and 288.7 eV, corresponding to the alkyl (C-C) group, ester group (C-O-C), and carbonyl group (O=C-O)(X. Chen et al., 2020), respectively.

6.3.5.5 XPS analysis conducted for Ni Alloy immersed till 1440 hours in JOB

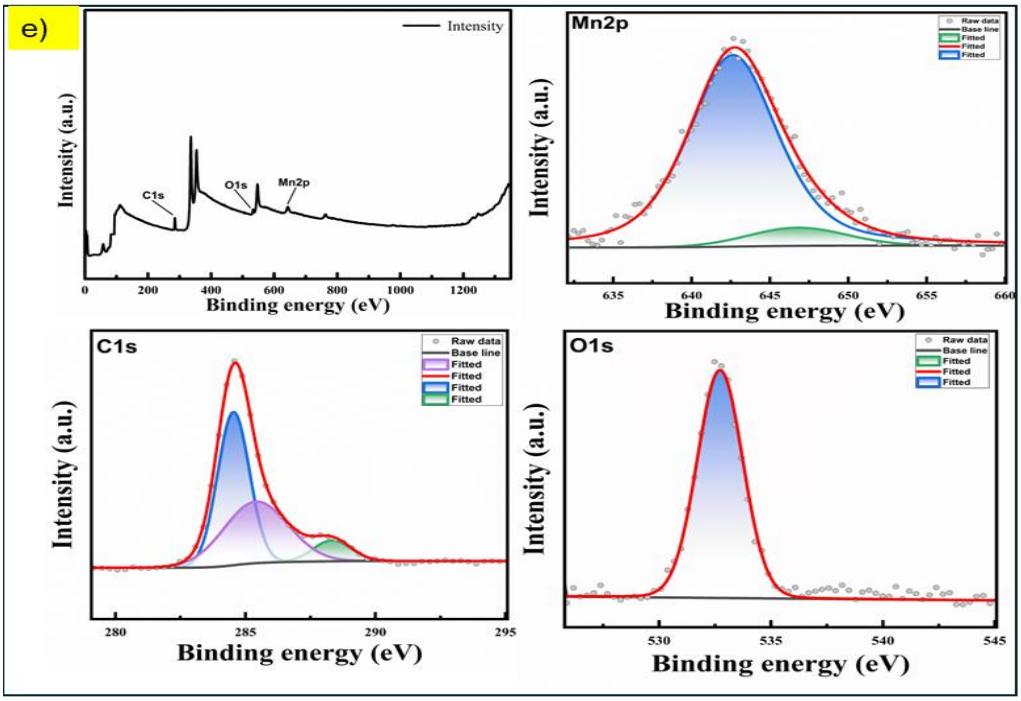

Figure 6.10. (e) XPS curve of the sample after 1440 hours of immersion in JOB

The XPS survey scan of the sample immersed in JOB for 1440 hours indicates the presence of elements in oxidation states, notably C1s, Mn2p, and O1s, as shown in Figure 6.10(e). A peak corresponding to a binding energy of 642.1 eV for MnO_2 was observed(Xiao & Xu, 2012).

6.3.5.6 XPS analysis conducted for Ni Alloy immersed till 2160 hours in JOB

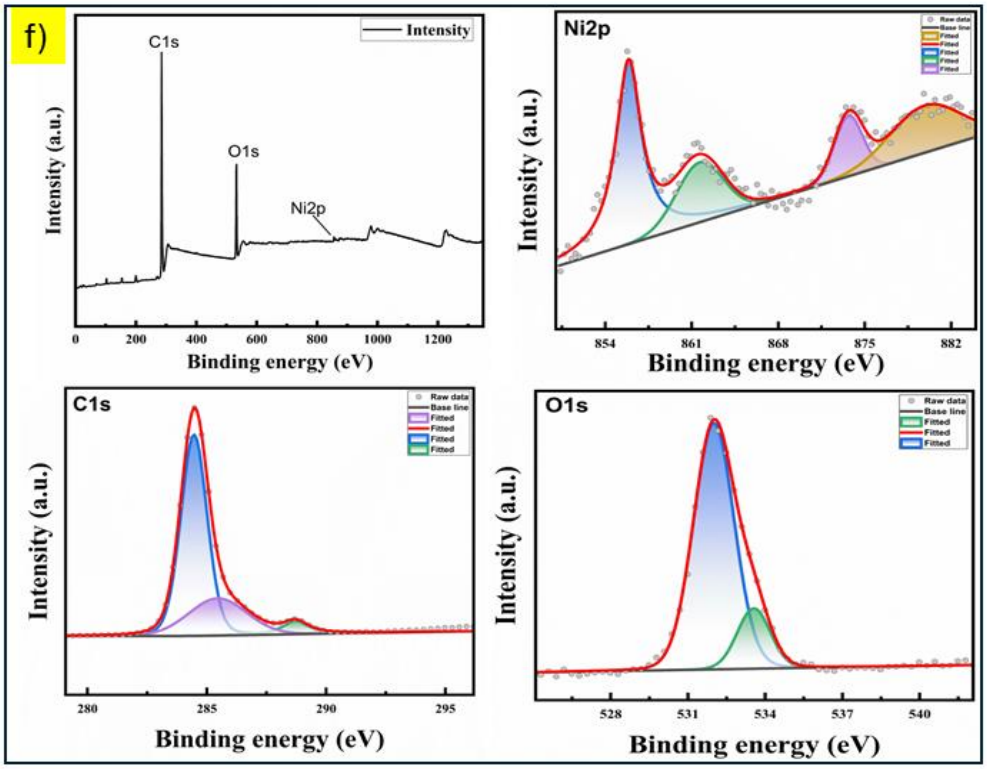

Figure 6.11. (f) XPS curve of the sample after 2160 hours immersion in JOB

The XPS survey curve of the sample immersed in JOB for 2160 hours reveals the presence of elements with oxidation states such as C1s, O1s, and Ni2p, as depicted in Figure 6.11(f). Upon peak fitting, peaks at binding energies of 835.8 eV for NiO, and 855.9 eV for $Ni(OH)_2$(Nesbitt et al., 2000) were observed.

6.3.5.7 XPS analysis conducted for Ni Alloy immersed till 720 hours in UCOB

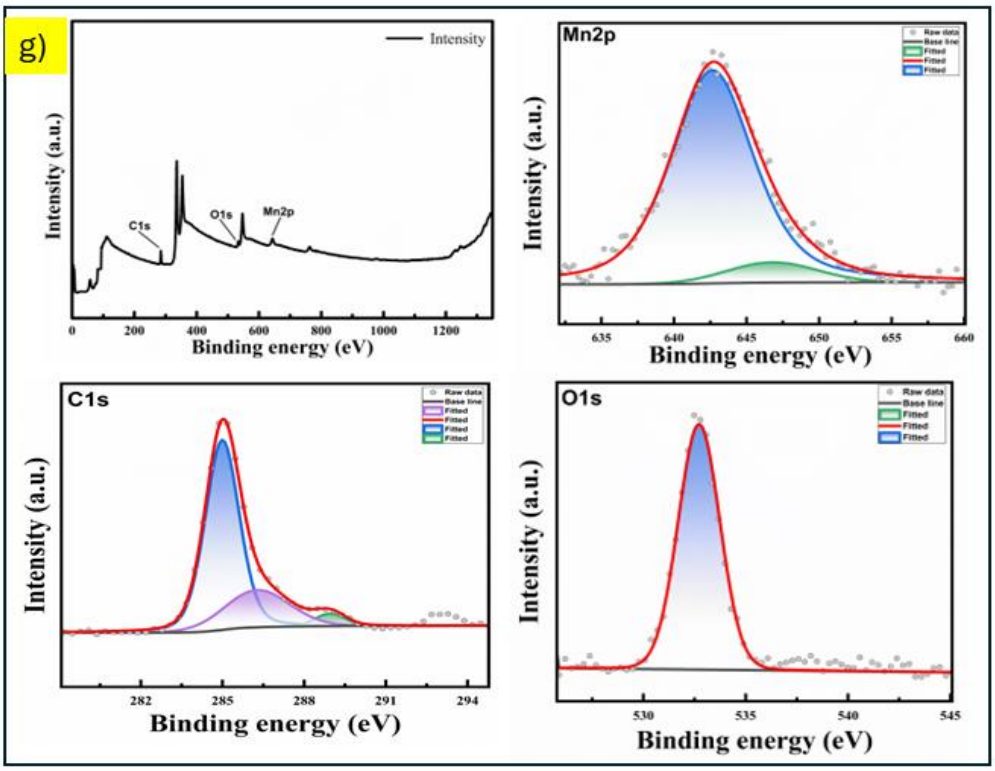

Figure 6.12. (g) XPS curve of the sample after 720 hours of immersion in UCOB

XPS survey scan for the sample immersed in UCO for 720 hours shows the presence of elements with oxidation states as C1s, O1s and Mn2p, as illustrated in Figure 6.12(g). After curve fitting, the formation of MnO_2 (642.43 eV) was confirmed (Z. Yang et al., 2015).

6.3.5.8 XPS analysis conducted for Ni alloy immersed till 1440 hours in UCOB

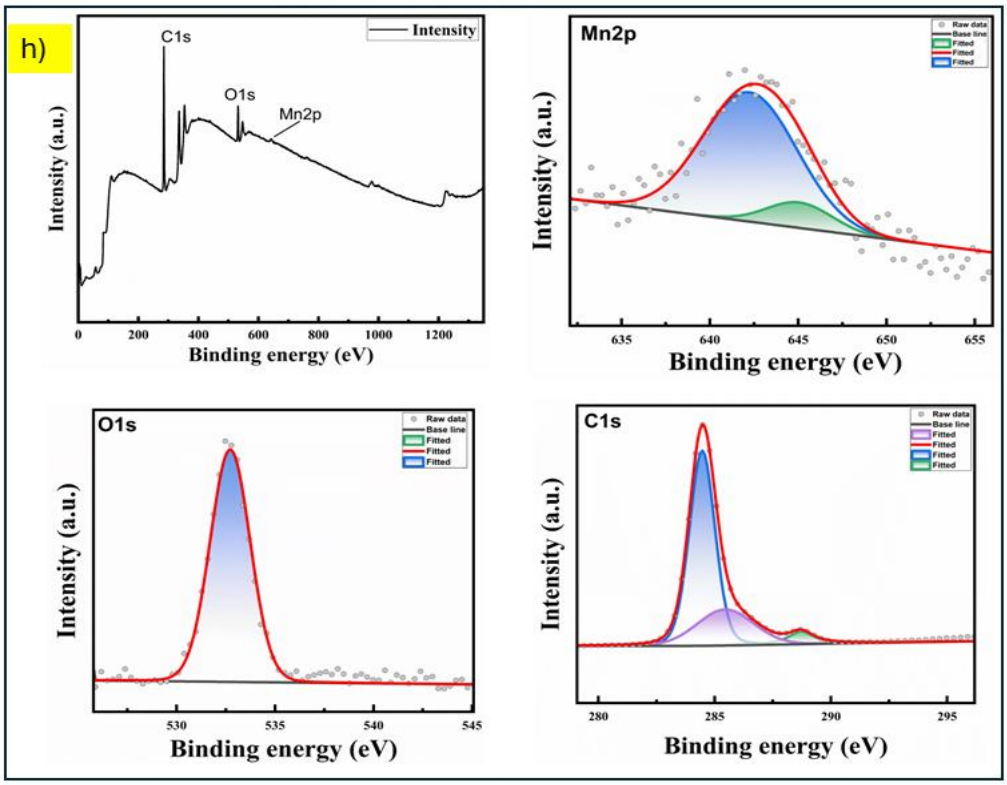

Figure 6.13. (h) XPS curve of the sample after 1440 hours of immersion in UCOB

The XPS survey scan of the sample immersed in UCO for 1440 hours reveals the presence of elements in oxidation states such as C1s, O1s, and Mn2p, as depicted in Figure 6.13(h). Upon peak fitting, peaks of O1s were observed corresponding to a binding energy of 532.3 eV,(Frankcombe & Liu, 2023) indicative of Organic C=O. Additionally, peaks were identified at binding energies of 284.9 eV, 286 eV, and 288.7 eV,(X. Chen et al., 2020) corresponding to the alkyl (C-C) group, ester group (C-O-C), and a carbonyl group (O-C=O), respectively.

6.3.5.9 XPS analysis conducted for Ni Alloy immersed till 2160 hours in UCOB

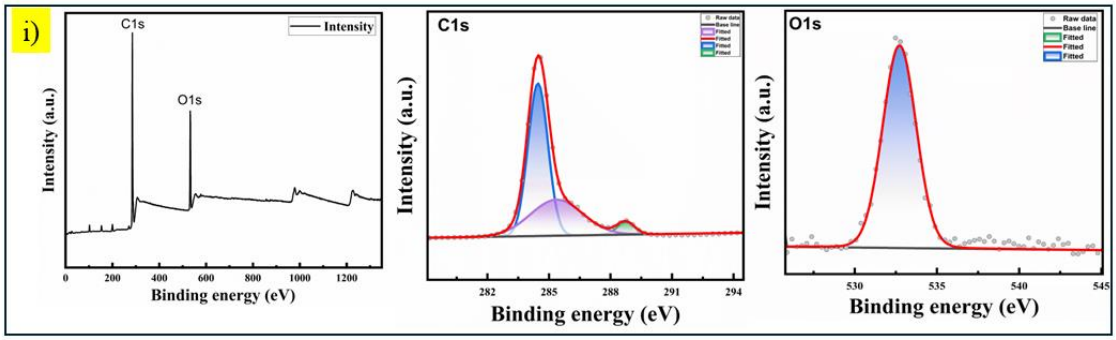

Figure 6.14.(i) XPS curve of the sample after 2160 hours immersion in UCOB

The XPS survey scan of the sample immersed in UCO for 2160 hours indicates the presence of elements with oxidation states such as C1s and O1s, as depicted in Figure 6.14(i). The peaks observed correspond to a binding energy of 284.55 eV for the alkyl (C-C) group, 286.4 eV for the ester group (C-O-C), 288.61 eV for the carbonyl group (O=C-O), and a binding energy of 532.3 eV for organic C=O(Abutalib et al., 2021).

6.4. Investigation of biodiesel degradation using FTIR

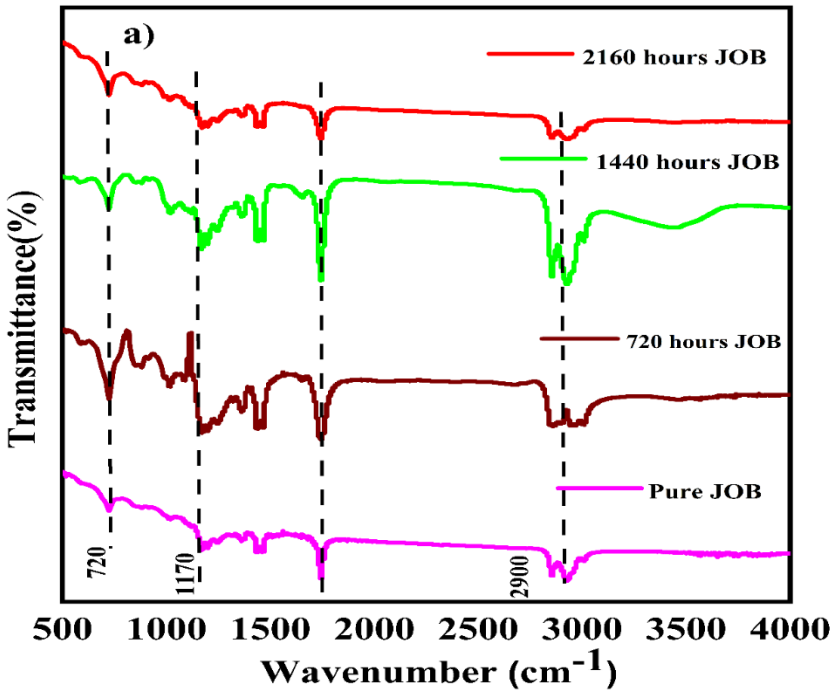

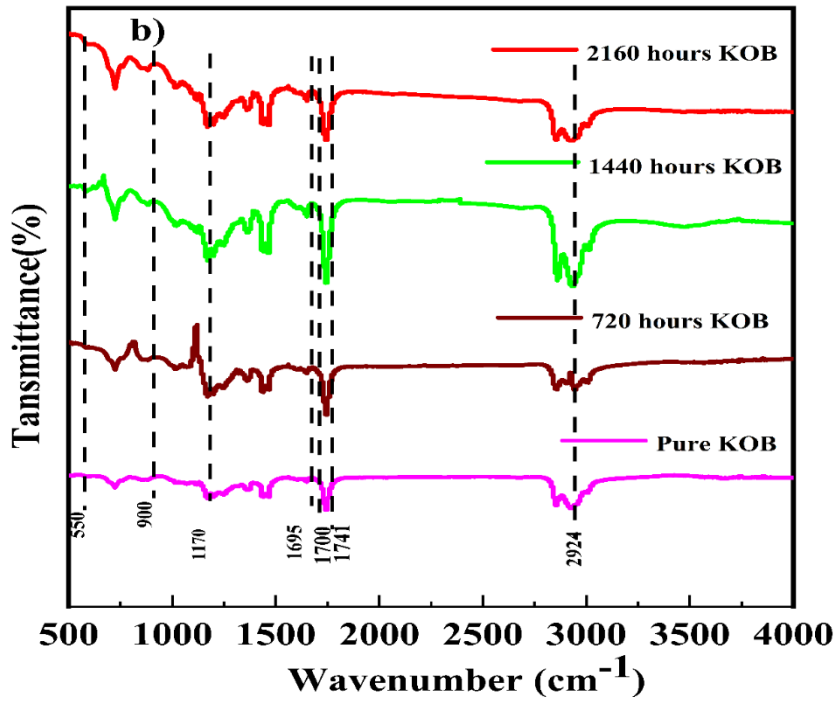

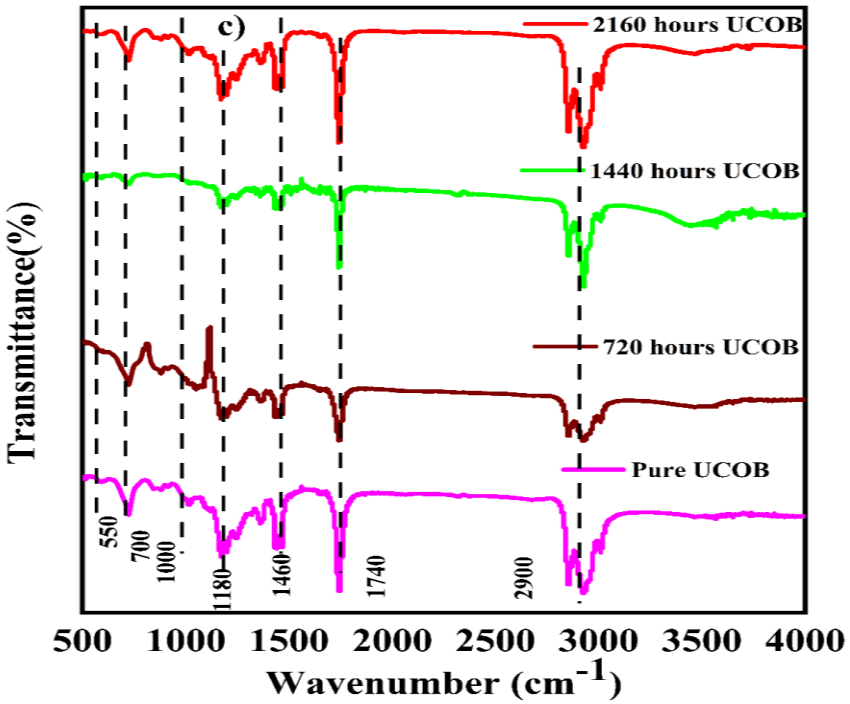

Figure 6.15. FTIR spectra were recorded for a) Jatropha biodiesel (JOB), b)Karanja biodiesel (KOB), and c) used cooking oil biodiesel (UCOB) at various time intervals

The degradation process of fuel samples was examined by analyzing the pre-immersion FTIR spectra of three biodiesel samples, depicted in Figure 6.15 (a), (b), and (c). This analysis confirmed the presence of common regions in JOB, KOB, and UCOB. In the pure jatropha spectrum, there was a notable reduction in O-CH_3 stretching and carbonyl absorption. Saturated aliphatic esters exhibit strong absorption between 1735-1750 cm^{-1}(Matwijczuk et al., 2017; L. D. S. Yadav, 2005), corresponding to the carbonyl absorption region. Peaks at lower frequencies may be attributed to the presence of multiple carbonyl-containing compounds besides ester chains. The appearance of peaks in the 1700-1740 cm^{-1} range suggests the presence of organic compounds such as carboxylic acids, ketones, and aldehydes ("Fatty Acids," 2015; Furlan et al., 2010a). The peak observed in the carbonyl region (1741 cm^{-1}) decreased with increased exposure time (Figure 6.15a), a change attributed to oxidation reactions that convert esters into non-

carbonylated substances (Furlan et al., 2010a; Zhou et al., 2017). Shoulders emerged around 1718, 1720, and 1724 cm^{-1} in the spectra of samples degraded for 720, 1440, and 2160 hours, respectively, indicating the formation of oxidation products like aldehydes, ketones, and fatty acids (Matwijczuk et al., 2017). A signal at approximately 1695 cm^{-1} confirmed the conjugation of the carbonyl group with a double bond. Peaks at 1170, 1195, and 1244 cm^{-1} were linked to C=O in long-chain methyl esters (Figure 5b & 5c) (Furlan et al., 2010a). Furlan et al.(Furlan et al., 2010b) clarified the relationship between carbonyl group peak intensity and the dissociation of methyl-ester linkages ($O\text{-}CH_3$) due to oxidation. The chemical composition of JOB, KOB, and UCOB depends on the initial feedstock characteristics. Feedstocks with double bonds encourage oxidation, leading to products with unsaturated fatty acids post-transesterification (Pullen & Saeed, 2012b), which have poor storage stability. The presence of double bonds was verified by peaks at 710 and 3009 cm^{-1} in FTIR (Figure 6.15 (a), (b) & (c)). UCO's degradation patterns resembled those of Jatropha and Karanja, and FTIR spectra were compared to illustrate fuel degradation after 2160 hours (as shown in Figure 6.15c). Occasionally, biodiesel degradation results in polymer formation, negatively impacting engine performance by clogging the fuel line (“Fatty Acids,” 2015; Mirghani et al., 2011; Parker et al., 2014; Sahoo & Biswas, 2009; Zhou et al., 2017).

6.5. Corrosion mechanisms

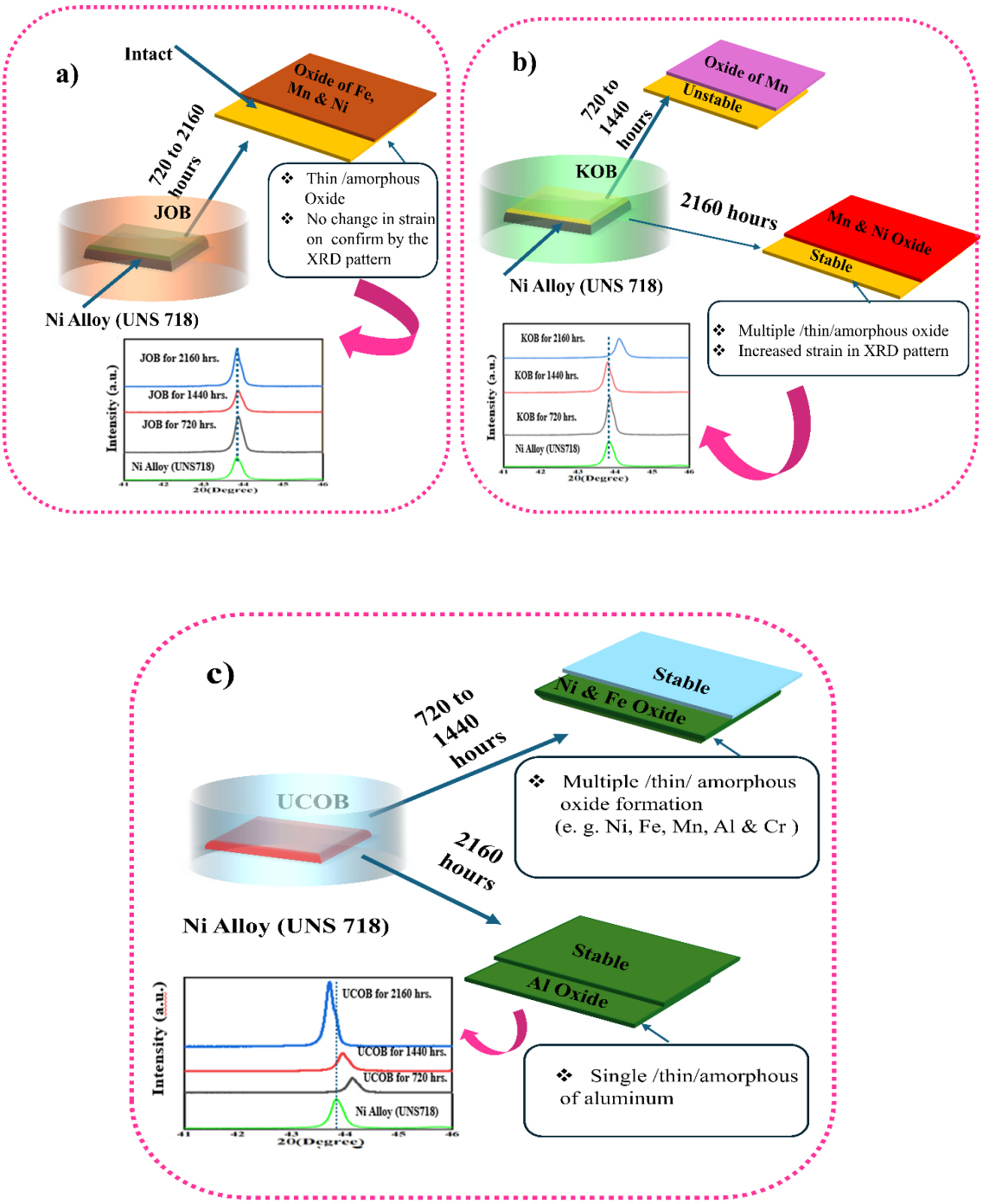

Figure 6.16. Elucidation of the proposed corrosion mechanism

The corrosion mechanism of Ni alloy was detailed in Figure 6.16 (a-c), with the results showing the formation of protective iron, nickel, and manganese oxides on the Ni alloy after exposure to JOB for 720 to 2160 hours (Figure 6.16 (a)). The corrosion rate for JOB was the lowest compared to KOB and UCO. Interestingly, Ni alloy samples exposed to

KOB for up to 1440 hours exhibited higher corrosion rates than those exposed to UCO, due to the formation of unstable Mn and Ni oxides (Figure 6.16 (b)). Further XRD analyses suggested that strain value was higher for the samples exposed to KOB for 1440 hours than for 2160 hours. This might be attributed to the stabilization of corrosion products by releasing strain. The nucleation and growth of oxide-based corrosion products, as shown by the XPS patterns for Ni alloy samples exposed to KOB for 2160 hours, featuring oxides like MnO, NiO, Ni $(OH)_2$ whereas Ni alloy samples exposed to KOB for 1440 hours exhibited MnO_2 formation. Intriguingly, prolonged exposure to KOB allowed the development of additional oxides such as NiO, Ni $(OH)_2$, which were absent in samples exposed for only 720 and 1440 hours. Therefore, a significant change in corrosion rate was observed after 1440 hours for the Ni alloy sample exposed to KOB. The corrosion rates increased more rapidly for Ni alloys exposed to UCO up until 1440 hours compared to those exposed after 2160 hours. This increase is due to the formation of various unstable oxides, such as those of Fe, Ni, Al, and Cr, which might have occurred via a diffusion mechanism until 1440 hours and have not been exhibited by XPS. However, beyond 2160 hours, no oxide was present as a passive layer on the Ni alloy, as confirmed by XPS, however, XRF confirmed some oxides like Cr_2O_3, Fe_2O_3, etc., not appearing in the XPS pattern (Figure 6.16(c)). Consequently, the Ni alloy immersed in UCO showed a higher corrosion rate before 2160 hours than after.

To evaluate the distinct effects of chemical components in various biodiesels, both pure and degraded, the unused cooking oil biodiesel (UCOB), degraded UCOB (DUCOB), Jatropha oil biodiesel (JOB), degraded JOB (DJOB), Karanja oil biodiesel (KOB), and degraded KOB (DKOB) were selected as samples for NMR. The ^1H NMR spectra of biodiesel and degraded biodiesel (after 90 days) were recorded and are displayed in Figure A5 (a), (b), and (c). The NMR spectra reveal that linoleic acid (L), also known as C18:2,

which was present in UCOB, is absent in the spectra for DUCOB. The peak at 2.74 ppm confirms the presence of linoleic acid (Parker et al., 2014). It should be noted that linoleic acid serves as a corrosion inhibitor, forming self-assembled monolayers on the substrate (Sahoo & Biswas, 2009). The NMR spectra for KOB & DKOB, JOB & DJOB, revealed the disappearance of a peak at 3.5 ppm in both cases, suggesting the biodiesel had degraded, with the ester groups either breaking down or converting into new molecules. This is illustrated in Figure A5 (b) & (c). Such degradation could result from hydrolysis, oxidation, or other chemical processes that cleave the ester bonds, releasing free fatty acids, alcohols, or other breakdown products (Parker et al., 2014).

Analysis of the corrosion rate reveals that the Ni alloy exposed to UCOB for 720 hours has a higher corrosion rate than when exposed for 2160 hours. Notably, the pH of DUCOB is significantly more acidic (pH 2.4) compared to UCOB (pH 4.5). Consequently, despite a more pronounced peak of linoleic acid in the NMR spectra for UCOB, the corrosion rate of Ni alloy after 2160 hours was lower than after 720 hours, attributable to the less effective corrosion environment for linoleic acid (at 720 hours). It is important to note that linoleic acid is a more effective corrosion inhibitor in acidic conditions than in neutral ones. The pH of DUCOB being highly acidic (pH 2.4) compared to UCOB (pH 4.5) is a significant factor in deciding the corrosion rate (Hermoso-Diaz et al., 2019).

6.6. Conclusion

The study examined the suitability of Ni alloy (UNS718) as a construction material for storing various biodiesels, including JOB, KOB, and UCOB. The Ni alloy exposed to UCOB exhibited the highest corrosion rate after 2160 hours compared to its exposure to KOB and JOB. However, KOB maintained a high level of corrosiveness until 1440 hours. Notably, JOB showed the least corrosiveness towards Ni alloy from 720 to 2160 hours.

The corrosion mechanisms of Ni alloy in contact with different biodiesels such as JOB, KOB, and UCOB were thoroughly investigated and explained. The study also emphasized the significance of multiple oxide formation in reducing Ni alloy corrosion. Consistency was observed in the surface, interface, and compositional analyses of the corroded Ni alloys, which corroborated well with one another.

In the next chapter, the overall conclusions of the present research work are summarised and briefly discussed, followed by recommendations for the future scope of study based on the findings achieved

Chapter 7
Conclusions and future recommendations

7.1 Conclusions

The following conclusions have been drawn from the present thesis:

(i) Unconventional reactor systems have proven effective in enhancing biodiesel production by improving heat and mass transfer, reducing reaction time, and enabling catalyst-free operation at lower temperatures.

(ii) Unconventional reactors show strong potential to enhance biodiesel production across various applications. However, each type comes with its own set of challenges that must be addressed before they can reliably replace traditional batch reactors and continuous stirred-tank reactors (CSTRs) for large-scale biodiesel generation.

(iii) A biodiesel production system was tested using a traditional batch reactor and continuous reactors: tubular coil and L- and U-shaped coiled flow inverters under optimal conditions (60 °C, 9:1 methanol-to-oil ratio, KOH catalyst).

(iv) The U-shaped CFI achieved the highest yield of 92.6% in under one minute, followed by the L-shaped CFI at 90%. The batch reactor required 2 hours to reach 90.63%, while the tubular coil reactor produced 82.52% yield in just over one minute.

(v) Four nanoparticles, ZnO, Mg-ZnO, TiO_2, and SiO_2, were synthesized, and their incorporation improved key physicochemical properties such as density, kinematic viscosity, oxidation stability, and heating value.

(vi) ZnO blends showed the highest calorific value and overall enhancement in fuel quality. SiO_2 blends exhibited lower density than TiO_2 but higher than Mg-ZnO and ZnO, while viscosity increased with all nanoparticles, with ZnO causing the least increase. Dosage variation (0–100 ppm) influenced both physicochemical and induction period properties.

(vii) A blend of waste tyre pyrolysis oil, UCO biodiesel, and biosynthesized SrO nanoparticles (B10TPO90SrO100) was tested in diesel engines, showing improved combustion with brake thermal efficiency increasing by 1.77% and fuel consumption decreasing by 5.18%.

(viii) The nano-enhanced blend also exhibited a heat release rate comparable to diesel and significantly reduced emissions of HC, CO, and NOx by 15.27%, 15.84%, and 1.89%, respectively. These results highlight the effectiveness of eco-friendly SrO nanoparticles in enhancing combustion performance and their potential for scalable practical use.

(ix) The corrosion behaviour of Ni alloy (UNS718) was evaluated in the presence of three biodiesels: JOB, KOB, and UCOB. UCOB caused the highest corrosion rate after 2160 hours, while KOB maintained significant corrosiveness until 1440 hours. JOB showed the least corrosive effect between 720 and 2160 hours.

(x) The study also emphasized the significance of multiple oxide formation in reducing Ni alloy corrosion. Consistency was observed in the surface, interface, and compositional analyses of the corroded Ni alloys, which corroborated well with one another.

7.2 Future recommendations

Based on this research, the following future recommendations are proposed:

(i) Future work should focus on scaling up the microreactor and coiled flow inverter (CFI) systems, especially the U-shaped CFI, to pilot and industrial scales.

(ii) Strategies for the continuous integration of these high-efficiency reactors into existing biodiesel production infrastructures must be explored.

(iii) A comprehensive life cycle analysis (LCA) and techno-economic assessment should be conducted to evaluate the environmental and financial viability of using unconventional reactors and nano-additives in large-scale biodiesel production.

(iv) Research should continue into the development of more advanced, cost-effective, and environmentally benign nanoparticles, including doped or hybrid nanostructures, to further improve biodiesel properties and combustion performance.

(v) Long-term engine tests using nano-enhanced fuel blends should be performed to assess engine wear, fuel injector compatibility, emission control system impacts, and overall durability.

(vi) It is important to evaluate the economic viability of integrating additives based on nanoparticles into the production of biodiesel and subsequent engine utilization. When considering the viability of such technologies, cost-effectiveness is a crucial determinant.

(vii) Advanced computational modelling of combustion in diesel engines is recommended to gain detailed insights into the behaviour of biodiesel blends with nano-additives. This will enable a thorough assessment of combustion parameters, aiding in the optimization of fuel formulations and engine settings to enhance performance and reduce emissions in future biodiesel applications.

(viii) Due to the corrosion of Ni alloys observed with various biodiesel types, future research should investigate protective coatings, alloy modifications, or corrosion inhibitors to enhance material compatibility, especially for biofuels with higher acid content.

(ix) Future research should investigate the stability of nano-additives in fuel blends, as well as the potential of surfactants to enhance nanoparticle dispersion and overall fuel stability.

References

References

Abdul Raman, A. A., Tan, H. W., & Buthiyappan, A. (2019). Two-Step Purification of Glycerol as a Value-Added by Product From the Biodiesel Production Process. *Frontiers in Chemistry, 7,* 439904. https://doi.org/10.3389/fchem.2019.00774/bibtex

Abdulqadir, L. B. (2017). Investigation of the Effects of Soot on the Wear of Automotive Engine Components.*Ph.D. Thesis*, The University of Seffered, Western Bank*, U.K.2017*

Abed, C., Bouzidi, C., Elhouichet, H., Gelloz, B., & Ferid, M. (2015). Mg doping induced high structural quality of sol-gel ZnO nanocrystals: Application in photocatalysis. *Applied Surface Science*, *349*, 855–863. https://doi.org/10.1016/j.apsusc.2015.05.078

Abishek, M. S., Kachhap, S., Rajak, U., Verma, T. N., Singh, T. S., Shaik, S., Cuce, E., & Alwetaishi, M. (2024). Alumina and titanium nanoparticles to diesel–Guizotia abyssinica (L.) biodiesel blends on MFVCR engine performance and emissions. *Sustainable Energy Technologies and Assessments*, *61*, 103580. https://doi.org/10.1016/j.seta.2023.103580

AbuTalib, N. H., LaGrow, A. P., Besenhard, M. O., Bondarchuk, O., Sergides, A., Famiani, S., Ferreira, L. P., Cruz, M. M., Gavriilidis, A., & Thanh, N. T. K. (2021). Shape controlled iron oxide nanoparticles: Inducing branching and controlling particle crystallinity. *CrystEngComm, 23(3)*, 550–561. https://doi.org/10.1039/d0ce01291b

Adamou, P., Harkou, E., Villa, A., Constantinou, A., & Dimitratos, N. (2024). Ultrasonic reactor set-ups and applications: A review. *Ultrasonics Sonochemistry*, *107*, 106925. https://doi.org/10.1016/J.ultsonch.2024.106925

Agarwal, M., Soni, S., Singh, K., Chaurasia, S. P., & Dohare, R. K. (2013). Biodiesel yield assessment in continuous-flow reactors using batch reactor conditions. *International Journal of Green Energy*, *10*(1), 28–40. https://doi.org/10.1080/15435075.2011.647171

Akcay, M., & Ozer, S. (2024). Experimental investigation on performance and emission characteristics of a CI diesel engine fueled with fusel oil/diesel fuel blends. *Energy Sources, Part A: Recovery, Utilization, and Environmental Effects, 46*(1), 2600–2615. https://doi.org/10.1080/15567036.2019.1689317

Alamsyah, R., Tambunan, A. H., Purwanto, Y. A., Kusdiana, D. ", Alamsyah, R., Tambunan, A. H., Purwanto, Y. A., & Kusdiana, D. (2010). Comparison of static-

mixer and blade agitator reactor in biodiesel production. *Agricultural Engineering International: CIGR Journal*, *12*(1). https://cigrjournal.org/index.php/Ejounral/article/view/1566

Ali Ijaz Malik, M., Kalam, M. A., Mujtaba Abbas, M., Susan Silitonga, A., & Ikram, A. (2024). Recent advancements, applications, and technical challenges in fuel additives-assisted engine operations. *Energy Conversion and Management*, *313*, 118643. https://doi.org/10.1016/j.enconman.2024.118643

Ali Ijaz Malik, M., Zeeshan, S., Khubaib, M., Ikram, A., Hussain, F., Yassin, H., & Qazi, A. (2024). A review of major trends, opportunities, and technical challenges in biodiesel production from waste sources. *Energy Conversion and Management: X*, *23*, 100675. https://doi.org/10.1016/j.ecmx.2024.100675

Amid, S., Aghbashlo, M., Tabatabaei, M., Hajiahmad, A., Najafi, B., Ghaziaskar, H. S., Rastegari, H., Hosseinzadeh-Bandbafha, H., & Mohammadi, P. (2020). Effects of waste-derived ethylene glycol diacetate as a novel oxygenated additive on performance and emission characteristics of a diesel engine fueled with diesel/biodiesel blends. *Energy Conversion and Management*, *203*, 112245. https://doi.org/10.1016/j.enconman.2019.112245

An, H., Yang, W. M., Chou, S. K., & Chua, K. J. (2012). Combustion and emissions characteristics of diesel engine fueled by biodiesel at partial load conditions. *Applied Energy*, *99*, 363–371. https://doi.org/10.1016/j.apenergy.2012.05.049

Anish, M., Bency, P., Jayaprabakar, J., Joy, N., Jayaprakash, V., Sahaya Susmi, S. K., Aravind Kumar, J., Ansar, S., & Rezania, S. (2022). An evaluation of biosynthesized nanoparticles in biodiesel as an enhancement of a VCR diesel engine. *Fuel*, *328*, 125299. https://doi.org/10.1016/j.fuel.2022.125299

Ansari Samani, M., Hosseinzadeh Samani, B., Ghasemi-Varnamkhasti, M., Rostami, S., & Ebrahimi, R. (2023). Biodiesel production from sunflower oil using a combined atmospheric cold plasma jet-hydrodynamic reactor. *Biofuels*, *14*(9), 895–905. https://doi.org/10.1080/17597269.2023.2190569

Aricetti, J. A., & Tubino, M. (2012). A green and simple visual method for the determination of the acid-number of biodiesel. *Fuel*, *95*, 659–661. https://doi.org/10.1016/J.fuel.2011.10.058

Asghari, M., Hosseinzadeh Samani, B., & Ebrahimi, R. (2022). Review on non-thermal plasma technology for biodiesel production: Mechanisms, reactors configuration, hybrid reactors. *Energy Conversion and Management*, *258*, 115514. https://doi.org/10.1016/j.enconman.2022.115514

Aslan, V. (2024). The analysis of classical, polynomial regression and cubic spline mathematical models in hemp biodiesel optimization: an experimental comparison. *Environmental Science and Pollution Research*, *31*(6), 9392–9407. https://doi.org/10.1007/S11356-023-31720-0

Atabani, A. E., Silitonga, A. S., Badruddin, I. A., Mahlia, T. M. I., Masjuki, H. H., & Mekhilef, S. (2012). A comprehensive review on biodiesel as an alternative energy resource and its characteristics. *Renewable and Sustainable Energy Reviews*, *16*(4), 2070–2093. https://doi.org/10.1016/j.rser.2012.01.003

Atadashi, I. M., Aroua, M. K., Abdul Aziz, A. R., & Sulaiman, N. M. N. (2012). Production of biodiesel using high free fatty acid feedstocks. *Renewable and Sustainable Energy Reviews*, *16*(5), 3275–3285. https://doi.org/10.1016/j.rser.2012.02.063

Athar, M., Zaidi, S., & Hassan, S. Z. (2020). Intensification and optimization of biodiesel production using microwave-assisted acid-organo catalyzed transesterification process. *Scientific Reports*, *10*(1), 1–19. https://doi.org/10.1038/s41598-020-77798-1

Atmanli, A., Ileri, E., & Yüksel, B. (2014). Experimental investigation of engine performance and exhaust emissions of a diesel engine fueled with diesel–n-butanol–vegetable oil blends. *Energy Conversion and Management*, *81*, 312–321. https://doi.org/10.1016/J.enconman.2014.02.049

Attarbachi, T., Kingsley, M. D., & Spallina, V. (2023). New trends on crude glycerol purification: A review. *Fuel*, *340*, 127485. https://doi.org/10.1016/j.fuel.2023.127485

Awogbemi, O., & Kallon, D. V. Von. (2022). Application of Tubular Reactor Technologies for the Acceleration of Biodiesel Production. *Bioengineering*, *9*(8). https://doi.org/10.3390/bioengineering9080347

Azam, N. A. M., Uemura, Y., Kusakabe, K., & Bustam, M. A. (2016). Biodiesel Production from Palm Oil Using Micro Tube Reactors: Effects of Catalyst Concentration and Residence Time. *Procedia Engineering*, *148*, 354–360. https://doi.org/10.1016/j.proeng.2016.06.462

Babu, D., & Anand, R. (2017). Effect of biodiesel-diesel-n-pentanol and biodiesel-diesel-n-hexanol blends on diesel engine emission and combustion characteristics. *Energy*, *133*, 761–776. https://doi.org/10.1016/j.energy.2017.05.103

Babu, D., & Anand, R. (2019). Biodiesel-diesel-alcohol blend as an alternative fuel for DICI diesel engine. *Advanced Biofuels: Applications, Technologies and Environmental Sustainability*, 337–367. https://doi.org/10.1016/B978-0-08-102791-2.00014-3

Badday, A. S., Abdullah, A. Z., Lee, K. T., & Khayoon, M. S. (2012). Intensification of biodiesel production via ultrasonic-assisted process: A critical review on fundamentals and recent development. *Renewable and Sustainable Energy Reviews*, *16*(7), 4574–4587. https://doi.org/10.1016/j.rser.2012.04.057

Barnard, T. M., Leadbeater, N. E., Boucher, M. B., Stencel, L. M., & Wilhite, B. A. (2007). Continuous-flow preparation of biodiesel using microwave heating. *Energy and Fuels*, *21*(3), 1777–1781. https://doi.org/10.1021/ef0606207

Bashir, M. A., Wu, S., Zhu, J., Krosuri, A., Khan, M. U., & Ndeddy Aka, R. J. (2022). Recent development of advanced processing technologies for biodiesel production: A critical review. *Fuel Processing Technology*, *227*. https://doi.org/10.1016/j.fuproc.2021.107120

Bedassa Gudeta, T. (2016). Chemical Composition, Bio-Diesel Potential and Uses of <i> Jatropha curcas</i> L. (Euphorbiaceae). *American Journal of Agriculture and Forestry*, *4*(2), 35. https://doi.org/10.11648/j.ajaf.20160402.15

Bernal, J. M., Lozano, P., García-Verdugo, E., Burguete, M. I., Sánchez-Gómez, G., López-López, G., Pucheault, M., Vaultier, M., & Luis, S. V. (2012). Supercritical Synthesis of Biodiesel. *Molecules*, *17*(7), 8696. https://doi.org/10.3390/molecules17078696

Bertoldi, C., Da Silva, C., Bernardon, J. P., Corazza, M. L., Filho, L. C., Oliveira, J. V., & Corazza, F. C. (2009). Continuous production of biodiesel from soybean oil in supercritical ethanol and carbon dioxide as cosolvent. *Energy and Fuels*, *23*(10), 5165–5172. https://doi.org/10.1021/ef900402r

Bhoi, R., Sen, N., Singh, K. K., Mahajani, S. M., Shenoy, K. T., Rao, H., & Ghosh, S. K. (2014). Transesterification of sunflower oil in microreactors. *International Journal of Chemical Reactor Engineering*, *12*(1), 47–62. https://doi.org/10.1515/ijcre-2013-0105

Bi, Y., Zhou, H., Jia, H., & Wei, P. (2017). A flow-through enzymatic microreactor immobilizing lipase based on layer-by-layer method for biosynthetic process: Catalyzing the transesterification of soybean oil for fatty acid methyl ester production. *Process Biochemistry*, *54*, 73–80. https://doi.org/10.1016/j.procbio.2016.12.008

Binnal, P., Amruth, A., Basawaraj, M. P., Chethan, T. S., Murthy, K. R. S., & Rajashekhara, S. (2021). Microwave-assisted esterification and transesterification of dairy scum oil for biodiesel production: kinetics and optimisation studies. *Indian Chemical Engineer*, *63*(4), 374–386. https://doi.org/10.1080/00194506.2020.1748124

Biodiesel Education. (n.d.). Retrieved May 23, 2025, from https://www.biodieseleducation.org/

BioEnergyTimes. (2025, March 15). India’s 5% biodiesel blending target requires Rs 2,500 crore investment by 2030: Ind-Ra. BioEnergy Times. https://bioenergytimes.com/indias-5-biodiesel-blending-target-requires-rs-2500-crore-investment-by-2030-ind-ra/

BioEnergy Times. (2025, February). Indonesia plans to implement B50 palm oil biodiesel mandate in 2026 - *BioEnergy Times*. https://bioenergytimes.com/indonesia-plans-to-implement-b50-palm-oil-biodiesel-mandate-in-2026/

Blagojevič, M., Rak, G., Bizjan, B., & Kolbl Repinc, S. (2023). A Review on Rotary Generators of Hydrodynamic Cavitation for Wastewater Treatment and Enhancement of Anaerobic Digestion Process. *Processes 2023, Vol. 11, Page 514*, *11*(2), 514. https://doi.org/10.3390/PR11020514

Blinov, A. V., Blinova, A. A., Kravtsov, A. A., Gvozdenko, A. A., Kobina, A. V., & Momot, E. V. (2019). Synthesis of multicomponent systems based on silicon dioxide and noble metal nanoparticles. *AIP Conference Proceedings*, *2188*(December 2019). https://doi.org/10.1063/1.5138420

Boffito, D. C., Martinez-Guerra, E., Gude, V. G., & Patience, G. S. (2015). Conversion of Refined and Waste Oils by Ultrasound-assisted Heterogeneous Catalysis. *Handbook of Ultrasonics and Sonochemistry*, 1–33. https://doi.org/10.1007/978-981-287-470-2_12-1

Bokhari, A., Yusup, S., Chuah, L. F., Klemeš, J. J., Asif, S., Ali, B., Akbar, M. M., & Kamil, R. N. M. (2017). Pilot scale intensification of rubber seed (Hevea brasiliensis) oil via chemical interesterification using hydrodynamic cavitation technology. *Bioresource Technology, 242*, 272–282. https://doi.org/10.1016/j.biortech.2017.03.046

Borugadda, V. B., & Goud, V. V. (2012a). Biodiesel production from renewable feedstocks: Status and opportunities. *Renewable and Sustainable Energy Reviews*, *16*(7), 4763–4784. https://doi.org/10.1016/j.rser.2012.04.010

Bouaid, A., Iliuta, G., & Marchetti, J. M. (2024). Cold flow properties of biodiesel from waste cooking oil and a new improvement method. *Heliyon*, *10*(17), e36756. https://doi.org/10.1016/j.heliyon.2024.e36756

Boukhalkhal, A. L., Kadi, M. E. A., Lasbet, Y., Loubar, K., Awad, S., Makhlouf, M., & Tazerout, M. (2020). A Continuous Biodiesel Production Process Using a Chaotic Mixer-Reactor. *Waste and Biomass Valorization*, *11*(11), 6159–6168. https://doi.org/10.1007/s12649-019-00880-x

Brahma, S., Nath, B., Basumatary, B., Das, B., Saikia, P., Patir, K., & Basumatary, S. (2022). Biodiesel production from mixed oils: A sustainable approach towards industrial biofuel production. *Chemical Engineering Journal Advances*, *10*, 100284. https://doi.org/10.1016/j.ceja.2022.100284

Branco, J. E. H., Prates, R. C., Oliveira, A. L. do N., & Carvalho, A. K. F. de. (2025). Evaluation of the greenhouse gas emissions of the Brazilian biodiesel and the impact of the mandatory blending of the biofuel into commercial diesel fuel. *Chemosphere*, *376*, 144268. https://doi.org/10.1016/j.chemosphere.2025.144268

Buasri, A., Rattanapan, T., Boonrin, C., Wechayan, C., & Loryuenyong, V. (2015). Oyster and pyramidella shells as heterogeneous catalysts for the microwave-assisted biodiesel production from jatropha curcas oil. *Journal of Chemistry*, *2015*. https://doi.org/10.1155/2015/578625

Buchori, L., Istadi, I., Purwanto, P., Kurniawan, A., & Maulana, T. I. (2016). Preliminary Testing of Hybrid Catalytic-Plasma Reactor for Biodiesel Production Using Modified-Carbon Catalyst. *Bulletin of Chemical Reaction Engineering & Catalysis*, *11*(1), 59–65. https://doi.org/10.9767/bcrec.11.1.416.59-65

Budi Utomo, W. (2013). Novel Oscillatory Flow Reactor to Improve Biodiesel Production Continuous System. *International Journal of Science and Research*, *4*, 2319–7064. www.ijsr.net

Çakmak, A., & Özcan, H. (2022). Analysis of combustion and emissions characteristics of a DI diesel engine fuelled with diesel/biodiesel/glycerol tert-butyl ethers mixture by altering compression ratio and injection timing. *Fuel*, *315*, 123200. https://doi.org/10.1016/j.fuel.2022.123200

Cako, E., Wang, Z., Castro-Muñoz, R., Rayaroth, M. P., & Boczkaj, G. (2022). Cavitation based cleaner technologies for biodiesel production and processing of hydrocarbon streams: A perspective on key fundamentals, missing process data and economic feasibility – A review. *Ultrasonics Sonochemistry*, *88*, 106081. https://doi.org/10.1016/j.ultsonch.2022.106081

Cao, X., Ahammed, S. M., Datta, S., Chowdhury, J., & Roy, P. K. (2024). Enhancement of Biodiesel Production via Ultrasound Technology: A Mathematical Study. *ACS Omega*. https://doi.org/10.1021/acsomega.4c01729

Carvalho, A. K. F., Bento, H. B. S., Izário Filho, H. J., & de Castro, H. F. (2018). Approaches to convert Mucor circinelloides lipid into biodiesel by enzymatic synthesis assisted by microwave irradiations. *Renewable Energy*, *125*, 747–754. https://doi.org/10.1016/j.renene.2018.03.012

Chai, M., Tu, Q., Lu, M., & Yang, Y. J. (2014). Esterification pretreatment of free fatty acid in biodiesel production, from laboratory to industry. *Fuel Processing Technology*, *125*, 106–113. https://doi.org/10.1016/j.fuproc.2014.03.025

Chandran, D., Raviadaran, R., Lau, H. L. N., Numan, A., Elumalai, P. V., & Samuel, O. D. (2023a). Corrosion characteristic of stainless steel and galvanized steel in water emulsified diesel, diesel and palm biodiesel. *Engineering Failure Analysis*, *147*, 107129. https://doi.org/10.1016/j.engfailanal.2023.107129

Chanthon, N., Ngaosuwan, K., Kiatkittipong, W., Wongsawaeng, D., Appamana, W., Quitain, A. T., & Assabumrungrat, S. (2021). High-efficiency biodiesel production using rotating tube reactor: New insight of operating parameters on hydrodynamic regime and biodiesel yield. *Renewable and Sustainable Energy Reviews*, *151*, 111430. https://doi.org/10.1016/j.rser.2021.111430

Chataut, G., Bhatta, B., Joshi, D., Subedi, K., & Kafle, K. (2023). Greenhouse gases emission from agricultural soil: A review. *Journal of Agriculture and Food Research*, *11*, 100533. https://doi.org/10.1016/j.jafr.2023.100533

Chaudhuri, A., Temelli, E. B., Hop, C. J. W., Sureshkumar, V. P., & Van Der Schaaf, J. (2022). Transesterification of Triglycerides in a Rotor-Stator Spinning Disc Reactor: Scale-Up and Solid Handling. *Industrial and Engineering Chemistry Research*, *61*(20), 6831–6844. https://doi.org/10.1021/acs.iecr.2c00690

Chen, K. J., & Chen, Y. S. (2014). Intensified production of biodiesel using a spinning disk reactor. *Chemical Engineering and Processing: Process Intensification*, *78*, 67–72. https://doi.org/10.1016/j.cep.2014.02.009

Chen, X., Wang, X., & Fang, D. (2020). A review on C1s XPS-spectra for some kinds of carbon materials. *Fullerenes, Nanotubes and Carbon Nanostructures*, 1048–1058. https://doi.org/10.1080/1536383x.2020.1794851

Choedkiatsakul, I., Ngaosuwan, K., Assabumrungrat, S., Mantegna, S., & Cravotto, G. (2015). Biodiesel production in a novel continuous flow microwave reactor. *Renewable Energy*, *83*, 25–29. https://doi.org/10.1016/j.renene.2015.04.012

Choedkiatsakul, I., Ngaosuwan, K., Cravotto, G., & Assabumrungrat, S. (2014). Biodiesel production from palm oil using combined mechanical stirred and ultrasonic reactor. *Ultrasonics Sonochemistry*, *21*(4), 1585–1591. https://doi.org/10.1016/j.ultsonch.2013.12.025

Choudhury, T., Kayani, U. N., Gul, A., Haider, S. A., & Ahmad, S. (2023). Carbon emissions, environmental distortions, and impact on growth. *Energy Economics, 126*, 107040. https://doi.org/10.1016/j.eneco.2023.107040

Cintas, P., Mantegna, S., Calcio, E., & Cravotto, G. (2010). Ultrasonics Sonochemistry A new pilot flow reactor for high-intensity ultrasound irradiation . Application to the synthesis of biodiesel. *Ultrasonics - Sonochemistry*, *17*(6), 985–989. https://doi.org/10.1016/j.ultsonch.2009.12.003

COSTELLO | Spinning Tube in a Tube Reactor. (n.d.). Retrieved March 9, 2024, from https://rccostello.com/spinning_tube.html

Cruz, P. C., Silva, C. R., Rocha, F. A., & Ferreira, A. M. (2021). Mixing performance of planar oscillatory flow reactors with liquid solutions and solid suspensions. *Industrial and Engineering Chemistry Research*, *60*(6), 2663–2676. https://doi.org/10.1021/acs.iecr.0c04991

Csontos, B., Bernemyr, H., Erlandsson, A. C., Forsberg, O., Pach, M., & Hittig, H. (2019). Characterization of Deposits Collected from Plugged Fuel Filters. *SAE International Journal of Advances and Current Practices in Mobility*, *2*(2), 672–680. https://doi.org/10.4271/2019-24-0140

Cursaru, D. L., Brănoiu, G., Ramadan, I., & Miculescu, F. (2014). Degradation of automotive materials upon exposure to sunflower biodiesel. *Industrial Crops and Products*, *54*, 149–158. https://doi.org/10.1016/j.indcrop.2014.01.032

Dai, J. Y., Li, D. Y., Zhao, Y. C., & Xiu, Z. L. (2014). Statistical optimization for biodiesel production from soybean oil in a microchannel reactor. *Industrial and Engineering Chemistry Research*, *53*(22), 9325–9330. https://doi.org/10.1021/ie4037005

De la Mata, P., Dominguez-Vidal, A., Bosque-Sendra, J. M., Ruiz-Medina, A., Cuadros-Rodríguez, L., & Ayora-Cañada, M. J. (2012). Olive oil assessment in edible oil blends by means of ATR-FTIR and chemometrics. *Food Control*, *23*(2), 449–455. https://doi.org/10.1016/j.foodcont.2011.08.013

De Marco Rodriguez, I., Laresgoiti, M. F., Cabrero, M. A., Torres, A., Chomón, M. J., & Caballero, B. (2001). Pyrolysis of scrap tyres. *Fuel Processing Technology*, *72*(1), 9–22. https://doi.org/10.1016/S0378-3820(01)00174-6

Demirbas, A. (2009). Progress and recent trends in biodiesel fuels. *Energy Conversion and Management*, *50*(1), 14–34. https://doi.org/10.1016/j.enconman.2008.09.001

Deshmane, V. G., & Adewuyi, Y. G. (2013). Synthesis and kinetics of biodiesel formation via calcium methoxide base catalyzed transesterification reaction in the absence and presence of ultrasound. *Fuel*, *107*, 474–482. https://doi.org/10.1016/j.fuel.2012.12.080

Devaraj, K., Mani, Y., Rawoof, S. A. A., Thanarasu, A., Dhanasekaran, A., & Subramanian, S. (2020). Feasibility of biodiesel production from waste cooking oil: lab-scale to pilot-scale analysis. *Environmental Science and Pollution Research*, *27*(20), 25828–25835. https://doi.org/10.1007/S11356-020-09068-6

Devasan, R., Ruatpuia, J. V. L., Gouda, S. P., Kodgire, P., Basumatary, S., Halder, G., & Rokhum, S. L. (2023). Microwave-assisted biodiesel production using bio-waste catalyst and process optimization using response surface methodology and kinetic study. *Scientific Reports 2023 13:1*, *13*(1), 1–17. https://doi.org/10.1038/s41598-023-29883-4

Di Serio, M., Ledda, M., Cozzolino, M., Minutillo, G., Tesser, R., & Santacesaria, E. (2006). Transesterification of soybean oil to biodiesel by using heterogeneous basic catalysts. *Industrial and Engineering Chemistry Research*, *45*(9), 3009–3014. https://doi.org/10.1021/ie051402o

Díaz, L., Horstmann, F., Brito, A., & González, L. A. (2023). A comprehensive review of the influence of co-solvents on the catalysed methanolysis process to obtain biodiesel. *Heliyon*, *9*(1). https://doi.org/10.1016/j.heliyon.2023.e13006

Dong, Z., Wen, Z., Zhao, F., Kuhn, S., & Noël, T. (2021). Scale-up of micro- and milli-reactors: An overview of strategies, design principles and applications. *Chemical Engineering Science: X, 10*, 100097. https://doi.org/10.1016/j.cesx.2021.100097

Dubé, M. A., Tremblay, A. Y., & Liu, J. (2007). Biodiesel production using a membrane reactor. *Bioresource Technology*, *98*(3), 639–647. https://doi.org/10.1016/j.biortech.2006.02.019

El-Shafay, A. S., Ağbulut, Ü., Attia, E. A., Touileb, K. L., & Gad, M. S. (2023). Waste to energy: Production of poultry-based fat biodiesel and experimental assessment of its usability on engine behaviors. *Energy*, *262*, 125457. https://doi.org/10.1016/j.energy.2022.125457

Emiroğlu, A. O., & Şen, M. (2018). Combustion, performance and exhaust emission characterizations of a diesel engine operating with a ternary blend (alcohol-biodiesel-diesel fuel). *Applied Thermal Engineering*, *133*, 371–380. https://doi.org/10.1016/j.applthermaleng.2018.01.069

Encinar, J. M., González, J. F., & Rodríguez-Reinares, A. (2007). Ethanolysis of used frying oil. Biodiesel preparation and characterization. *Fuel Processing Technology*, *88*(5), 513–522. https://doi.org/10.1016/j.fuproc.2007.01.002

Encinar, J. M., Pardal, A., Sánchez, N., & Nogales, S. (2018). Biodiesel by Transesterification of Rapeseed Oil Using Ultrasound: A Kinetic Study of Base-Catalysed Reactions. *Energies, 11*(9), 2229. https://doi.org/10.3390/en11092229

Erol, D., Kadir Yeşilyurt, M., Yaman, H., & Doğan, B. (2023). Evaluation of the use of diesel-biodiesel-hexanol fuel blends in diesel engines with exergy analysis and sustainability index. *Fuel*, *337*. https://doi.org/10.1016/j.fuel.2022.126892

Fadara, O. A., Falowo, O. A., Ojumu, T. V., & Betiku, E. (2021). Process optimization of microwave irradiation-aided transesterification of kariya seed oil by Taguchi orthogonal array: pawpaw trunk as a novel biocatalyst. *Biofuels, Bioproducts and Biorefining*, *15*(4), 1006–1020. https://doi.org/10.1002/bbb.2193

Fakhri, S. N., Ramadhani, S. D., & Bismo, S. (2018). Coaxial dielectric barrier discharge plasma reactor for biodiesel production from palm oil and methanol. *E3S Web of Conferences*, *67*, 02009. https://doi.org/10.1051/e3sconf/20186702009

Fallah Kelarijani, A., Gholipour Zanjani, N., & Kamran Pirzaman, A. (2020). Ultrasonic Assisted Transesterification of Rapeseed Oil to Biodiesel Using Nano Magnetic Catalysts. *Waste and Biomass Valorization*, *11*(6), 2613–2621. https://doi.org/10.1007/s12649-019-00593-1

Farobie, O., & Matsumura, Y. (2015a). Biodiesel Production in Supercritical Methanol Using a Novel Spiral Reactor. *Procedia Environmental Sciences, 28*, 204–213. https://doi.org/10.1016/j.proenv.2015.07.027

Farobie, O., & Matsumura, Y. (2015b). Effectiveness of spiral reactor for biodiesel production using supercritical t-butyl methyl ether (MTBE). *Journal of the Japan Petroleum Institute, 58*(2), 110–117. https://doi.org/10.1627/jpi.58.110

Farobie, O., Samanmulya, T., & Matsumura, Y. (2016). Application of spiral reactor for biodiesel production in supercritical methanol and ethanol: process evaluation *Conference: The 3rd Asian Conference on Biomass Science (ACBS2016)* At: Nigata, Japan,

Farobie, O., Sasanami, K., & Matsumura, Y. (2015). A novel spiral reactor for biodiesel production in supercritical ethanol. *Applied Energy*, *147*, 20–29. https://doi.org/10.1016/j.apenergy.2015.02.033

Farvardin, M., Hosseinzadeh Samani, B., Rostami, S., Abbaszadeh-Mayvan, A., Najafi, G., & Fayyazi, E. (2022). Enhancement of biodiesel production from waste cooking oil: ultrasonic- hydrodynamic combined cavitation system. *Energy Sources, Part A: Recovery, Utilization and Environmental Effects*, *44*(2), 5065–5079. https://doi.org/10.1080/15567036.2019.1657524

Fayyazi, E., Ghobadian, B., Van De Bovenkamp, H. H., Najafi, G., Hosseinzadehsamani, B., Heeres, H. J., & Yue, J. (2018). Optimization of Biodiesel Production over Chicken Eggshell-Derived CaO Catalyst in a Continuous Centrifugal Contactor Separator. *Industrial and Engineering Chemistry Research*, *57*(38), 12742–12755. https://doi.org/10.1021/acs.iecr.8b02678

Feng, Z., Fan, X., Wang, Z., Yu, Y., Chen, L., Du, Y., & Dong, L. (2021). Corrosion Behavior and Passive Film Composition of Alloy 825 in High Temperature and High H2S-CO2 Containing Environment. *Frontiers in Materials*, *8*. https://doi.org/10.3389/fmats.2021.728898

Fernandes, D. M., Squissato, A. L., Lima, A. F., Richter, E. M., & Munoz, R. A. A. (2019). Corrosive character of Moringa oleifera Lam biodiesel exposed to carbon steel under simulated storage conditions. *Renewable Energy*, *139*, 1263–1271. https://doi.org/10.1016/j.renene.2019.03.034

Foutch, G. L., & Johannes, A. H. (2003). Reactors in Process Engineering. In R. A. Meyers (Ed.), *Encyclopedia of Physical Science and Technology (Third Edition)* (pp. 23–43). Academic Press. https://doi.org/10.1016/B0-12-227410-5/00654-2

Frankcombe, T. J., & Liu, Y. (2023). Interpretation of Oxygen 1s X-ray Photoelectron Spectroscopy of ZnO. *Chemistry of Materials*, *35*(14), 5468–5474. https://doi.org/10.1021/acs.chemmater.3c00801

Frankel, E. N. (2012). Photooxidation of unsaturated fats. *Lipid Oxidation*, 51–66. https://doi.org/10.1533/9780857097927.51

Frankel, G. S., & Sridhar, N. (2008). Understanding localized corrosion. *Materials Today*, *11*(10), 38–44. https://doi.org/10.1016/s1369-7021(08)70206-2

Freedman, B., Pryde, E. H., & Mounts, T. L. (1984). Variables affecting the yields of fatty esters from transesterified vegetable oils. *Journal of the American Oil Chemists Society*, *61*(10), 1638–1643. https://doi.org/10.1007/bf02541649

Fuels and lubes. (2024, March). *Brazil prepares to boost biodiesel blending goals - F&L Asia*. https://www.fuelsandlubes.com/fli-article/brazil-prepares-to-boost-biodiesel-blending-goals/

Furlan, P. Y., Wetzel, P., Johnson, S., Wedin, J., & Och, A. (2010). Investigating the Oxidation of Biodiesel From Used Vegetable Oil by FTIR Spectroscopy: Used Vegetable Oil Biodiesel Oxidation Study by FTIR. *Spectroscopy Letters*, *43*(7–8), 580–585. https://doi.org/10.1080/00387010.2010.510708

García-Martín, J. F., Barrios, C. C., Alés-Álvarez, F. J., Dominguez-Sáez, A., & Alvarez-Mateos, P. (2018). Biodiesel production from waste cooking oil in an oscillatory flow reactor. Performance as a fuel on a TDI diesel engine. *Renewable Energy*, *125*, 546–556. https://doi.org/10.1016/j.renene.2018.03.002

García-Martínez, O., Rojas, R. M., Vila, E., & de Vidales, J. L. M. (1993). Microstructural characterization of nanocrystals of ZnO and CuO obtained from basic salts. *Solid State Ionics*, *63–65*(C), 442–449. https://doi.org/10.1016/0167-2738(93)90142-p

Gaurav, K., Neeti, K., & Singh, R. (2024). Microalgae-based biodiesel production and its challenges and future opportunities: A review. *Green Technologies and Sustainability*, *2*(1), 100060. https://doi.org/10.1016/j.grets.2023.100060

Geller, D. P., Adams, T. T., Goodrum, J. W., & Pendergrass, J. (2008). Storage stability of poultry fat and diesel fuel mixtures: Specific gravity and viscosity. *Fuel*, *87*(1), 92–102. https://doi.org/10.1016/j.fuel.2007.03.043

Gengenbach, T. R., Major, G. H., Linford, M. R., & Easton, C. D. (2021). Practical guides for x-ray photoelectron spectroscopy (XPS): Interpreting the carbon 1s spectrum IN. *J. Vac. Sci. Technol. A*, *39*, 13204. https://doi.org/10.1116/6.0000682

Ghaini, A., Kashid, M. N., & Agar, D. W. (2010). Effective interfacial area for mass transfer in the liquid–liquid slug flow capillary microreactors. *Chemical Engineering and Processing: Process Intensification*, *49*(4), 358–366. https://doi.org/10.1016/j.cep.2010.03.009

Ghanbari, M., Mozafari-Vanani, L., Dehghani-Soufi, M., & Jahanbakhshi, A. (2021). Effect of alumina nanoparticles as additive with diesel–biodiesel blends on performance and emission characteristic of a six-cylinder diesel engine using response surface methodology (RSM). *Energy Conversion and Management: X*, *11*, 100091. https://doi.org/10.1016/j.ecmx.2021.100091

Ghazi, A. T. I. M., Resul, M. F. M. G., Yunus, R., & Shean Yaw, T. C. (2008). Preliminary design of oscillatory flow biodiesel reactor for continuous biodiesel

production from jatropha triglycerides. *Journal of Engineering Science and Technology*, *3*(2), 138–145.

Global Bioenergy Statistics Report 2024. (2024). *Global Bioenergy Statistics Report 2024 Summary*.

Gnaneswar Gude, V., Patil, P., Martinez-Guerra, E., Deng, S., & Nirmalakhandan, N. (2013). *Microwave energy potential for biodiesel production*. http://www.sustainablechemicalprocesses.com/content/1/5/5

Gonzalez-Quiroga, A., Djokic, M. R., Van Geem, K. M., & Marin, G. B. (2016). Conversion of Solid Waste to Diesel via Catalytic Pressureless Depolymerization: Pilot Scale Production and Detailed Compositional Characterization. *Energy and Fuels*, *30*(10), 8292–8303. https://doi.org/10.1021/acs.energyfuels.6b01639

Guan, G., Kusakabe, K., Moriyama, K., & Sakurai, N. (2009). Transesterification of sunflower oil with methanol in a microtube reactor. *Industrial and Engineering Chemistry Research*, *48*(3), 1357–1363. https://doi.org/10.1021/ie800852x

Gude, V. G., & Martinez-Guerra, E. (2015). *Green Chemistry of Microwave-Enhanced Biodiesel Production*. 225–250. https://doi.org/10.1007/978-94-017-9612-5_11

Gude, V. G., Patil, P., Martinez-Guerra, E., Deng, S., & Nirmalakhandan, N. (2013). Microwave energy potential for biodiesel production. *Sustainable Chemical Processes 2013 1:1*, *1*(1), 1–31. https://doi.org/10.1186/2043-7129-1-5

Guillén, M. D., & Cabo, N. (1997). Infrared spectroscopy in the study of edible oils and fats. *Journal of the Science of Food and Agriculture*, *75*(1), 1–11. https://doi.org/10.1002/(sici)1097-0010(199709)75

Gupta, J., Agarwal, M., & Dalai, A. K. (2019). Intensified transesterification of mixture of edible and nonedible oils in reverse flow helical coil reactor for biodiesel production. *Renewable Energy*, *134*, 509–525. https://doi.org/10.1016/j.renene.2018.11.057

Hamidi, R., Damizia, M., De Filippis, P., Patrizi, D., Verdone, N., Vilardi, G., & de Caprariis, B. (2023). Recent developments and future outlooks of hydrodynamic cavitation as an intensification technology for renewable biofuels production. *Journal of Environmental Chemical Engineering*, *11*(5), 110819. https://doi.org/10.1016/j.jece.2023.110819

Hapońska, M., Nurra, C., Abelló, S., Makkee, M., Salvadó, J., & Torras, C. (2019). Membrane reactors for biodiesel production with strontium oxide as a heterogeneous catalyst. *Fuel Processing Technology, 185*, 1–7. https://doi.org/10.1016/j.fuproc.2018.11.010

Harmsen, G. J. (2007). Reactive distillation: The front-runner of industrial process intensification. A full review of commercial applications, research, scale-up, design

and operation. *Chemical Engineering and Processing: Process Intensification*, *46*(9 SPEC. ISS..), 774–780. https://doi.org/10.1016/j.cep.2007.06.005

Harvey, A. P., Mackley, M. R., & Seliger, T. (2003). Process intensification of biodiesel production using a continuous oscillatory flow reactor. *Journal of Chemical Technology & Biotechnology*, *78*(2–3), 338–341. https://doi.org/10.1002/jctb.782

Haseeb, A. S. M. A., Masjuki, H. H., Ann, L. J., & Fazal, M. A. (2010). Corrosion characteristics of copper and leaded bronze in palm biodiesel. *Fuel Processing Technology*, *91*(3), 329–334. https://doi.org/10.1016/j.fuproc.2009.11.004

Hassan Pranta, M., & Muk Cho, H. (2025). A comprehensive review of the evolution of biodiesel production technologies. *Energy Conversion and Management, 328*, 119623. https://doi.org/10.1016/j.enconman.2025.119623

Hazrat, M. A., Rasul, M. G., Khan, M. M. K., Ashwath, N., Fattah, I. M. R., Ong, H. C., & Mahlia, T. M. I. (2023). Biodiesel production from transesterification of Australian Brassica napus L. oil: optimisation and reaction kinetic model development. *Environment, Development and Sustainability*, *25*(11), 12247–12272. https://doi.org/10.1007/S10668-022-02506-0

Hazrat, M. A., Rasul, M. G., Mofijur, M., Khan, M. M. K., Djavanroodi, F., Azad, A. K., Bhuiya, M. M. K., & Silitonga, A. S. (2020). A Mini Review on the Cold Flow Properties of Biodiesel and its Blends. *Frontiers in Energy Research*, *8*, 598651. https://doi.org/10.3389/fenrg.2020.598651/bibtex

Hendi1, A. H. Y., Al-Kuhaili, M. F., & Durrani, S. M. A. (2016). Chemical and optical properties of MnO_2 thin films prepared by reactive evaporation of manganese. *IJRET: International Journal of Research in Engineering and Technology*. http://ijret.esatjournals.org320

Hermoso-Diaz, I. A., Foroozan, A. E., Flores-De los Rios, J. P., Landeros-Martinez, L. L., Porcayo-Calderon, J., & Gonzalez-Rodriguez, J. G. (2019). Electrochemical and quantum chemical assessment of linoleic acid as a corrosion inhibitor for carbon steel in sulfuric acid solution. *Journal of Molecular Structure*, *1197*, 535–546. https://doi.org/10.1016/j.molstruc.2019.07.085

Hirani, A. H., Javed, N., Asif, M., Basu, S. K., & Kumar, A. (2018). A Review on First- and Second-Generation Biofuel Productions. *Biofuels: Greenhouse Gas Mitigation and Global Warming: Next Generation Biofuels and Role of Biotechnology*, 141–154. https://doi.org/10.1007/978-81-322-3763-1_8

Hood, Z. D., Adhikari, S. P., Evans, S. F., Wang, H., Li, Y., Naskar, A. K., Chi, M., Lachgar, A., & Paranthaman, M. P. (2018). Tire-derived carbon for catalytic preparation of biofuels from feedstocks containing free fatty acids. *Carbon Resources Conversion, 1*(2), 165–173. https://doi.org/10.1016/j.crcon.2018.07.007

Hoque, M. E., Gee, L. P., Hoque, M. E., & Gee, L. P. (2013). Biodiesel from Plant Resources—Sustainable Solution to Ever Increasing Fuel Oil Demands. *Journal of Sustainable Bioenergy Systems*, *3*(3), 163–170. https://doi.org/10.4236/jsbs.2013.33023

Hosseinzadeh Samani, B., Ansari Samani, M., Shirneshan, A., Fayyazi, E., Najafi, G., & Rostami, S. (2020). Evaluation of an enhanced ultrasonic-assisted biodiesel synthesized using safflower oil in a diesel power generator. *Biofuels*, *11*(4), 523–532. https://doi.org/10.1080/17597269.2019.1646542

Hussain, Z. (2018a). Non-Catalytic and Catalytic Routes for Biodiesel Production. December.*Ph.D. Thesis*, Rajiv Gandhi Institute of Petroleum Technology, Jais (Amethi), India, 2018.

Ilyin, A. M. (2017). Auger Electron Spectroscopy. *Microscopy Methods in Nanomaterials Characterization*, 363–381. https://doi.org/10.1016/b978-0-323-46141-2.00011-0

Islam, M. R., Islam, M. N., Mustafi, N. N., Rahim, M. A., & Haniu, H. (2013). Thermal Recycling of Solid Tire Wastes for Alternative Liquid Fuel: The First Commercial Step in Bangladesh. *Procedia Engineering*, *56*, 573–582. https://doi.org/10.1016/j.proeng.2013.03.162

Islam, M. T., Rashid, F., & Arefin, M. A. (2021). Numerical analysis of the performance and NOx emission of a diesel engine fueled with algae biofuel-diesel blends. *Energy Sources, Part A: Recovery, Utilization and Environmental Effects*. https://doi.org/10.1080/15567036.2021.1895916;subpage:string:full

Istiningrum, R. B., Aprianto, T., & Pamungkas, F. L. U. (2017). Effect of reaction temperature on biodiesel production from waste cooking oil using lipase as biocatalyst. *AIP Conference Proceedings*, *1911*(1), 20031. https://doi.org/10.1063/1.5016024/720773

Jachuck, R., Pherwani, G., & Gorton, S. M. (2009). Green engineering: Continuous production of biodiesel using an alkaline catalyst in an intensified narrow channel reactor. *Journal of Environmental Monitoring, 11*(3), 642–647. https://doi.org/10.1039/B807390M

Jafari, M., Vanoppen, M., van Agtmaal, J. M. C., Cornelissen, E. R., Vrouwenvelder, J. S., Verliefde, A., van Loosdrecht, M. C. M., & Picioreanu, C. (2021). Cost of fouling in full-scale reverse osmosis and nanofiltration installations in the Netherlands. *Desalination*, *500*, 114865. https://doi.org/10.1016/j.desal.2020.114865

Jalali, E., Maghsoudi, S., & Noroozian, E. (2020). A novel method for biosynthesis of different polymorphs of TiO2 nanoparticles as a protector for Bacillus thuringiensis from Ultra Violet. *Scientific Reports*, *10*(1), 1–9. https://doi.org/10.1038/s41598-019-57407-6

Jamil, M. F., Uemura, Y., Kusakabe, K., Ayodele, O. B., Osman, N., Majid, N. M. N. A., & Yusup, S. (2016). Transesterification of Mixture of Castor Oil and Sunflower Oil in Millichannel Reactor: FAME Yield and Flow Behaviour. *Procedia Engineering*, *148*(December), 378–384. https://doi.org/10.1016/j.proeng.2016.06.487

Jayabal, R. (2025). Environmental impact of adding hybrid nanoparticles and hydrogen to the algae biodiesel-diesel blend on engine emissions. *Process Safety and Environmental Protection*, *198*, 107102. https://doi.org/10.1016/j.psep.2025.107102

Jayaprabakar, J., Dawn, S. S., Anish, M., Giri, J., Sudhakar, K., Alarfaj, A. A., & Guru, A. (2024). Development of Free Fatty Acid (FFA) monitoring device for evaluation of oil samples used for biodiesel production. *Heliyon*, *10*(17), e37118. https://doi.org/10.1016/j.heliyon.2024.e37118

Jazie, A. A., Abed, S. A., Nuhma, M. J., & Mutar, M. A. (2020). Continuous biodiesel production in a packed bed reactor from microalgae Chlorella sp. using DBSA catalyst. *Engineering Science and Technology, an International Journal*, *23*(3), 642–649. https://doi.org/10.1016/j.jestch.2019.08.002

Jeremy Moorhouse, E. A.-R. E. M. A. G. (2024, February). *India could triple its biofuel use and accelerate global deployment – Analysis - IEA*. https://www.iea.org/commentaries/india-could-triple-its-biofuel-use-and-accelerate-global-deployment

Kamari, A., Ishak, S., Hussin, M. I. A. M., Wong, S. T. S., Jumadi, J., & Yahaya, N. M. (2020). Optimisation and characterisation studies of biodiesel production from black soldier fly larvae fed by soya residue. *IOP Conference Series: Materials Science and Engineering*, *980*(1), 012057. https://doi.org/10.1088/1757-899x/980/1/012057

Karagoz, M., Uysal, C., Agbulut, U., & Saridemir, S. (2020). Energy, exergy, economic and sustainability assessments of a compression ignition diesel engine fueled with tire pyrolytic oil−diesel blends. *Journal of Cleaner Production*, *264*, 121724. https://doi.org/10.1016/j.jclepro.2020.121724

Kashyap, S. S., Gogate, P. R., & Joshi, S. M. (2019). Ultrasound assisted synthesis of biodiesel from karanja oil by interesterification: Intensification studies and optimization using RSM. *Ultrasonics Sonochemistry*, *50*, 36–45. https://doi.org/10.1016/j.ultsonch.2018.08.019

Kaya, C., & Kökkülünk, G. (2023). Biodiesel as alternative additive fuel for diesel engines: An experimental and theoretical investigation on emissions and performance characteristics. *Energy Sources, Part A: Recovery, Utilization, and Environmental Effects*, *45*(4), 10741–10763. https://doi.org/10.1080/15567036.2020.1774685

Keskin, A., Gürü, M., & Altiparmak, D. (2007). Biodiesel production from tall oil with synthesized Mn and Ni based additives: Effects of the additives on fuel consumption and emissions. *Fuel*, *86*(7–8), 1139–1143. https://doi.org/10.1016/j.fuel.2006.10.021

Khan, H. M., Iqbal, T., Mujtaba, M. A., Soudagar, M. E. M., Veza, I., & Fattah, I. M. R. (2021). Microwave Assisted Biodiesel Production Using Heterogeneous Catalysts. *Energies 2021, 14*(23), 8135. https://doi.org/10.3390/en14238135

Khan, M. A., & Adewuyi, Y. G. (2019). Techno-economic modeling and optimization of catalytic reactive distillation for the esterification reactions in bio-oil upgradation. *Chemical Engineering Research and Design*, *148*, 86–101. https://doi.org/10.1016/j.cherd.2019.05.037

Khan, O., Alsaduni, I., Equbal, A., Parvez, M., & Yadav, A. K. (2024). Performance and emission analysis of biodiesel blends enriched with biohydrogen and biogas in internal combustion engines. *Process Safety and Environmental Protection*, *183*, 1013–1037. https://doi.org/10.1016/j.psep.2024.01.049

Khedri, B., Mostafaei, M., & Safieddin Ardebili, S. M. (2019). A review on microwave-assisted biodiesel production. *Energy Sources, Part A: Recovery, Utilization, and Environmental Effects, 41*(19), 2377–2395. https://doi.org/10.1080/15567036.2018.1563246

Khelafi, M., Djaafri, M., Kalloum, S., Atelge, M. R., Abut, S., Dahbi, A., Bekirogullari, M., & Atabani, A. E. (2022). Effect of stirring speeds on biodiesel yield using an innovative oscillatory reactor and conventional STR (A comparative study). *Fuel*, *325*, 124856. https://doi.org/10.1016/j.fuel.2022.124856

Khond, V. W., & Kriplani, V. M. (2016). Effect of nanofluid additives on performances and emissions of emulsified diesel and biodiesel fueled stationary CI engine: A comprehensive review. *Renewable and Sustainable Energy Reviews*, *59*, 1338–1348. https://doi.org/10.1016/j.rser.2016.01.051

Knothe, G., & Razon, L. F. (2017). Biodiesel fuels. *Progress in Energy and Combustion Science*, *58*, 36–59. https://doi.org/10.1016/j.pecs.2016.08.001

Kombe, G. G. (2024). Exploring the landscape of ultrasonic transesterification: Unveiling priority research areas through bibliometric insights. *Energy Conversion and Management: X*, *23*, 100586. https://doi.org/10.1016/j.ecmx.2024.100586

Kong, H., Li, W., Lu, X., Wang, J., Olagunju, O. A., Musonge, P., & Kiambi, S. L. (2022). Production and Optimization of Biodiesel in a Membrane Reactor, Using a Solid Base Catalyst. *Membranes 2022, Vol. 12, Page 674*, *12*(7), 674. https://doi.org/10.3390/membranes12070674

Kouhifaiegh, M., Hosseinzadeh Samani, B., Ebrahimi, R., & Taki, K. (2024). Design and construction of a single orifice oscillatory flow reactor for the continuous

production of biodiesel from sunflower oil. *Biofuels, 15*(8), 1041–1050. https://doi.org/10.1080/17597269.2024.2330187

Krishna, D. N. G., & Philip, J. (2022). Review on surface-characterization applications of X-ray photoelectron spectroscopy (XPS): Recent developments and challenges. *Applied Surface Science Advances*, *12*, 100332. https://doi.org/10.1016/j.apsadv.2022.100332

Kumar Biswas, P., Pohit, S., & Kumar, R. (2010). Biodiesel from jatropha: Can India meet the 20% blending target? *Energy Policy, 38*(3), 1477–1484. https://doi.org/10.1016/j.enpol.2009.11.029

Kumar, T. S., & Ashok, B. (2023). Corrosion behaviour analysis of SI engine components for ethanol-gasoline blends in flex fuel vehicular application. *Fuel Processing Technology*, *240*, 107574. https://doi.org/10.1016/j.fuproc.2022.107574

Kumaravel, S. T., Murugesan, A., & Kumaravel, A. (2016). Tyre pyrolysis oil as an alternative fuel for diesel engines – A review. *Renewable and Sustainable Energy Reviews, 60*, 1678–1685. https://doi.org/10.1016/j.rser.2016.03.035

Kuppusamy, S., Azhagesan, A., Kumar, P., Sahu, D., Verma, S., & Almutairi, B. O. (2024). Production and characterization of biodiesel fuel produced from third-generation feedstock. *Frontiers in Materials*, *11*, 1454120. https://doi.org/10.3389/fmats.2024.1454120

Kuznetsov, V. V. (2011). Heat and Mass Transfer With Phase Change and Chemical Reactions in Microscale. *2010 14th International Heat Transfer Conference, IHTC 14*, *8*, 209–228. https://doi.org/10.1115/ihtc14-22570

Labhane, P. K., Huse, V. R., Patle, L. B., Chaudhari, A. L., & Sonawane, G. H. (2015). Synthesis of Cu Doped ZnO Nanoparticles: Crystallographic, Optical, FTIR, Morphological and Photocatalytic Study. *Journal of Materials Science and Chemical Engineering*, *03*(07), 39–51. https://doi.org/10.4236/msce.2015.37005

Leevijit, T., Wisutmethangoon, W., Prateepchaikul, G., Tongurai, C., & Allen, M. (2006). Design and test of a continuous reactor for palm oil transesterification. *Songklanakarin Journal of Science and Technology*, *28*(4), 791–802.

Li, W., Li, G., Wang, F., Zhu, H., He, W., & Huang, J. (2022). Optimization and Comparison of Biodiesel Production Process by Electric Heating and Microwave-Assisted Heating Transesterification for Waste Cooking Oil via One-Way Experiments and ANOVA. *Frontiers in Environmental Science*, *10*, 885453. https://doi.org/10.3389/fenvs.2022.885453/bibtex

Linke, J., Du, J., Loewenhoff, T., Pintsuk, G., Spilker, B., Steudel, I., & Wirtz, M. (2019). Challenges for plasma-facing components in nuclear fusion. *Matter and Radiation at Extremes*, *4*(5), 56201. https://doi.org/10.1063/1.5090100/253043

Liu, H., Lukić, I., Miladinović, M. R., Veljković, V. B., Zdujić, M., Zhu, X., Zhang, Y., & Skala, D. U. (2018). Continuous biodiesel production under subcritical condition of methanol – Design of pilot plant and packed bed reactor with MnCO3/Na-silicate catalyst. *Energy Conversion and Management, 168*, 494–504. https://doi.org/10.1016/j.enconman.2018.05.028

Liu, J., Dong, J., Li, X., Xu, T., Li, Z., Ampah, J. D., Ikram, M., Zhang, S., Jin, C., Geng, Z., Sun, T., & Liu, H. (2023). Technical analysis of blending fusel to reduce carbon emission and pollution emission of diesel engine. *Fuel Processing Technology*, *241*, 107560. https://doi.org/10.1016/j.fuproc.2022.107560

Lodha, H., Jachuck, R., & Suppiah Singaram, S. (2012a). Intensified biodiesel production using a rotating tube reactor. *Energy and Fuels*, *26*(11), 7037–7040. https://doi.org/10.1021/ef301235t

López-Guajardo, E., Ortiz-Nadal, E., Montesinos-Castellanos, A., & Nigam, K. D. P. (2017). Coiled flow inverter as a novel alternative for the intensification of a liquid-liquid reaction. *Chemical Engineering Science*, *169*, 179–185. https://doi.org/10.1016/J.CES.2017.01.016

López-Guajardo, Enrique Ortiz-Nadal, Enrique Montesinos-Castellanos, A., & Nigam, K. D. P. (2017). Process Intensification of Biodiesel Production Using a Tubular Micro-Reactor (TMR): Experimental and Numerical Assessment. *Chemical Engineering Communications*, *204*(4), 467–475. doi: 10.1080/00986445.2016.1277521

Lott, P., & Deutschmann, O. (2023). Heterogeneous chemical reactions—A cornerstone in emission reduction of local pollutants and greenhouse gases. *Proceedings of the Combustion Institute*, *39*(3), 3183–3215. https://doi.org/10.1016/j.proci.2022.06.001

Madhawan, A., Arora, A., Das, J., Kuila, A., & Sharma, V. (2018). Microreactor technology for biodiesel production: a review. *Biomass Conversion and Biorefinery*, *8*(2), 485–496. https://doi.org/10.1007/S13399-017-0296-0/METRICS

Madiwale, S., Karthikeyan, A., & Bhojwani, V. (2017). A Comprehensive Review of Effect of Biodiesel Additives on Properties, Performance, and Emission. *IOP Conference Series: Materials Science and Engineering*, *197*(1). https://doi.org/10.1088/1757-899x/197/1/012015

Mahamuni, N. N., & Adewuyi, Y. G. (2009). Optimization of the synthesis of biodiesel via ultrasound-enhanced base-catalyzed transesterification of soybean oil using a multifrequency ultrasonic reactor. *Energy and Fuels*, *23*(5), 2757–2766. https://doi.org/10.1021/ef900047j

Mahamuni, N. N., & Adewuyi, Y. G. (2010). Application of taguchi method to investigate the effects of process parameters on the transesterification of soybean

oil using high frequency ultrasound. *Energy and Fuels*, *24*(3), 2120–2126. https://doi.org/10.1021/ef901488g

Maheshwari, P., Haider, M. B., Yusuf, M., Klemeš, J. J., Bokhari, A., Beg, M., Al-Othman, A., Kumar, R., & Jaiswal, A. K. (2022). A review on latest trends in cleaner biodiesel production: Role of feedstock, production methods, and catalysts. *Journal of Cleaner Production*, *355*, 131588. https://doi.org/10.1016/j.jclepro.2022.131588

Malani, R. S., Shinde, V., Ayachit, S., Goyal, A., & Moholkar, V. S. (2019). Ultrasound–assisted biodiesel production using heterogeneous base catalyst and mixed non–edible oils. *Ultrasonics Sonochemistry*, *52*, 232–243. https://doi.org/10.1016/j.ultsonch.2018.11.021

Malaysia: Biofuels Annual(USDA). (2023, November). *Malaysia: Biofuels Annual | USDA Foreign Agricultural Service*. https://www.fas.usda.gov/data/malaysia-biofuels-annual-7

Martinez-Guerra, E., & Gude, V. G. (2014). Transesterification of used vegetable oil catalyzed by barium oxide under simultaneous microwave and ultrasound irradiations. *Energy Conversion and Management*, *88*, 633–640. https://doi.org/10.1016/j.enconman.2014.08.060

Matwijczuk, A., Zając, G., Kowalski, R., Kachel-Jakubowska, M., & Gagoś, M. (2017). Spectroscopic Studies of the Quality of Fatty Acid Methyl Esters Derived from Waste Cooking Oil. *Polish Journal of Environmental Studies*, *26*(6), 2643–2650. https://doi.org/10.15244/pjoes/70431

Meenakshi, H. N., & Shyamala, R. (2015). Effect of flow and dissolved oxygen on the compatibility of pongamia pinnata biodiesel with common construction materials used in storage and transportation. *International Journal of Chemical Engineering*, *2015*. https://doi.org/10.1155/2015/463064

Mehboob, A., Nisar, S., Rashid, U., Shean, T., Choong, Y., Khalid, T., & Qadeer, H. A. (2016). Reactor designs for the production of biodiesel. *Ijcbs*, *10*, 87–94.

Meher, L. C., Vidya Sagar, D., & Naik, S. N. (2006). Technical aspects of biodiesel production by transesterification - A review. *Renewable and Sustainable Energy Reviews*, *10*(3), 248–268. https://doi.org/10.1016/j.rser.2004.09.002

Meza-Ramírez, D. B., Hernández-Benítez, C., Contreras-Arias, A., Godínez, L. A., & Rodríguez-Valadez, F. J. (2021). Optimization of an ultrasonic reactor on a semi-pilot scale for biodiesel production. *Fuel, 288*, 119645. https://doi.org/10.1016/j.fuel.2020.119645

Mia, M., Islam, A., Rubel, R. I., & Islam, M. R. (2017). Fractional Distillation & Characterization of Tire Derived Pyrolysis Oil. *International journal of engineering technologies*, *3*(1).

Milano, J., Umar, H., Shamsuddin, A. H., Silitonga, A. S., Irfan, O. M., Sebayang, A. H., Fattah, I. M. R., & Mofijur, M. (2021). Experimental Study of the Corrosiveness of Ternary Blends of Biodiesel Fuel. *Frontiers in Energy Research*, *9*(November), 1–20. https://doi.org/10.3389/fenrg.2021.778801

Ministry of Petroleum & Natural Gas (PIB Delhi). (2024, July 25). *Press Release:Press Information Bureau*. https://www.pib.gov.in/PressReleasePage.aspx?PRID=2036867

Mirghani, M. E. S., Kabbashi, N. A., Alam, M. Z., Qudsieh, I. Y., & Alkatib, M. F. R. (2011). Rapid Method for the Determination of Moisture Content in Biodiesel Using FTIR Spectroscopy. *Journal of the American Oil Chemists' Society*, *88*(12), 1897–1904. https://doi.org/10.1007/S11746-011-1866-0

Mishra, B., Thakare, A., Mukherjee, A., Mullick, A., Moulik, S., & Roy, A. (2022). Sustainable Approach to Biodiesel Production Using Hydrodynamic Cavitation Route. *Environmental Science and Engineering*, 1093–1119. https://doi.org/10.1007/978-3-030-96554-9_73

Mofijur, M., Ahmed, S. F., Ahmed, B., Mehnaz, T., Mehejabin, F., Shome, S., Almomani, F., Chowdhury, A. A., Kalam, M. A., Badruddin, I. A., & Kamangar, S. (2024). Impact of nanoparticle-based fuel additives on biodiesel combustion: An analysis of fuel properties, engine performance, emissions, and combustion characteristics. *Energy Conversion and Management: X*, *21*, 100515. https://doi.org/10.1016/j.ecmx.2023.100515

Mohadesi, M., Aghel, B., Maleki, M., & Ansari, A. (2020). The use of KOH/Clinoptilolite catalyst in pilot of microreactor for biodiesel production from waste cooking oil. *Fuel*, *263*(November), 116659. https://doi.org/10.1016/j.fuel.2019.116659

Mohamed Shameer, P., Ramesh, K., Sakthivel, R., & Purnachandran, R. (2017). Effects of fuel injection parameters on emission characteristics of diesel engines operating on various biodiesel: A review. *Renewable and Sustainable Energy Reviews*, *67*, 1267–1281. https://doi.org/10.1016/j.rser.2016.09.117

Mohd, A., Kushaari, K., Azeem, B., Yusup, S., Chin, J., & Denecke, J. (2020). Rapid production of biodiesel in a microchannel reactor at room temperature by enhancement of mixing behaviour in methanol phase using volume of fluid model. *Chemical Engineering Science*, *219*, 115532. https://doi.org/10.1016/j.ces.2020.115532

Mondal, B., & Jana, A. K. (2019). Techno-economic Feasibility of Reactive Distillation for Biodiesel Production from Algal Oil: Comparing with a Conventional Multiunit System. *Industrial and Engineering Chemistry Research*, *58*(27), 12028–12040. https://doi.org/10.1021/acs.iecr.9b00347

Monika, Banga, S., & Pathak, V. V. (2023). Biodiesel production from waste cooking oil: A comprehensive review on the application of heterogenous catalysts. *Energy Nexus*, *10*, 100209. https://doi.org/10.1016/j.nexus.2023.100209

Motasemi, F., & Ani, F. N. (2012). A review on microwave-assisted production of biodiesel. *Renewable and Sustainable Energy Reviews*, *16*(7), 4719–4733. https://doi.org/10.1016/j.rser.2012.03.069

Mrabet, Z., Alsamara, M., Saleh, A. S., & Anwar, S. (2019). Urbanization and non-renewable energy demand: A comparison of developed and emerging countries. *Energy, 170*, 832–839. https://doi.org/10.1016/j.energy.2018.12.198

Mumtaz, M. W., Adnan, A., Mukhtar, H., Rashid, U., & Danish, M. (2017). Biodiesel Production Through Chemical and Biochemical Transesterification: Trends, Technicalities, and Future Perspectives. *Clean Energy for Sustainable Development: Comparisons and Contrasts of New Approaches*, 465–485. https://doi.org/10.1016/b978-0-12-805423-9.00015-6

Murugesan, P., Hoang, A. T., Perumal Venkatesan, E., Santosh Kumar, D., Balasubramanian, D., Le, A. T., & Pham, V. V. (2022). Role of hydrogen in improving performance and emission characteristics of homogeneous charge compression ignition engine fueled with graphite oxide nanoparticle-added microalgae biodiesel/diesel blends. *International Journal of Hydrogen Energy*, *47*(88), 37617–37634. https://doi.org/10.1016/j.ijhydene.2021.08.107

Musa, I. A. (2016). The effects of alcohol to oil molar ratios and the type of alcohol on biodiesel production using transesterification process. *Egyptian Journal of Petroleum*, *25*(1), 21–31. https://doi.org/10.1016/j.ejpe.2015.06.007

N, A. L., B, A. A., E, K. . E., & A, R. M. (2014). Corrosion and Engine Test Analysis of Neem *(Azadirachta indica)* Oil Blends in a Single Cylinder, Four Stroke, and Air-cooled Compresion Ignition Engine. *American Journal of Mechanical Engineering*, *2*(6), 151–158. https://doi.org/10.12691/ajme-2-6-1

Na, S. H., & Park, C. H. (2009). First-Principles Study of the Surface of Wurtzite ZnO and ZnS - Implications for Nanostructure Formation. *Journal of the Korean Physical Society*, *54*(9), 867–872. https://doi.org/10.3938/jkps.54.867

Najafi, G. (2018). Diesel engine combustion characteristics using nano-particles in biodiesel-diesel blends. *Fuel*, *212*, 668–678. https://doi.org/10.1016/j.fuel.2017.10.001

Nanthagopal, K., Ashok, B., Saravanan, B., Patel, D., Sudarshan, B., & Aaditya Ramasamy, R. (2018). An assessment on the effects of 1-pentanol and 1-butanol as additives with Calophyllum Inophyllum biodiesel. *Energy Conversion and Management*, *158*, 70–80. https://doi.org/10.1016/j.enconman.2017.12.048

Natarajan, Y., Nabera, A., Salike, S., Dhanalakshmi Tamilkkuricil, V., Pandian, S., Karuppan, M., & Appusamy, A. (2019). An overview on the process intensification of microchannel reactors for biodiesel production. *Chemical Engineering and Processing - Process Intensification*, *136*, 163–176. https://doi.org/10.1016/j.cep.2018.12.008

Nema, V. K., Singh, A., Chaurasiya, P. K., Gogoi, T. K., Verma, T. N., & Tiwari, D. (2023). Combustion, performance, and emission behavior of a CI engine fueled with different biodiesels: A modelling, forecasting and experimental study. *Fuel*, *339*, 126976. https://doi.org/10.1016/j.fuel.2022.126976

Nesbitt, H. W., & Banerjee, D. (1998a). Interpretation of XPS Mn(2p) spectra of Mn oxyhydroxides and constraints on the mechanism of MnO2 precipitation. *American Mineralogist*, *83*(3–4), 305–315. https://doi.org/10.2138/am-1998-3-414

Nesbitt, H. W., Legrand, D., & Bancroft, G. M. (2000). Interpretation of Ni2p XPS spectra of Ni conductors and Ni insulators. *Physics and Chemistry of Minerals*, *27*(5), 357–366. https://doi.org/10.1007/s002690050265

Ng, J.-H., Yang, J. K. Y., Subramaniam, K., Wong, K. Y., Chiong, M. C., & Chong, C. T. (2023). Microwave-Heated Tubular Reactor for Enhanced Biodiesel Transesterification Process. *Chemical Engineering Transactions, 106*, 667–672. https://doi.org/10.3303/cet23106112

Nguyen, V. P., Nguyen, H. H. M., Nguyen, D. T., Nguyen, H. L., & Huynh, T. M. (2018). Optimization of biodiesel production from waste cooking oil using static mixer technology in Vietnam. *Biofuels*, *9*(5), 567–574. https://doi.org/10.1080/17597269.2018.1426165

Nollet, L. M. L., & Toldra, F. (Eds.). (2015). Handbook of Food Analysis—Two Volume Set (3rd ed.). *CRC Press*. https://doi.org/10.1201/b18668

Nomanbhay, S., & Ong, M. Y. (2017). A Review of Microwave-Assisted Reactions for Biodiesel Production. *Bioengineering 2017, Vol. 4, Page 57*, *4*(2), 57. https://doi.org/10.3390/bioengineering4020057

Noshadi, I., Amin, N. A. S., & Parnas, R. S. (2012). Continuous production of biodiesel from waste cooking oil in a reactive distillation column catalyzed by solid heteropolyacid: Optimization using response surface methodology (RSM). *Fuel*, *94*, 156–164. https://doi.org/10.1016/j.fuel.2011.10.018

Nurhidayanti, N. (2021). The Effect of Use Microwave Irradiation in Produce Biodiesel Nyamplung Oil (Calophyllum inophyllum Linn) Using KOH Catalyst. *Journal of Physics: Conference Series*, *1845*(1), 012064. https://doi.org/10.1088/1742-6596/1845/1/012064

Olagunju, O. A., & Musonge, P. (2017). Production of Biodiesel Using a Membrane Reactor to Minimize Separation Cost. *IOP Conference Series: Earth and Environmental Science*, *78*(1). https://doi.org/10.1088/1755-1315/78/1/012019

Oliveira, P. A., Baesso, R. M., Morais, G. C., Alvarenga, A. V., & Costa-Félix, R. P. B. (2021). Ultrasound-assisted transesterification of soybean oil using low power and high frequency and no external heating source. *Ultrasonics Sonochemistry*, *78*, 105709. https://doi.org/10.1016/j.ultsonch.2021.105709

Oni, B. A., Sanni, S. E., Ezurike, B. O., & Okoro, E. E. (2022). Effect of corrosion rates of preheated Schinzochytrium sp. Microalgae biodiesel on metallic components of a diesel engine. *Alexandria Engineering Journal, 61*(10), 7509–7528. https://doi.org/10.1016/j.aej.2022.01.005

Osman, A. I., Fang, B., Zhang, Y., Liu, Y., Yu, J., Farghali, M., Rashwan, A. K., Chen, Z., Chen, L., Ihara, I., Rooney, D. W., & Yap, P. S. (2024). Life cycle assessment and techno-economic analysis of sustainable bioenergy production: a review. *Environmental Chemistry Letters 2024 22:3*, *22*(3), 1115–1154. https://doi.org/10.1007/S10311-023-01694-Z

Osman, A. I., Nasr, M., Farghali, M., Rashwan, A. K., Abdelkader, A., Al-Muhtaseb, A. H., Ihara, I., & Rooney, D. W. (2024). Optimizing biodiesel production from waste with computational chemistry, machine learning and policy insights: a review. *Environmental Chemistry Letters 2024 22:3*, *22*(3), 1005–1071. https://doi.org/10.1007/S10311-024-01700-Y

Oza, S., Kodgire, P., Kachhwaha, S. S., Lam, M. K., Yusup, S., Chai, Y. H., & Rokhum, S. L. (2024). A review on sustainable and scalable biodiesel production using ultra-sonication technology. *Renewable Energy*, *226*, 120399. https://doi.org/10.1016/J.renene.2024.120399

Pandey, S. P., Upadhyay, R., Prakash, R., & Kumar, S. (2023). Performance and emission analysis of blends of bio-oil obtained by catalytic pyrolysis of Argemone mexicana seeds with diesel in a CI engine. *Environmental Science and Pollution Research*, *30*(60), 125034–125047. https://doi.org/10.1007/s11356-022-24648-4

Panithasan, M. S., Gopalakichenin, D., Venkadesan, G., & Malairajan, M. (2020). Evaluating the working characters of a diesel engine fueled with biodiesel blends added with rice husk Nano particles. *Energy Sources, Part A: Recovery, Utilization, and Environmental Effects*. https://doi.org/10.1080/15567036.2020.1767726

Parikh, H. B., Prajapati, V. M., & Thakkar, K. H. (n.d.). Performance evaluation and emission analysis of 4-s, i.c. engine using ethanol bio-diesel blended with diesel fuel. *IJRET: International Journal of Research in Engineering and Technology*. Retrieved September 2, 2024, from http://www.ijret.org

Park, S. H., Cha, J., Kim, H. J., & Lee, C. S. (2012). Effect of early injection strategy on spray atomization and emission reduction characteristics in bioethanol blended diesel fueled engine. *Energy (Oxford)*, *39*(1), 375–387. https://doi.org/10.1016/j.energy.2011.12.050

Parker, T., Limer, E., Watson, A. D., Defernez, M., Williamson, D., & Kemsley, E. K. (2014). 60 MHz 1H NMR spectroscopy for the analysis of edible oils. *TrAC Trends in Analytical Chemistry*, *57*, 147–158. https://doi.org/10.1016/j.trac.2014.02.006

Patel, C., Chandra, K., Hwang, J., Agarwal, R. A., Gupta, N., Bae, C., Gupta, T., & Agarwal, A. K. (2019). Comparative compression ignition engine performance, combustion, and emission characteristics, and trace metals in particulates from Waste cooking oil, Jatropha and Karanja oil derived biodiesels. *Fuel*, *236*, 1366–1376. https://doi.org/10.1016/j.fuel.2018.08.137

Payne, B. P., Biesinger, M. C., & Mcintyre, N. S. (2012). Use of oxygen/nickel ratios in the XPS characterisation of oxide phases on nickel metal and nickel alloy surfaces. *Journal of Electron Spectroscopy and Related Phenomena*, *185*, 159–166. https://doi.org/10.1016/j.elspec.2012.06.008

Peer, M. S., Kasimani, R., Rajamohan, S., & Ramakrishnan, P. (2017). Experimental evaluation on oxidation stability of biodiesel/diesel blends with alcohol addition by rancimat instrument and FTIR spectroscopy. *Journal of Mechanical Science and Technology*, *31*(1), 455–463. https://doi.org/10.1007/s12206-016-1248-5

Peigang, C., Tremblay, A. Y., Dubé, M. A., & Morse, K. (2007). Effect of membrane pore size on the performance of a membrane reactor for biodiesel production. *Industrial and Engineering Chemistry Research*, *46*(1), 52–58. https://doi.org/10.1021/ie060555o

Pérez-Cisneros, E. S., Mena-Espino, X., Rodríguez-López, V., Sales-Cruz, M., Viveros-García, T., & Lobo-Oehmichen, R. (2016). An integrated reactive distillation process for biodiesel production. *Computers & Chemical Engineering*, *91*, 233–246. https://doi.org/10.1016/J.compchemeng.2016.01.008

Petchsoongsakul, N., Ngaosuwan, K., Kiatkittipong, W., Aiouache, F., & Assabumrungrat, S. (2017). Process design of biodiesel production: Hybridization of ester-and transesterification in a single reactive distillation. *Energy Conversion and Management*, *153*, 493–503. https://doi.org/10.1016/j.enconman.2017.10.013

Poddar, T., Jagannath, A., & Almansoori, A. (2015). Biodiesel Production using Reactive Distillation: A Comparative Simulation Study. *Energy Procedia*, *75*, 17–22. https://doi.org/10.1016/j.egypro.2015.07.129

Pote, R. N., & Patil, R. K. (2019). Combustion and emission characteristics analysis of waste tyre pyrolysis oil. *SN Applied Sciences*, *1*(4), 1–17. https://doi.org/10.1007/s42452-019-0308-8

Prabhu, C., Navaneetha Krishnan, B., Prakash, T., Rajasekar, V., Balasubramanian, D., Le, V. V., Linh Le, N. V., Phong Nguyen, P. Q., & Nguyen, V. N. (2023). Biodiesel unsaturation and the synergic effects of hydrogen sharing rate on the characteristics of a compression ignition engine in dual-fuel mode. *Fuel*, *334*, 126699. https://doi.org/10.1016/j.fuel.2022.126699

Pradana, Y. S., Hidayat, A., Prasetya, A., & Budiman, A. (2017). Biodiesel production in a reactive distillation column catalyzed by heterogeneous potassium catalyst. *Energy Procedia*, *143*, 742–747. https://doi.org/10.1016/j.egypro.2017.12.756

Prajapati, A. K., Yadawa, Y., Dwivedi, D., & Kumar, R. (2024). Fuel property enhancement of Jatropha biodiesel by blending with nanoparticles. *Chemical Engineering & Technology, 47*(1), 200-207.

Prasetyo, J., Kusmardini, D., Sa'adah, T. N., Sari, D. P., Dahnum, D., Adelia, N., Kurniati, E., Wibisana, A., Hidayat, H., & Ndruru, S. T. C. L. (2024). Optimization of used cooking oil for biodiesel using CaO-derived of bovine bone catalyst. *South African Journal of Chemical Engineering*, *48*(1), 95–102. https://doi.org/10.1016/j.sajce.2024.01.008

Priscilla, S. J., Daniel, R., Dhakshayani, Y., Caroline, S. C., & Sivaji, K. (2019). Effect of magnesium dopant on the structural, morphological and electrical properties of ZnO nanoparticles by sol-gel method. *Materials Today: Proceedings*, *36*(xxxx), 793–796. https://doi.org/10.1016/j.matpr.2020.07.005

Pu, J., Jin, X., Wang, J., Cui, F., Chu, S., Sheng, E., & Wang, Z. (2013). Shape-controlled synthesis of ternary nickel cobaltite and their application in supercapacitors. *Journal of Electroanalytical Chemistry*, *707*, 66–73. https://doi.org/10.1016/J.jelechem.2013.08.021

Pullen, J., & Saeed, K. (2012a). An overview of biodiesel oxidation stability. *Renewable and Sustainable Energy Reviews*, *16*(8), 5924–5950. https://doi.org/https://doi.org/10.1016/j.rser.2012.06.024

Purwanto, P., Buchori, L., & Istadi, I. (2020). Reaction rate law model and reaction mechanism covering effect of plasma role on the transesterification of triglyceride and methanol to biodiesel over a continuous flow hybrid catalytic-plasma reactor. *Heliyon, 6*(10), e05164. https://doi.org/10.1016/j.heliyon.2020.e05164

Qiu, Z., Engineering, P., & Members, C. (2010). Intensification of Liquid-Liquid Contacting Processes, *University of Kansas*, *https://hdl.handle.net/1808/6755*

Qiu, Z., Petera, J., & Weatherley, L. R. (2012). Biodiesel synthesis in an intensified spinning disk reactor. *Chemical Engineering Journal*, *210*, 597–609. https://doi.org/10.1016/j.cej.2012.08.058

Qiu, Z., Zhao, L., & Weatherley, L. (2010). Process intensification technologies in continuous biodiesel production. *Chemical Engineering and Processing: Process Intensification*, *49*(4), 323–330. https://doi.org/10.1016/j.cep.2010.03.005

R, G., Thangarasu, V., Vinayakaselvi M, A., & Ramanathan, A. (2022). A critical review of recent advancements in continuous flow reactors and prominent integrated microreactors for biodiesel production. *Renewable and Sustainable Energy Reviews*, *154*. https://doi.org/10.1016/j.rser.2021.111869

Rahimi, A., Moradi, G., Abolhasan Alavi, S., & Ardjmand, M. (2018). Simultaneous Extraction of Rapeseed Oil and Conversion to Biodiesel Using Hetrogenous and Homogenous Catalysts. *Environmental Progress & Sustainable Energy*, *37*(1), 518–523. https://doi.org/https://doi.org/10.1002/ep.12679

Rahimi, M., Mohammadi, F., Basiri, M., Parsamoghadam, M. A., & Masahi, M. M. (2016). Transesterification of soybean oil in four-way micromixers for biodiesel production using a cosolvent. *Journal of the Taiwan Institute of Chemical Engineers*, *64*, 203–210. https://doi.org/10.1016/j.jtice.2016.04.023

Rajpoot, A. S., Shende, V., Chelladurai, H. M., Dwivedi, G., Verma, T. N., & Choudhary, T. (2025). Exploring the potential and progress of microalgae biomass production, harvesting, and pre-treatment for sustainable biofuel production: a comprehensive review. *Environment, Development and Sustainability 2025*, 1–51. https://doi.org/10.1007/S10668-025-05984-0

Ramadhas, A. S., Jayaraj, S., & Muraleedharan, C. (2005). Biodiesel production from high FFA rubber seed oil. *Fuel*, *84*(4), 335–340. https://doi.org/10.1016/j.fuel.2004.09.016

Ramos, M. J., Fernández, C. M., Casas, A., Rodríguez, L., & Pérez, Á. (2009). Influence of fatty acid composition of raw materials on biodiesel properties. *Bioresource Technology*, *100*(1), 261–268. https://doi.org/10.1016/j.biortech.2008.06.039

Ranjbari, M., Shams Esfandabadi, Z., Shevchenko, T., Scagnelli, S. D., Lam, S. S., Varjani, S., Aghbashlo, M., Pan, J., & Tabatabaei, M. (2022). An inclusive trend study of techno-economic analysis of biofuel supply chains. *Chemosphere*, *309*, 136755. https://doi.org/10.1016/j.chemosphere.2022.136755

Rathore, V., Tyagi, S., Newalkar, B., & Badoni, R. P. (2015). Jatropha and Karanja oil derived DMC–biodiesel synthesis: A kinetics study. *Fue*l, *140,* 597–608. https://doi.org/10.1016/j.fuel.2014.10.003

Reay, D., Ramshaw, C., & Harvey, A. (Eds.). (2008). Chapter 5—Reactors. In Process Intensification (pp. 103–186). *Butterworth-Heinemann.* https://doi.org/10.1016/B978-0-7506-8941-0.00006-7

Riayatsyah, T. M. I., Sebayang, A. H., Silitonga, A. S., Padli, Y., Fattah, I. M. R., Kusumo, F., Ong, H. C., & Mahlia, T. M. I. (2022). Current Progress of Jatropha Curcas Commoditisation as Biodiesel Feedstock: A Comprehensive Review. *Frontiers in Energy Research, 9*. https://doi.org/10.3389/fenrg.2021.815416

Rimkus, A., Vipartas, T., Matijošius, J., Stravinskas, S., & Kriaučiūnas, D. (2021). Study of Indicators of CI Engine Running on Conventional Diesel and Chicken Fat Mixtures Changing EGR. *Applied Sciences 2021, Vol. 11, Page 1411*, *11*(4), 1411. https://doi.org/10.3390/APP11041411

Rocha, A. da C., Pereira, G. R., Rocha, A. da C., & Pereira, G. R. (2020). Identification and Quantification of Phases in Steels by X Ray Diffraction Using Rietveld Refinement. *Inelastic X-Ray Scattering and X-Ray Powder Diffraction Applications*. https://doi.org/10.5772/intechopen.91823

Ron Kotrba. (2025). *Brazil temporarily suspends biodiesel increase*. https://www.biobased-diesel.com/post/brazil-temporarily-suspends-biodiesel-increase

Rosset, M., & Perez-Lopez, O. W. (2019). FTIR spectroscopy analysis for monitoring biodiesel production by heterogeneous catalyst. *Vibrational Spectroscopy*, *105*, 102990. https://doi.org/10.1016/j.vibspec.2019.102990

Sadiq Ali, S., Asif, M., & Basu, A. (2019). Design and simulation of high purity biodiesel reactive distillation process. *Pol. J. Chem. Tech*, *21*(3). https://doi.org/10.2478/pjct-2019-0022

Safar, M., Bertrand, D., Robert, P., Devaux, M. F., & Genot, C. (1994). Characterization of edible oils, butters and margarines by Fourier transform infrared spectroscopy with attenuated total reflectance. *Journal of the American Oil Chemists' Society*, *71*(4), 371–377. https://doi.org/10.1007/bf02540516

Safieddin Ardebili, S. M., Ge, X., & Cravotto, G. (2019). Flow-mode biodiesel production from palm oil using a pressurized microwave reactor. *Green Processing and Synthesis*, *8*(1), 8–14. https://doi.org/10.1515/gps-2017-0116/machinereadablecitation/ris

Safieddin Ardebili, S. M., Hashjin, T. T., Ghobadian, B., Najafi, G., Mantegna, S., & Cravotto, G. (2015). Optimization of biodiesel synthesis under simultaneous ultrasound-microwave irradiation using response surface methodology (RSM). *Green Processing and Synthesis*, *4*(4), 259–267. https://doi.org/10.1515/gps-2015-0029

Sahoo, R. R., & Biswas, S. K. (2009). Frictional response of fatty acids on steel. *Journal of Colloid and Interface Science*, *333*(2), 707–718. https://doi.org/10.1016/j.jcis.2009.01.046

Sahoo, R. R., & Jain, A. (2019). Experimental analysis of nanofuel additives with magnetic fuel conditioning for diesel engine performance and emissions. *Fuel*, *236*(May 2018), 365–372. https://doi.org/10.1016/j.fuel.2018.09.027

Saini, R., Osorio-Gonzalez, C. S., Brar, S. K., & Kwong, R. (2021). A critical insight into the development, regulation and future prospects of biofuels in Canada. *Bioengineered*, *12*(2), 9847–9859. https://doi.org/10.1080/21655979.2021.1996017

Samani, B. H., Behruzian, M., Najafi, G., Fayyazi, E., Ghobadian, B., Behruzian, A., Mofijur, M., Mazlan, M., & Yue, J. (2021). The rotor-stator type hydrodynamic cavitation reactor approach for enhanced biodiesel fuel production. *Fuel*, *283*, 118821. https://doi.org/10.1016/j.fuel.2020.118821

Sandaka, B. P., & Kumar, J. (2023). Alternative vehicular fuels for environmental decarbonization: A critical review of challenges in using electricity, hydrogen, and biofuels as a sustainable vehicular fuel. *Chemical Engineering Journal Advances, 14*, 100442. https://doi.org/10.1016/j.ceja.2022.100442

Savvopoulos, S., Hussain, M. N., Hatzikirou, H., & Janajreh, I. (2023). A computational approach in automating the continuous sonicated biodiesel production. *Sustainable Energy Technologies and Assessments*, *60*, 103509. https://doi.org/10.1016/J.SETA.2023.103509

Saxena, V., Kumar, N., & Saxena, V. K. (2017). A comprehensive review on combustion and stability aspects of metal nanoparticles and its additive effect on diesel and biodiesel fuelled C.I. engine. *Renewable & Sustainable Energy Reviews*, *70*, 563–588. https://doi.org/10.1016/j.rser.2016.11.067

Shahridzuan Abdullah, I., Khalid, A., Jaat, N., Saputra Nursal, R., Koten, H., & Karagoz, Y. (2021). A study of ignition delay, combustion process and emissions in a high ambient temperature of diesel combustion. *Fuel*, *297*, 120706. https://doi.org/10.1016/j.fuel.2021.120706

Shalaby., E. A., & Nour Sh. El-gendy. (2012). Two steps alkaline transesterification of waste cooking oil and quality assessment of produced biodiesel. *International Journal of Chemical and Biochemical Sciences*, *1*, 30–35.

Sharma, A. K., Jaryal, S., Sharma, S., Dhyani, A., Tewari, B. S., & Mahato, N. (2025). Biofuels from Microalgae: A Review on Microalgae Cultivation, Biodiesel Production Techniques and Storage Stability. *Processes 2025, Vol. 13, Page 488*, *13*(2), 488. https://doi.org/10.3390/pr13020488

Sharon, H., Jai Shiva Ram, P., Jenis Fernando, K., Murali, S., & Muthusamy, R. (2013). Fueling a stationary direct injection diesel engine with diesel-used palm oil–butanol blends – An experimental study. *Energy Conversion and Management*, *73*, 95–105. https://doi.org/10.1016/j.enconman.2013.04.027

Shilpita Das, A. S. (2024). *India: Biofuels Annual | USDA Foreign Agricultural Service*. https://www.fas.usda.gov/data/india-biofuels-annual-9

Shokravi, H., Heidarrezaei, M., Shokravi, Z., Ong, H. C., Lau, W. J., Din, M. F. M., & Ismail, A. F. (2022). Fourth-generation biofuel from genetically modified algal biomass for bioeconomic development. *Journal of Biotechnology*, *360*, 23–36. https://doi.org/10.1016/j.jbiotec.2022.10.010

Shrivastava, P., Salam, S., Verma, T. N., & Samuel, O. D. (2020). Experimental and empirical analysis of an IC engine operating with ternary blends of diesel, karanja and roselle biodiesel. *Fuel*, *262*, 116608. https://doi.org/10.1016/j.fuel.2019.116608

Silva, R. J. M. C. L., Tschoeke, I. C. P., Melo, J. C., Silva, J. P., Pacheco, J. G. A., Silva, J. M. F., & Souza, T. P. C. (2019). Comparison between experimental and simulated results of biodiesel production by reactive distillation and energetic assessment. *Brazilian Journal of Chemical Engineering*, *36*(1), 351–359. https://doi.org/10.1590/0104-6632.20190361S20170266

Simasatitkul, L., Siricharnsakunchai, P., Patcharavorachot, Y., Assabumrungrat, S., & Arpornwichanop, A. (2011). Reactive distillation for biodiesel production from soybean oil. *Korean Journal of Chemical Engineering*, *28*(3), 649–655. https://doi.org/10.1007/S11814-010-0440-Z

Singh, A., Nigam, P. S., & Murphy, J. D. (2011). Renewable fuels from algae: An answer to debatable land based fuels. *Bioresource Technology*, *102*(1), 10–16. https://doi.org/10.1016/j.biortech.2010.06.032

Singh, T. S., & Verma, T. N. (2019). Biodiesel production from Momordica Charantia (L.): Extraction and engine characteristics. *Energy*, *189*. https://doi.org/10.1016/j.energy.2019.116198

Singh, Y., Khattar, J. I. S., Singh, D. P., & Singh, R. P. (Eds.). (2025). *Industrial and Biotechnological Applications of Algae*. https://doi.org/10.1007/978-981-96-1844-6

Sorate, K. A., & Bhale, P. V. (2015). Biodiesel properties and automotive system compatibility issues. *Renewable and Sustainable Energy Reviews, 41,* 777–798. https://doi.org/10.1016/j.rser.2014.08.079

Soudagar, M. E. M., Nik-Ghazali, N. N., Abul Kalam, M., Badruddin, I. A., Banapurmath, N. R., & Akram, N. (2018). The effect of nano-additives in diesel-biodiesel fuel blends: A comprehensive review on stability, engine performance and emission characteristics. *Energy Conversion and Management*, *178*, 146–177. https://doi.org/10.1016/j.enconman.2018.10.019

Speight, J. G. (2011). Chapter 10—Combustion of Hydrocarbons. In J. G. Speight (Ed.), *Handbook of Industrial Hydrocarbon Processes* (pp. 355–393). Gulf Professional Publishing. https://doi.org/10.1016/b978-0-7506-8632-7.10010-6

Srinivasan, G. R., Shankar, V., Chandra Sekharan, S., Munir, M., Balakrishnan, D., Mohanam, A., & Jambulingam, R. (2020). Influence of fatty acid composition on process optimization and characteristics assessment of biodiesel produced from waste animal fat. *Energy Sources, Part A: Recovery, Utilization and Environmental Effects*. https://doi.org/10.1080/15567036.2020.1771477

Statista Research Department. (2025, February). *EU-27: biofuels consumption for transportation| Statista*. https://www.statista.com/statistics/613238/biofuels-consumption-transport-eu/

Sterpu, A. E., Simedrea, B. G., Chis, T. V., & Săpunaru, O. V. (2024). Corrosion Effect of Biodiesel-Diesel Blend on Different Metals/Alloy as Automotive Components Materials. *Fuels*, *5*(1), 17–32. https://doi.org/10.3390/fuels5010002

Stevie, F. A., & Donley, C. L. (2020). Introduction to x-ray photoelectron spectroscopy. *Journal of Vacuum Science & Technology A: Vacuum, Surfaces, and Films*, *38*(6). https://doi.org/10.1116/6.0000412/1024200

Su, Y., Chen, F., Wu, Z., & Wang, H. (2013). Corrosion characteristics of biodiesel in storage. *ICMREE 2013 - Proceedings: 2013 International Conference on Materials for Renewable Energy and Environment*, *1*, 200–202. https://doi.org/10.1109/icmree.2013.6893647

Subedi, S., Anand, M., Gokul Ragavendra, S., & Ranjitha, J. (2020). Production and Characterization of Biodiesel from Hevea Brasiliensis and Diesel like Fuel from Waste Engine Oil. *IOP Conference Series: Materials Science and Engineering*, *923*(1), 012071. https://doi.org/10.1088/1757-899x/923/1/012071

Sui, T., Ding, M., Ji, C., Yan, S., Wei, J., Wang, A., Zhao, F., & Fei, J. (2018). Dispersibility and rheological behavior of functionalized silica nanoparticles as lubricant additives. *Ceramics International*, *44*(15), 18438–18443. https://doi.org/10.1016/j.ceramint.2018.07.061

Sun, J., Ju, J., Ji, L., Zhang, L., & Xu, N. (2008). Synthesis of biodiesel in capillary microreactors. *Industrial and Engineering Chemistry Research*, *47*(5), 1398–1403. https://doi.org/10.1021/ie070295q

Tabatabaei, M., Aghbashlo, M., Dehhaghi, M., Panahi, H. K. S., Mollahosseini, A., Hosseini, M., & Soufiyan, M. M. (2019). Reactor technologies for biodiesel production and processing: A review. *Progress in Energy and Combustion Science*, *74*, 239–303. https://doi.org/10.1016/j.pecs.2019.06.001

Tadele, K., Verma, S., Gonzalez, M. A., & Varma, R. S. (2017). A sustainable approach to empower the bio-based future: Upgrading of biomass via process intensification. *Green Chemistry*, *19*(7), 1624–1627. https://doi.org/10.1039/c6gc03568j

Takase, M. (2022). Biodiesel Yield and Conversion Percentage from Waste Frying Oil Using Fish Shell at Elmina as a Heterogeneous Catalyst and the Kinetics of the Reaction. *International Journal of Chemical Engineering*, *2022*. https://doi.org/10.1155/2022/8718638

Talam, S., Karumuri, S. R., & Gunnam, N. (2012). Synthesis, Characterization, and Spectroscopic Properties of ZnO Nanoparticles. *ISRN Nanotechnology*, *2012*, 1–6. https://doi.org/10.5402/2012/372505

Tamizhdurai, P., Arthi, P., Mangesh, V. L., Krishnan, P. S., Kumar, N. S., Saravanan, P., Subramani, A., Sasikumar, P., Alotibi, M. F., Alreshaidan, S. B., Abahussain, A. A. M., Al-Fatesh, A. S., & Kumaran, R. (2025). Clean energy technology: Hydro-processing of waste tyre pyrolysis oil (WTPO) to diesel fuel in a continuous reactor using Co/SBA-15 catalyst. *Applications in Energy and Combustion Science, 21*, 100305. https://doi.org/10.1016/j.jaecs.2024.100305

Tanawannapong, Y., Kaewchada, A., & Jaree, A. (2013). Biodiesel production from waste cooking oil in a microtube reactor. *Journal of Industrial and Engineering Chemistry*, *19*(1), 37–41. https://doi.org/10.1016/j.jiec.2012.07.007

Tariq, A. I., & Saleh, A. M. (2023). An experimental investigation into the combustion properties, performance, emissions, and cost reduction of using heavy and light fuel oils. *Case Studies in Thermal Engineering*, *44*, 102832. https://doi.org/10.1016/j.csite.2023.102832

Tariq, M., Ali, S., Ahmad, F., Ahmad, M., Zafar, M., Khalid, N., & Khan, M. A. (2011). Identification, FT-IR, NMR (1H and 13C) and GC/MS studies of fatty acid methyl esters in biodiesel from rocket seed oil. *Fuel Processing Technology*, *92*(3), 336–341. https://doi.org/10.1016/j.fuproc.2010.09.025

Tesfay, A. H., Asfaw, S. H., & Bidir, M. G. (2019). Comparative evaluation of biodiesel production and engine characteristics of Jatropha and Argemone Mexicana oils. *SN Applied Sciences*, *1*(9). https://doi.org/10.1007/s42452-019-1075-2

Tesfaye Lamore, M., Seyoum Zeleke, D., & Yitayew Kassa, B. (2023). A comparative study on the effect of nano-additives on performance and emission characteristics of CI engine run on castor biodiesel blended fuel. *Energy Conversion and Management: X*, *20*, 100493. https://doi.org/10.1016/j.ecmx.2023.100493

Thangamani, S., Sundaresan, S. N., Kannappan S., S., Barawkar, V. T., & Jeyaseelan, T. (2021). Impact of biodiesel and diesel blends on the fuel filter: A combined experimental and simulation study. *Energy*, *227*, 120526. https://doi.org/10.1016/j.energy.2021.120526

Thangarasu, V., & Anand, R. (2019). Comparative evaluation of corrosion behavior of Aegle Marmelos Correa diesel, biodiesel, and their blends on aluminum and mild steel metals. *Advanced Biofuels: Applications, Technologies and Environmental Sustainability*, 443–471. https://doi.org/10.1016/B978-0-08-102791-2.00017-9

Thompson, J. C., & He, B. B. (2007). Biodiesel Production Using Static Mixers. *Transactions of the ASABE*, *50*(1), 161–165. https://doi.org/10.13031/2013.22389

Tran, T.-K., Nguyen, M.-K., Lin, C., Hoang, T.-D., Nguyen, T.-C., Lone, A. M., Khedulkar, A. P., Gaballah, M. S., Singh, J., Chung, W. J., & Nguyen, D. D. (2024). Review on fate, transport, toxicity and health risk of nanoparticles in natural ecosystems: Emerging challenges in the modern age and solutions toward a sustainable environment. *Science of The Total Environment, 912*, 169331. https://doi.org/10.1016/j.scitotenv.2023.169331

Tsoutsos, T., Tournaki, S., Gkouskos, Z., Paraíba, O., Giglio, F., García, P. Q., Braga, J., Adrianos, H., & Filice, M. (2019). Quality Characteristics of Biodiesel Produced from Used Cooking Oil in Southern Europe. *ChemEngineering, 3*(1), 19. https://doi.org/10.3390/chemengineering3010019

Tumala, M. M., Salisu, A., & Nmadu, Y. B. (2023). Climate change and fossil fuel prices: A GARCH-MIDAS analysis. *Energy Economics, 124*, 106792. https://doi.org/10.1016/j.eneco.2023.106792

Turner, N. H., & Schreifels, J. A. (2000). Surface analysis: X-ray photoelectron spectroscopy and Auger electron spectroscopy. *Analytical Chemistry*, *72*(12). https://doi.org/10.1021/A10000110

United States Environmental Protection Agency. (2024, November). *Timeline of Major Accomplishments in Transportation, Air Pollution, and Climate Change | US EPA*. https://www.epa.gov/transportation-air-pollution-and-climate-change/timeline-major-accomplishments-transportation-air

Universitesi, I. M., & Soyhan, H. S. (2019). *Microwave-assisted pilot-scale biodiesel production and engine tests*. *February*. https://doi.org/10.1680/jener.18.00006

U.S. Energy Information Administration, M. E. R. R. energy,. (2023, September). *Biofuels explained - U.S. Energy Information Administration (EIA)*. https://www.eia.gov/energyexplained/biofuels/

Valentino, G., Corcione, F. E., Iannuzzi, S. E., & Serra, S. (2012). Experimental study on performance and emissions of a high speed diesel engine fuelled with n-butanol diesel blends under premixed low temperature combustion. *Fuel*, *92*(1), 295–307. https://doi.org/10.1016/j.fuel.2011.07.035

Vellaiyan, S., Subbiah, A., & Chockalingam, P. (2018). Combustion, performance, and emission analysis of diesel engine fueled with water-biodiesel emulsion fuel and

nanoadditive. *Environmental Science and Pollution Research*, *25*(33), 33478–33489. https://doi.org/10.1007/s11356-018-3216-3

Venkatesan, S. P., & Kadiresh, P. N. (2016). Influence of an aqueous cerium oxide nanofluid fuel additive on performance and emission characteristics of a compression ignition engine. *International Journal of Ambient Energy*, *37*(1), 64–67. https://doi.org/10.1080/01430750.2014.882863

Verghese, G., & Saeed, K. (2024). Advances in the measurements of the biodiesel oxidative stability. *Biofuels*. https://doi.org/10.1080/17597269.2024.2428024

Visscher, F., van der Schaaf, J., Nijhuis, T. A., & Schouten, J. C. (2013). Rotating reactors – A review. *Chemical Engineering Research and Design*, *91*(10), 1923–1940. https://doi.org/10.1016/j.cherd.2013.07.021

Vo, D. H., Vo, A. T., & Ho, C. M. (2024). Urbanization and renewable energy consumption in the emerging ASEAN markets: A comparison between short and long-run effects. *Heliyon, 10*(9), e30243. https://doi.org/10.1016/j.heliyon.2024.e30243

Vural Gürsel, I., Kurt, S. K., Aalders, J., Wang, Q., Noël, T., Nigam, K. D. P., Kockmann, N., & Hessel, V. (2016). Utilization of milli-scale coiled flow inverter in combination with phase separator for continuous flow liquid–liquid extraction processes. *Chemical Engineering Journal*, *283*, 855–868. https://doi.org/10.1016/j.cej.2015.08.028

Walter, S., Malmberg, S., Schmidt, B., & Liauw, M. A. (2005). Mass transfer limitations in microchannel reactors. *Catalysis Today*, *110*(1–2), 15–25. https://doi.org/10.1016/j.cattod.2005.09.019

Wancura, J. H. C., Fantinel, A. L., Ugalde, G. A., Donato, F. F., Vladimir de Oliveira, J., Tres, M. V., & Jahn, S. L. (2021). Semi-continuous production of biodiesel on pilot scale via enzymatic hydroesterification of waste material: Process and economics considerations. *Journal of Cleaner Production*, *285*(October 2018). https://doi.org/10.1016/j.jclepro.2020.124838

Wang, L., Mercier, D., Zanna, S., Seyeux, A., Laurent-Brocq, M., Perrière, L., Guillot, I., & Marcus, P. (2020). Study of the surface oxides and corrosion behaviour of an equiatomic CoCrFeMnNi high entropy alloy by XPS and ToF-SIMS. *Corrosion Science*, *167*, 108507. https://doi.org/10.1016/j.corsci.2020.108507

Wang, L., & Muhammed, M. (1999). Synthesis of zinc oxide nanoparticles with controlled morphology. *Journal of Materials Chemistry*, *9*(11), 2871–2878. https://doi.org/10.1039/a907098b

Wang, X., Zhang, Y., Karthikeyan, C., Boomadevi, P., Maroušek, J., Nasif, O., Alharbi, S. A., & Xia, C. (2022). Role of injection pressure on fuel atomization and spray

penetration on the Thevetia peruviana and Jatropha curcas biodiesel blends with nanoparticle. *Fuel*, *324*, 124527. https://doi.org/10.1016/j.fuel.2022.124527

World bioenergy Association. (2024). *Global Bioenergy Statistics Report 2024 Summary*.https://www.worldbioenergy.org/uploads/241023%20GBS%20Report%20Short%20Version.pdf

Wu, S., Bashir, M. A., Hsieh, H., Krosuri, A., & McDonald, A. (2019). Highly efficient biodiesel conversion from soybean oil using liquid-phase plasma discharge technology. *Transactions of the ASABE*, *62*(5), 1129–1134. https://doi.org/10.13031/trans.13534

Xiao, F., & Xu, Y. (2012). Pulse Electrodeposition of Manganese Oxide for High-Rate Capability Supercapacitors. *International Journal of Electrochemical Science*, *7*(8), 7440–7450. https://doi.org/10.1016/S1452-3981(23)15795-6

Xu, W., Gao, L., Wang, S., & Xiao, G. (2013). Biodiesel Production from Soybean Oil in a Membrane Reactor over Hydrotalcite Based Catalyst: An Optimization Study. *Energy & Fuels, 27*(11), 6738–6742. https://doi.org/10.1021/ef401823z

Yadav, L. D. S. (2005). Infrared (IR) Spectroscopy. *Organic Spectroscopy*, 52–106. https://doi.org/10.1007/978-1-4020-2575-4_3

Yadav, N., Yadav, G., & Ahmaruzzaman, M. (2023). Microwave-assisted biodiesel production using –SO3H functionalized heterogeneous catalyst derived from a lignin-rich biomass. *Scientific Reports 2023 13:1*, *13*(1), 1–17. https://doi.org/10.1038/s41598-023-36380-1

Yang, L., & Jensen, K. F. (2013). Mass transport and reactions in the tube-in-tube reactor. *Organic Process Research and Development*, *17*(6), 927–933. https://doi.org/10.1021/op400085a

Yang, L., Wang, R., Zare, A., Hunicz, J., Bodisco, T. A., & Brown, R. J. (2025). Development of a Reduced Chemical Reaction Kinetic Mechanism with Cross-Reactions of Diesel/Biodiesel Fuels. *Journal of Marine Science and Application*, 1–15. https://doi.org/10.1007/s11804-025-00634-3

Yang, Z., Lv, J., Pang, H., Yan, W., Qian, K., Guo, T., & Guo, Z. (2015). Facile Synthesis of Coaxial CNTs/MnOx-Carbon Hybrid Nanofibers and Their Greatly Enhanced Lithium Storage Performance. *Scientific Reports 2015 5:1*, *5*(1), 1–10. https://doi.org/10.1038/srep17473

Yeh, S. I., Huang, Y. C., Cheng, C. H., Cheng, C. M., & Yang, J. T. (2016). Development of a millimetrically scaled biodiesel transesterification device that relies on droplet-based co-axial fluidics. *Scientific Reports*, *6*(101), 1–7. https://doi.org/10.1038/srep29288

Yuan, H., Yang, B. L., & Zhu, G. L. (2009). Synthesis of biodiesel using microwave absorption catalysts. *Energy and Fuels*, *23*(1), 548–552. https://doi.org/10.1021/ef800577j

Zara, K., Anisa, S. F., Nabilla, S., & Bismo, S. (2019). Biodiesel synthesis in DBD plasma reactor using hot mixture of castor oil and used palm oil - Methanol. *AIP Conference Proceedings*, *2175*(1). https://doi.org/10.1063/1.5134570/1002947

Zareh, P., Zare, A. A., & Ghobadian, B. (2017). Comparative assessment of performance and emission characteristics of castor, coconut and waste cooking based biodiesel as fuel in a diesel engine. *Energy*, *139*, 883–894. https://doi.org/10.1016/j.energy.2017.08.040

Zhang, Q., Xia, J., Wang, J., He, Z., Zhao, W., Qian, Y., Zheng, L., Liu, R., & Lu, X. (2022). Experimental study on ignition and combustion characteristics of biodiesel-butanol blends at different injection pressures. *Renewable and Sustainable Energy Reviews*, *160*, 112289. https://doi.org/10.1016/j.rser.2022.112289

Zhang, S., Hou, L., Du, H., Wei, H., Liu, B., & Wei, Y. (2020). A study on the interaction between chloride ions and CO2 towards carbon steel corrosion. *Corrosion Science*, *167*, 108531. https://doi.org/10.1016/j.corsci.2020.108531

Zhang, Y., Zhong, Y., Wang, J., Tan, D., Zhang, Z., & Yang, D. (2021). Effects of Different Biodiesel-Diesel Blend Fuel on Combustion and Emission Characteristics of a Diesel Engine. *Processes 2021, Vol. 9, Page 1984*, *9*(11), 1984. https://doi.org/10.3390/pr9111984

Zheng, F., & Cho, H. M. (2025). Study on Biodiesel Production: Feedstock Evolution, Catalyst Selection, and Influencing Factors Analysis. *Energies 2025, Vol. 18, Page 2533*, *18*(10), 2533. https://doi.org/10.3390/en18102533

Zhou, J., Xiong, Y., Gong, Y., & Liu, X. (2017). Analysis of the oxidative degradation of biodiesel blends using FTIR, UV–Vis, TGA and TD-DES methods. *Fuel*, *202*, 23–28. https://doi.org/10.1016/j.fuel.2017.04.032

Zuo, L., Wang, J., Mei, D., Dai, S., & Adu-Mensah, D. (2022). Experimental investigation on combustion and (regulated and unregulated) emissions performance of a common-rail diesel engine using partially hydrogenated biodiesel-ethanol-diesel ternary blend. *Renewable Energy*, *185*, 1272–1283. https://doi.org/10.1016/j.renene.2021.12.085

Appendix

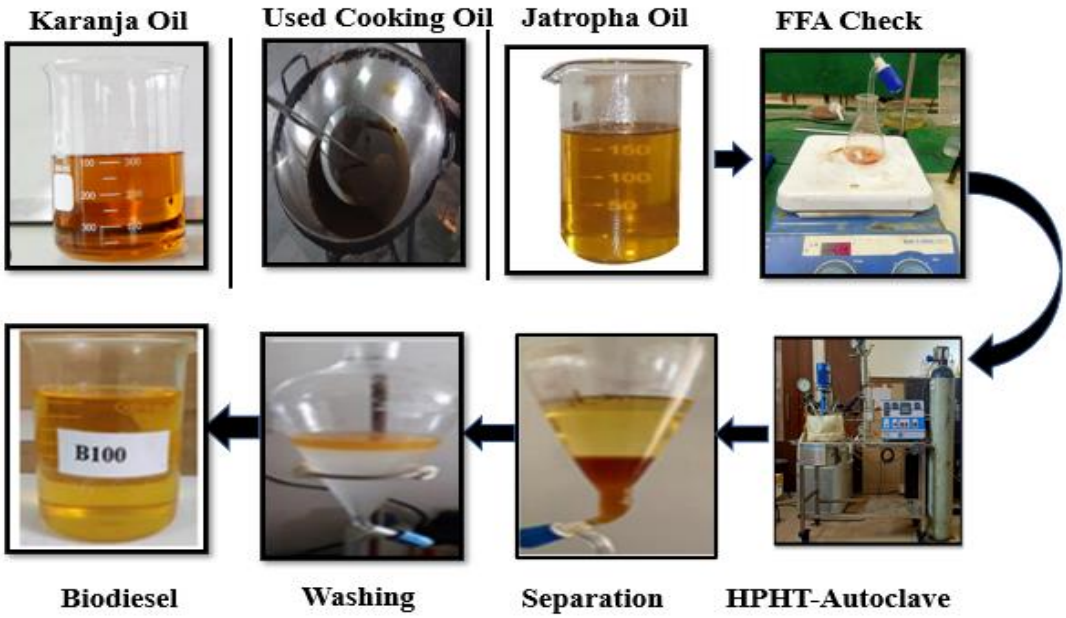

Figure A1 Steps involved in the production of biodiesel using high pressure-high temperature (HPHT) autoclave

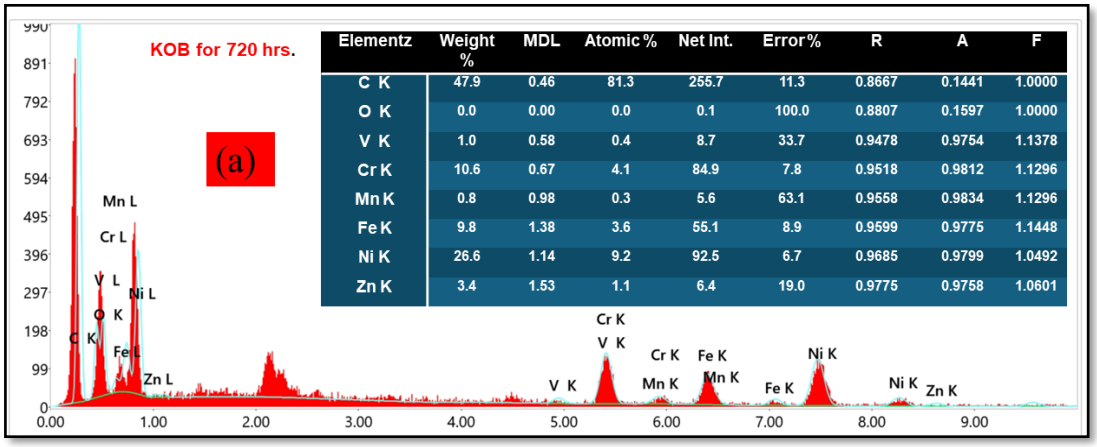

Elementz	Weight %	MDL	Atomic %	Net Int.	Error %	R	A	F
C K	47.9	0.46	81.3	255.7	11.3	0.8667	0.1441	1.0000
O K	0.0	0.00	0.0	0.1	100.0	0.8807	0.1597	1.0000
V K	1.0	0.58	0.4	8.7	33.7	0.9478	0.9754	1.1378
Cr K	10.6	0.67	4.1	84.9	7.8	0.9518	0.9812	1.1296
Mn K	0.8	0.98	0.3	5.6	63.1	0.9558	0.9834	1.1296
Fe K	9.8	1.38	3.6	55.1	8.9	0.9599	0.9775	1.1448
Ni K	26.6	1.14	9.2	92.5	6.7	0.9685	0.9799	1.0492
Zn K	3.4	1.53	1.1	6.4	19.0	0.9775	0.9758	1.0601

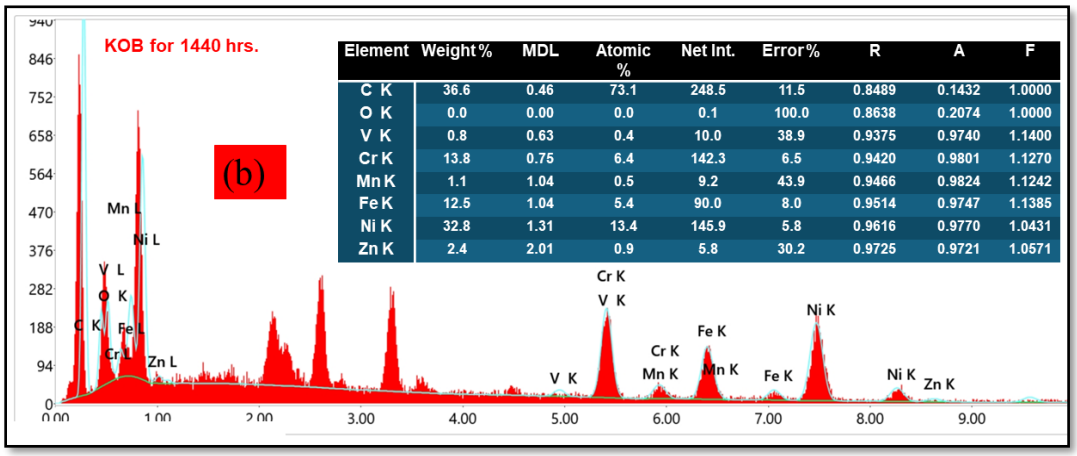

Element	Weight %	MDL	Atomic %	Net Int.	Error %	R	A	F
C K	36.6	0.46	73.1	248.5	11.5	0.8489	0.1432	1.0000
O K	0.0	0.00	0.0	0.1	100.0	0.8638	0.2074	1.0000
V K	0.8	0.63	0.4	10.0	38.9	0.9375	0.9740	1.1400
Cr K	13.8	0.75	6.4	142.3	6.5	0.9420	0.9801	1.1270
Mn K	1.1	1.04	0.5	9.2	43.9	0.9466	0.9824	1.1242
Fe K	12.5	1.04	5.4	90.0	8.0	0.9514	0.9747	1.1385
Ni K	32.8	1.31	13.4	145.9	5.8	0.9616	0.9770	1.0431
Zn K	2.4	2.01	0.9	5.8	30.2	0.9725	0.9721	1.0571

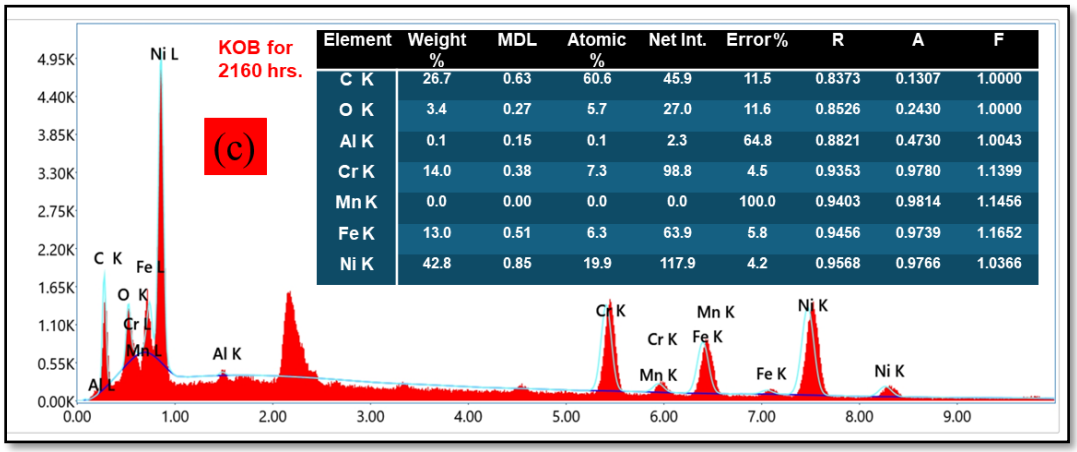

Element	Weight %	MDL	Atomic %	Net Int.	Error %	R	A	F
C K	26.7	0.63	60.6	45.9	11.5	0.8373	0.1307	1.0000
O K	3.4	0.27	5.7	27.0	11.6	0.8526	0.2430	1.0000
Al K	0.1	0.15	0.1	2.3	64.8	0.8821	0.4730	1.0043
Cr K	14.0	0.38	7.3	98.8	4.5	0.9353	0.9780	1.1399
Mn K	0.0	0.00	0.0	0.0	100.0	0.9403	0.9814	1.1456
Fe K	13.0	0.51	6.3	63.9	5.8	0.9456	0.9739	1.1652
Ni K	42.8	0.85	19.9	117.9	4.2	0.9568	0.9766	1.0366

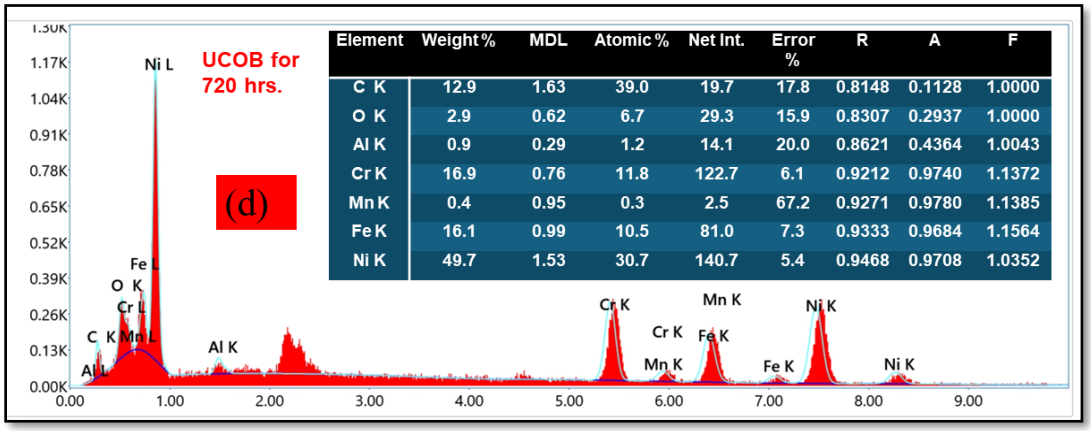

Element	Weight %	MDL	Atomic %	Net Int.	Error %	R	A	F
C K	12.9	1.63	39.0	19.7	17.8	0.8148	0.1128	1.0000
O K	2.9	0.62	6.7	29.3	15.9	0.8307	0.2937	1.0000
Al K	0.9	0.29	1.2	14.1	20.0	0.8621	0.4364	1.0043
Cr K	16.9	0.76	11.8	122.7	6.1	0.9212	0.9740	1.1372
Mn K	0.4	0.95	0.3	2.5	67.2	0.9271	0.9780	1.1385
Fe K	16.1	0.99	10.5	81.0	7.3	0.9333	0.9684	1.1564
Ni K	49.7	1.53	30.7	140.7	5.4	0.9468	0.9708	1.0352

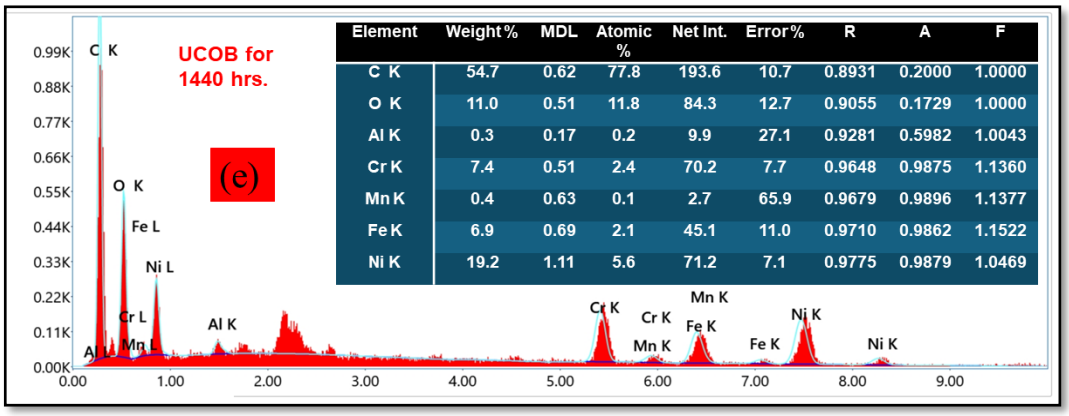

Element	Weight %	MDL	Atomic %	Net Int.	Error %	R	A	F
C K	54.7	0.62	77.8	193.6	10.7	0.8931	0.2000	1.0000
O K	11.0	0.51	11.8	84.3	12.7	0.9055	0.1729	1.0000
Al K	0.3	0.17	0.2	9.9	27.1	0.9281	0.5982	1.0043
Cr K	7.4	0.51	2.4	70.2	7.7	0.9648	0.9875	1.1360
Mn K	0.4	0.63	0.1	2.7	65.9	0.9679	0.9896	1.1377
Fe K	6.9	0.69	2.1	45.1	11.0	0.9710	0.9862	1.1522
Ni K	19.2	1.11	5.6	71.2	7.1	0.9775	0.9879	1.0469

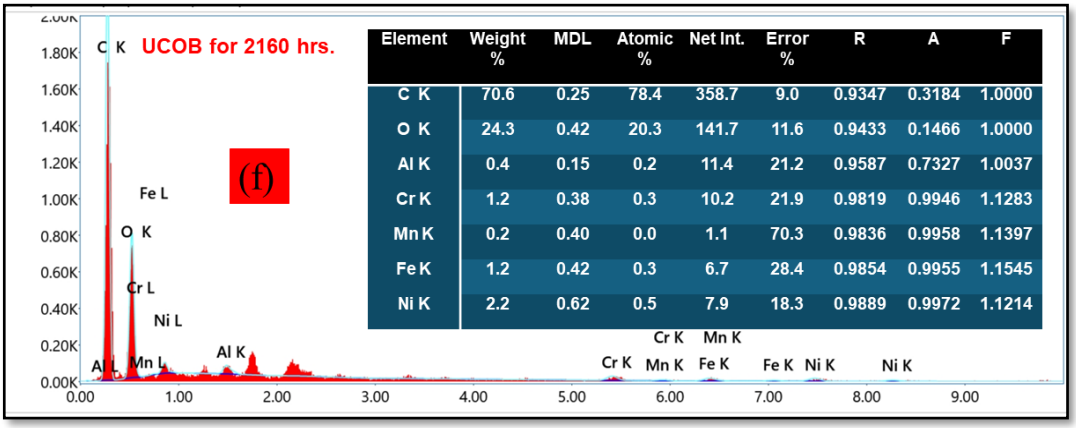

Element	Weight %	MDL	Atomic %	Net Int.	Error %	R	A	F
C K	70.6	0.25	78.4	358.7	9.0	0.9347	0.3184	1.0000
O K	24.3	0.42	20.3	141.7	11.6	0.9433	0.1466	1.0000
Al K	0.4	0.15	0.2	11.4	21.2	0.9587	0.7327	1.0037
Cr K	1.2	0.38	0.3	10.2	21.9	0.9819	0.9946	1.1283
Mn K	0.2	0.40	0.0	1.1	70.3	0.9836	0.9958	1.1397
Fe K	1.2	0.42	0.3	6.7	28.4	0.9854	0.9955	1.1545
Ni K	2.2	0.62	0.5	7.9	18.3	0.9889	0.9972	1.1214

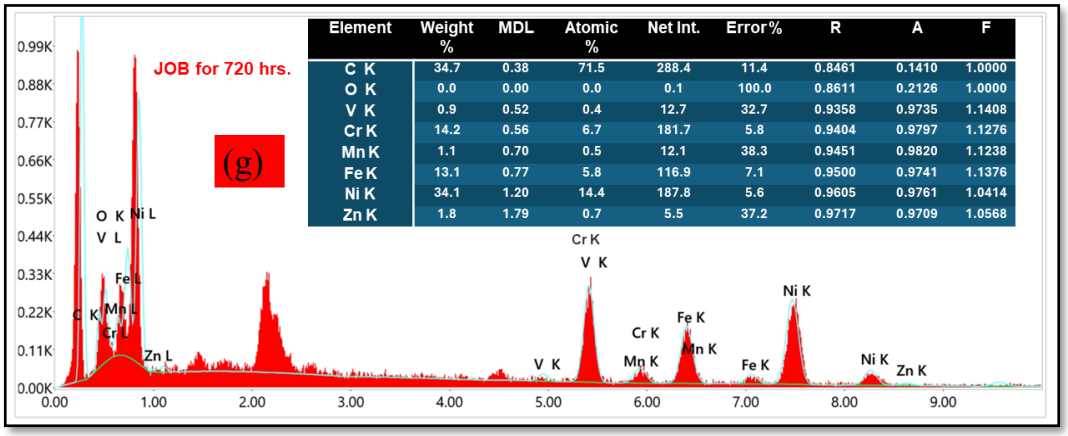

Element	Weight %	MDL	Atomic %	Net Int.	Error %	R	A	F
C K	34.7	0.38	71.5	288.4	11.4	0.8461	0.1410	1.0000
O K	0.0	0.00	0.0	0.1	100.0	0.8611	0.2126	1.0000
V K	0.9	0.52	0.4	12.7	32.7	0.9358	0.9735	1.1408
Cr K	14.2	0.56	6.7	181.7	5.8	0.9404	0.9797	1.1276
Mn K	1.1	0.70	0.5	12.1	38.3	0.9451	0.9820	1.1238
Fe K	13.1	0.77	5.8	116.9	7.1	0.9500	0.9741	1.1376
Ni K	34.1	1.20	14.4	187.8	5.6	0.9605	0.9761	1.0414
Zn K	1.8	1.79	0.7	5.5	37.2	0.9717	0.9709	1.0568

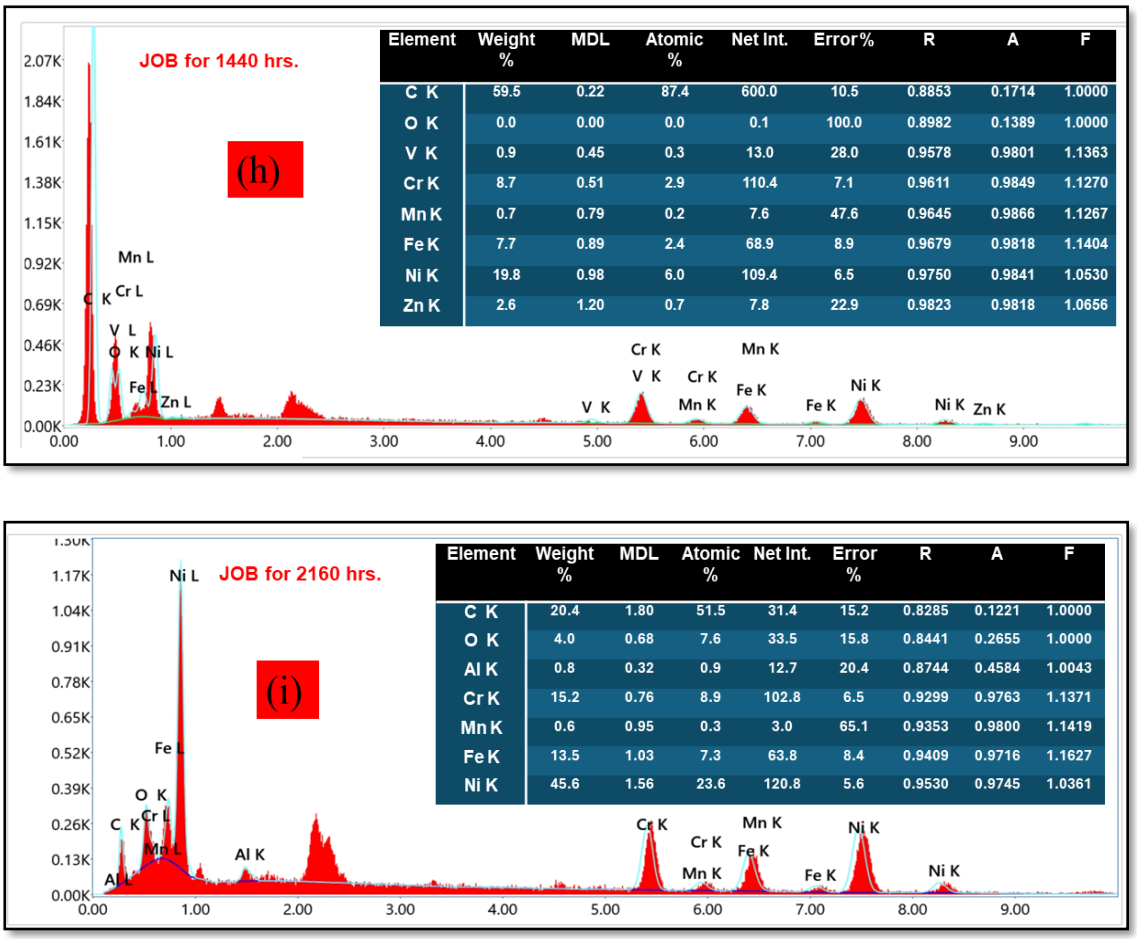

Figure A2 Elemental EDS spectrums of Ni alloys exposed in KOB (a-c), UCOB (d-f) and JOB (g-i).

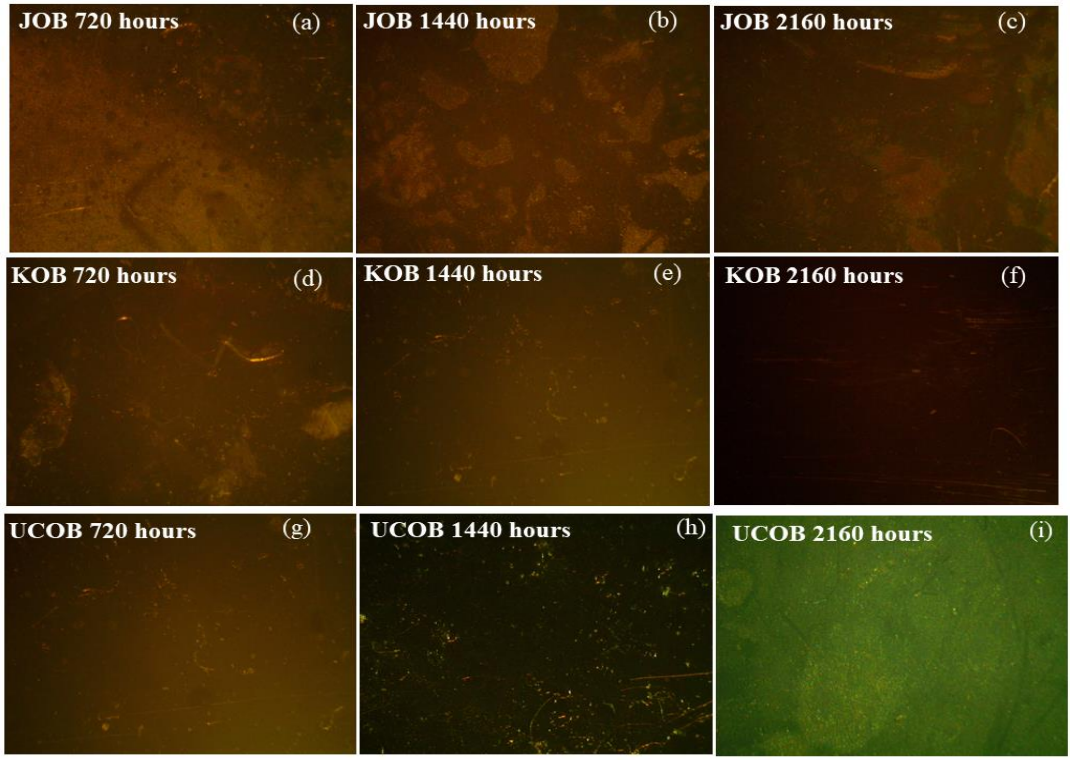

Figure A3 Optical microscopic images of corroded samples of Ni alloy (UNS 718)

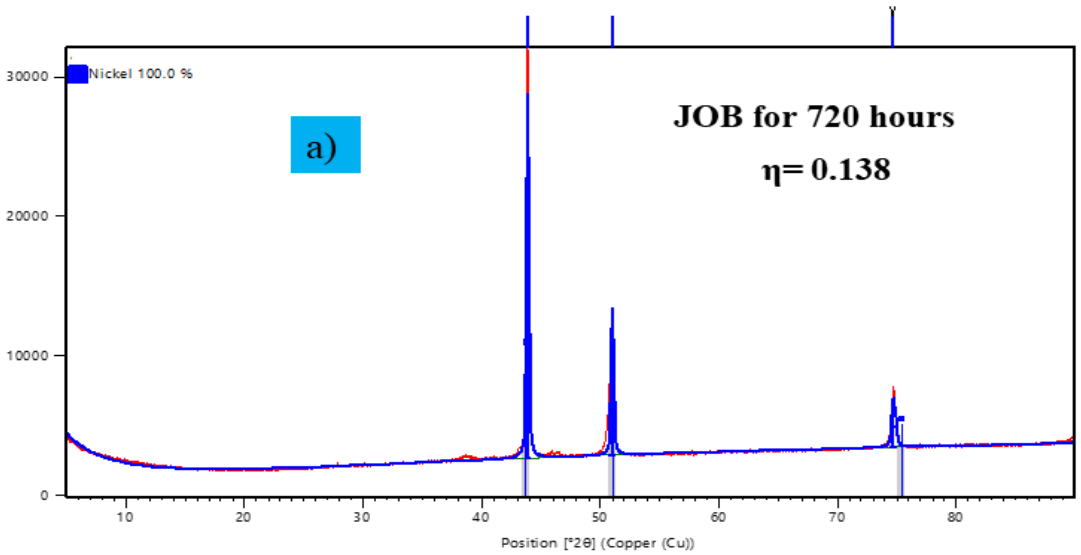

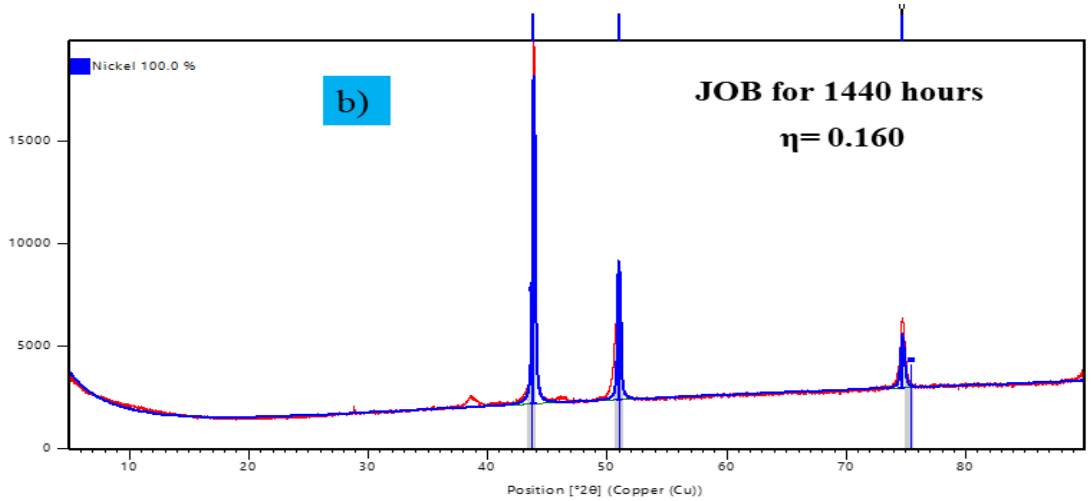
Nickel 100.0 %
b)
JOB for 1440 hours
η= 0.160
15000
10000
5000
0
10
20
30
40
50
60
70
80
Position [°2θ] (Copper (Cu))

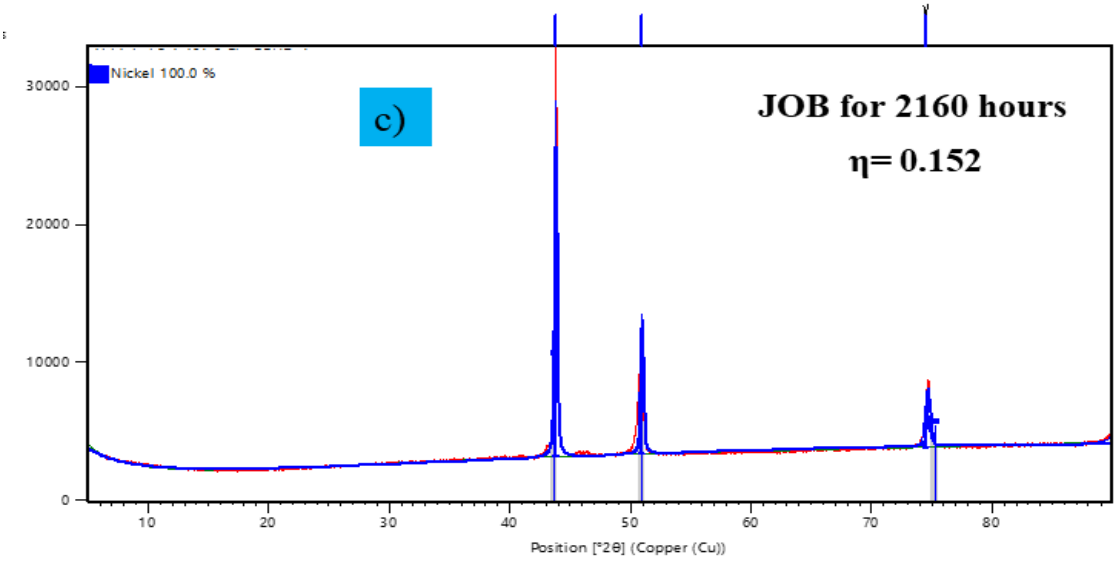
Nickel 100.0 %
c)
JOB for 2160 hours
η= 0.152
30000
20000
10000
0
10
20
30
40
50
60
70
80
Position [°2θ] (Copper (Cu))

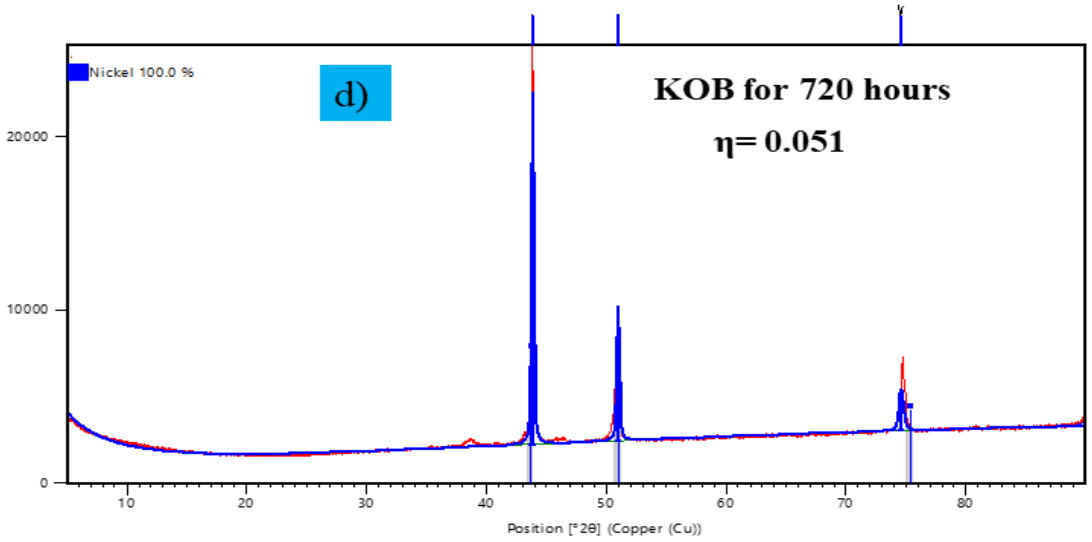
Nickel 100.0 %
d)
KOB for 720 hours
η= 0.051
20000
10000
0
10
20
30
40
50
60
70
80
Position [°2θ] (Copper (Cu))

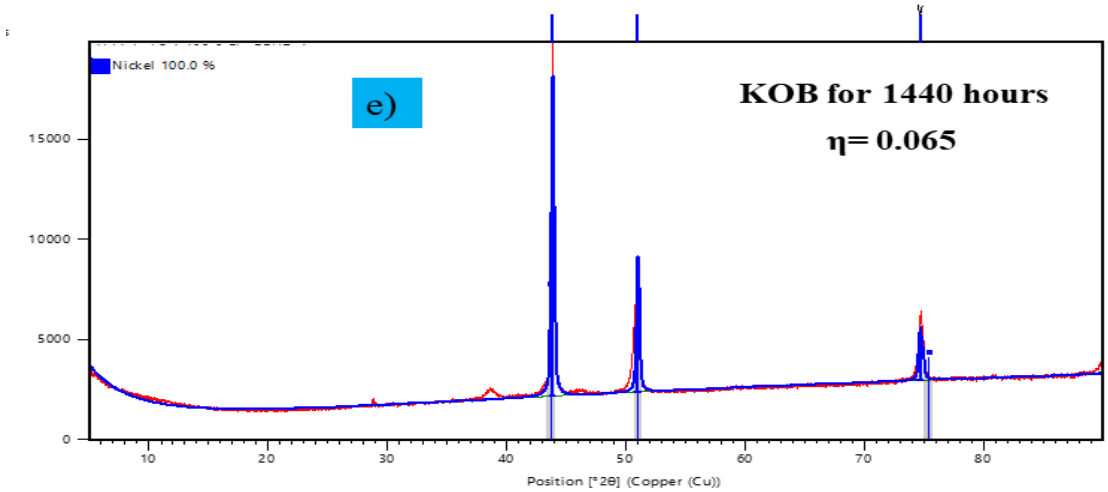
Nickel 100.0 %
e)
KOB for 1440 hours
η= 0.065
15000
10000
5000
0
10
20
30
40
50
60
70
80
Position [°2θ] (Copper (Cu))

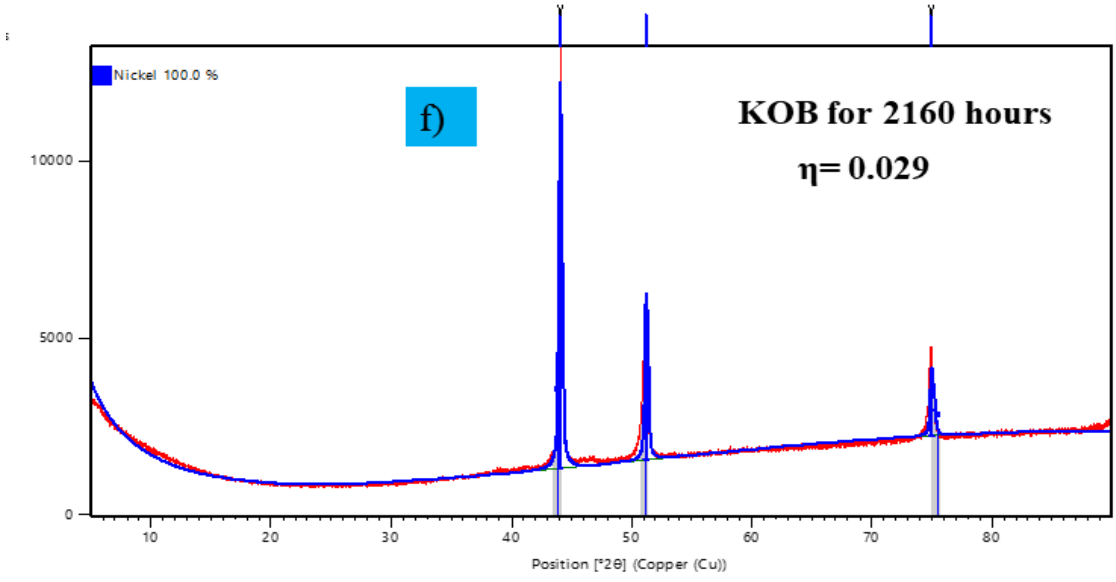
Nickel 100.0 %
f)
KOB for 2160 hours
η= 0.029
10000
5000
0
10
20
30
40
50
60
70
80
Position [°2θ] (Copper (Cu))

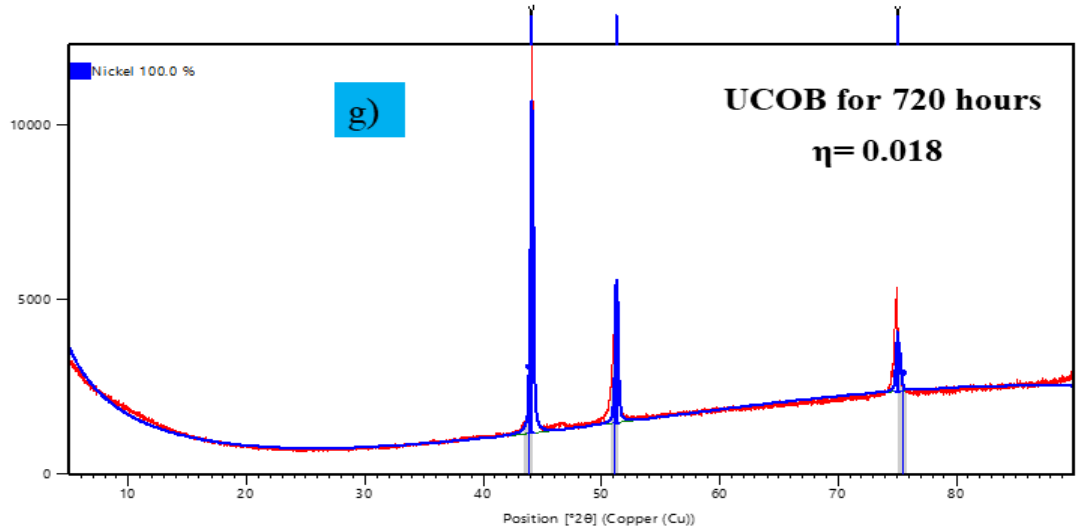
Nickel 100.0 %
g)
UCOB for 720 hours
η= 0.018
10000
5000
0
10
20
30
40
50
60
70
80
Position [°2θ] (Copper (Cu))

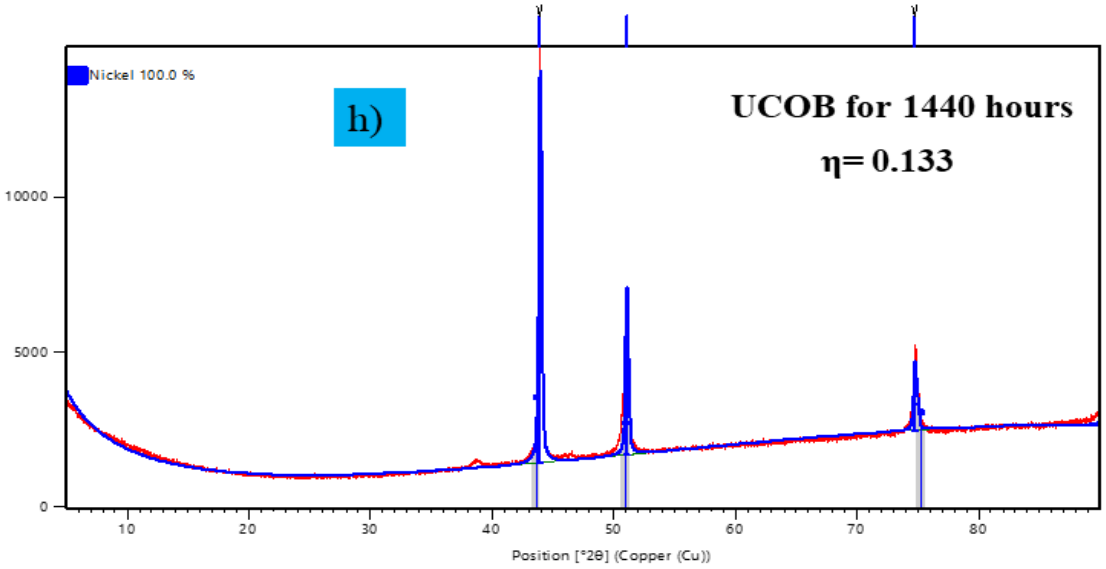
Nickel 100.0 %
h)
UCOB for 1440 hours
η= 0.133
10000
5000
0
10
20
30
40
50
60
70
80
Position [°2θ] (Copper (Cu))

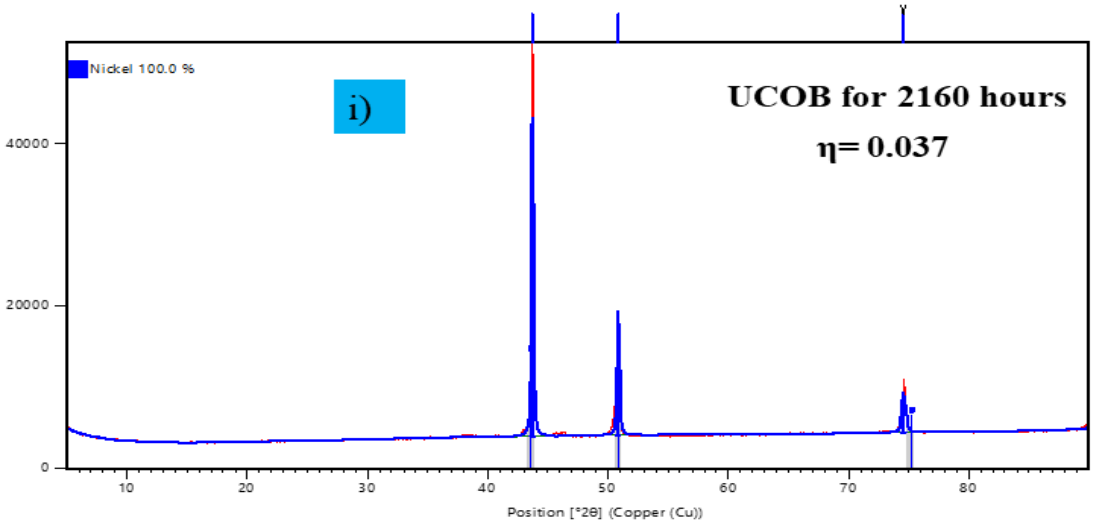
Nickel 100.0 %
i)
UCOB for 2160 hours
η= 0.037
40000
20000
0
10
20
30
40
50
60
70
80
Position [°2θ] (Copper (Cu))

Figure A4 Rivetweld strain refinement for Ni alloy exposed to JOB (a-c), KOB (d-f) and UCOB (g-i) for 720,1440 and 2160 hours respectively.

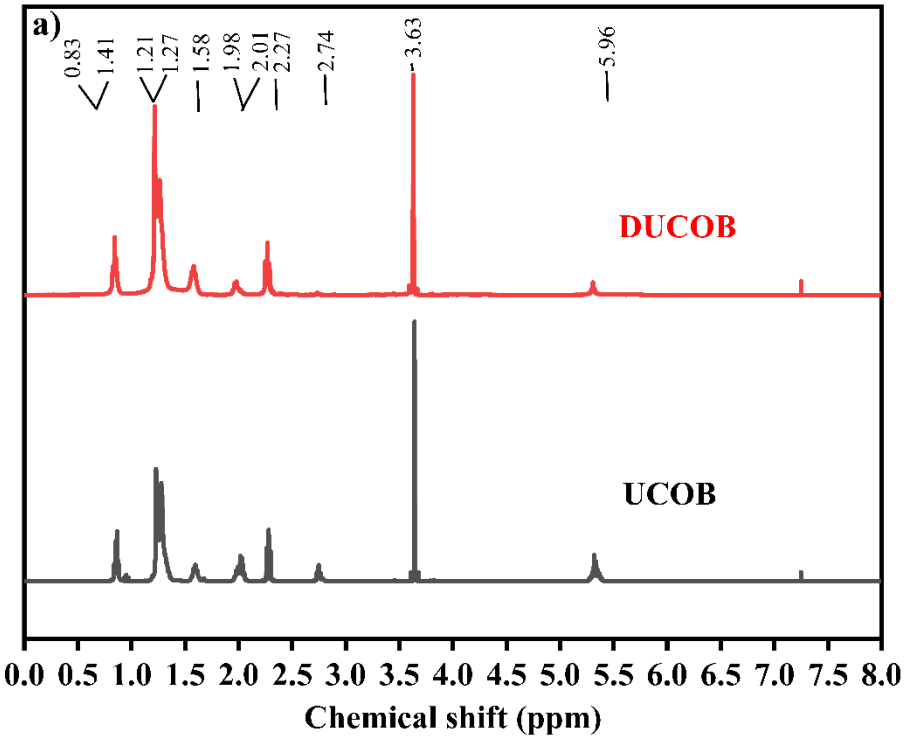

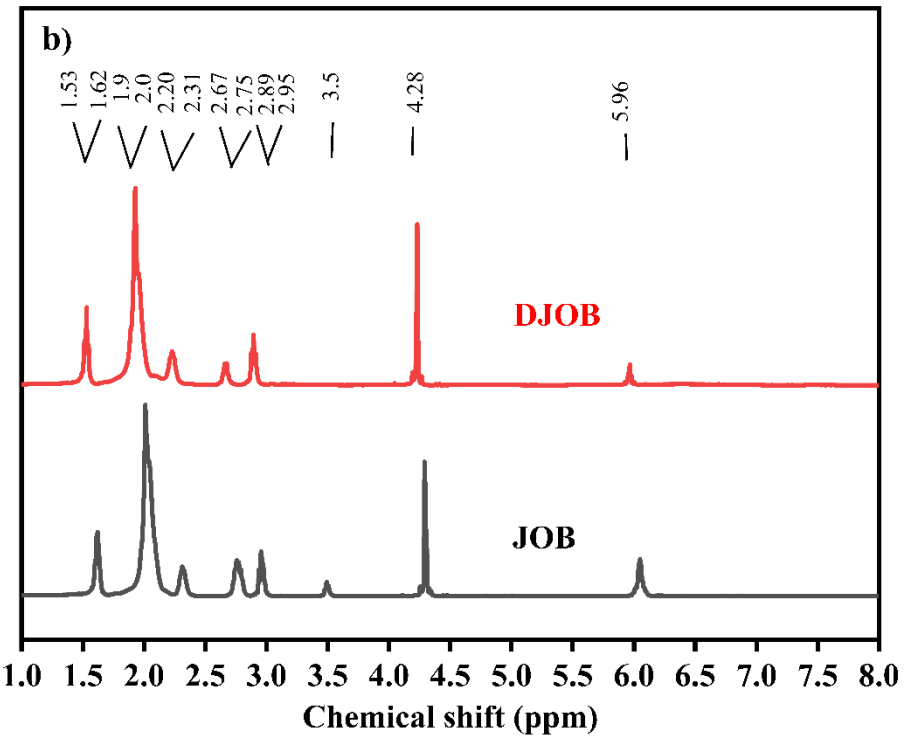

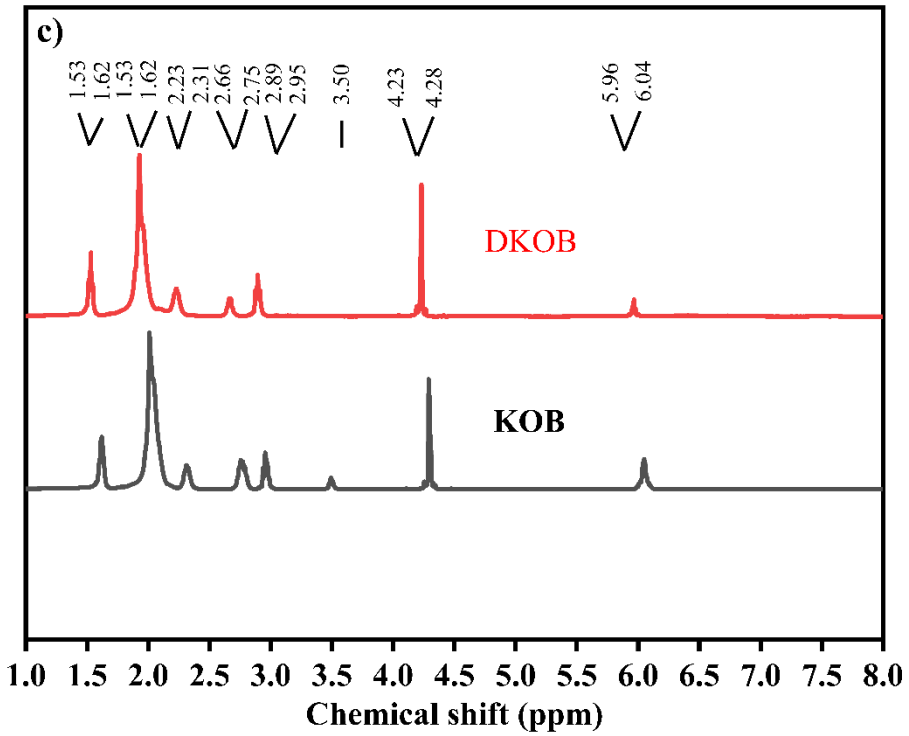

Figure A5 ^{1}H NMR spectrum: a) DUCOB and UCOB, b) DJOB & JOB,c) DKOB &KOB

Thesis outcomes

1. **Prajapati AK**, Yadawa Y, Dwivedi D, Kumar R. Fuel property enhancement of Jatropha biodiesel by blending with nanoparticles. Chemical Engineering & Technology. **2023** Jan;47(1):200-7.

2. **Prajapati AK,** Yadav S, Gomey AK, Choubey AK, Kumar R. Assessment of performance and emission characteristics of CI engine using tyre pyrolysis oil and biodiesel blends by nano additives: An experimental study. Journal of the Energy Institute. **2024** Dec 1;117:101825.

3. **Prajapati AK**, Saini A, Atal S, Kumar S, Mani G, Vellaichamy RP, Melcureraj L, Kumar R, Dwivedi D. Assessing the effect of different biodiesels on corrosion of nickel alloy. Materials Today Sustainability. **2024** Dec 1;28:100968.

4. **Prajapati AK**, Ali SS, Ansari KB, Athar M, Al Mesfer MK, Shah M, Danish M, Kumar R, Raheman AS. Process intensification in biodiesel production using unconventional reactors. Fuel. **2025** Jan 15;380:133263.

5. **Prajapati AK**, Gomey AK, Dwivedi D, Kumar R. "Evaluating the performance of batch, tubular coiled and coil flow invertor reactors in biodiesel production from karanja and used cooking oil".Chemical Engineering and Processing - Process Intensification, **2025**, 110375, https:doi.org/10.1016/j.cep.2025.110375

List of all publications

a) List of peer-reviewed publications in International Journals

1. **Prajapati AK**, Yadawa Y, Dwivedi D, Kumar R. Fuel property enhancement of Jatropha biodiesel by blending with nanoparticles. Chemical Engineering & Technology. **2023** Jan;47(1):200-7.

2. **Prajapati AK,** Yadav S, Gomey AK, Choubey AK, Kumar R. Assessment of performance and emission characteristics of CI engine using tyre pyrolysis oil and biodiesel blends by nano additives: An experimental study. Journal of the Energy Institute. **2024** Dec 1;117:101825.

3. **Prajapati AK**, Saini A, Atal S, Kumar S, Mani G, Vellaichamy RP, Melcureraj L, Kumar R, Dwivedi D. Assessing the effect of different biodiesels on corrosion of nickel alloy. Materials Today Sustainability. **2024** Dec 1;28:100968.

4. **Prajapati AK**, Ali SS, Ansari KB, Athar M, Al Mesfer MK, Shah M, Danish M, Kumar R, Raheman AS. Process intensification in biodiesel production using unconventional reactors. Fuel. **2025** Jan 15;380:133263.

5. **Prajapati AK**, Gomey AK, Dwivedi D, Kumar R. "Evaluating the performance of batch, tubular coiled and coil flow invertor reactors in biodiesel production from karanja and used cooking oil".Chemical Engineering and Processing - Process Intensification, **2025**, 110375, https:doi.org/10.1016/j.cep.2025.110375

b) Communications at the revision stage

6. Gomey A K, **Prajapati AK**, Tripathi MM, Haider MB, Kumar R " Performance, Combustion and Emission Study of Biodiesel Synthesized Using Azadirachta Indica Oil and Deep Eutectic Solvents as Catalyst". Bioresource Technology, Elsevier. (**Under Review**)

7. **Prajapati AK,** Panday P, Awasthi V, Singh S, Kumar R, Comparative Assessment of Performance, Combustion, and Emissions of Multifuel Blends in a Variable Compression Ratio CI Engine. Journal of Cleaner Production, Elsevier. (**Revised submission**)

8. **Prajapati AK**, Kumar R "Techno-Environmental Assessment of Biodiesel Production from Waste Cooking Oil: A Computational Perspective". Fuel. (**Correction stage**)

9. **Prajapati AK**, Kumar A, Kumar R. "AI/ML-Based Comparative Analysis of Engine Performance, Combustion, and Emissions for Multifuel Blends in a VCR CI Engine. Journal of Energy (**Correction stage**)

c) Additional publication in International Journals

10. **Prajapati AK**, Kumar P, Atal S, Kumar R, Dwivedi, D "Biodiesel feasibility study: An evaluation of material compatibility in the pipeline, corrosion, and future aspects." Journal of Loss Prevention in the Process Industries **(Under review).**

11. Ansari KB, **Prajapati AK**, Ali SS, Mesfer MK, Elkhaleefa A, Raheman AS, Kumar R, Trinh QT. Comprehensive Review on Biomass Chemical Looping Combustion: Feedstock Type, Operating Conditions, Reactor Design, Technological Advancement, Mechanistic Insights, and Economics. Journal of Environmental Chemical Engineering. 2025 May 10:116947.

12. Ansari KB, **Prajapati AK**, Ali SS, Rajnandni, Kumar R, Rahman AS, Mesfer MKAl, Alwan BAl, MXene-Polymer Composites for Energy Storage: Recent Developments, Applications, Future Perspectives. Journal of Energy Storage Materials (**Under review**).

13. **Prajapati AK**, Mahajan A, Jadhav S, Kumar K, Kumar R "Fourth generation (4G) biodiesel: Paving the way for a greener and sustainable energy future in emerging

economies”, Renew. Sustain. Energy Rev. 225 (2026) 116103. https://doi.org/10.1016/j.rser.2025.116103.

14.

Curriculam Viate (CV)

AJEET KUMAR PRAJAPATI

PhD Scholar in the Department of Chemical Engineering and Engineering Science, Rajiv Gandhi Institute of Petroleum Technology Jais, Amethi, Up., India (An Institution of National Importance, Ministry of Petroleum & Natural Gas, MoPNG)

Researcher IDs Links:
Google Scholar: https://scholar.google.com/citations?user=dA6GK6oAAAAJ&hl=en Web of Science Researcher ID: LVR-0324-2024 Scopus ID: 278641 LinkedIn Profile: www.linkedin.com/in/ajeet-prajapati-077a48209
Mobile: +91-9179208949 E-mail:20ce0002@rgipt.ac.in, drajeet514@gmail.com DOB: August 4, 1991; Nationality: Indian

EDUCATIONAL QUALIFICATION					
Degree	**Specializations**	**Institute/University**	**Years**	**CGPA/CPI**	**Class**
PhD	Chemical & Biochemical Engineering	Rajiv Gandhi Institute of Petroleum Technology Jais **(An Institution of National Importance)**	2020-2025	7.4	1st
M.E.	Heat Power Engineering	University Institute of Technology -RGPV Bhopal M.P.	2013-2015	8.35	1st
B.E.	Mechanical Engineering	Lakshmi Narain College of Technology, Bhopal, M.P.	2009-2013	77.28	1st

RESEARCH AND TEACHING INTERESTS

Research interest: Biodiesel synthesis using various reactor systems and enhancement of its properties through additives, focusing on performance, combustion characteristics, emissions, and corrosion compatibility with engine materials, along with compatibility studies of tyre pyrolysis oil in variable compression ratio (VCR) diesel engines. Additionally, the work includes a techno-economic analysis of biodiesel production from diverse feedstocks such as Karanja, jatropha, used cooking oil, algae oil, and bio-oil.

Thesis title: "**Synergistic approach for the optimization of biodiesel production and property enhancement via nano-additive**".

PROFESSIONAL EXPERIENCE

1. Plant maintenance engineer in the Force Motor Pithampur Indore M.P. (6 months)

Date of joining: 12/08/2015 **Date of leaving**: 02/02/2016 Duration:6 month

Activities: To check breakdowns, machine maintenance,

2. Assistant Professor in the Department of Mechanical Engineering, Government Engineering College Nowgong, Chhatarpur, M.P., India (Ad hoc basis).

Date of joining: 04/08/2016 **Date of leaving**: 16/07/2020 Duration: 4 years

Activities: Teaching, Research, Mentoring, student induction program, Sports coordinator

PUBLICATION's SUMMARY

Journals: No of SCI/SCIE/SSCI:05 No. of other peer-reviewed journals:02 No. of review journals:03

No.of Q1 journals:04 ,

Conference: National conference: 08 International conference:01 (Alternative fuels held in Bali, Indonesia)

Book chapters (BCs): 04

PUBLICATIONS

JOURNAL PAPER

1. **Ajeet Kumar Prajapati**, Ravindra Randa, Experimental Study on Utilization of Biogas in IC Engine, Int. J. Eng. Sci. Res. Technol. 9655 (**2015**) 827–835.

2. **Ajeet Kumar Prajapati**, Vipin Patel, "A review paper on comparative analysis of Diesel blends with different proportions of karanja oil Biodiesel" Published in International Journal of Trend in Scientific Research and Development (ijtsrd), ISSN: 2456-6470, Volume-2 | Issue-4, June **2018**, pp.419-424, URL: https://www.ijtsrd.com/papers/ijtsrd12896.pdf DOI: https://doi.org/10.31142/ijtsrd12896

3. **Ajeet Kumar Prajapati,** Yogendra Yadawa, Deepak Dwivedi, and Rakesh Kumar. "Fuel Property Enhancement of Jatropha Biodiesel by Blending with Nanoparticles.*" **Chemical Engineering & Technology, Wiley**,* Vol. 47, no. 1 (**2023**): 200-207. https://doi.org/10.1002/ceat.202300150. (Indexing: SCIE/SCOPUS, **IF:2.2**, SCImago Journal Rank: Q2,)

4. **Ajeet Kumar Prajapati**, Syed Saim Ali, Khursheed B. Ansari, Moina Athar, Mohammed K. Al Mesfer, Mumtaj Shah, Mohd Danish, Rakesh Kumar, and AR Shakeelur Raheman. "Process intensification in biodiesel production using unconventional reactors." Fuel, Elsevier, Vol. 380 (**2025**): 133263. https://doi.org/10.1016/j.fuel.2024.133263. (Indexing: SCIE/SCOPUS, **IF: 6.7**, SCImago Journal Rank: **Q1**)

5. **Ajeet Kumar Prajapati,** Shalu Yadav, Amit Kumar Gomey, Abhay Kumar Choubey, and Rakesh Kumar. "Assessment of Performance and Emission Characteristics of CI Engine Using Tyre Pyrolysis Oil and Biodiesel Blends by Nano Additives: An Experimental Study." Journal of the Energy Institute, Elsevier, Vol. 117, (**2024**): 101825. https://doi.org/10.1016/j.joei.2024.101825. (Indexing: SCIE/SCOPUS, **IF: 5.7**, SCImago Journal Rank: **Q1**)
6. **Ajeet Kumar Prajapati**, Abhishek Saini, Siddharth Atal, Saurabh Kumar, Gajendiran Mani, Ramesh Prabhu Vellaichamy, Lavanya Melcureraj, Rakesh Kumar, and Deepak Dwivedi. "Assessing the effect of different biodiesels on corrosion of nickel alloy." Materials Today Sustainability, Elsevier, Vol. 28, (**2024**): 100968. https://doi.org/10.1016/j.mtsust.2024.100968 (Indexing: SCIE/SCOPUS, **IF: 7.1**, SCImago Journal Rank: **Q1**)
7. **Ajeet Kumar Prajapati**, Amit Kumar Gomey, Deepak Dwivedi, Rakesh Kumar. "Evaluating the performance of batch, tubular coiled and coil flow invertor reactors in biodiesel production from karanja and used cooking oil". **Chemical Engineering and Processing - Process Intensification**, Elsevier, (Indexing: SCIE/SCOPUS, **IF: 3.8**, SC Imago Journal Rank: **Q1**) (**Under review**).
8. **Ajeet Kumar Prajapati**, Khursheed B. Ansari*, Syed Saim Ali, Mohammed K Al. Mesfer, Abubakr Elkhaleefa, Shakeelur Raheman A.R., Rakesh Kumar, Quang Thang Trinh "Comprehensive Review on Biomass Chemical Looping Combustion: Feedstock Type, Operating Conditions, Reactor Design, Technological Advancement, Mechanistic Insights, and Economics" Journal of Environmental Chemical Engineering**,** Elsevier, Vol.13 (**2025**) 116947. https://doi.org/10.1016/j.jece.2025.116947. (Indexing: SCIE/SCOPUS, **IF: 7.4**, SC Imago Journal Rank: **Q1**)
9. **Ajeet Kumar Prajapati**, Ananaya Mahajan, Shraddha Jadhav, Karan Kumar * Fourth-Generation Biodiesel: Paving the Way for a Greener and Sustainable Energy Future in India. Renewable and Sustainable Energy Reviews. Elsevier, (Indexing: SCIE/SCOPUS, **IF: 16.1**, SC Imago Journal Rank: **Q1**) (**Under review**).
10. **Ajeet Kumar Prajapati**, Pooja Panday, Vinayak Awasthi, Samyak, Rakesh Kumar, Comparative Assessment of Performance, Combustion, and Emissions of Multifuel Blends in a Variable Compression Ratio (VCR) CI Engine. Journal of Cleaner Production, Elsevier. (Indexing: SCIE/SCOPUS, **IF: 9.8**, SC Imago Journal Rank: **Q1**) (**Under review**).
NATIONAL AND INTERNATIONAL CONFERENCES

1. Presented paper in the 17th annual session of students "Chemical Engineering Congress **SCHEMCON-2021**" Organized by MANIT & IISER Bhopal(M.P.), on 22nd – 23rd, October 2021.

2. Presented paper at the International Conference on "Recent Trends in Energy Science and Engineering (**ICRTESE 2021**) " Organized by Rajiv Gandhi Institute of Petroleum Technology Jais, Amethi, on 26th -28th October 2021.

3. Presented poster in the "**SEFCO-2022**" entitled "Enhancement of Physiochemical Properties of Biodiesel and Diesel Blend with Nanoparticles" Organized by the CSIR-IIP Dehradun Uttarakhand India on 26th-27th August 2022.

4. Presented paper in the 18th annual session of students "Chemical Engineering Congress **SCHEMCON-2022**" Organized by NIT WARANGAL, on 23rd – 24th, September 2022.

5. Presented paper in the "**75th Chemical Engineering Congress CHEMCON-2022**" entitled "Application of nanoparticles for enhancement of fuel properties of jatropha –derived biodiesel and Corrosion impact" Organized by the HBTU Kanpur U.P. India on 27th-30th December 2022.

6. Oral presentation - International Conference on "**Trends in Energy and Environmental Research for Sustainable Development" (TEERSD-2023**), Guru Ghasidas Vishwavidyalaya, Bilaspur, C.G.

7. Presented paper in "**IIChe-Chemcon 2023**" entitled "Exploring the Fuel Properties of Tire Pyrolysis Oil through the Synergistic" Organized by HIT Kolkata, West Bengal, India on 27th-30th December 2023.

8. Attend a conference on Emissions Monitoring, **CEM India 2024** New Delhi, India, 20th - 22nd February 2024

9. Presented paper at the "**International Conference and Research Innovations (ICRI-2025)**" entitled "Sustainable Biodiesel from Novel Feedstocks: Synthesis, Optimization, and Combustion Insights" Organized by ISRA, EIST (EU) held in **Bali, Indonesia** on 5th-6th May 2025.

WORKING MANUSCRIPT

1. **Ajeet Kumar Prajapati**, Aditya Kashyap, & Rakesh Kumar "An Experimental and Numerical Investigation of the Performance, Combustion and Emission Characteristics of a VCR Diesel Engine Fueled with Cassia fistula Biodiesel" will be submitted to the Journal of Mechanical Design (JMD), ASME. (Indexing: SCIE/SCOPUS, **IF: 2.9**, SC Imago Journal Rank: **Q1**)

2. **Ajeet Kumar Prajapati,** Aditya Kashyap, & Rakesh Kumar " Impact of Dual Fuel Ammonia-Diesel –Tyre Pyrolysis Oil on Combustion and Emissions in Compression-Ignition Engines" will be submitted to the Journal of **Energy,** Elsevier, (Indexing: SCIE/SCOPUS, **IF: 9.0**, SC Imago Journal Rank: **Q1**).

3. **Ajeet Kumar Prajapati,** Abhijeet Kumar, & Rakesh Kumar. "AI/ML-Based Comparative Analysis of Engine Performance, Combustion, and Emissions for Multifuel Blends in a VCR CI Engine" will be submitted to the Journal of Combustion and Flame, Elsevier, (Indexing: SCIE/SCOPUS, **IF: 5.0**, SC Imago Journal Rank: **Q1**).

BOOK CHAPTERS

1. **Prajapati, A. K**., Aryan, S., Singh, S., Dwivedi, D., Serikova, N., & Purohit, B. K. Application of Functional Ceramics in Oil and Gas Industries: Properties and Current Status. In Functional Materials for the Oil and Gas Industry (pp. 39-50), (2024)CRC Press.

2. **Prajapati, A.K**., Yadawa, Y. Science and Engineering of Functional Coatings used in Energy Sectors", In the book: Functional Coatings: Innovations & Challenges" Chapter 32 (2023), John Wiley & Sons, Inc., NJ, USA, ISBN: 9781394207275

3. **Prajapati A.K**., Aditya Kashyap, Rakesh Kumar, Hardik Valera, Avinash Kumar Agarwal "Various Fuel Injection Techniques, Such as Port Fuel Injection and High-Pressure Direct Injection, Enable Ammonia, Methanol, and Hydrogen Combustion" In the book: Ammonia, Methanol, and Hydrogen as Emerging Fuels for De-Fossilized Transport Sector" Springer Nature, **eBook** ISBN, 978-981-96-6620-1
4. **Prajapati A.K.,** Aditya Kashyap, Rakesh Kumar, Andreas Bartl, Prof. Franz Winter, Prof. Stefan Pflügl, Avinash Kumar Agarwal " Alcohol for fueling IC Engines " In the book: Alcohol Production Processes and their Utilization in the Transport Sector" Springer Nature, **eBook** ISBN,978-981-96-7384-1

AWARDS AND ACHIEVEMENTS
1. Received the **Young Achiever Award -2025** at the RCS International Awards & Honors-2025 in Bali, Indonesia.
2. Won **Best Paper oral presentation award** at ICRI-2025 organized by the Research Cultural Society (ISRA), Bali, Indonesia, from 5th-6th May 2025.
3. Received the **International Travel Grant (ITG)** from the CSIR-HRDG, to attend the International Conference and Expo on Biofuels and Bioenergy, Italy, on 11th - 12th April 2024.
4. Won **Best Paper Award in an oral presentation at IICHE-CHEMCON-2023** organized by the Heritage Institute of Technology Kolkata, W.B., India, from 27th-30th December 2023.
5. Won **3rd** prize in Oral presentation and a cash prize of Rs.2000/- at SCHEMCON-2022 organized by NIT Warangal, Karnataka, India, during 23rd – 24th, September 2022
6. Won **3rd prize** in Oral presentation at SCHEMCON-2021 organized by Maulana Azad National Institute of Technology Bhopal,(MANIT) Madhya Pradesh, India, during 22nd – 23rd, October 2021.
7. **Scholarship awarded** by MHRD (Indian Govt.) in Aug 2020 (for Ph.D. Program, GATE-20)
8. **Appreciation** for the "MARUTI ENGINE EXHAUST ANALYSIS" led to better understanding for the students and the employees.

SKILLS
Software proficiency: Lab view software, Design expert, Minitab, CAD, CFD (Learning), MS Office Package, LCA (learning)

ACTIVITIES

Workshops/Short-term courses attended	• Attended a Workshop on "**Ionic Liquids and Deep Eutectic Solvents with Nature**" Conducted by IIT Guwahati Assam in March 2021 • Attended National Seminar on "**Global Energy Trends: Petroleum vs Other Energy**" at Chandigarh University, 2-7th September 2021. (**Online**) • Attended virtual summit of "**NextGen Chemical & Petrochemical Summit 2021**", 7-8th October 2021. • Attended National Workshop on "**Additive Manufacturing & Digital Twin for Turbomachinery**" Organized by ASME (International Gas Turbine Institute), on 31st July-1 August 2021. • Workshop on "**Efficient Technology for Waste Heat Recovery**". SERB, SITRC, Nashik, Maharashtra, India • Webinar on **Fundamental Hydrogen-Air Mixing, Combustion and Particulate Formation Processes in Hydrogen in Internal Combustion Engine (H_2ICE).** • CERI-Talk, **Engineering Our Wicked Problems the Case for Prioritizing Maintenance.** • Short-term course on GIAN initiatives offered by the IIT Kanpur "**Fuel/Engine Interactions in Practical Internal Combustion Engines for Future Emission Compliance and Efficiency Improvement**" from 17/06/2023 to 26/11/2023. • Attend the workshop on "**Biodiesel Production Using Deep Eutectic Solvents and Solid Acid Based Catalyst**." • Attended the workshop on "**Intensified Biodiesel Production using CFI, Batch and Coil tube reactor.**" • Attended the workshop on "**Recent Trends in Alternative Automotive Fuels**" • Attend the workshop on **Funding 101: Master the Art of Research Proposal Writing.** • Attend the workshop on **IPR Awareness and Skill Development with Special Reference to Patents and Start-ups,** India, conducted by the IPR Cell, NIT Mizoram. • Attend the workshop on **Intellectual Property Rights,** conducted by the RGIPT jais Amethi, U.p. India. • Short course on **Corrosion in Refineries and Petrochemicals**, from 16th-20th January 2023, Noida New Delhi, India • Attending the pre-conference webinar entitled " **Sustainable Manufacturing: Leveraging Additive Technologies and Materials** to Meet SDGs organized by the Chitkara University, Chandigarh-Patiala National Highway, Rajpura, Punjab, India • **Attend the workshop Recent Advances in Sustainable Energy IIT Jodhpur**, Rajasthan, India 26th -29th December 2024.
Team leader	Played the role of team leader in my research team.

Academic/Administrative Responsibility till PhD	• Worked as a teaching assistant (TA) from July 2021 to July 2024 while pursuing PhD at RGIPT Jais. • Elected as the student representative (DPGC) at Dept. of Chemical Engineering and Biochemical Engineering, Rajiv Gandhi Institute of Petroleum Technology Jais, Amethi, U.P. India (from 2023-2024)

PROFESSIONAL MEMBERSHIP

- Member of The American Society of Mechanical Engineers (ASME).
- Member of the Society of Automotive Engineers (SAE)
- International Association of Engineers (IAENG)
- RSIS International - Research and Scientific Innovation Society (Member)
- Institute For Engineering Research and Publication (IFERP)

RESEARCH COLLABORATIONS

Abroad	India
• King Khalid University Abha, Saudi Arabia. • Queensland Micro and Nanotechnology Centre, Griffith University, Nathan, Queensland, Australia • RWTH Aachen University, Worringer Weg Aachen, Germany	• Council of Scientific and Industrial Research Indian Institute of Petroleum Dehradun (CSIR-IIP) Dehradun, Uttarakhand • Indian Institute of Technology, Patna, Bihar • India Institute of Technology, Madras, Tamil Nadu • India Institute of Technology, Kanpur U.P.

REFERENCES

1. Dr. Rakesh Kumar (PhD Supervisor) Associate Professor, Dept. of Chemical Engineering and Biochemical Engineering, Rajiv Gandhi Institute of Petroleum Technology Jais, Amethi U.P., India Mobile:+91-9450352043 E-mail: rkumar@rgipt.acin	2. Dr Deepak Dwivedi Assistant Professor, Dept. of Chemical Engineering and Biochemical Engineering, Rajiv Gandhi Institute of Petroleum Technology Jais, Amethi U.P., India Mobile:+91-9691062352 E-mail: ddwivedi@rgipt.ac.in
3. Dr. Khursheed A.B. Ansari Assistant Professor, Dept. of Chemical Engineering, King Khalid University Abha, Saudi Arabia., Mobile: +91-9045104440 E-mail: khansari@kku.edu.sa	4. Dr.Venkata Subbarayudu Sistla Associate Professor, Dept. of Chemical Engineering and Biochemical Engineering, Rajiv Gandhi Institute of Petroleum Technology Jais, Amethi U.P., India Mobile: +91-9935967357 , E-mail: vsistla@rgipt.ac.in